TECHNISCHE UNIVERSITÄT WIEN

Dissertation

Pioneering Light, Air, and Photosensitizing Proteins for the Degradation of Polyolefins

ausgeführt zum Zwecke der Erlangung des akademischen Grades einer Doktorin der Naturwissenschaften unter der Leitung von

Associate Prof. Dr. Florian Rudroff
Institut für Angewandte Synthesechemie, E163

eingereicht an der Technischen Universität Wien Fakultät für Technische Chemie

von
Lydia Suchy, MSc, MSc

01205005

Wien, Jänner 2025

There were times when it felt as though everything and everyone was conspiring against the process. But the thing about adversities is that they force you out of your comfort zone. The bad outcome is that you might drift into the void, but the other outcome is that you might gain amazing tools for growth and knowledge.

– *Alfonso Cuaron on directing "Gravity"*

Declaration of contribution

Anna Krapfenbauer contributed to chapters 3.2, 3.3, and 3.6 as part of her bachelor thesis internship. She contributed substantially to protein production, purification, and development of ROS-specific assays for the characterization of the unmodified photosynthesizer proteins. Moreover, she conducted five molecular cloning experiments as part of a one-month internship.

Morris Glowacki contributed to chapters 3.6, 3.7, and 3.8 as part of his bachelor thesis internship. He conducted several cloning experiments, produced, and purified fusion proteins and partially characterized fusion proteins regarding their ROS-production.

Markus Sauer contributed to chapters 3.9.3.3, and 3.11.3. He conducted all XPS measurements for the analysis of protein adsorption to PE and degradation of PE.

Lukas Brunnbauer contributed to chapter 3.11.3. He conducted LIBS measurements of PE degradation experiments.

Table of contents

Declaration of contribution iv

Table of contents v

Acknowledgments viii

Abstract x

Kurzfassung xii

1 Introduction 14

1.1 The problem with plastic *14*
Polyolefins and their waste management 16
1.1.1 Aging of polyolefins in the environment – formation of microplastic 17
1.1.2 Degradation methodologies of polyolefins in microplastic 19

1.2 Background to reactive oxygen species (ROS) *25*
1.2.1 ROS production by a photosensitizer 25
1.2.2 Limitations and detection of ROS 26

1.3 Genetically encoded photosensitizer proteins *29*
1.3.1 Homologs of Green Fluorescent Protein (GFP) 29
1.3.2 Flavin-binding Light-Oxygen-Voltage sensing domain (LOV) proteins 31
1.3.3 Applications of ROS-producing PSPs 32

1.4 Hydrophobins - the surface-active proteins *34*

1.5 Methods for polyolefin-surface analysis *36*
1.5.1 Selected methods for the analysis of protein-polyolefin interaction 36
1.5.2 Selected methods for the analysis of polyolefin surface oxidation and degradation 41

2 Research question and aims 47

3 Results and discussion 49

3.1 Design of plasmids for expression and cloning *49*

3.2 Protein production analysis of unmodified PSPs *50*

3.3 Characterization of PSPs and selection of highest ROS producers *51*
3.3.1 Spectroscopic characterization 51
3.3.2 Quantification of reactive oxygen species production 52

3.4 Attempts to establish a model reaction for PE degradation *66*

3.5 Design of plasmids for cloning – fusion proteins with hydrophobins *69*

3.6 Assembly of fusion protein constructs *71*

3.7 Protein production analysis of fusion proteins *73*

3.8 Characterization of selected fusion proteins *78*
3.8.1 Spectroscopic characterization 78
3.8.2 Quantification of reactive oxygen species production 88
3.8.3 Oxygen consumption 96

3.9 Analysis of the interaction between fusion protein and polymer *100*

3.9.1 Generation of a smooth polymer surface: spin coating 100
3.9.2 Analysis of the pristine polymer surface 101
3.9.3 Analysis of the adsorption of fusion proteins to the polymer surface 103
3.9.4 Analysis of the desorption of fusion proteins from the polymer surface 110

3.10 Quantification of HO• production on the polymer surface *115*

3.11 Polyolefin degradation *117*
3.11.1 Positive control – Fenton reaction 117
3.11.2 Incubation with the selected fusion protein and negative control 118
3.11.3 Analysis by ATR-FTIR, LIBS, and XPS 120

4 Conclusion **125**

5 Material and methods **128**

5.1 Stock solutions *128*

5.2 Media *128*

5.3 Buffers and other solutions *129*

5.4 Cultivation of bacteria *131*
5.4.1 Overnight culture 131
5.4.2 Preparation of cryostocks 131
5.4.3 Cultivation on LB-agar plates (recovery of bacteria from cryostock) 131

5.5 Preparation of chemically competent (RbCl) E. coli cells *132*

5.6 Transformation of chemically competent (RbCl) E. coli cells *132*

5.7 Plasmid DNA isolation and quantification *132*

5.8 Verification of DNA by sequencing *133*

5.9 Dilution of primers *133*

5.10 Colony PCR *133*

5.11 Gel electrophoresis *134*

5.12 Molecular cloning - NEBuilder® HiFi DNA assembly *134*
5.12.1 Primer design 134
5.12.2 PCR amplification of target DNA fragments 134
5.12.3 Gel purification of PCR-amplified DNA fragments 136
5.12.4 Assembly 136
5.12.5 Chemical transformation and verification 137

5.13 Molecular cloning – Q5® site-directed mutagenesis *137*
5.13.1 Step 1: Exponential amplification 137
5.13.2 Step 2: KLD reaction 138
5.13.3 Step 3: Chemical transformation and verification 138

5.14 Protein production in E. coli BL21(DE3) *138*
5.14.1 Cultivation in autoinduction media[178] 138

5.15 Protein purification *139*
5.15.1 Cell harvesting 139
5.15.2 Cell lysis 139
5.15.3 Purification by IMAC 139

5.16 Determination of protein concentration *140*

5.17 Protein production analysis by SDS-PAGE (Sodium Dodecyl Sulfate Polyacrylamide Gel Electrophoresis) *141*

5.18 Characterization of fusion proteins *142*

5.18.1 Spectroscopic characterization of fusion proteins 142
5.18.2 Quantification of ROS production 142
5.18.3 O_2 consumption analysis 143

5.19 Surface analysis *144*
5.19.1 Spin coating for the preparation of a smooth polymer surface 144
5.19.2 Ellipsometry 144
5.19.3 SPR (Surface Plasmon Resonance) 145
5.19.4 WCA (Water Contact Angle measurement) 145
5.19.5 ATR-FTIR (Attenuated Total Reflectance Fourier Transform InfraRed Spectroscopy) 145
5.19.6 XPS (X-Ray Photoelectron Spectroscopy) 145
5.19.7 LIBS (Laser Induced Breakdown Spectroscopy) 146
5.19.8 AFM (Atomic Force Microscopy) 146

5.20 Quantification of $HO^{\bullet}$ production on the polymer surface *147*

5.21 Polyethylene degradation experiments *147*
5.21.1 Degradation experiments with Fenton reaction 147
5.21.2 Degradation experiments with protein 148

6 Appendix **149**

6.1 Protein library *149*

6.2 Gene sequences *151*

6.3 List of primers *165*

6.4 Molecular cloning – specifications *167*

6.5 Light intensity measurement *170*

6.6 ABTS assay *170*

6.7 FMN photobleaching experiment *171*

6.8 Supplementary Figures *173*
6.8.1 Fluorescence spectra 173
6.8.2 Gel Electrophoresis 174
6.8.3 WCA 182
6.8.4 ATR-FTIR spectra 182
6.8.5 XPS spectra 185

7 Abbreviations **189**

8 Curriculum Vitae **192**

9 References **195**

Acknowledgments

I want to thank my supervisor Florion Rudroff for the possibility to conduct my PhD thesis in the BSC working group at the Institute for Applied Synthetic Chemistry, TU Vienna. I am grateful for all his support and the chance to work on such an interesting new topic. Although it was very challenging to start from scratch in a new project (spending most of the time on the development of fluorescent assays and surface analysis methods), the topic represents an approach towards plastic waste reduction, which is important for environmental protection, and of my personal interests.

I would like to thank the other seniors who complete our working group, Marko D. Mihovilovic, Michael Schnürch, and Christian Stanetty, for all their input during seminars and for making our working group so versatile.

Furthermore, I want to thank all the people who offered their expertise and collaboration for different subjects during my research project: Brigitte Holzer and Birgit Meindl for their help during the planning and implementation of SPR measurements; Dogukan Hazar Apaydin for his help with the spin coating of polymers; Lukas Brunnbauer and Andreas Limbeck for conducting the LIBS measurements and particularly Markus Sauer and Annette Foelske for their advice and conducting the numerous XPS measurements.

At this point, I would like to thank my two students who worked on this research project, who are both very curious scientists, good thinkers, and super nice people. Anna helped me at the very beginning of the project with the first steps of protein production and the development of assays for the detection of ROS. Morris helped me during the cloning process to create fusion proteins and analyze the first fusion proteins.

Next, (my favorite part) I want to thank all my colleagues in the BSC group. I want to start with my two office pals, Julia and Tom, for all their knowledge and help throughout my whole time. It was the best Bio-office I can imagine. Then, I want to thank all my other colleagues in the Bio-team for all their support and help and fun time together: Astrid for being absolutely the nicest person, Chrise for his friendship and his dark humor, Freddy for being my best friend and making every day the best day, Jorge for bringing some fresh Spanish wind into the group, Max for being Max and funny, Richie for always being nice and chill, Stefan for always seeing things from a different perspective, and Verena for being always so honest and having her heart always in the right place. Also, I want to thank all former “Bios”: Clemens, Hamid, Heci, and Hubert, I missed you all after you were gone.

I want to thank all the other people in our big, diversified working group. I am very grateful for all the scientific help as well as all the nice and funny moments: Ashadi, Björn, Christoph St., Christoph Su., Dominik, Eleni, Emmanuel, Fanny, Farooq, Johanna, Kathi, Nanditha, Nika, Nina, Pierre, Raheleh, Simon, Tobi, and Viktor.

I would also like to extend my gratitude to all other staff members at the institute, whose contributions are vital for keeping up the research.

Lastly, I also want to thank all my friends and family who have always been supporting and encouraging me during my studies and my PhD. Thank you for cheering me up during challenging times and for always being on my side and showing me the different aspects of life. In this regard, I want to thank my partner for being my favorite person in the world and for all the love, support, and endurance throughout this time.

Abstract

Single-use plastics are essential but cause significant environmental issues, particularly due to inadequate recycling. The large-scale production of plastic, its long lifetime, and its pollution due to landfilling necessitate the development of new, more sustainable, and more effective recycling strategies. Polyolefins like polyethylene (PE) and polypropylene (PP), are very inert to biodegradation and chemical recycling. Most current chemical recycling methodologies rely on high-energy processes or require harsh conditions like high temperatures or toxic chemicals. Especially the generation and distribution of microplastic represent a growing environmental problem and require alternative methodologies for its degradation. One possibility for the degradation of polyolefin microplastic is photoinduced oxidative degradation. Photocatalysts like TiO_2 accelerate the formation of hydroxyl radical ($HO^{\bullet}$), a reactive oxygen species (ROS), which is a powerful oxidant that initiates the degradation of polyolefins.

In this study we explored a novel bio-based approach for PE degradation using light-driven protein-based photocatalysts that create ROS upon visible light exposure, promoting the oxidative degradation of PE. Different photosensitizing proteins (PSPs) were analyzed, regarding their ROS-producing activity. Two representatives of LOV (light-oxygen-voltage-sensing) domain proteins, which harbor a blue-light sensitive flavin chromophore, were selected. Due to the short lifetime of ROS, efficient adsorption of the LOV protein to the hydrophobic polyolefin surface would improve oxidation efficiency. A previously reported concept was implemented, where different hydrophobins (small fungal proteins containing a hydrophobic patch) were fused to the LOV proteins. Therefore, different genetic constructs encoding the fusion proteins were created by molecular cloning. Fusion proteins were produced in *Escherichia coli* and purified by immobilized metal affinity chromatography (IMAC).

Improved adsorption of the fusion proteins to a PE/PP surface was proven by different surface analysis methods. Among these, water contact angle measurement (WCA) and attenuated total reflectance Fourier transform infrared spectroscopy (ATR-FTIR) resulted to be the most suitable methods. In this context, protocols for the generation of smooth polymer surfaces by spin coating were developed. Besides the analysis of the adsorption behavior of the fusion proteins, the stability of the fusion proteins towards blue light was analyzed by fluorescence and oxygen consumption measurements. Moreover, ROS-specific assays (including $HO^{\bullet}$, $^1O_2$, H_2O_2, and $O_2^{\bullet-}$) were conducted for the evaluation of ROS production by the fusion proteins. The LOV protein DsFbFpM49I (*Dinoroseobacter shibae*) fused to the hydrophobin mHGF1 (*Grifola frondosa*) showed the highest ROS production.

For the verification of in situ generation of $HO^{\bullet}$ by the protein on a polyolefin surface, a $HO^{\bullet}$ specific assay was incorporated into a PE layer. The production of $HO^{\bullet}$ directly on the PE surface by the adsorbed fusion protein could be proven, while with solubilized protein no $HO^{\bullet}$ production could be detected.

Finally, the concept that the protein is capable of oxidative polyolefin degradation was proven. A degradation experiment was conducted with the fusion protein mHGF1-

DsFbFpM49I and commercially available PE. A positive control for the oxidation of the PE surface (with Fenton's reagent) was conducted. The oxidation of the PE surface was analyzed by ATR-FTIR, laser-induced breakdown spectroscopy (LIBS), and X-ray photoelectron spectroscopy (XPS). Surface-bound oxygen could be detected, suggesting surface oxidation by the protein.

Kurzfassung

Einwegkunststoffe sind zwar unverzichtbar, verursachen jedoch erhebliche Umweltprobleme, insbesondere durch unzureichendes Recycling. Die großflächige Produktion, die lange Lebensdauer und die Umweltverschmutzung durch Deponierung des Plastikabfalls erfordern die Entwicklung neuer, nachhaltiger und effizienter Recyclingmethoden. Polyolefine wie Polyethylen (PE) und Polypropylen (PP) sind besonders resistent gegenüber biologischem Abbau und chemischem Recycling. Die meisten chemischen Recyclingverfahren basieren auf energieintensiven Prozessen oder erfordern extreme Bedingungen wie hohe Temperaturen oder giftige Chemikalien. Besonders die Entstehung und Verbreitung von Mikroplastik stellen ein wachsendes Umweltproblem dar und erfordern alternative Abbaumethoden. Eine Möglichkeit für den Abbau von Polyolefin-Mikroplastik ist der photoinduzierte oxidative Abbau. Photokatalysatoren wie TiO_2 beschleunigen die Bildung von Hydroxylradikalen ($HO^{\bullet}$), einer reaktiven Sauerstoffspezies (ROS), welche ein starkes Oxidationsmittel ist und den Abbau von Polyolefinen initiiert.

In dieser Studie wurde ein neuartiger biobasierter Ansatz für den PE-Abbau mittels lichtgetriebener, Protein-Photokatalysatoren untersucht, die bei Belichtung mit sichtbarem Licht ROS erzeugen und somit den oxidativen Abbau von PE einleiten. Verschiedene photosensibilisierende Proteine (PSP) wurden hinsichtlich ihrer ROS-Produktion untersucht. Zwei Vertreter der LOV-Domänen (light-oxygen-voltage-sensing) Proteine, die einen Blaulicht-empfindlichen Flavin-Chromophor enthalten, wurden ausgewählt. Aufgrund der kurzen Lebensdauer von ROS würde eine effiziente Adsorption der LOV-Proteine an der hydrophoben Polyolefin-Oberfläche die Oxidationseffizienz verbessern. Ein bekanntes Konzept wurde umgesetzt, bei dem unterschiedliche Hydrophobine (kleine, hydrophobe Pilzproteine) an die LOV-Proteine fusioniert wurden. Die genetischen Konstrukte wurden durch Klonierung erstellt, die Fusionsproteine wurden in *Escherichia coli* produziert und mittels immobilisierter Metallchelat-Affinitätschromatographie (IMAC) gereinigt.

Die verbesserte Adsorption der Fusionsproteine an PE/PP-Oberflächen wurde durch verschiedene Oberflächenanalysemethoden nachgewiesen, wobei Wasserkontaktwinkel-Messungen (WCA) und abgeschwächte Totalreflexion Fourier-Transformations-Infrarotspektroskopie (ATR-FTIR) am geeignetsten waren. Hierbei wurden Protokolle für die Herstellung glatter Polymeroberflächen mittels Spin-Coating entwickelt. Neben der Analyse des Adsorptionsverhaltens der Fusionsproteine wurde deren Stabilität während Blaulichtbestrahlung mittels Fluoreszenz- und Sauerstoff-Messungen analysiert. Außerdem wurde die ROS-Produktion ($HO^{\bullet}$, $^1O_2$, H_2O_2, and $O_2^{\bullet-}$) mittels spezifischer Assays analysiert. Das LOV-Protein DsFbFpM49I (*Dinoroseobacter shibae*) fusioniert mit dem Hydrophobin mHGF1 (*Grifola frondosa*), zeigte die höchste ROS-Produktion.

Um die $HO^{\bullet}$-Erzeugung in situ auf einer Polyolefin-Oberfläche nachzuweisen, wurde ein $HO^{\bullet}$-spezifischer Test in eine PE-Schicht integriert. Dabei konnte die $HO^{\bullet}$-Produktion durch adsorbiertes Fusionsprotein nachgewiesen werden, jedoch nicht, wenn das Protein in einer Lösung verwendet wurde.

Schließlich wurde nachgewiesen, dass das Protein den oxidativen Abbau von Polyolefinen ermöglicht. In einem Experiment wurde kommerzielles PE mit dem Fusionsprotein mHGF1-DsFbFpM49I behandelt. Eine positive Kontrolle für die Oxidation der PE-Oberfläche durch Fenton-Reagenz wurde durchgeführt. Die Oxidation der PE-Oberfläche wurde mittels ATR-FTIR, Laserinduzierte Plasmaspektroskopie (LIBS) und Röntgenphotoelektronenspektroskopie (XPS) nachgewiesen. Es konnte sauerstoffgebundene Oxidation nachgewiesen werden, was auf eine Protein-vermittelte Oberflächenoxidation hinweist.

1 Introduction

1.1 The problem with plastic

Plastics, especially single-use plastics such as bags, bottles, and packaging are used in all aspects of life (Figure 1, a), and thus are an indispensable part of today's society. Packaging is the largest world plastic market, followed by building & construction applications.[1] The global plastic production is increasing steadily, generating millions of tons every year.[1,2] Plastic production is cheap and mainly petroleum-based.[3] Petroleum-based plastics show advantageous properties as they are lightweight, safe, durable, chemically inert, have excellent thermal stability, and have outstanding electrical insulation.[4] However, plastics desired durability has a down part. Currently, the accumulation of plastic waste due to insufficient/inefficient methods for the recycling of commodity polymers represents a growing environmental problem. Less than 10 % of post-consumer plastics are being recycled (Figure 1, b). Plastic disposal and waste management are not considered enough.[5] Irresponsible disposal leads to pollution impacting wildlife and the environment.[6] Plastic's high persistency towards most chemicals, light, and extreme temperatures, leads to long degradation times. This explains their growing role in the pollution of all ecosystems.

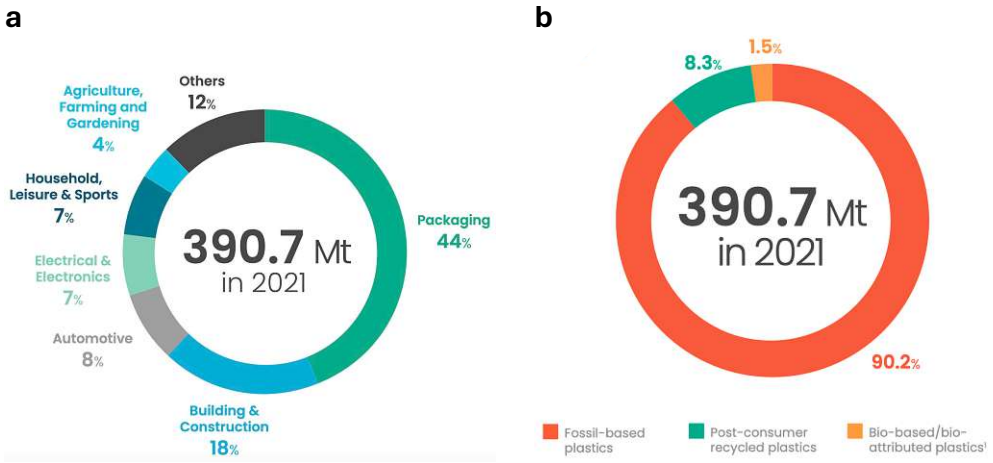

Figure 1| Plastic's use and production. The above data are rounded estimations. The figures are adapted from Plastics Europe (Nova-Institute 2022; data for bio-based structural polymers, preliminary estimations for 2021).[1,7] **a**, Distribution of the use of the global plastic by application. **b**, World plastics production in 2021.

As plastic gets broken down into tiny fragments, but not degraded completely, a new unknown factor arises by so-called microplastic. It can be formed in all processes that involve plastics (building and construction, industry, packaging), but also in daily processes, e.g., coming off tires on roads or during the washing of synthetic clothes. It is formed by mechanical degradation, photodegradation, and biodegradation. Followingly, it is distributed and can be detected in most environments, e.g. rivers, seawater, soil, and air (Figure 2).[8] Its small size (smaller than 5 mm) allows its transportation throughout biological membranes. The alarming fact about microplastic is its ability to absorb

hydrophobic pollutants and its containment of additives with potentially hazardous chemical properties. The impacts on our environment and health, especially the long-term effects of plastic pollution, are yet to be fully understood.[2,9]

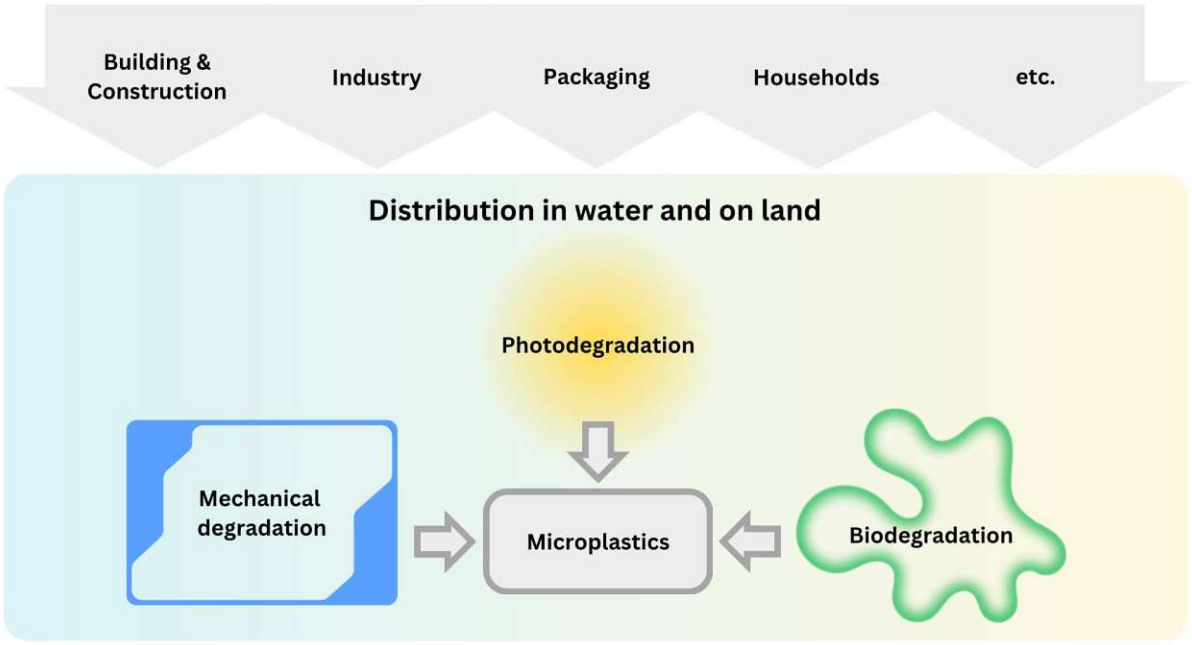

Figure 2| Sources of microplastic in the environment. Microplastic can be formed during all processes that involve plastic. It is formed by mechanical degradation, photodegradation, and biodegradation and followingly distributed in all environments.

Several aspects must be considered when tackling the global plastic pollution problem. First and foremost, it can be tackled by reducing plastic production. A different way to tackle the problem represents the development of sustainable plastic alternatives. New materials with reduced environmental impact are being developed.[10,11] However, it is not probable nor possible to stop plastic production or to switch entirely to degradable alternatives. Therefore, waste management infrastructure (collection and sorting of plastic waste) represents the most integral factor for the successful handling of plastics. However, this is an organizational and legislative matter which will not be tackled in this thesis. After collection and sorting, generally, it can be distinguished between four main pathways for plastic waste. It can be incinerated for energy recovery, stored in landfills, recycled mechanically, or recycled chemically. The deposition in landfills has long-term risks for soil and groundwater. Finally, an important aspect is the improvement of efficient degradation and recycling technologies. Waste management represents the key to the improvement of recycling rates. Regarding recycling technologies, mechanical recycling (melting or extrusion) is often limited to thermoplastics and is very dependent on prior waste pre-processing via sorting, cleaning, drying, etc. Consequently, mechanically recycled plastics often show decreased quality due to impurities.[12] Therefore, next to mechanical recycling, an important measure is the development of efficient recycling technologies, especially chemical and bio-recycling methods.[10,13]

Polyolefins and their waste management

Polyolefins are the most produced plastics and are mainly used for short-lived packaging materials (Figure 3).

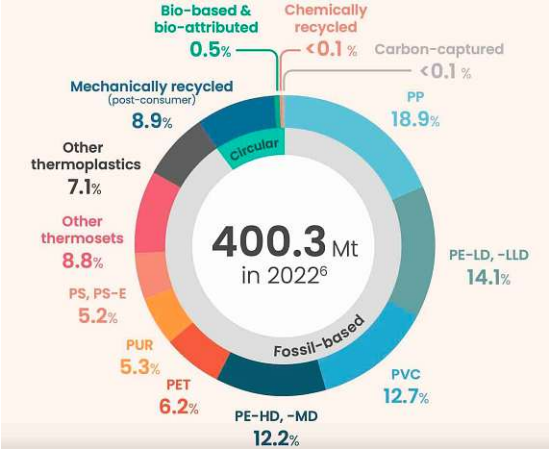

Figure 3| Global plastics production by polymer. The above data are rounded estimations.[1] Includes polybutylene terephthalate (PBT), polyetheretherketone (PEEK), polyetherimide (PEI), polyoxymethylene (POM), polyphthalamide (PPA), polysulfone/ polyethersulfone/ polyphenylsulfone (PSU/PES/PPSU), polytetrafluoroethylene (PTFE), polyvinylidene fluoride (PVDF) and other thermoplastics not listed separately. The figure is adapted from Plastics Europe.[7]

They are characterized by their saturated carbon backbone, which consists of only carbon-carbon single bonds (C-C) and carbon-hydrogen bonds (C-H), without any functional groups (Figure 4). Polyethylene (PE) and polypropylene (PP) represent the most common polyolefins. PE is classified into four main types: High-Density Polyethylene (HDPE), Low-Density Polyethylene (LDPE), Linear Low-Density Polyethylene (LLDPE), and Ultra High Molecular Weight Polyethylene (UHMWPE). While HDPE has minimal branching making it rigid and resistant, LDPE has a highly branched structure making it very flexible. LLDPE has shorter branches and is therefore more durable than LDPE. UHMWPE has extremely long polymer chains and therefore the most durable type.[14]

Polyethylene (PE) **Polypropylene (PP)**

Figure 4| The chemical structures of the most common polyolefins: PE and PP.

The waste management of polyolefins is difficult. The composition of polyolefins (mainly in packaging) varies, which makes the sorting very difficult. Therefore, recycling is not well established. At the end of their lifetime, they are either burned or more often stored in landfills. Moreover, they pile up on land or in waterways, especially oceans.[15] Therefore, polyolefins contribute substantially to the formation of microplastic.

1.1.1 Aging of polyolefins in the environment – formation of microplastic

The lack of functional groups in polyolefins makes them chemically very inert. Other hydrolyzable plastic types with functional groups, such as ester-linked monomers (e.g., in polyethylene terephthalate (PET)) can be degraded by microorganisms. These microorganisms harbor enzymes that can hydrolytically cleave e.g., ester bonds. On the contrary, for the breakdown of polyolefins like PE or PP a non-hydrolytic oxidative pathway is necessary, which explains their persistency in the environment.[16] Especially C-H and C-C bonds are very stable covalent bonds. Their cleavage usually requires a radical mechanism. Polyolefin aging in the environment is a combination of photo- and thermo-oxidative degradation and biological follow-up treatment by microorganisms.[17]

Reactive oxygen species (ROS, chapter 1.2) play a significant role in the first step of polyolefin degradation in the environment, especially the degradation of microplastic (fragmentation, size reduction, and surface changes). ROS are generated in the environment through various pathways such as UV radiation, atmospheric reactions, photosynthesis, and redox reactions in air, soil, and water (Figure 5, a).[18] Solar UV radiation can directly produce singlet oxygen ($^1O_2$) and indirectly generate ROS through photochemical reactions involving organic matter. Hydroxyl radical ($HO^\bullet$), which is one of the most powerful oxidizing agents known, is primarily generated through photo-Fenton reactions, the photolysis of nitrates and nitrites, and the breakdown of natural organic matter (NOM). Additionally, reduced species like ferrous iron (Fe^{2+}) and sulfur ions (S^{2-}) in soils and sediments also contribute to $HO^\bullet$ formation. Even biological systems produce ROS, with cellular respiration, peroxisomal metabolism, and immune cell activity. Lastly, ROS are generated on the surfaces of the microplastic itself through several mechanisms, including photochemical, biological, and chemical pathways.[19]

The first and rate-determining step is oxidative degradation (photooxidation), which is a radical process dependent on ROS. PE and PP are initially resistant to photooxidation due to the absence of light-absorbing chromophoric groups. However, external impurities can initiate photodegradation.[20] PP was reported to be less stable than PE because of its greater susceptibility of the tertiary carbons to hydrogen abstraction.[21] $HO^\bullet$ can attack C-H groups, creating alkyl radicals that react with oxygen to form peroxy radicals and carboxylic groups.[22,23] Aromatic polymers like PS react with $HO^\bullet$ to form alcohols. Aliphatic polymers such as PP, PE, and polyvinyl chloride (PVC) undergo hydrogen abstraction, forming radicals, followed by peroxidation (Figure 5, b).[24,25] These radicals further react with ROS or the polymer itself, breaking down the polymer chains into shorter fragments.[22]

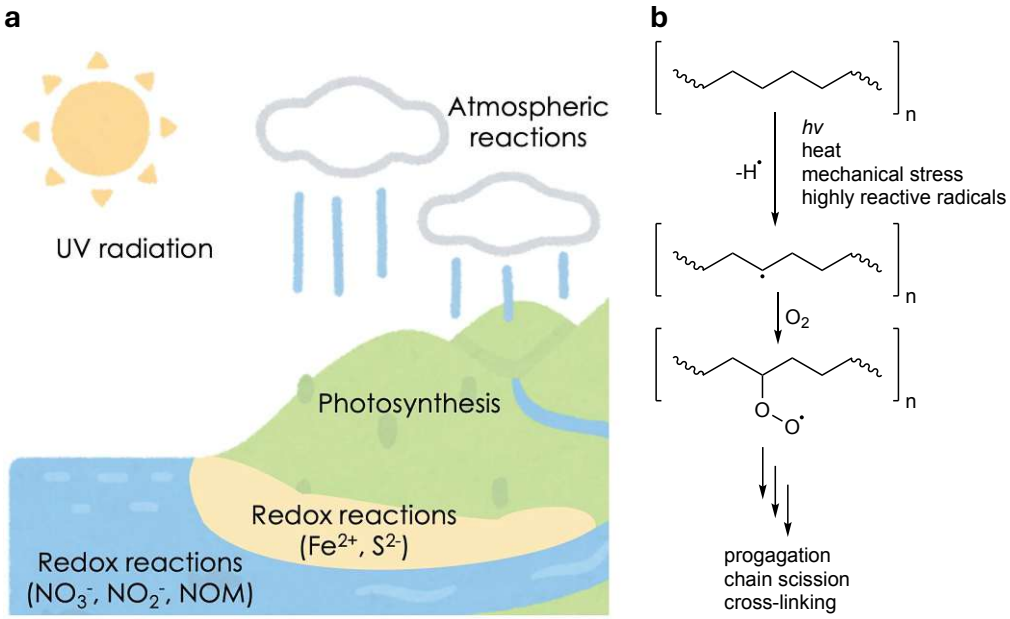

Figure 5| The first steps of PE degradation. a, Sources of ROS in the environment. **b**, Simplified generalized scheme of the first steps of the oxidative degradation of PE. These are hydrogen abstraction and peroxidation, followed by propagation, chain scission, and cross-linking reactions.[21,24,26-30]

This oxidative degradation of PE results in a variety of products including alkanes, alkenes, ketones, aldehydes, alcohols, carboxylic acids, keto-acids, dicarboxylic acids, lactones, and esters (Figure 6). Additives (e.g., photocatalysts, chapter 1.1.2.2) can be added to accelerate its auto-oxidation process, to improve the accessibility of oxidation products for the second degradation step - microbial degradation. Nevertheless, biodegradability remains very limited when exposed to microorganisms.[17]

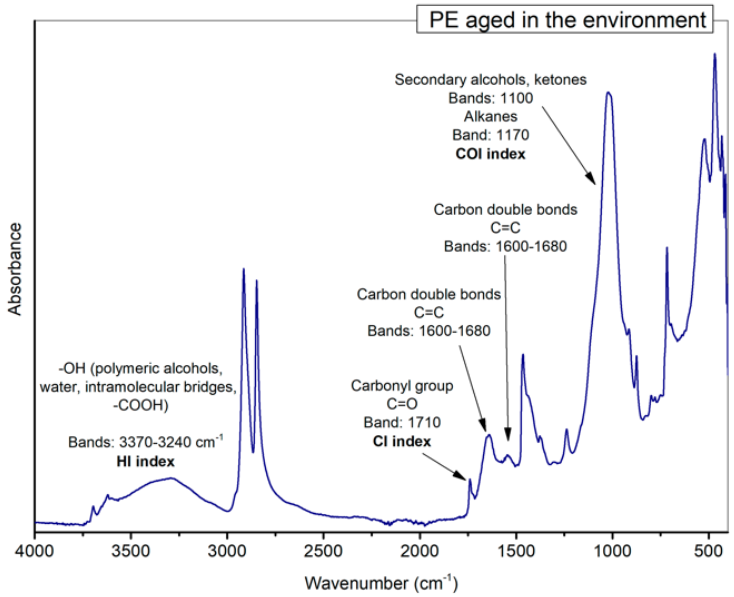

Figure 6| PE aging in the environment. An exemplary FTIR spectrum of naturally weathered polyethylene (PE) shows the formation of new functional groups because of the degradation process. The figure is adapted from Campanale et al.[31]

1.1.2 Degradation methodologies of polyolefins in microplastic

In recent years, various techniques have been developed to degrade polyolefins focusing on microplastic-degradation, including pyrolysis, gasification, hydroconversion, and different oxidative degradation technologies (Figure 7).

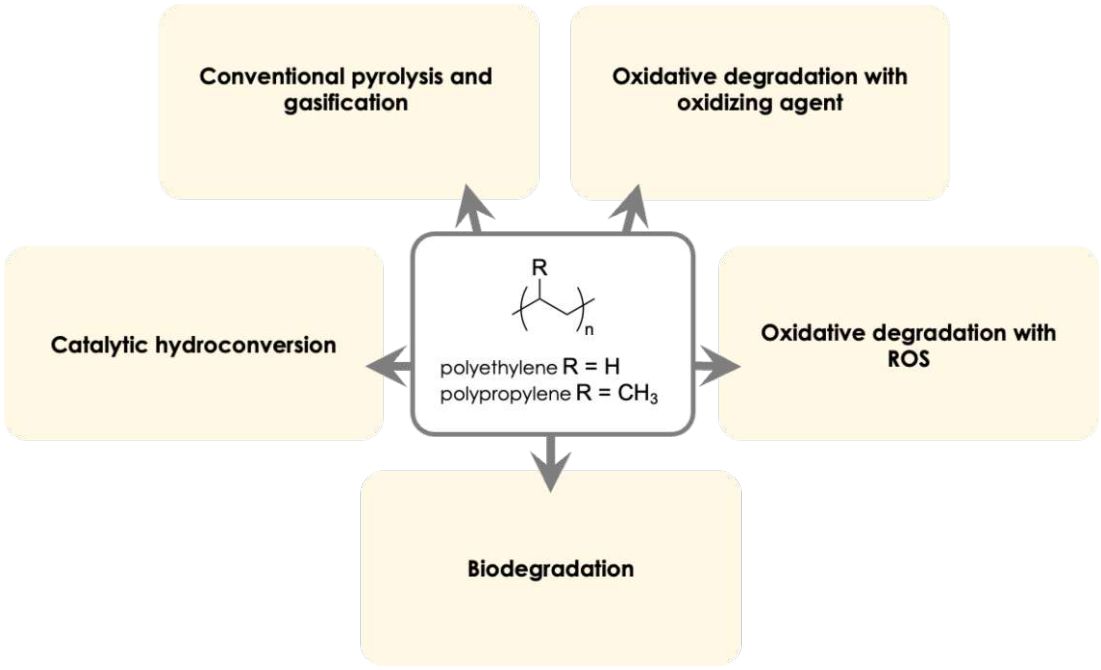

Figure 7| An overview of different methods for the breakdown of polyolefins. Pyrolysis and gasification, catalytic hydroconversion, oxidative degradation by oxidizing agents, and oxidative degradation methods with ROS.

1.1.2.1 Conventional and catalytic chemical methods

Conventional chemical degradation and recycling are very dependent on the type of plastic and usually require harsh reaction conditions and high costs.[32] Thermal degradation methods for polyolefins are pyrolysis and gasification. Pyrolysis, where the material is thermally decomposed in the absence of oxygen, requires a temperature of 300 – 700 °C. Liquid or gaseous products composed of smaller molecules are formed. These can further be used as feedstock for the production of fuels, chemicals, or new plastics. Gasification is the conversion to syngas using using air and/or steam as gasifying agents. Syngas primarily consists of H_2, CO, CH_4, and CO_2, and can be used for energy, hydrogen production, or as feedstock for various refining processes. It requires temperatures of 700 – 1200 °C (Figure 8, a). Polyolefins are chemically very inert and thus, conventional chemical recycling methods for polyolefins require very high temperatures, which makes them very inefficient.

The catalytic degradation of polyolefins has been subject to many experimental studies.[33] However, they usually require either harsh reaction conditions or aggressive chemicals. Moreover, most methods need a preceding collection and pre-treatment, which represents a difficulty, especially for smaller polymer residues and microplastic,

e.g., in wastewater. Catalytic hydroconversion (hydrocracking, hydrogenolysis) has gained significant attention as a promising method for upcycling these materials into fuels, lubricants, and waxes. It requires a temperature between 200 and 300 °C, usually making use of transition metal catalysts (e.g. Ru, Pt, Zr), also applied multi-step processes with alkene metathesis (Figure 8, b).[34,35] Hydroconversion has gained significant attention as a promising method for upcycling these materials into fuels, lubricants, and waxes. Also, methods for catalytic functionalization and oxidation have been explored, e.g. hydrothermal oxidation using nitric acid at 180 °C or diluted H_2O_2, which yields dicarboxylic acids (Figure 8, c).[36-38]

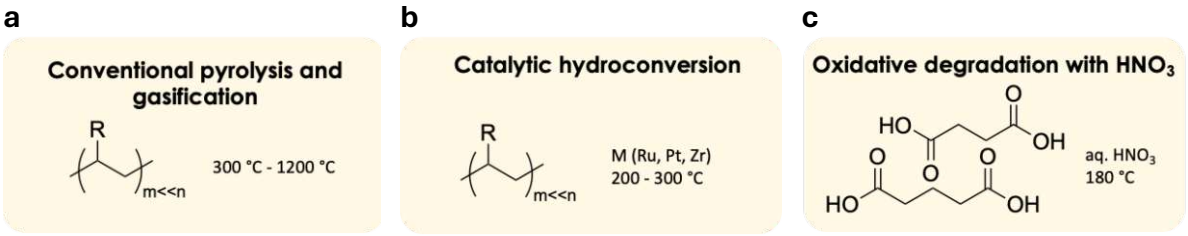

Figure 8| Conventional and catalytic chemical methods for the breakdown of polyolefins. **a**, Pyrolysis and gasification require very high temperatures from 300 °C to 1200 °C and yield short-chain alkanes which are used for fuel, waxes, or gas.[34] **b**, Catalytic hydroconversion requires moderately high temperatures from 200 °C to 300 °C, transition metal catalysts (e.g. Ru, Pt, Zr), and yields liquid alkanes or waxes.[34] **c**, Oxidative degradation by oxidizing agents requires moderately high temperatures & aggressive chemicals. An example is a hydrothermal procedure employing HNO_3 at 180 °C, which yields dicarboxylic acids as the main products.[36,38]

1.1.2.2 ROS-mediated polyolefin degradation

Conventional and catalytic chemical methods target solid-state polyolefins or microplastics. Wastewater treatment plants remove most microplastic, but, not entirely. There exist techniques for adsorption and filtration of microplastic, but further treatment after adsorption/filtration is required.[39] In the environment, ROS play a significant role during polymer degradation (chapter 1.1.1). This is especially important for the degradation of polyolefins. Therefore, another possibility for polyolefin degradation, especially for microplastic degradation in aqueous systems, is the targeted use of ROS.[18] Oxidative degradation methods using ROS follow a radical oxidation mechanism leading to oxy-functionalization of the polyolefin and final mineralization products CO_2 and H_2O (Figure 9). The products can serve as nutrients for microorganism utilization to fix carbon and minimize carbon emissions.[40]

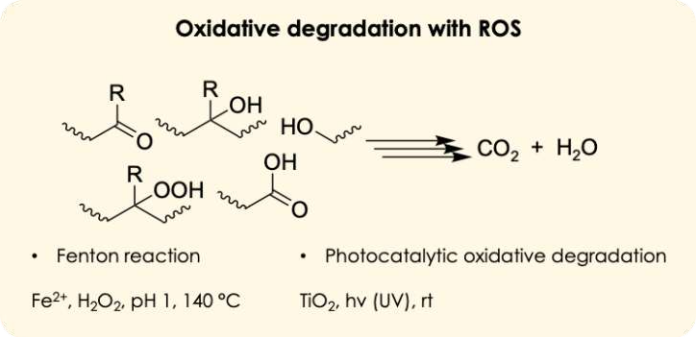

Figure 9| Oxidative degradation methods with ROS for the breakdown of polyolefins. Oxidative degradation methods with ROS follow a radical oxidation mechanism leading to oxy-functionalization of the polyolefin and final mineralization products CO_2 and H_2O.

One approach for polyolefin degradation by ROS is the use of Fenton's reagent (Fe^{2+}/H_2O_2) (Scheme 1) which can be used in an aqueous environment. It is widely used for wastewater treatment (degradation of organic pollutants) and advanced oxidation processes (AOPs). It produces HO•, which was shown to oxidatively degrade polyolefins in microplastic .[41] There is some research on the degradation of polyethylene by Fenton's reagent. A successful example is a hydrothermal Fenton reaction, where Fe^{2+} and H_2O_2 were used at pH 1 and 140 °C (Figure 10). Microplastic polymers in water were degraded, leading to significant chemical and structural changes.[42]

$$Fe^{2+} + H_2O_2 \longrightarrow Fe^{3+} + HO^{\bullet} + HO^{-}$$

Scheme 1| Fenton's reagent.

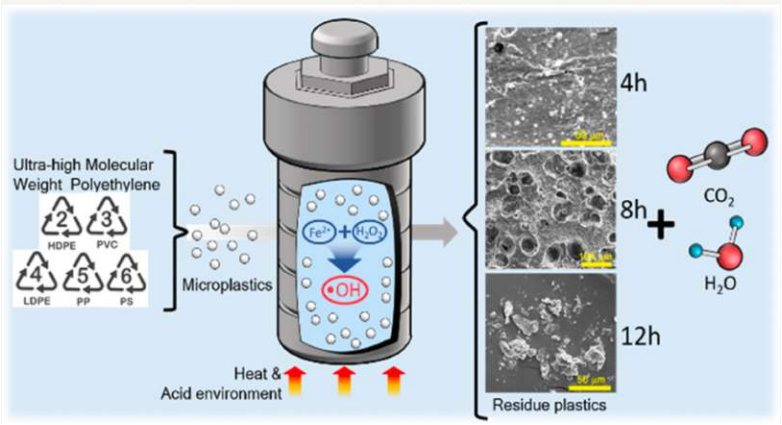

Figure 10| The hydrothermal Fenton reaction for the degradation of PE and other petroleum-based plastics. The figure is adapted from Hu et al.[42]

A different innovative strategy allowing for milder reaction conditions is the use of light as an energy source, as in its natural degradation process. Polyolefin aging by light and ROS (chapter 1.2) can be accelerated via photocatalysis (e.g. using the photocatalyst TiO_2, ZnO, NbO_5). It is a promising method for microplastic waste degradation from the environment.[3,4,43,44] These photocatalysts accelerate the formation of the powerful oxidant HO•. It absorbs light, generating charge carriers (electrons e^- and holes h^+). The h^+ reacts with H_2O to form HO• and H^+, while the e^- reacts with ground-state oxygen (O_2) to produce superoxide ($O_2^{\bullet -}$). These radicals lead to the formation of H_2O_2, which further decomposes into more HO• (Figure 11).[45,46]

The photocatalytic degradation of PE follows three key stages: Initiation, propagation, and termination. During initiation, HO• attacks the polymer chains, forming polymer radicals (P•). During propagation, P• reacts with O_2 to form peroxyl radicals (POO•), leading to chain scission and the formation of oxygen-containing groups, like carbonyls. The reactions continue as radicals like POO• and alkoxy radicals (PO•) further break down the polymer chains. During termination, the free radicals react with each other, forming stable products like alkenes, aldehydes, ketones, and carboxylic acids. This mechanism highlights how photocatalysis can break down PE into functionalized/biodegradable degradation products (Figure 12).[47,48]

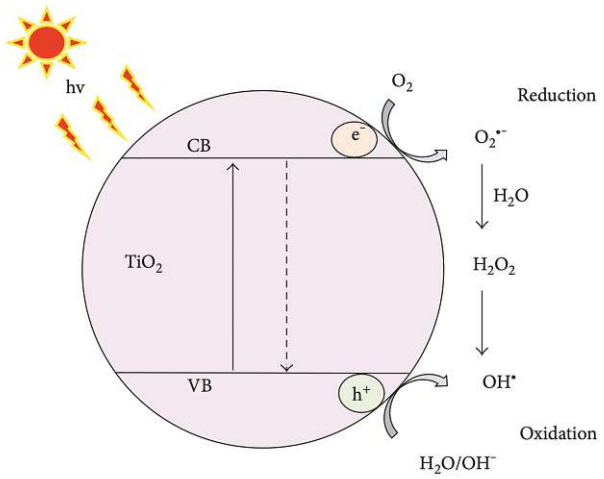

Figure 11| The mechanism of the photocatalyst TiO_2. The catalyst requires UV light. The figure is adapted from Gutierrez-Mata et al.[45]

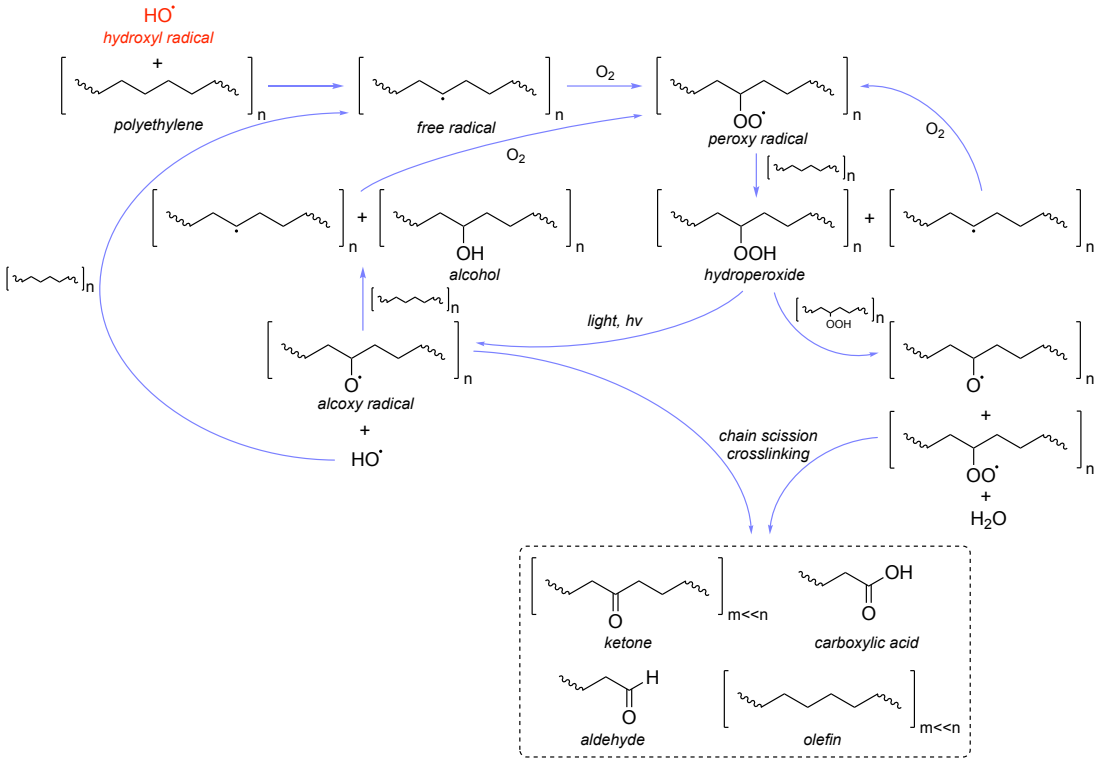

Figure 12| Pathway of PE degradation by photocatalysis. The initiation step by HO•, further propagation, and termination steps are depicted.[47]

An example was the degradation of HDPE microplastics using C,N-TiO_2 powders.[49] In this work, Vital-Grappin et al. proposed to use this photocatalytic process for the implementation in wastewater treatment plants for the elimination of microplastic pollution. In a different study, Nabi et al. presented the complete photocatalytic mineralization of microplastic on a TiO_2 nanoparticle film.[50] They explored how different TiO_2 preparation methods affect photocatalytic performance. TiO_2-based films could be applied to microplastic filters for effective decomposition under UV light. A different study examined the degradation of fragmented LDPE microplastic residues using visible light-induced heterogeneous photocatalysis, activated by ZnO nanorods.[51]

1.1.2.3 Biodegradation of polyolefins

Opposed to chemical methodologies for polyolefin degradation and recycling, a vast amount of research has focused on improving the biodegradation of petroleum-based plastics. Recently, the use of polymer-degrading biocatalysts by (micro)organisms like bacteria, fungi, biofilms, microalgae, but also insect larvae, has been subject to many studies. (Micro)organisms with the ability to break down plastics through enzymatic actions are being studied more and more in recent years.[52-54] Research focuses on the determination of the enzymes responsible for the degradation of the polymers.[55] Successful examples of the degradation of plastic types like PET through enzymatic hydrolysis (hydrolases) have been studied and improved extensively.[56-58] In this regard, the biotech company CARBIOS has developed pioneering technologies for the bio recycling of PET.[59,60] On the other hand, very few enzymes are known to catalyze the oxidation of inert C-H or C-C bonds present in polyolefins. Therefore, the first step of polyolefin-degradation, the oxidation, presumably still relies on a non-enzymatic mechanism.[61] The proposed degradation mechanism involves four stages: abiotic treatment (e.g., UV, heat, or chemical oxidation, chapter 1.1.1), biofragmentation (degradation by extracellular enzymes into shorter segments), assimilation of small fragments by microorganisms and subsequent mineralization into CO_2 (Figure 13).[61]

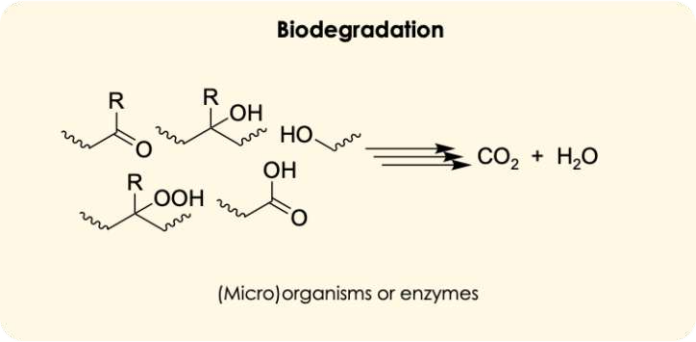

Figure 13| Biodegradation for the breakdown of polyolefins. Biodegradation requires a preceding non-enzymatic oxidation step, followed by biofragmentation and subsequent mineralization to CO_2 and H_2O by the (micro)organisms/enzymes.

Several studies have used various (micro)organisms and shown the degradation of polyolefins to some extent.[52,62] Natural strains, natural microbial consortia, as well as enzymes and artificial microbial consortia have been reported. More than 100 species have been found with the ability to degrade PE to some extent. Fungi are generally considered more efficient in degrading PE than bacteria, due to their ability to attach to

hydrophobic surfaces and secrete extracellular enzymes.[61] Recently, the role of ROS in polystyrene (PS) degradation in the gut of superworms (*Zophobas atratus* larvae) has been reported (Figure 14).[63] In this work, Chen et al proposed that degradation of PS was achieved by the synergistic effect of ROS (with a focus on HO•) and complex functional microbes and enzymes (like extracellular oxidases) in the gut of larvae. Following this, the role of ROS like hydroxyl radical in the first step of polyolefin degradation becomes increasingly evident.[18]

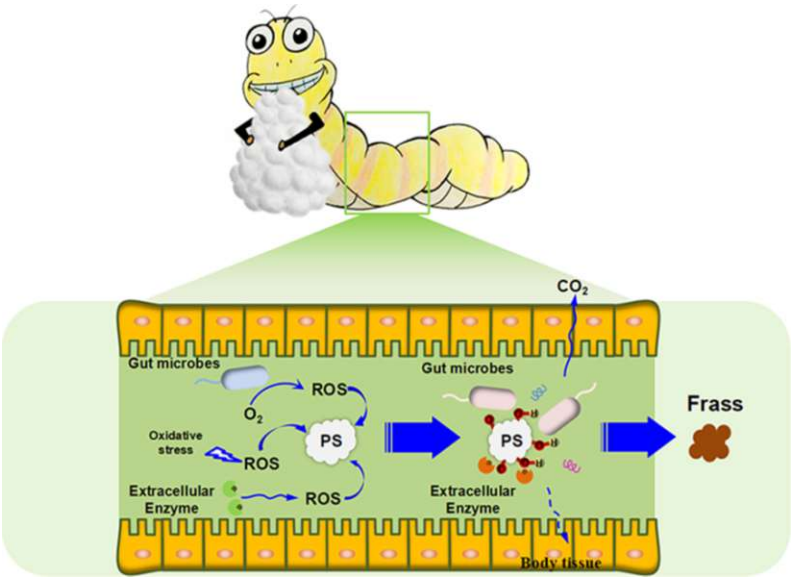

Figure 14| The ROS-mediated degradation of PS in superworms (*Zophobas atratus* larvae). The figure is adapted from Chen et al.[63]

Similar to the challenges in chemically depolymerizing polyolefins, using enzymes to efficiently break down C-C bonded polymers will require significant advancements to produce useful industrial products. In most studies for biodegradation of polyolefins, data are inconclusive, and no specific enzyme could be linked to polyolefin degradation, full enzymatic pathways are still unclear. There is a lack of standardized methods to evaluate the degradation efficiency of (micro)organisms or enzymes. Moreover, results should be taken with caution due to the ambiguity of most analysis methods (chapter 1.5.2).

1.2 Background to reactive oxygen species (ROS)

As already established, ROS play a crucial role during the aging of polyolefin microplastic in the environment, as well as its targeted degradation (chapters 1.1.1 and 1.1.2.2). Here, the classification of ROS, and the mechanism of production and detection are summarized.

ROS are highly reactive molecules that contain oxygen atoms. While oxygen in its ground state (triplet oxygen) is a stable molecule, in its different excited states it becomes very reactive.[46,64,65] ROS include oxygen radicals as well as non-radical oxygen species. The main ROS are singlet oxygen $^1O_2$, the radical anion superoxide $O_2^{\bullet-}$, hydrogen peroxide H_2O_2, and hydroxyl radical $HO^\bullet$ (Figure 15).

$^1O_2$ has a very unstable electron configuration, where all electrons are spin-paired. It cannot directly convert to other ROS. Meanwhile, one electron reduction of oxygen leads to the formation of $O_2^{\bullet-}$ which can be the precursor for other ROS. E.g., dismutation of $O_2^{\bullet-}$ leads to H_2O_2, which is the most stable among the four mentioned ROS (chapter 1.2.2). The last ROS, $HO^\bullet$ is thought to be the most reactive ROS towards the reaction with covalent bonds. Therefore, it possibly is the most important ROS regarding the oxidative degradation of polyolefins.[66,67]

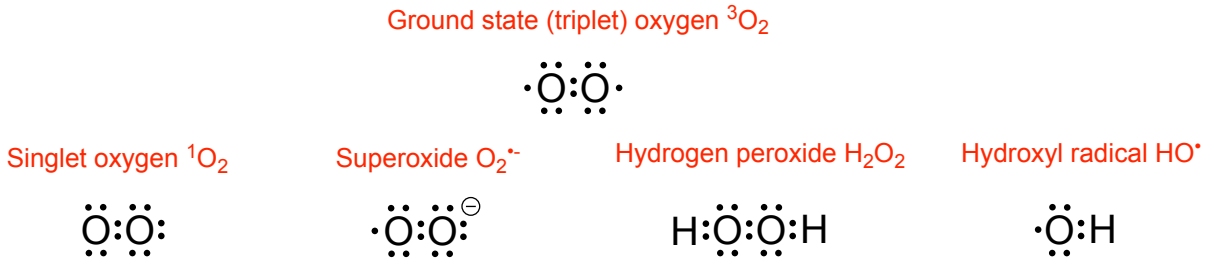

Figure 15| Reactive oxygen species (ROS). The chemical formula and structure of ground state oxygen and the four main ROS is depicted.

In biology, ROS play a dual role. They serve as signaling molecules which gives them an important role in cell regulatory mechanisms. On the other hand, they are also a potential source of cellular damage through oxidative stress, which can result in pathological processes, like Alzheimer's disease, cancer etc. However, this can be exploited in biomedical applications e.g., in cancer therapy.[67-69] In environmental chemistry, ROS play a role in air quality, but also in the degradation of pollutants. An example is the use of ROS in water treatment e.g., by the (photo)-Fenton processes.[70,71] In material science, ROS can be used for surface modifications (e.g., plasma treatment of polymers).[72,73]

1.2.1 ROS production by a photosensitizer

In chapter 1.1.2.2, the use of photocatalysis for polyolefin-degradation was presented. Photosensitization and photocatalysis are closely related processes, and the terms are often used interchangeably depending on the scientific community.[74] Whereas the term

photocatalysis is mostly used in environmental science or materials science, photosensitization is mostly used in biomedicine and photodynamic therapy. The proteins used during this research project are referred to as photosensitizers.

A photosensitizer (PS) is a molecule that is excited by the absorption of light and then transfers the energy to nearby molecules (such as O_2), initiating a photochemical creation of ROS (Figure 16). First, the PS is excited by the absorption of light at a specific wavelength. The excited singlet state (PS_1^*) is converted via intersystem crossing (ISC) to a more stable excited triplet state (PS_3^*). Following the type I mechanism, PS_3^* is reduced by a neighboring auxiliary e^- donor (X) to $PS^{\bullet-}$ which can transfer the e^- to O_2 to generate the radical species $O_2^{\bullet-}$. A cascade of follow-up reactions results in the formation of other ROS like H_2O_2 or $HO^\bullet$.[75] Following the type II mechanism, the PS_3^* is transformed to the ground state (PS_0) via direct energy transfer to O_2 yielding excited singlet state $^1O_2$. However, the relaxation of the PS to its electrical ground state by fluorescence competes with the production of ROS.[76,77] For the formation of ROS, the PS in its excited state must collide with molecular oxygen.[66] For the generation of ROS by a photosensitizer only O_2 and a light source are needed.

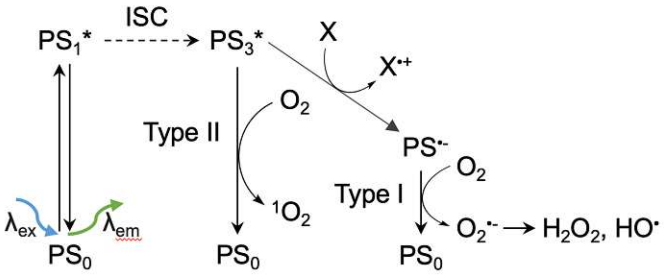

Figure 16| Generation of ROS by a PS. A PS is excited by the absorption of light at a specific wavelength. The excited singlet state (PS_1^*) is converted via intersystem crossing (ISC) to a more stable excited triplet state (PS_3^*). Following the type II mechanism, the PS_3^* is transformed to the ground state (PS_0) via direct energy transfer to O_2 yielding excited singlet oxygen $^1O_2$. Following the type I mechanism, PS_3^* is reduced by an e^- donor (X) to $PS^{\bullet-}$ which can transfer the e^- to O_2 to generate superoxide $O_2^{\bullet-}$. $O_2^{\bullet-}$ can lead to the production of H_2O_2 and $HO^\bullet$.[75,76]

1.2.2 Limitations and detection of ROS

ROS are very reactive molecules due to their radical or excited state. However, this is also the reason for their very short lifetime, setting limits to the distance of diffusion in an aqueous solution (Table 1).[67]

Table 1: Approximate half-lives of ROS[78,79]

Molecule		Half-life
Singlet oxygen	$^1O_2$	10^{-6} s
Superoxide	$O_2^{\bullet-}$	10^{-6} s
Hydrogen peroxide	H_2O_2	stable
Hydroxyl radical	$HO^\bullet$	10^{-10} s

The short lifetime of ROS makes it very challenging to find reliable methods for their detection and quantification. Several methods for the detection of ROS exist.[46] Some ROS e.g., $^1O_2$ can be measured directly via phosphorescence. However, ROS are usually detected indirectly via an assay. Thereby, a ROS-specific probe reacts with the specific species forming a more stable analyte that can be measured spectrophotometrically.[69] Systems where the fluorescence of the assay product is measured proved to be the most efficient ones.[80] However, for the different ROS, different specific detection methods and assays exist.

Singlet oxygen $^1O_2$ can revert to its stable triplet form without engaging in chemical reactions or electron transfer. However, in solution, energy transfer to surrounding molecules can happen. Detection methods for $^1O_2$ include direct emission of phosphorescence, electron magnetic resonance (ESR), or fluorescence probes. $^1O_2$ emits phosphorescence in the near-IR region at 1270 nm (Figure 17).[81] In ESR spectroscopy, the absorption of microwave energy by unpaired electrons in a magnetic field is observed and measured.[82]

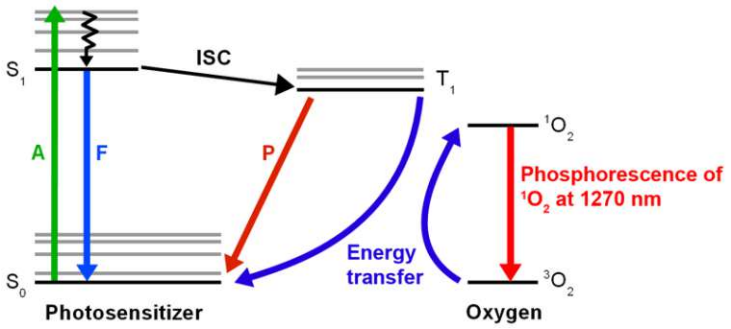

Figure 17| Jablonski diagram showing the energy transfer from a PS to $^3O_2$ and subsequent phosphorescence of $^1O_2$ to $^3O_2$. The figure is adapted from www.picoquant.com.[83]

Regarding the superoxide anion $O_2^{\bullet-}$, most detection methods are indirect. These methods rely on different principles: $O_2^{\bullet-}$'s redox properties, binding, trapping, or the formation of stable, detectable products.[84,85] Electrochemical as well as spectrophotometric detection techniques exist. Among the latter, absorbance or fluorescence (chromogenic or fluorogenic probes) can be measured, or vibrational spectroscopy techniques (e.g., ESR, etc.) can be employed (Figure 18). Detecting $O_2^{\bullet-}$ in cells is challenging due to the limited sensitivity of current techniques.[86]

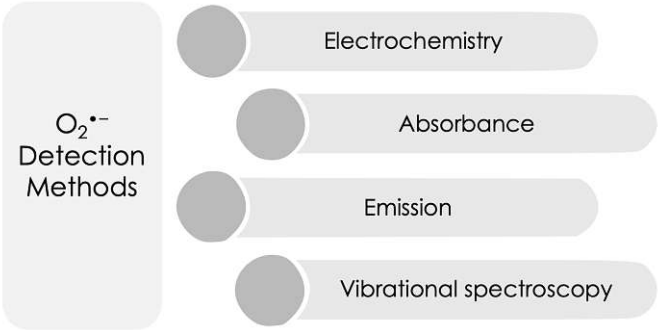

Figure 18| $O_2^{\bullet-}$ detection methods. Various detection methods exist, like electrochemical and spectrophotometric techniques such as measurement of absorbance, emission, and vibrational spectroscopy techniques.

Among ROS, hydrogen peroxide H_2O_2 is the only stable molecule, allowing it to be detected separately after the decay of other ROS. For the quantification of H_2O_2, various detection methods have been developed, either by direct absorption in UV or by the use of indirect detection of chromogenic or fluorescent probes.[46,87] A large variety of substances that can be oxidized by horseradish peroxidase (HRP) and H_2O_2 are commercially available. They change their color or become fluorescent when oxidized, which enables simple and efficient H_2O_2 detection (Figure 19).[88] $O_2^{\bullet-}$ can be converted to H_2O_2 by superoxide dismutase (SOD) and therefore $O_2^{\bullet-}$ can be also detected using the same assay.

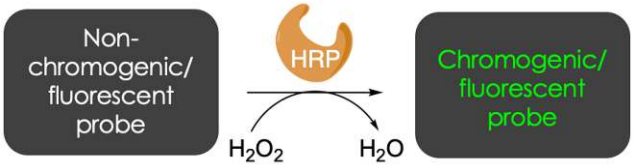

Figure 19| Schematic representation of H_2O_2 detection via a chromogenic or fluorescent probe. A non-chromogenic/fluorescent probe is converted by horseradish peroxidase (HRP) and the substrate H_2O_2 to a chromogenic/fluorescent probe, which can be detected and quantified.

Lastly, the short-lived hydroxyl radical HO$^{\bullet}$ which is considered the most reactive among ROS, several methods are used. One possibility is the use of DMPO (5,5-dimethyl-1-pyrroline N- oxide) as a spin-trapping reagent. Unstable HO$^{\bullet}$ reacts with DMPO to convert to stable DMPO–OH radical which could be detected by ESR spectroscopy (Figure 20).[46] Moreover, many fluorescent or chemiluminescent probes exist.[89]

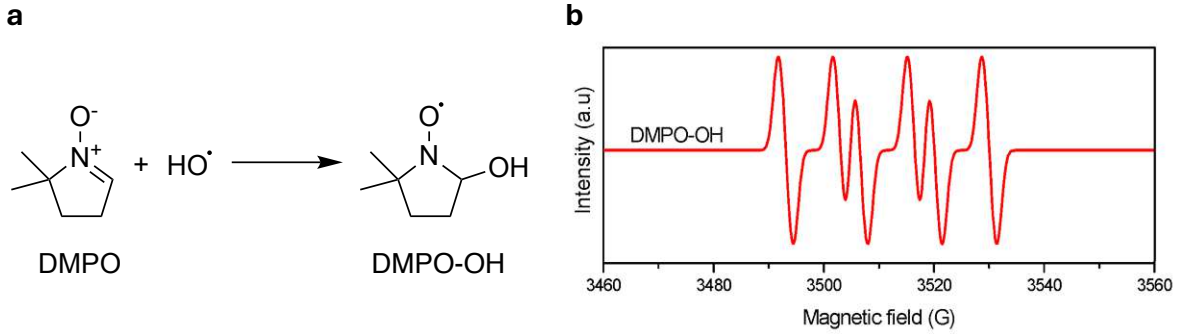

Figure 20| Detection of HO$^{\bullet}$ by indirect ESR spectroscopy. a, Scheme of the reaction of DMPO with HO$^{\bullet}$. **b**, An ESR spectrum of DMPO-OH. The figure is adapted from Li et al.[90]

Absolute quantification of ROS is not always possible, because the assay calibration is very difficult for very reactive and short-lived ROS. For H_2O_2, calibration is possible, however, in the micro-and nanomolar range, it is very error-prone. Therefore, the use of relative quantification is preferred allowing comparative conclusions.

During this research project, for the detection of ROS, three different fluorometric assays proved the be suitable: The Amplex Red assay for the detection of H_2O_2 and $O_2^{\bullet-}$, the Singlet Oxygen Sensor Green (SOSG) assay for the detection of $^1O_2$ and the Aminophenyl Fluorescein (APF) assay for the detection of HO$^{\bullet}$. The respective principles and implementation of the assays are explained in chapter 3.3.2.

1.3 Genetically encoded photosensitizer proteins

Non-genetic photosensitizers are small-molecule-based photosensitizers, usually based on tetrapyrrole derivatives, heavy-atom-containing fluorescent dyes, and transition metal complexes.[91] Genetically encoded photosensitizers or in this thesis referred to as photosensitizer proteins (PSPs) are proteins that are photosensitizers. They harbor a photosensitizer (PS) chromophore molecule, which absorbs light of a specific wavelength. PSPs photochemically produce ROS when illuminated (Figure 21).[67,76,77,92]

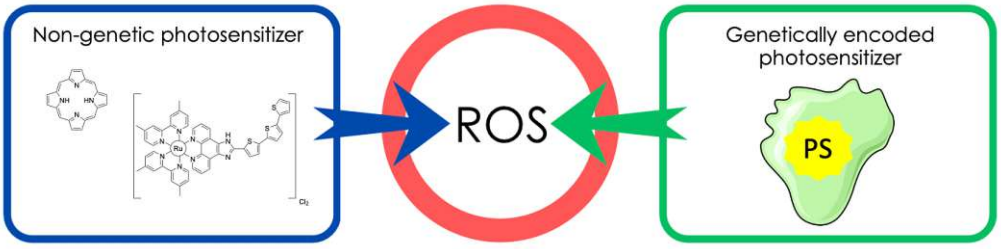

Figure 21| Non-genetic photosensitizers and genetically encoded photosensitizers. Non-genetic photosensitizers can be e.g., tetrapyrrole derivatives or transition metal complexes, like the ruthenium-based photosensitizer TLD1433. Genetically encoded photosensitizers are proteins harboring a photosensitizer (PS) chromophore molecule.

Two main classes of PSPs exist: fluorescent proteins similar to green fluorescent protein (GFP), and flavin-binding fluorescent proteins from the light-oxygen-voltage (LOV) photoreceptor domain proteins. Key examples include the GFP-like protein KillerRed and the LOV protein miniSOG.[93] Even though there are two main mechanisms of ROS production by a PS, in some cases it is still not precisely known how ROS are produced by different PSPs. Most PSPs undergo both mechanisms of ROS production (type I and type II, chapter 1.2.1). In protein-encased photosensitizers, the surrounding amino acids can act as electron donors for the type II mechanism.[75] Because $HO^{\bullet}$ is believed to be the most reactive ROS towards the degradation of polyolefins, it should be focused on during the selection of the best ROS-generating PSP. However, the literature focuses mainly on the production of $^1O_2$, $O_2^{\bullet-}$ and H_2O_2.

1.3.1 Homologs of Green Fluorescent Protein (GFP)

Green fluorescent protein GFP from a jellyfish from the hydrozoan order Leptomedusae is a well-studied fluorescence protein. Therefore, it is an essential labeling tool in various applications in molecular biology.[94] The ideal fluorescent protein chromophore should efficiently absorb light and have a high fluorescence quantum yield with little intersystem crossing. However, fluorescence proteins like GFP can also have a high rate of intersystem crossing to form the excited triplet state and subsequently generate ROS (chapter 1.2.1).[67] Therefore, GFP has been reported to generate low amounts of ROS during illumination, primarily $^1O_2$.[76,95]

The GFP-like protein KillerRed was the first fluorescent protein that was designed to be an efficient photosensitizer and therefore phototoxic (applications of these properties are described in chapter 1.3.3). It was developed from the anm2CP, a homolog protein of GFP from the jellyfish of the hydrazoan order *Anthomedusae*.[92] It is a dimeric red fluorescent protein, which gets excited by green light. Its structure is similar to GFP, consisting of an 11-stranded β-barrel with loop caps at both sides and a chromophore in the middle of an internal α-helix.[96] The encapsulated chromophore consists of the three amino acids QYG (Figure 22, a and b). The most important feature responsible for its phototoxicity is hypothesized to be a water-filled channel leading to the chromophore.[97]

New PSP variants with improved or changed photosensitizing properties were developed from KillerRed. SuperNova is a monomeric version derived from KillerRed, which exhibits improved photostability and is less prone to aggregation.[98] The monomeric character can be of advantage for proper function if used in a fusion protein, which has been shown by fusion to different cellular proteins.[99] Spectroscopic characteristics as well as ROS generation are reported to be similar to KillerRed.[98]

KillerOrange is a variant of KillerRed with shifted spectroscopic characteristics (different excitation wavelengths), obtained by random mutagenesis.[100] The chromophore with a tryptophan core changes the protein's color to orange (Figure 22, c and d). [101] This allows the simultaneous use of the two proteins in a single system. Meanwhile, it maintains a similar ROS-generating ability as KillerRed.[100]

Whether photosensitization by KillerRed and other GFP-like proteins occurs via the type I or II ROS-generating pathway has been debated. However, most literature suggests that the dominant path of ROS generation by KillerRed and other GFP-like proteins is reported to be type I, therefore primarily producing $O_2^{\bullet-}$ and H_2O_2.[92,93] Moreover, it is important to note that GFP and all GFP-like proteins rely on oxygen to activate fluorescence.[102]

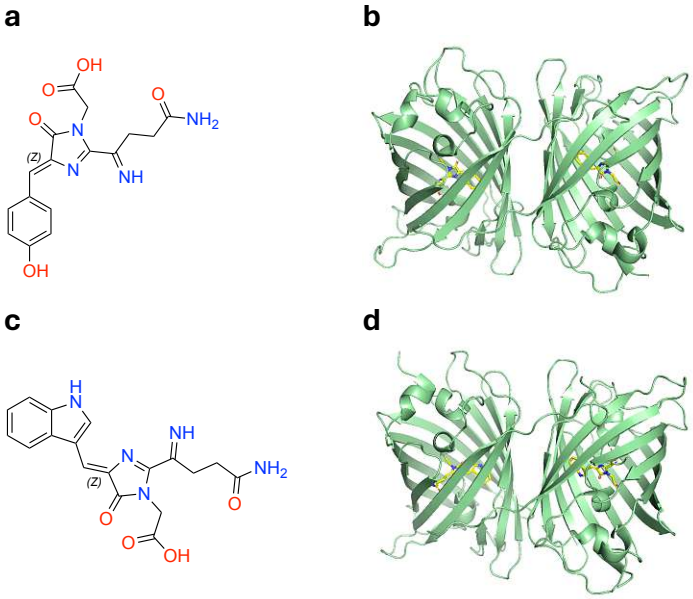

Figure 22| Chromphore and protein structures of GFP-like PSPs. a, Chromophore QYG (KillerRed, SuperNova). **b**, Structure of KillerRed.[103] **c**, Chromophore QWG (KillerOrange). d, Structure of KillerOrange.[104]

1.3.2 Flavin-binding Light-Oxygen-Voltage sensing domain (LOV) proteins

The second type of genetically encoded photosensitizers are light-oxygen-voltage sensing domain (LOV) proteins.[77] These LOV domains are small photosensors present in various organisms (plants, fungi, bacteria, etc.), which have been initially identified in phototropins. Their primary function is to sense environmental conditions like blue light, regulating processes such as gene expression, phototropism, and circadian rhythms.[105,106] LOV proteins are smaller in size compared to other GFP-like photosensitizer proteins. They bind to the cofactor flavin mononucleotide (FMN) which acts as a chromophore and therefore is responsible for their fluorescence and photosensitizing properties (Figure 23, a). The FMN cofactor is produced endogenously within the cells.[107] Upon excitation, FMN is linked to cysteine which activates a kinase and further induces a signal by phosphorylation, altering the protein's activity e.g., for phototropism. Like GFP-like fluorescence proteins, LOV proteins can be used as fluorescence tags or for the engineering of photoswitchable proteins.[107,108] LOV-based PSPs show their fluorescence also under anaerobic conditions. This makes them suitable reporter proteins for *in vivo* analysis of oxygen-limited cellular systems. They are valuable reporters for various biotechnological approaches.[107,109] However, blue-light excitation can also lead to the production of ROS.

One of the first engineered LOV proteins is MiniSOG (Mini Singlet Oxygen Generator), which was created through the mutagenesis of the LOV2 domain of the *Arabidopsis thaliana* PHOT2 gene.[110,111] Its structure is depicted in Figure 23, b. Many variants of MiniSOG have been developed due to inefficient molecular oxygen diffusion through the protein. MiniSOGQ103V is a mutant of MiniSOG with improved ROS-generating efficiency.[112,113] For MiniSOG, the primary pathway for ROS production is not clear, or rather different statements were made, and the oxidant species remains unclear in many of these applications. Nevertheless, it is evident that it produces ROS via both, type I yielding $O_2^{\bullet-}$ and H_2O_2, and type II yielding $^1O_2$.[114]

SOPP (Singlet Oxygen Photosensitizing Protein) and its enhanced version SOPP3 are variants of MiniSOG. Several studies suggest that both are very potent producers of ROS, with a primary focus on singlet oxygen.[115] SOPP3 has the highest $^1O_2$ yield through type-II photochemistry among LOV-based PSPs.[115] In these variants the electron donation of amino acid residues near the active center and the hydrogen bonding to the cofactor FMN were decreased. However, the FMN cofactor enclosed within the protein structure of SOPP3 easily undergoes bleaching upon irradiation in contrast to MiniSOG.[115,116]

DsFbFpM49I (Flavin-Binding Fluorescent Protein) is a novel PSP of the LOV family derived from *Dinoroseobacter shibae*. It is a variant of the wildtype protein DsFbFp, generated by the insertion of one mutation.[117] There is only limited research on DsFbFpM49I, however, high ROS production was reported.[77,109]

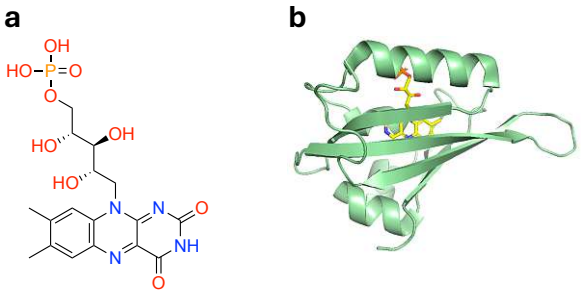

Figure 23| Chromphore and protein structure of a LOV protein. a, The chromophore of all LOV proteins - flavin mononucleotide (FMN). **b**, Structure of LOV protein miniSOG.[118]

1.3.3 Applications of ROS-producing PSPs

Apart from their use as fluorescent reporters, applications of GFP-related but also LOV-based PSPs have been reported where their ability to produce ROS is exploited. Some examples are targeted inactivation of genes/proteins via chromophore-assisted light inactivation (CALI), photodynamic therapy (PDT) e.g., for cancer cell destruction, ROS-mediated signaling or correlative light-electron microscopy (CLEM) (Figure 24).[67,99]

In CALI, ROS are used to selectively deactivate a target protein. In this regard, the fusion of PSPs to the target protein keeps the diffusion distance of the ROS short.[119] Upon illumination, the generated ROS affect residues in the target protein, altering its function. Therefore, CALI is a useful tool for studying the loss or gain of function of a protein. Light exposure and intensity have to be tightly controlled to avoid unintentional damage.[67,120]

Another important application is cancer therapy in the context of photodynamic therapy (PDT), which uses ROS generated to kill cancer cells. PDT has become a widely used approach for cancer treatment over the past 40 years, using different light-activated PSs. In this regard, genetically encoded PSPs have also been investigated. Challenges can arise because of limited light penetration, PS and oxygen dependence, or PS localization.[121] On the other hand, not only cells can be the target for selective inactivation but also bacteria in antimicrobial photodynamic inactivation, for microbiological and biomedical applications. This technique could be used for the localized treatment of microbial infections. In a study by Endres et al. ROS generation and antimicrobial effects of different PSPs were analyzed.[77]

Another important application is ROS-mediated cellular signaling studies. Signaling by ROS is crucial for cellular homeostasis, however, challenging to study due to the localized production of short-lived ROS. In this context, PSPs provide new tools to induce controlled and localized ROS production. This could lead to a better understanding of the effect of different ROS on cellular functions like metabolism, transcription, or apoptosis. An example was the use of targeted variants of KillerRed to analyze the interplay between peroxisomes and cellular oxidative stress by Wang et al.[122]

Correlative light and electron microscopy (CLEM) is a valuable technique for analyzing cell and tissue structures at high resolution. It combines the unique strengths of both

light and electron microscopy to enhance understanding of protein expression, trafficking, and function. The PSP MiniSOG has been applied as an effective tool for CLEM.[110] The production of $^1O_2$ by MiniSOG catalyzes the polymerization of the reagent 3,3'-diaminobenzidine (DAB) which can be stained and imaged with a high resolution (< 10 nm). Thereby, proteins can be visualized which is not possible by other means (e.g., electron microscopy).[99] Different flavoproteins have been evaluated as photosensitizers for CLEM.[112]

An interesting new concept is the use of ROS-producing PSPs in biocatalysis. Following the principle of CALI, PSPs have been used by et al Gerlach et al. for selective, light-dependent control of enzymes in multi-step biocatalysis. The selective inactivation of enzymes after specific biotransformations could reduce cross-reactivity.[123] In a different study, Püllmann et al. linked PSPs with unspecific peroxygenases (UPOs) which utilize H_2O_2, produced by the PSP upon illumination, as a cosubstrate for oxy-functionalization reactions.[124]

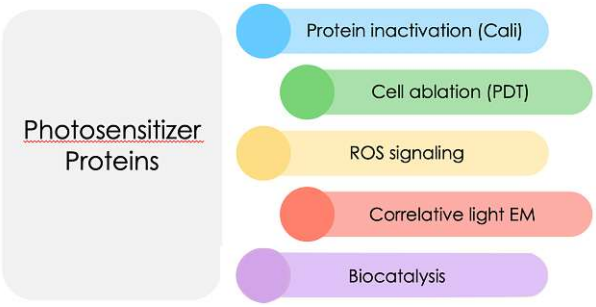

Figure 24| Applications of photosensitizer proteins (PSPs). PSPs can be used for protein inactivation in chromophore-assisted light inactivation (Cali), cell ablation through photodynamic therapy (PDT), ROS signaling studies, correlative light and electron microscopy (CLEM), or biocatalysis.

Opposed to all presented applications, the use of ROS produced by PSPs for the degradation of polymers, in particular polyolefins, has not been the topic of any research and will be presented in this thesis as a new concept. As previously established, ROS have a very short half-life (chapter 1.2.2). A protein needs an aqueous system to be active, while polymers such as polyolefins are highly hydrophobic and water-insoluble. Thus, for the ROS to be able to attack a polymer, it is necessary to bring the ROS-producing protein very close to the hydrophobic surface. However, the difference in hydrophilicity prevents the adsorption of high amounts of protein to the polymer surface. Methods to improve protein-polymer interaction have been explored over the last few years. One option is the fusion of the PSP to proteins with hydrophobic character, e.g., hydrophobins.

1.4 Hydrophobins - the surface-active proteins

Hydrophobins are small (10-15 kDa) fungal proteins that assemble on lipophilic surfaces or self-assemble in aqueous media and form micellar systems. Fusion of a protein to a hydrophobin represents one option to enhance substrate binding to a hydrophobic surface.[125,126]

Originally, hydrophobins are involved in mediating contact and communication between the fungus and its environment. They lower the water surface tension, allowing hyphae to breach the medium-air interface. Various other functions are known, e.g., in fungal growth and development.[127] Hydrophobins have a patch consisting of hydrophobic side chains on the protein surface. This feature is the reason for their amphiphilic behavior.[128] They share a core structural feature which contains eight cysteine residues forming intramolecular disulfide bridges and thereby stabilizing the amphiphilic structure.[125] As they self-assemble spontaneously on different interfaces, they can change the properties of this surface either from hydrophilic to hydrophobic or also the other way around. Hydrophobins are grouped into two classes. Class I hydrophobins form highly insoluble, rod-shaped nanostructures (rodlets) with an amyloid-like structure that can only be broken down by strong acids like formic acid. Class II hydrophobins create molecular films that can be disrupted by alcohol-detergent mixtures and do not exhibit rodlet morphology. The spacing between cysteine residues in the protein is highly conserved. However, classification seems to be more complex according to more recent literature.[129] Due to their amphipathic nature and their self-aggregation, expression as well as purification of hydrophobins can be challenging.[130]

Hydrophobins have been explored in various applications (Figure 25). They have been used for protein purification, the development of water-repellent coatings, or to enhance the stability of emulsions. Moreover, they have been used in the development of biofilms (protein or cell immobilization), biosensors, or drug delivery systems (drug solubilization) for medical applications.[125] Moreover, there have been examples where hydrophobins were fused to other enzymes to improve the biodegradation of polymers. In one example, two class I hydrophobins (RolA and HGF1) improved the activity of PETase to hydrolyze both semi-crystalline PET fiber and high-crystalline PET bottles. It highlights the role of self-assembled class I hydrophobins in boosting PET fiber hydrolysis for recycling purposes.[131] In a different example, the fungus *Aspergillus oryzae* is grown in a medium containing the biodegradable polyester polybutylene succinate-coadipate (PBSA). The fungus showed increased production of the hydrophobin RolA. Additionally, it produced CutL1, a cutinase enzyme that degrades PBSA. Pre-incubation of PBSA with RolA enhanced its degradation by CutL1.[132] Finally, PET hydrolysis efficiency has also been improved by the fusion of hydrophobins to a PET hydrolase. Hereby, it was explored whether the fusion of a bacterial cutinase to hydrophobins would further improve PET degradation. It significantly enhanced PET hydrolysis compared to the free enzyme. This was likely due to the binding of hydrophobin to the PET surface and changes in the enzyme's active site conformation.[133,134]

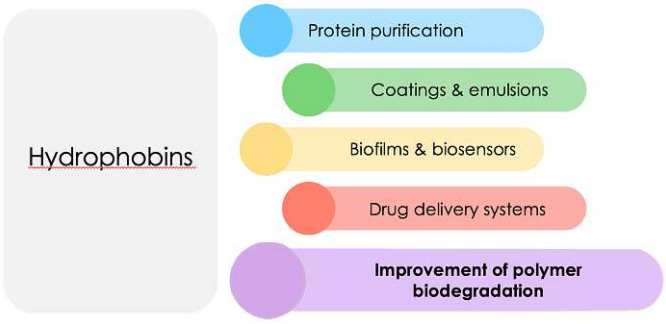

Figure 25| Applications of hydrophobins. Hydrophobins are used in protein purification, water-repellent coatings, emulsions, biofilms, biosensors, drug delivery systems, and in the improvement of polymer biodegradation by fusion to polymer-degrading enzymes.

Three hydrophobins were selected for this work. HFB1 or HFB2 are class II hydrophobins from *Trichoderma reesei* which, harbor an exposed hydrophobic patch on their surface (Figure 26).[127] They are well-researched hydrophobins that have been found to form highly ordered monolayer films.[135] Among other things, they have been used for surface modification of Mica and poly(dimethylsiloxane), modification of a gold surface for electrochemical biosensing applications, and also for the binding of a perfluoropolyether to PS, PP, and LDPE surfaces.[136-138] The third selected hydrophobin was HGF1. HGF1 is an 8 kDa class I hydrophobin derived from the mushroom *Grifola frondosa*.[139] The mutant mHGF1 exhibits improved soluble expression in a bacterial host compared to the original protein. Therefore, it was used in this research project.[140]

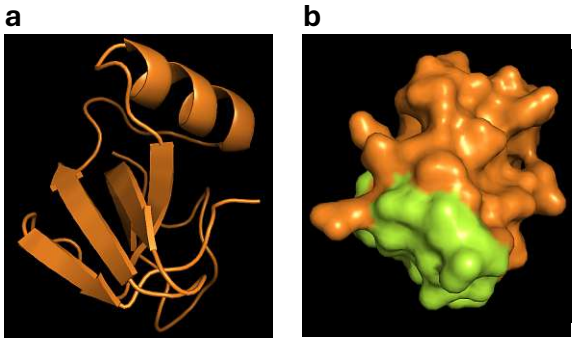

Figure 26| 3D Structure of HFB1. a, The structure of HFB1 is shown in cartoon representation. **b**, The structure of HFB1 is shown in a surface representation with exposed hydrophobic areas (hydrophobic patch) in green and polar exposed surfaces in orange.

1.5 Methods for polyolefin-surface analysis

A wide array of surface analysis methods exists which have been used for the analysis of polyolefin surfaces. This research project aimed to analyze, on the one hand, the adsorption of protein to the polymer surface and, on the other hand, the oxidation and, therefore, the degradation of the polymer surface. In previous research, many different methods have been used, depending on the polyolefin composition and properties, the method and extent of polyolefin degradation, but primarily depending on the available instrumentation, time, and financial resources. In the following chapter, the methods that were used during this research project are highlighted.

1.5.1 Selected methods for the analysis of protein-polyolefin interaction

Different surface analysis methods are commonly used for the analysis of the adsorption of protein to hydrophobic surfaces. One straightforward option is the analysis of the wettability of the surface. This can be analyzed via water contact angle (WCA) measurement, determining how hydrophilic/hydrophobic a surface is. Adsorption of a protein to a hydrophobic surface increases the hydrophilicity of the surface and thereby leads to a change in WCA (Figure 27). Therefore, WCA measurements can be proof of protein adsorption, but also adsorption affinities of different proteins can be compared.[131,138,141]

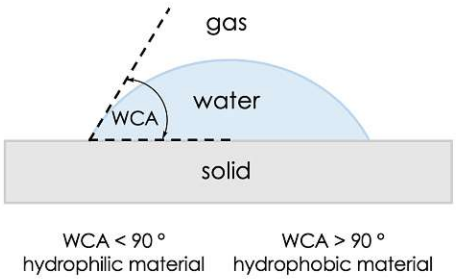

Figure 27| The principle of WCA measurement. The definition of a WCA and the difference between a hydrophilic or hydrophobic surface according to WCA measurement.

A different method for the analysis of the chemical composition of a plastic surface is Attenuated Total Reflection Fourier Transform Infrared Spectroscopy (ATR-FTIR). In this spectroscopic method, an IR beam penetrates the sample and is absorbed, depending on the chemical composition (functional groups) of the sample (Figure 28). The penetration depth into the sample ranges from 0.5 to 2 µm. An advantage is that samples can be examined directly in the solid state, making it a suitable method to analyze a polyolefin surface. The adsorption of a protein to the polyolefin surface can be analyzed through changes in the composition on the surface. However, ATR-FTIR has limited applicability for the analysis of protein adsorption to plastic polymers due to overlapping signals in the protein and the respective polymer analyzed. However, it can be used for the analysis of polyolefins which do not contain any functional groups.[142]

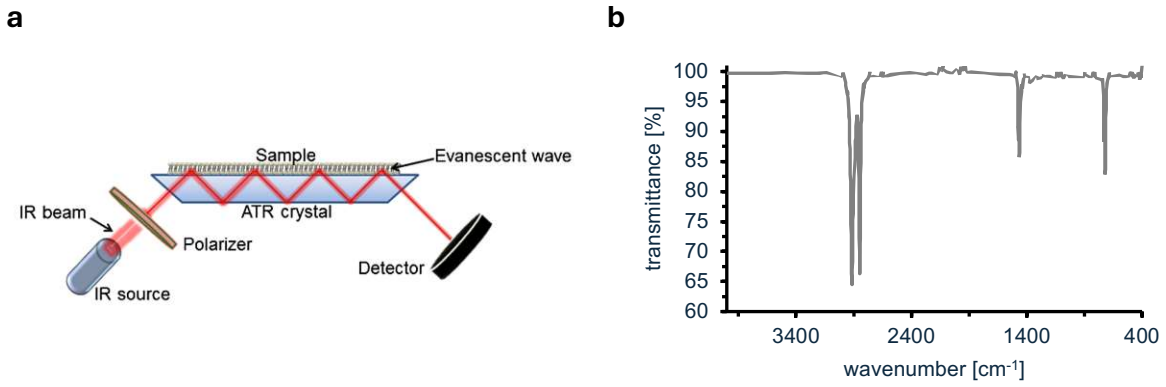

Figure 28| The principle of ATR-FTIR. a, Schematic representation of an ATR-FTIR system. The infrared beam passes through the ATR crystal covered on the top by the sample. The figure is adapted from Ausili et al.[143] **b**, An exemplary ATR-FTIR spectrum of PE.

X-ray Photoelectron Spectroscopy (XPS) offers the possibility to analyze a material's surface chemistry. The principle of XPS is the irradiation of a material with X-rays, causing the emission of core electrons, whose kinetic energy is measured. Thereby, the elemental composition and chemical states (e.g., C-H, C-O, C-N, etc.) can be analyzed, making it a useful technique for the analysis of the surface of materials e.g., polymers or surface oxides (Figure 29). The penetration depth typically is 1-10 nm. One important application of XPS is detecting surface contamination. The adsorption of protein can be detected by identifying nitrogen N (and functional groups, e.g., C-N and N-C=O) or by observing how adsorbed proteins reduce substrate signals. Changes in elemental ratios (such as N:C) help identify the deposition of biomolecules. Estimation of the amount of adsorbed protein is possible, however, difficult, because it cannot be differentiated between adsorbed protein and e.g., other contaminations. Distinguishing between similar biomolecules is not possible due to their elemental composition.[144]

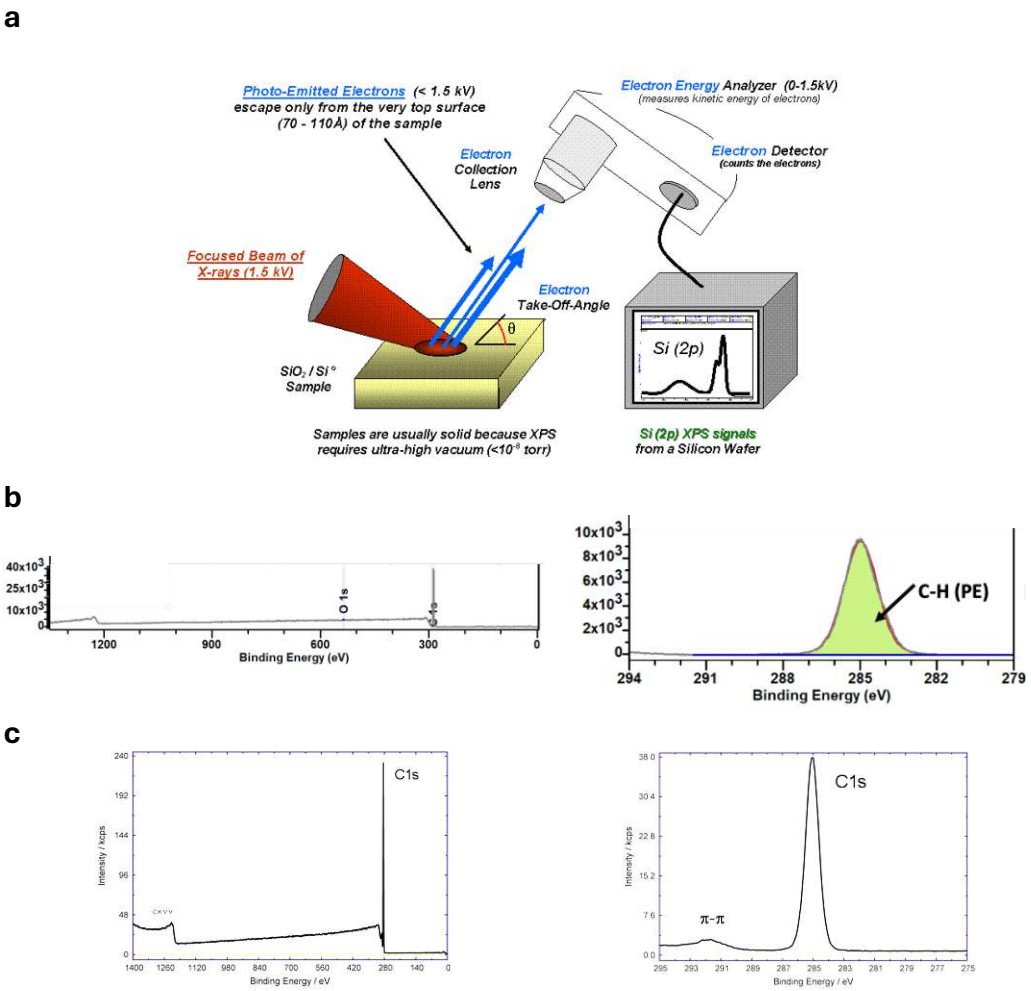

Figure 29| The principle of XPS. a, Schematic representation of an XPS device. The figure is adapted from www.wikipedia.org.[145] **b**, XPS survey spectrum (left) and C1s scan (right) of untreated polyethylene (PE). **c**, XPS survey spectrum (left) and C1s scan (right) of untreated polystyrene. The figure is adapted from Walton et al.[146]

With the optical method surface plasmon resonance (SPR) the real-time analysis of the adsorption of an analyte to a surface is possible. The principle of SPR is the detection of an analyte of interest by measuring the change of the refractive index in the target solution. In a standard SPR setup, polarized light hits a gold-coated sensor chip. At a certain angle, some light is absorbed by the electrons in the gold, generating charged density waves called “surface plasmons” that move along the metal surface. Plasmon resonance reduces the reflected light's intensity. At a specific angle (resonance angle) the intensity of refracted light is most significantly reduced. This angle depends on the refractive index near the gold surface. This refractive index changes when an analyte binds. Shifts in this resonance angle are recorded as a sensogram, reflecting interactions at the surface (Figure 30). Therefore, an increase in the SPR signal indicates the adsorption of the target protein to the surface. The biggest application of SPR is in biotechnology, medical diagnostics, or drug screening, detecting interactions between a solution-based analyte and a biomolecular recognition element. However, the interaction does not have to be between an analyte and a ligand. SPR can be also used in materials characterization e.g., the analysis of interactions of a polymer layer with an analyte.[147,148]

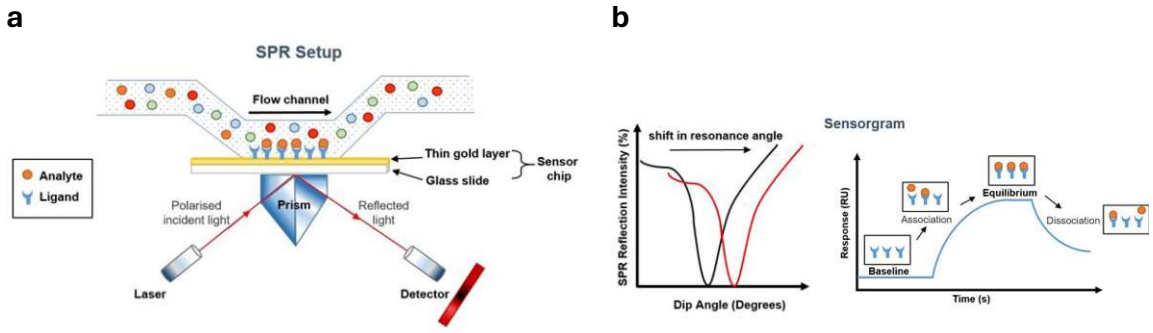

Figure 30| The principle of SPR. The figures are adapted from Marion J. Limo, ISAC, School of Pharmacy, University of Nottingham.[148] **a**, The setup of a SPR measurement. Here, the analyte binds to a ligand which is attached to the sensor chip. However, the analyte could also bind to a coating (e.g., a polymer coating) on the sensor chip. **b**, The shift in the resonance angle and representation in a sensogram.

Atomic force microscopy (AFM) represents another method to look at the surface of a material and analyze the change in morphology when protein is adsorbed. An AFM consists of four main components: a cantilever with a sharp tip, a reflective coating on the cantilever's back, a laser, and a sensitive photodetector. The laser is aimed at the cantilever's reflective surface, and the reflected light is detected by the photodetector. This system is controlled by an electric controller that scans the cantilever, laser, and detector. The cantilever functions as a force sensor, bending in response to the force between its tip and the sample (Figure 31, a). By scanning the surface of the material, the AFM can produce high-resolution topographical images at the nanoscale (Figure 31, b). Applications of AFM include imaging of biological molecules, cellular components, cells or tissues in biochemistry applications, polymers, nanostructures, or other materials. In this regard, AFM is commonly employed to measure the heights of protein molecules immobilized on a solid surface.[149,150]

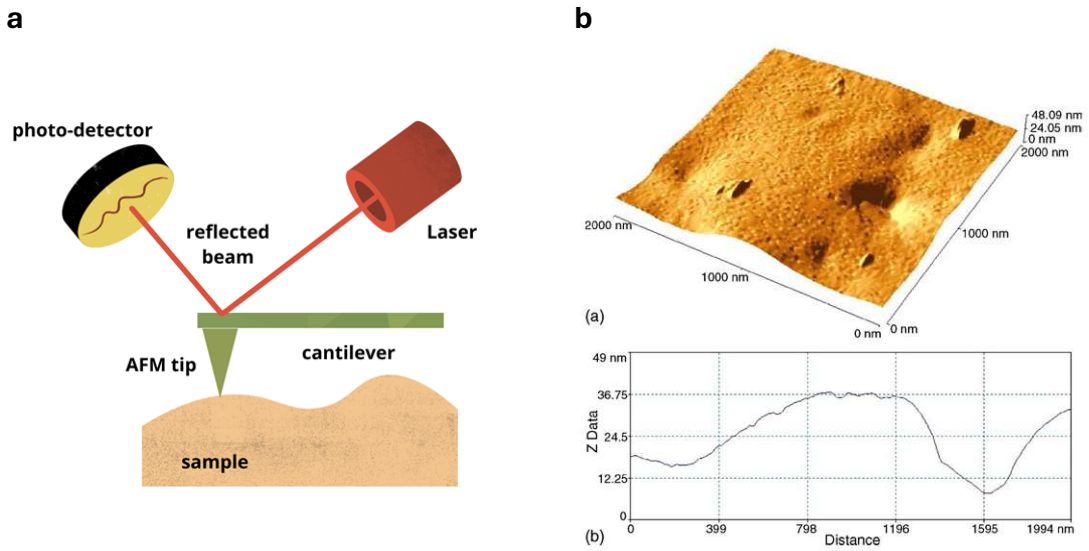

Figure 31| The principle of AFM. a, Schematic representation of the basic principle of AFM. Image Credit: Ilamaran Sivarajah. The figure is adapted from www.azooptics.coml.[149] **b**, (a) 3D AFM scan of a glass slide coated with hemoglobin. (b) Z data show the surface topography on a 2 mm length. The figure is adapted from Turner et al.[151]

Most studies that apply these techniques for the analysis of the adhesion of proteins/peptides to different surfaces make use of a combination of surface analysis techniques.[152,153] In a study by Gazzera et al., the adsorption of the hydrophobin HFB2 (serving as a primer layer for the binding of Fluorolink F10) to different hydrophobic polymer surfaces is shown using different surface analysis methods. They compared the WCA of pure PE to PE with adsorbed protein, detected typical protein bands in the ATR-FTIR after adsorption to LDPE, and also showed the adsorption of the protein to PS by AFM imaging (Figure 32).[138]

A

Sample	WCA
LDPE	91 ± 1 °
LDPE + HFB2	61 ± 1 °

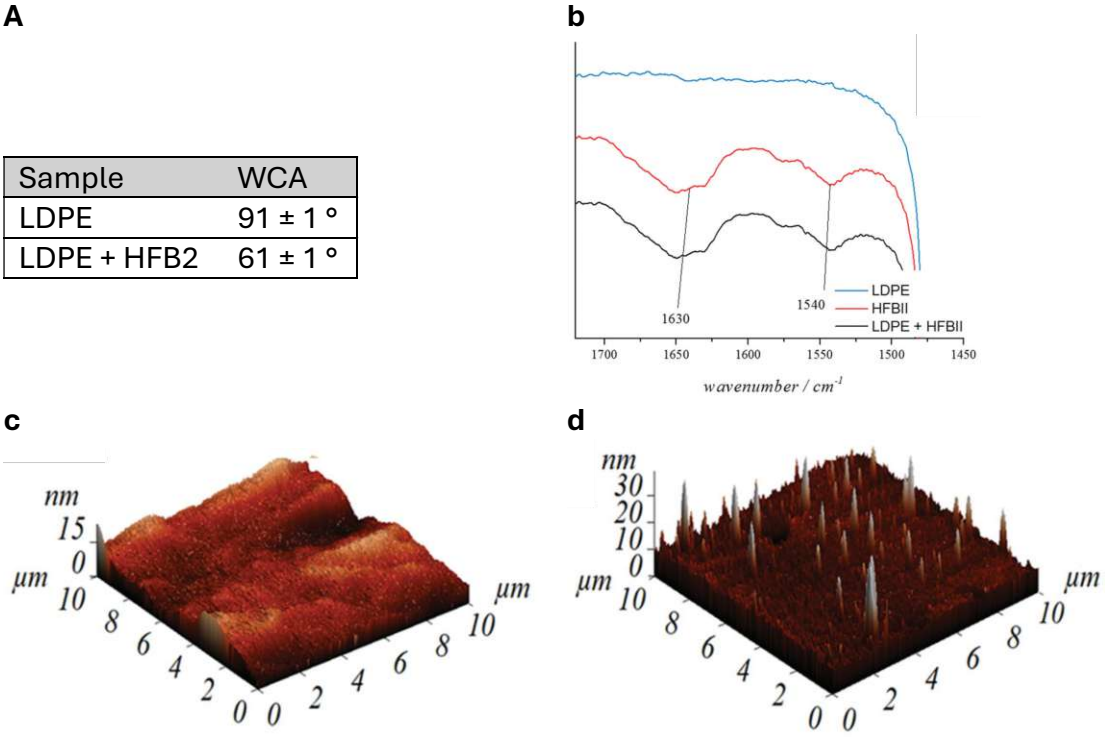

Figure 32| Analysis of protein adsorption to polymer surfaces by different surface analysis methods. The figures are adapted from Gazzera et al.[138] a, WCA measurement of untreated LDPE and upon treatment with HFB2. **b**, ATR-FTIR magnified and superimposed spectra of LDPE (blue), pure HFB2 (red), and LDPE coated with HFB2 (black) between 1720 and 1450 cm^{-1}. **c**, 3D AFM image of PS. The area displayed is 10 x 10 µm. **d**, 3D AFM image of PS treated by HFB2 and Fluorolink F10 solution. The area displayed is 10 x 10 µm.

A frequently used method which has not been used during this work, is the analysis of protein adsorption with a quartz crystal microbalance (QCM). It measures the mass of protein adsorbed onto the surface by detecting frequency changes in a quartz crystal resonator. As the protein binds to the surface, the mass changes cause a shift in the frequency, allowing for real-time monitoring of adsorption.[138,154] Moreover, following a similar principle as SPR, also ellipsometry can be used for the analysis of protein adsorption to a polymer surface.[155]

1.5.2 Selected methods for the analysis of polyolefin surface oxidation and degradation

How can we analyze the degradation/ breakdown of a polyolefin? First, the degradation of any polymer can be analyzed by the weight loss of the respective polymer. Weight loss is a common method for evaluating plastic degradation. Therefore, gravimetric analysis is done with a balance.[156,157] Moreover, the reduction of molecular weight can be analyzed. Gel permeation chromatography (GPC) is used to assess changes in molecular weight, helping to understand the breakdown process. These are the most common methods to analyze polyolefin degradation.[33] However, the analysis of weight loss is very error-prone due to sample treatment. Careful sample cleaning is essential to avoid misinterpreting results. Also, it is only applicable if there is substantial degradation. The analysis of molecular weight reduction by GPC is applicable for easily soluble polymers, however, for polymers with low solubility, it becomes a challenge and requires special equipment. Moreover, GPC is limited because early degradation happens mainly at the polymer surface.[61] A different approach is the analysis of changes in morphology or mechanical properties. Surface changes such as color shifts, cracks, and roughness can be analyzed by imaging techniques like scanning electron microscopy (SEM) and atomic force microscopy (AFM).[26,50,158,159] Advanced techniques such as X-ray powder diffraction (XRD) or differential scanning calorimetry (DSC), and others can provide further details for the elucidation of the degradation mechanisms.[49] There are some examples where the degradation of a polymer is monitored with SPR, by showing the decrease in thickness of the polymer layer.[160-163] Another possibility is the measurement of product formation. As an example, the measurement of CO_2 and CH_4 can provide information during microbial biodegradation of a polyolefin. However, this possibility is only applicable if the mechanism of degradation is known, and products can be calibrated for quantitative analysis. Lastly, the analysis of surface oxidation by the formation of new functional groups. FTIR can identify chemical changes. An increase in carbonyl groups (C=O) is associated with degradation. However, the results of these measurements can be affected by plastic additives or other impurities. Other techniques, such as XPS and nuclear magnetic resonance (NMR), can also identify chemical components formed during degradation. Mass spectrometry (MS) could also help track degradation by identifying metabolic intermediates.[61]

Most importantly, all these mentioned different approaches and techniques are used as complementary methods for the detection of polyolefin degradation.[164] Depending on the field of research, different methods are used preferably. Imaging methods like SEM and AFM are usually used as complementary approaches for the analysis of degradation, often combined with spectroscopic methods like FTIR and XPS. Moreover, the presented techniques are also very different regarding sample preparation, setup, costs, and instrumentation. While the measurement of weight loss or WCA does not require special/expensive instrumentation, other techniques like XRD or XPS require special expertise and instrumentation.

The focus of this research project was the analysis of chemical changes and the formation of new functional groups on a PE surface. The measurement of WCA could potentially serve as the first hint for the oxidation of a hydrophobic PE surface.[26]

However, this method is not suitable for this research project. WCA measurement is very error-prone due to impurities from e.g., solvents. Moreover, protein adsorption influences the WCA. With ATR-FTIR (chapter 1.5.1), the generation of functional groups by oxidative degradation of PE can be monitored. In most research regarding the degradation of PE via an oxidative pathway, FTIR is used as one tool for analysis. There are certain characteristic IR absorption bands for the oxidation of PE (Table 2). However, different reaction conditions used during the degradation process (such as temperature, solvent, catalyst, etc.) lead to differences in the degradation mechanism. Therefore, the respective formed functional groups are dependent on the used reaction conditions.

Table 2: Characteristic IR-bands for functional groups generated during oxidative PE degradation

Functional group	Mode of vibration	Wavenumber [cm^{-1}]
Alcohol	O-H stretch	3600-3200
Carbonyl	C=O stretch	1870-1650
Alkene	C=C stretch	1670-1600
Alcohol, ether, ester, anhydride, acetal	C-O stretch	1300-1020

In a study by Hu et al., they used Fenton's reagent under hydrothermal conditions for the efficient degradation of PE in water.[42] FTIR was used to observe chemical changes in PE microplastics after oxidation. An increase in peak intensity of both C=O and C-O groups was observed (Figure 33, a). In a different study by Yao et al., PE films were treated with UV irradiation (254 nm) at high temperatures (70 °C).[158] Samples were taken each 24 h and analyzed by FTIR (Figure 33, b). A prominent C=O peak increased with thermal UV treatment time. However, a different tendency for the formation of functional groups is observed under different conditions, as presented in a study by Campanale et al.[31] In this study, the aim was to mimic natural weathering conditions. Therefore, different PE samples were irradiated with UVA light (340 nm) under controlled environmental conditions (22 °C, 60 % humidity) (Figure 33, c). Here, the C=O peak was not as pronounced. However, the absorption regions for O-H and C-O groups showed an increase.

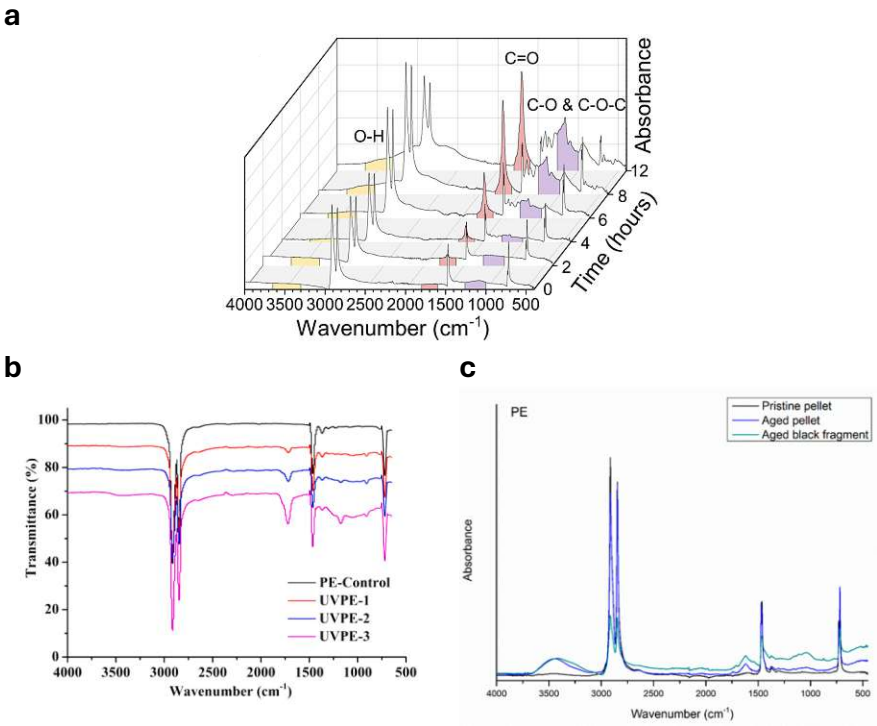

Figure 33| FTIR analysis of PE oxidative degradation under different conditions. **a**, PE microplastics after 12 h treatment with Fenton's reagent at 140 °C. Experimental conditions: 4 mM Fe^{2+}, 200 mM H_2O_2, 1 g/L UHMWPE microplastics, 140 °C. The figure is adapted from Hu et al.[42] **b**, PE after UV treatment at 70 °C. Samples for FTIR were taken in 24 h intervals. The figure is adapted from Yao et al.[158] **c**, Comparison of pristine PE pellet to two different aged PE samples (aged pellet, aged black fragment) after 20 days of UVA irradiation under controlled conditions. The figure is adapted from Campanale et al.[31]

In a study by Tofa et al., the photocatalytic (ZnO) degradation of LDPE microplastic residues was monitored by FTIR.[51] After photodegradation, new functional groups (carbonyls, hydroperoxides, peroxides, and unsaturated groups) appeared. Detailed analysis revealed the formation of alcohol species, peroxides, and carbonyl compounds such as carboxylic acids, ketones, aldehydes, and esters. Additionally, photo-oxidation of ketones produced vinylidene and vinyl groups (Figure 34).

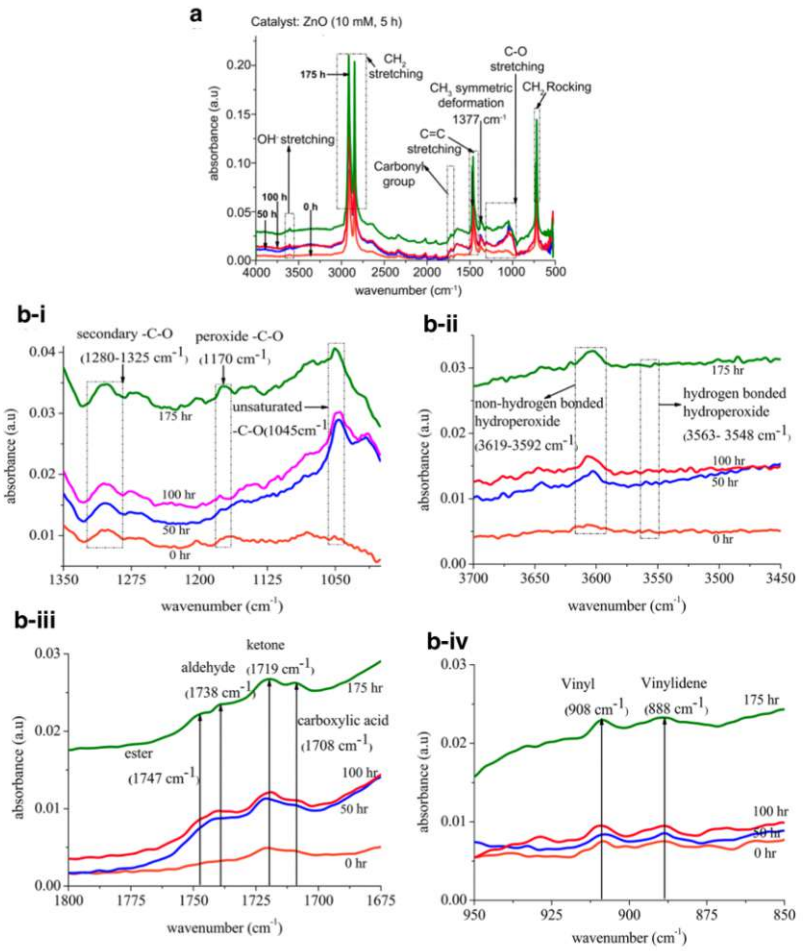

Figure 34| Detailed FTIR spectra of LDPE film over 175 h of visible light photocatalysis. The experiment was conducted in the presence of ZnO nanorods (10 mM, 5 h). The figure is adapted from Tofa et al.[51] **a**, The whole FTIR spectrum. **b**, Different functional groups are depicted, b-i peroxides, b-ii hydroperoxides, b-iii carbonyl, and b-iv unsaturated.

Laser-induced Breakdown Spectroscopy (LIBS) is a surface analysis method that is less common for the analysis of oxidation of a polymer surface. It identifies a material's composition by atomic emission. A pulsed laser is focused on the sample, vaporizing it, and forming plasma with the surrounding atmosphere. As the plasma cools down, element-specific light is emitted and detected by a spectrometer, which enables the identification of specific elements like oxygen (Figure 35). It is a fast method and applicable to all material states. In solid samples, the laser ablation leads to the generation of small craters. Moreover, repeated measurements allow for a deeper analysis of the material's composition. Sommer et al. demonstrated the applicability of LIBS for the analysis of the oxidation of different polymers (PE, PP, PS). The polymers were aged under controlled conditions. Through laser ablation, the oxygen content on the surface and its penetration depth into the respective polymer were analyzed. The findings demonstrate that LIBS represents an effective and rapid method for quantifying surface oxidation.[165,166] In similar studies by Willner and Brunnbauer et al., LIBS was combined with laser ablation-inductively coupled plasma-mass spectrometry (LA-ICP-MS) for the spatially resolved analysis of polymer thin films (polyimide, polystyrene, and polyvinylpyrrolidone) exposed to UV treatment and a corrosive conditions. [167,168]

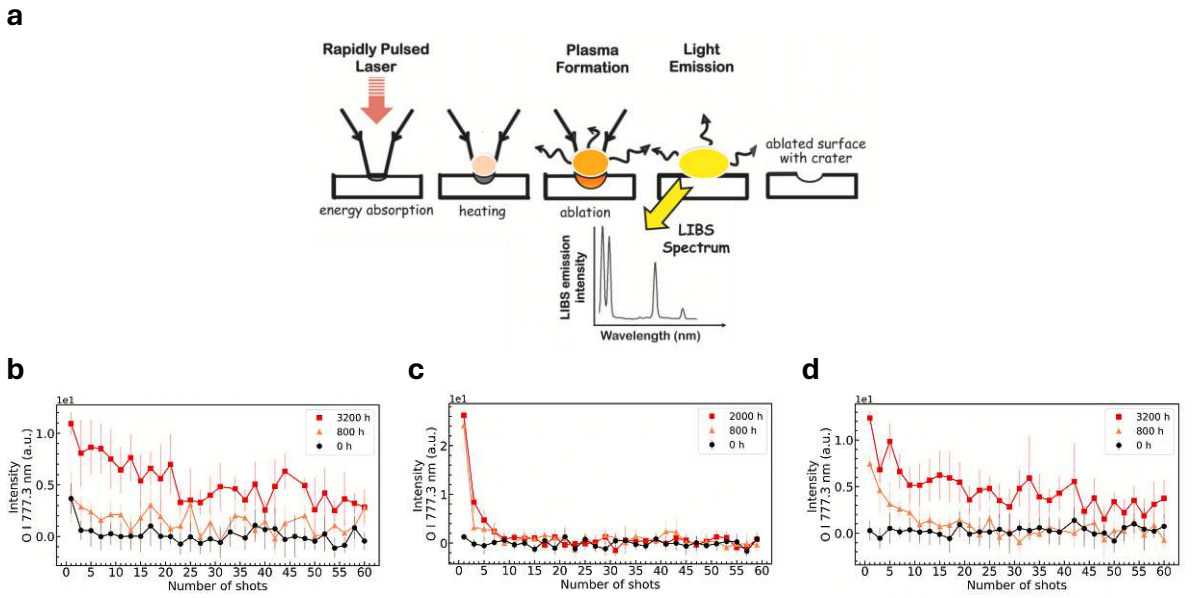

Figure 35| Analysis of polymer surface oxidation by LIBS. a, Schematic representation of the LIBS process. The figure is adapted from Harmon et al.[169] **b**, **c**, and **d**, Oxygen intensity with an increasing number of shots for PP, PS, and PE, respectively, during 3200 h of weathering. Values are mean ± σ for n = 3. The figures are adapted from Sommer et al.[165]

XPS (chapter 1.5.1) represents another suitable method for the analysis of functional group generation by oxidation of the PE surface (e.g., C-O, C=O, etc.).[170] In a study by Dorey et al., the effects of gamma (γ)-irradiation on PE were analyzed. XPS was used to analyze the surface composition and chemical changes after irradiation at different doses, indicating the potential presence of ROS (Figure 36).[171]

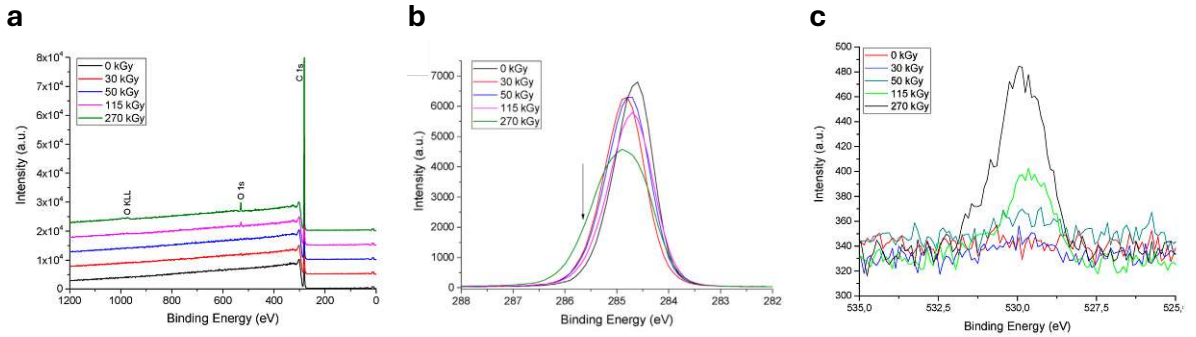

Figure 36| Analysis of PE surface oxidation by XPS. The figures are adapted from Dorey et al.[171] **a**, XPS survey spectra of a PE film irradiated at different γ-doses. **b**, C1s XPS spectra of a PE film irradiated at different γ-doses. **c**, O1s XPS spectra of a PE film irradiated at different γ-doses.

In a study by Chen et al. PS oxidation and degradation in superworms (*Zophobas atratus* Larvae) (chapter 1.1.2.3), were monitored by XPS and FTIR analysis.[63] XPS analysis shows the formation of C=O and C-O bonds. However, the possibility of overlapping protein signals that interfere with oxidation signals was completely omitted. In the XPS spectra shown, there is also nitrogen present which can be explained by adsorbed protein (Figure 37). This interferes with the analysis of PS oxidation signals. Therefore, results from protein-based plastic degradation studies should be interpreted with caution because sources of error are not always taken into consideration.

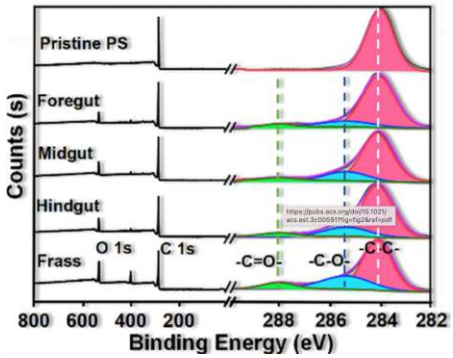

Figure 37| XPS survey and C1s spectra of PS in different regions of the gut and frass of superworms (*Zophobas atratus* Larvae). A signal for nitrogen is visible at approx. 400 eV. The figure is adapted from Chen et al.[63]

In this regard, an important feature during XPS analysis is depth profiling. Traditional depth profiling with monoatomic ion sources (e.g., Ar ions) can significantly damage organic materials such as polymers. However, new ion sources, such as large organic molecule clusters (e.g., C24, C60) or Ar gas clusters, have been developed. By distributing the impact energy over many atoms, the energy is localized to the top surface and reduces subsurface damage. This allows for better analysis of polymers without altering their chemical structure and makes the removal of loosely bound material possible.[172-174]

2 Research question and aims

Previously, the Fenton reaction[41,42,70] or photocatalysts like TiO_2[3,4,43,44] have been used for oxidative polyolefin microplastic degradation, which both function by producing hydroxyl radicals ($HO^{\bullet}$) and other ROS.[18] Inspired by this, the idea arose, to find a biological equivalent, namely to use a protein for the generation of highly reactive oxygen radicals for the oxidation of a polyolefin surface, accelerating the first step of its degradation.[21,24,26-30,63] Thus, the idea was to use a protein as a photocatalyst for PE degradation, combining photodegradation and biodegradation. In this completely bio-based approach, polyolefin microplastic degradation would only be mediated by the protein and light and would omit high reaction temperatures or aggressive or expensive chemicals. Moreover, this approach would come along with all positive aspects of biocatalysis, e.g., avoidance of the synthesis of metal catalysts, no organic solvents, biodegradability of the catalyst, etc. The envisioned protein should produce reactive oxygen species, particularly $HO^{\bullet}$, upon illumination with visible light.

Following this, a potent radical-generating protein was needed. It should produce highly reactive oxygen species like $HO^{\bullet}$, upon illumination with visible light. Photosensitizer proteins (PSP) are bio-based photosensitizers, that harbor a photosensitizer molecule that absorbs light and initiates the photochemical creation of ROS. These proteins were evaluated and selected based on their ROS-producing activity.[76,92] Their use for polymer degradation is a new concept. However, as ROS have a very short lifetime, it would be beneficial to bring the protein very close to the hydrophobic polyolefin surface, to improve degradation efficiency.[4] For better adsorption of the protein to the polyolefin surface, the hypothesis was to introduce a hydrophobic element (hydrophobic "anchor"). A previously reported concept was implemented, where hydrophobins which are small fungal proteins that contain a hydrophobic patch, were used.[131,133,134,136,138] They were attached to the PSP, creating fusion proteins. The aim was to show the improved adsorption of the fusion protein, to analyze its ability to generate ROS, and finally to prove the concept that the protein is capable of oxidatively degrading polyolefins (using PE as the model polyolefin) (Figure 38). Therefore, fusion proteins were created and produced, assays for the detection of ROS were conducted and methods for surface analysis were developed, for the analysis of protein adsorption and oxidation of the PE surface.

The approach used in this thesis represents a green alternative to conventional methods for polyolefin degradation. Like other photocatalytic approaches, this approach is an energy-efficient alternative to heat-based methods, as the biocatalyst is activated by light. Moreover, mild reaction conditions (no organic solvents, ambient temperature), a degradable catalyst, and no chemical waste are some big benefits.

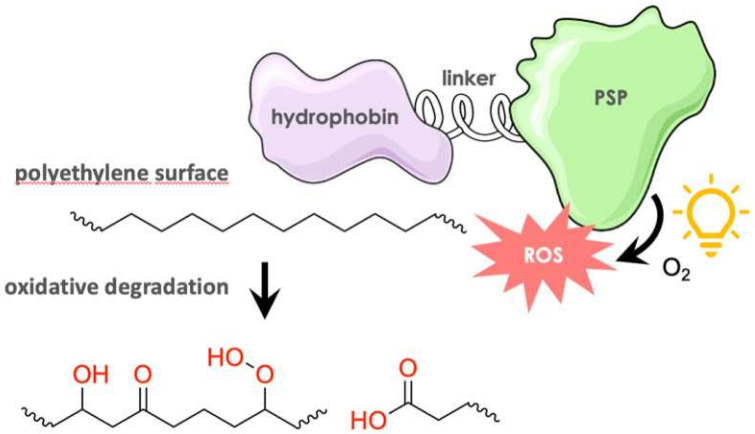

Figure 38| Bio-photocatalytic oxidative degradation of PE. Schematic representation of the new bio-photocatalytic approach to oxidative PE degradation. The photocatalytic photosensitizer protein (PSP) is linked to a hydrophobin, which leads to an attachment of the protein to the PE surface for an in situ generation of ROS upon exposure to oxygen and visible light.

3 Results and discussion

3.1 Design of plasmids for expression and cloning

To begin with, based on the literature, an array of PSPs with promising ROS-producing activity from two different protein types were chosen for this research project. Three selected PSPs were proteins related to the green fluorescent protein (GFP) family (KillerRed, SuperNova, and KillerOrange) and another three PSPs belonged to flavin-binding fluorescent proteins, more specifically light-oxygen-voltage sensing domain (LOV) proteins (MiniSOGQ103V, SOPP3 and DsFbFpM49I) (as described in chapter 1.3). The genetic sequences of these six proteins were codon optimized for production in *E. coli* using online tools for codon optimization.[175,176] Then, the company Twist Bioscience was chosen for the DNA synthesis of the genes of interest. The expression vector pET29b(+) with the T7 expression system for high yield production in E. *coli* BL21(DE3) was chosen for all six genes and a C-terminal 6 x His tag was included for purification via immobilized metal affinity chromatography (IMAC). A plasmid map showing the organization of respective genetic fragments is shown in Figure 39. After the design of those six plasmids in silico they were ordered from Twist Bioscience.[177] A library of all proteins and all genetic sequences is listed in chapters 6.1 and 6.2.

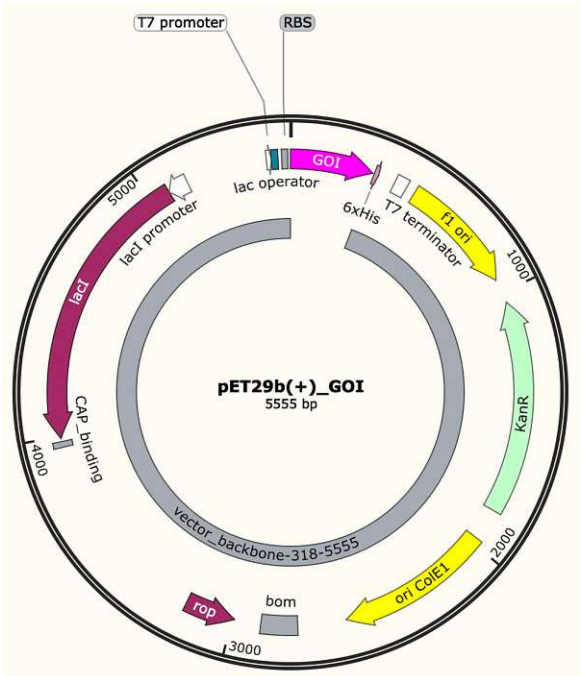

Figure 39| An exemplary plasmid map showing the organization of the genetic fragments. The pET29b(+) vector contains the gene of interest (GOI), a 6 x His tag embedded in a T7 expression cassette (lac inhibitor (lacI) with lacI promoter, T7 promoter, lac operator, ribosome binding site (RBS) and T7 terminator). Other relevant genetic elements are the kanamycin resistance (KanR) and a high-copy-number ColE1 origin of replication.

3.2 Protein production analysis of unmodified PSPs

After plasmid DNA was obtained, for expression, plasmids were transformed in chemically competent *E. coli* BL21(DE3) cells. Cells were cultivated overnight for the preparation of cryostocks. Moreover, plasmids were isolated from overnight cultures for storage of additional plasmid aliquots and verification of correct gene sequences by sequencing. Then, for protein production, an autoinduction protocol using media containing the inducer α-lactose was followed.[178] Already during expression, the color of the respective PSPs was visible (Figure 40, a). Cultures were harvested and protein purification was done via IMAC. After purification and concentration of the protein solutions, the strong color of the respective PSPs became very apparent (Figure 40, b).

Figure 40| The colors of the six PSPs. a, *E. coli* BL21(DE3) cultures expressing the PSP KillerRed. **b**, The PSPs after purification, from left to right: KillerOrange, KillerRed, SuperNova, MiniSOGQ130V, SOPP3, DsFbFPM49I.

For Verification of the production of correct proteins, sodium dodecyl sulfate polyacrylamide gel electrophoresis (SDS-PAGE) was done. SDS-PAGE separates proteins based on their size by using an electric field to navigate proteins through a gel matrix containing SDS. SDS denatures and provides a negative charge to the proteins. This allows them to migrate only based on size. All PSPs showed a strong band at the correct size (Figure 41).

a

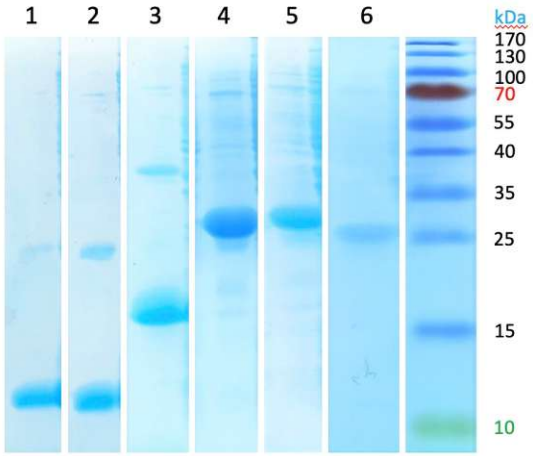

b

	Protein	Size [kDa]
1	SOPP3	13.2
2	MiniSOGQ103V	13.4
3	DsFbFpM49I	16.8
4	SuperNova	27.4
5	KillerRed	27.5
6	KillerOrange	27.4

Figure 41| Verification of protein production by SDS-PAGE. Protein content was normalized to 5 µg protein per lane, and a 17.5 % acrylamide gel was used. **a**, SDS-PAGE of purified PSPs. Bands with the expected size are visible for all proteins. **b**, The expected molecular weight (size) of the six PSPs.

3.3 Characterization of PSPs and selection of highest ROS producers

To elucidate the photosensitizing efficiency of the PSPs and ultimately find out which one produces the highest amount of ROS, their behavior during illumination had to be characterized and assays for the detection of ROS had to be implemented. For illumination, different light sources were used. The measurement of their respective light intensities is described in chapter 6.5.

3.3.1 Spectroscopic characterization

To verify the fluorescence behavior of the PSPs, fluorescence spectra were measured. It was normalized to an absorption of 0.02. Therefore, the absorption of PSPs was measured close to their absorption maxima reported in the literature. KillerRed and SuperNova were measured at 595 nm, LOV proteins (MiniSOGQ103V, SOPP3, and DsFbFpM49I) and KillerOrange were measured at 450 nm. However, to obtain fluorescence emissions spectra, a sufficiently big difference between excitation and emission wavelength had to be ensured. Therefore, LOV proteins were excited at 440 nm. KillerOrange was excited at 455 nm, KillerRed and SuperNova were excited at 540 nm. Fluorescence spectra are depicted in Figure 42. From these measurements, approximate fluorescence maxima were determined: 490 nm for MiniSOGQ103V and SOPP3, 507 nm for DsFbFpM49I, 605 nm for KillerRed and SuperNova, 540 nm for KillerOrange.

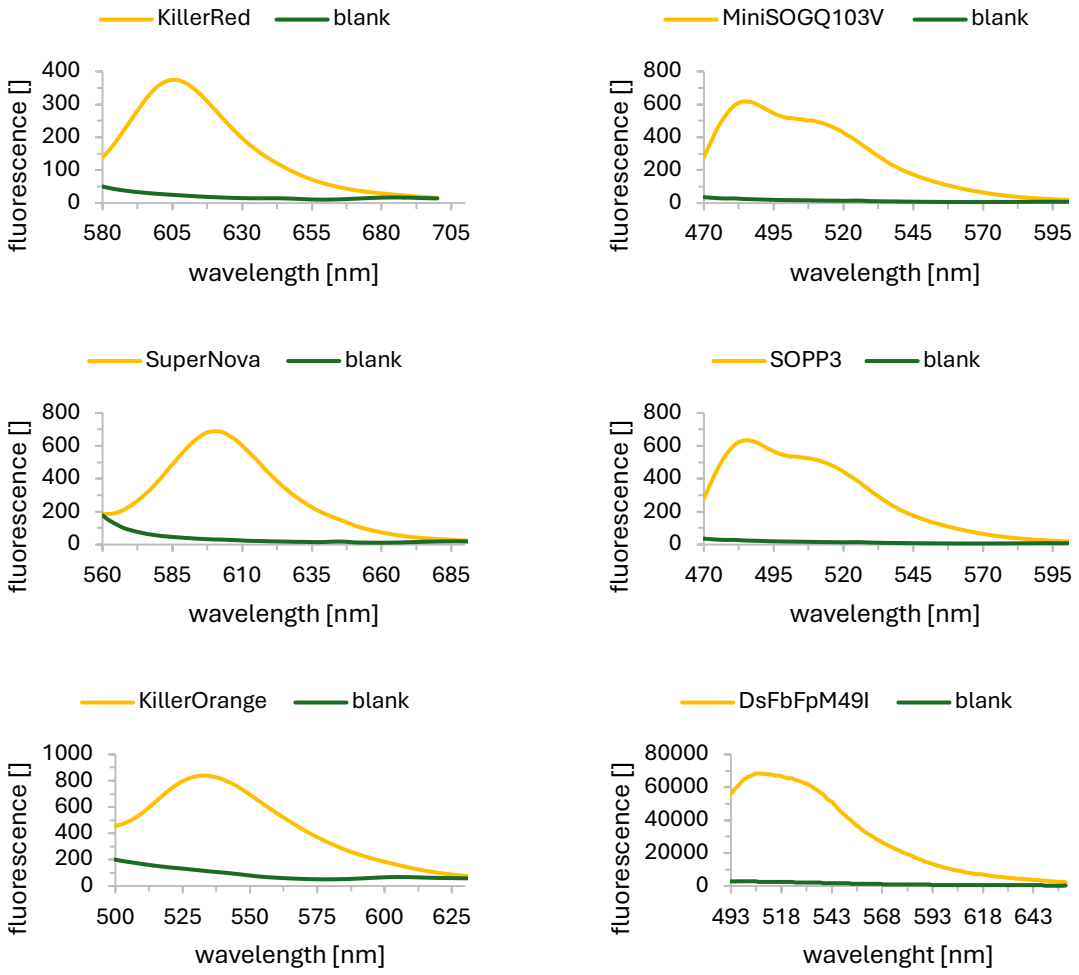

Figure 42| Fluorescence emission spectra of all PSPs: KillerRed, SuperNova, KillerOrange, MiniSOGQ103V, SOPP3, and DsFbFpM49I. a, Protein solutions of all proteins except DsFbFpM49I were normalized to absorption of 0.02 and were prepared in 50 mM NaPi buffer (pH 7.2) in a final volume of 100 µL. As a blank, the buffer was measured. The plate reader "Fluorescence spectrometer PerkinElmer LS-55" was used for the measurements. **b**, DsFbFpM49I was normalized to chromophore concentration 50 µM, prepared in Milli-Q H_2O in a final volume of 100 µL. The chromophore FMN was measured as well. As a blank, Milli-Q H_2O was measured. The plate reader "Spark® Multimode Microplate Reader, Tecan" was used for the measurement.

3.3.2 Quantification of reactive oxygen species production

To determine the best candidate for polyolefin degradation, different assays for the detection of ROS production by the PSPs were established. For all assays, a daylight lamp was used for illumination (Megaman Helix, 1.02 mW/cm^2). PSPs were normalized to an absorption of 0.02, as described in the previous chapter 3.3.1. This approach to normalization was used because it was previously described in a very similar setting.[77,93] A different approach to normalization would be by measuring protein content and calculating molar concentration (e.g. via BCA assay, chapter 3.8). Even though normalization was done by absorption, the protein content of the PSP solution was

additionally determined via BCA assay. When comparing the molar concentrations, DsFbFpM49I was slightly less concentrated than the other LOV proteins. The samples of the GFP-family PSPs were also lower concentrated (KillerRed 0.02 µmol/mL, SuperNova 0.02 µmol/mL, KillerOrange 0.01 µmol/mL, MiniSOGQ103V 0.05 µmol/mL, SOPP3 0.05 µmol/mL, DsFbFpM49I 0.03 µmol/mL).

For all assays, it must be considered that highly reactive ROS can react unpredictably with all surroundings, assay reagents, assay products, buffer components, or other proteins. This introduces complexity to the fluorescence measurements. Furthermore, the fluorescence of the PSP itself can interfere with the output signal, or quenching effects can occur. Also, the autoxidation of the assay reagents must be considered. Therefore, the autoxidation of the respective assay reagent was subtracted from all measurements. Very small amounts were used to set up the reaction mixture of the assay, which led to a high variability in the results. Therefore, a given ROS-specific assay was usually conducted in one day for all PSPs. Moreover, variations in assay composition or experimental setup were avoided if possible.

To exclude errors due to photobleaching, it was tested if the light intensity (1.02 mW/cm^2) led to a decrease in the fluorescence intensity of the PSPs. It was illuminated for 15, 30, 60, 120, and 180 min. However, this low light intensity had no significant influence as the fluorescence of the PSPs, which was measured at their respective fluorescence maxima (previous chapter 3.3.1), did not decrease over time. So, it could be concluded that no photobleaching occurred under the assay conditions.

3.3.2.1 Quantification of H_2O_2 and $O_2^{\bullet-}$ production

First, the quantification of the most stable reactive oxygen species, H_2O_2, was tested. The assumption was that the PSPs produce H_2O_2 when illuminated with white light. The observed H_2O_2 concentrations would be an indication of ROS production via the type-I photosensitizing mechanism. For its quantification, several chromogenic substrates exist (chapter 1.2.2). One widely used chromogenic substrate is ABTS (2,2'-azino-bis(3-ethylbenzothiazoline-6-sulfonate), which is oxidized by horseradish peroxidase (HRP) and H_2O_2. HRP uses H_2O_2 for the one-electron oxidation of ABTS into the radical cation ABTS$^{\bullet+}$ (Scheme 2). The absorption of this stable, green-colored radical cation can be measured at 405 nm for quantification. The assay was conducted by mixing the different PSPs with the reagent ABTS and illuminating for different periods to see a rise in ABTS$^{\bullet+}$ formation (measured at 405 nm). However, in the presence of the PSPs, the formation of ABTS$^{\bullet+}$ could not be observed. After many trials, with negative and positive controls, it became clear that the radical cation ABTS$^{\bullet+}$ is not stable in the presence of the PSPs and light. Probably, the respective PSP itself reacts with ABTS$^{\bullet+}$ to form the over-oxidation product ABTS^{2+} (which is usually formed in the presence of excess H_2O_2). ABTS^{2+} is not stable in aqueous solutions and decomposes into colorless products (chapter 6.6).[179]

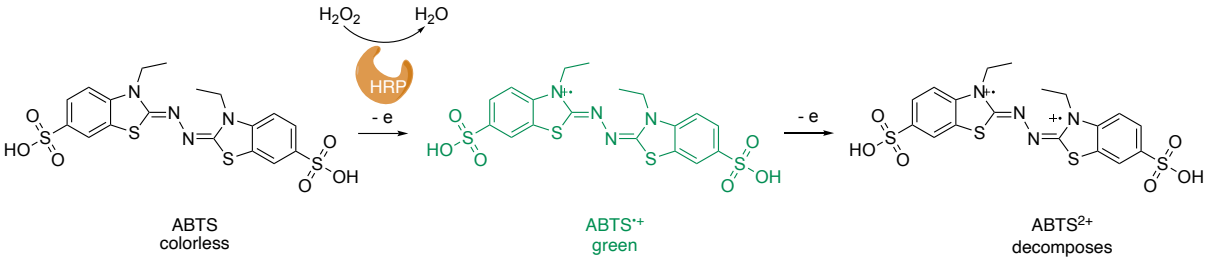

Scheme 2| Oxidation of ABTS by HRP and H_2O_2 to its detectable form $ABTS^{\bullet+}$ and over-oxidation to $ABTS^{2+}$.[180] The radical cation $ABTS^{\bullet+}$, which is detected by its absorption at 405 nm, is highlighted in green.

Therefore, a different assay for quantification of H_2O_2 production was chosen, the Amplex Red (10-acetyl-3,7-dihydroxyphenoxazine) assay. The fluorogenic assay is widely used in biological applications (e.g. for the investigation of oxidative stress).[181] It relies on the oxidation of the non-fluorescent dye Amplex Red to the fluorescent oxidation product Resorufin (7-hydroxy-3*H*-phenoxazin-3-one) by horseradish peroxidase in the presence of H_2O_2 in a 1:1 stoichiometry.[182] First, one-electron oxidation of the compound creates a radical species which then disproportionates and hydrolyzes to the final stable product Resorufin (Scheme 3).[183] The fluorescence of Resorufin can be detected and correlated to the H_2O_2 concentration. The assay is very sensitive and can detect H_2O_2 in the nanomolar range.

Furthermore, the same assay can be used in combination with superoxide dismutase (SOD) for the quantification of superoxide $O_2^{\bullet-}$. This enzyme, which is an important defense mechanism of cells against oxidative stress, converts $O_2^{\bullet-}$ into H_2O_2 and ground state O_2.[184] Consequently, the formed H_2O_2 can be measured by the Amplex Red assay in the same way as previously described. By comparing the results with and without the addition of SOD, the amount of formed $O_2^{\bullet-}$ can be estimated.

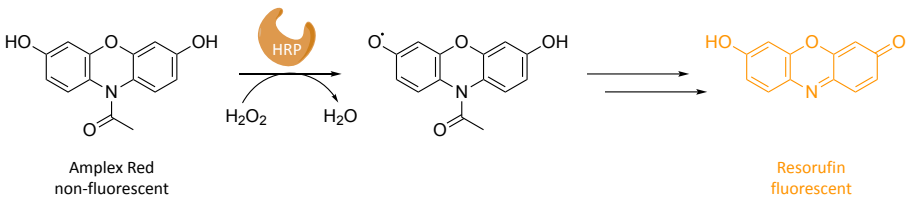

Scheme 3| Oxidation of the reagent Amplex Red to fluorescent Resorufin.[183] In the first step, one-electron oxidation by HRP and H_2O_2 occurs, followed by disproportionation and hydrolysis to the fluorescent product Resorufin (highlighted in orange).

In the first attempts to perform this assay, it became clear that the H_2O_2 concentrations quickly exceeded the linear range of the assay, and the results could not be interpreted anymore. This was observed by a rapid rise of the fluorescence signal, followed by a fast drop due to the assumed overoxidation of the assay product Resorufin. Therefore, various assay conditions were screened. In the end, higher Amplex Red reagent concentrations combined with low protein concentrations and low light intensities were chosen to ensure that the linear range of the assay was not exceeded.

Dark controls omitting light illumination of the samples were performed. As expected, there was no significant increase in fluorescence over time, proving the necessity of light for ROS production by the PSPs (Figure 43). Moreover, the autoxidation of Amplex Red by

light illumination was measured. Results show a slight increase in fluorescence with illumination time (Figure 44). This problem, which represents a source of error and reduces the sensitivity and comparability of the assay, has been described before.[185]

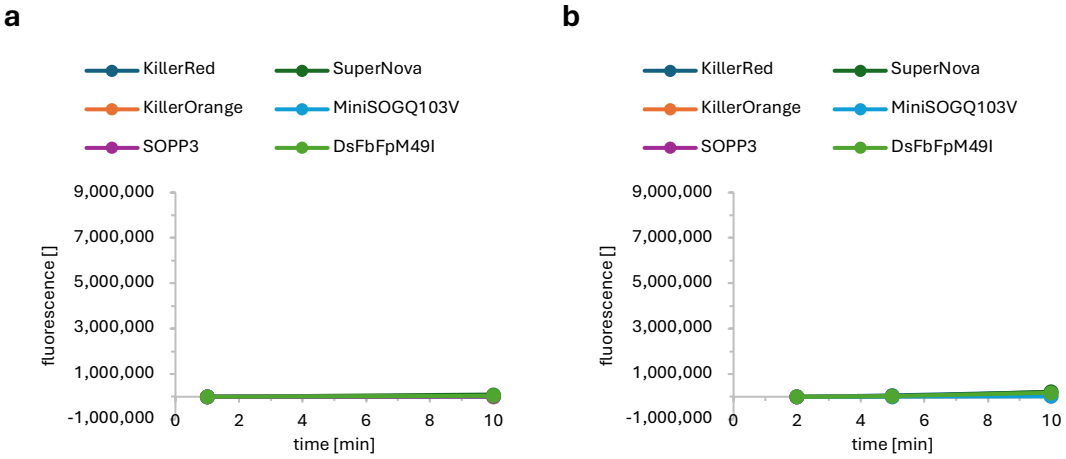

Figure 43| Dark controls for the Amplex Red assay for H_2O_2 and $O_2^{\bullet-}$ detection. Reaction mixtures with the respective PSPs were incubated in the dark. Almost no rise in fluorescence was observed. 0.2 U/mL HRP and 0.05 mM Amplex Red were used, without (**a**) or with (**b**) the addition of 2 U/mL SOD. PSPs were adjusted to absorption of 0.02 at their absorption maximum (ex 450 nm for LOV proteins and KillerOrange and ex 595 nm for KillerRed and SuperNova) in 50 mM NaPi pH 7.2, in a total volume of 100 µL. The increase in fluorescence was measured at ex 550 nm / em 595 nm and corrected by the average fluorescence of the initial mixture, values are mean ± σ for n = 3.

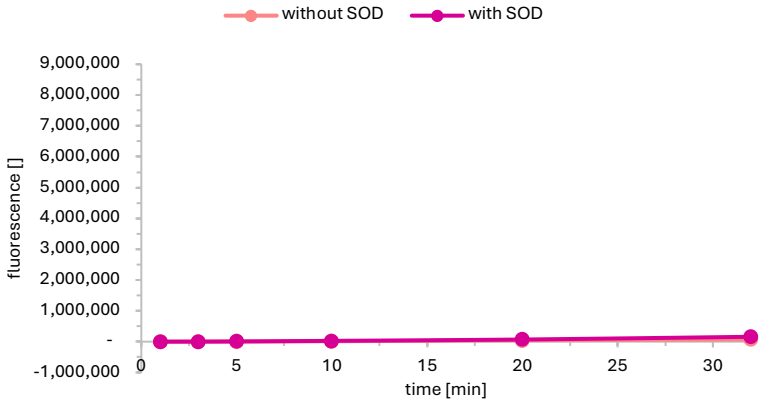

Figure 44| Autoxidation of Amplex Red by light. Only a slight increase in fluorescence signals was observed without or with SOD. 0.2 U/mL HRP and 0.05 mM Amplex Red were used, without or with the addition of 2 U/mL SOD, in 50 mM NaPi pH 7.2, in a total volume of 100 µL. It was illuminated with Megaman Helix daylight lamp (1.02 mW/cm^2). The increase in fluorescence was measured at ex 550 nm / em 595 nm and corrected by the average fluorescence of the initial mixture, values are mean ± σ for n = 3.

The results of the first experiments showed a bigger rise in fluorescence, therefore higher H_2O_2 production by MiniSOGQ103V, SOPP3, and DsFbFPM49I (LOV proteins) than by KillerRed, SuperNova, and KillerOrange (GFP-like proteins), which has been described in the literature (Figure 45).[92] The observed H_2O_2 production is an indication of ROS production via the type-I photosensitizing mechanism. DsFbFPM49I showed the highest

increase in fluorescence. After the addition of SOD for the conversion of $O_2^{\bullet-}$ into H_2O_2, similar results were observed (Figure 46). The LOV protein DsFbFpM49I showed the highest production of H_2O_2 and $O_2^{\bullet-}$. The GFP-like protein KillerRed exhibited the lowest production of H_2O_2 and $O_2^{\bullet-}$.

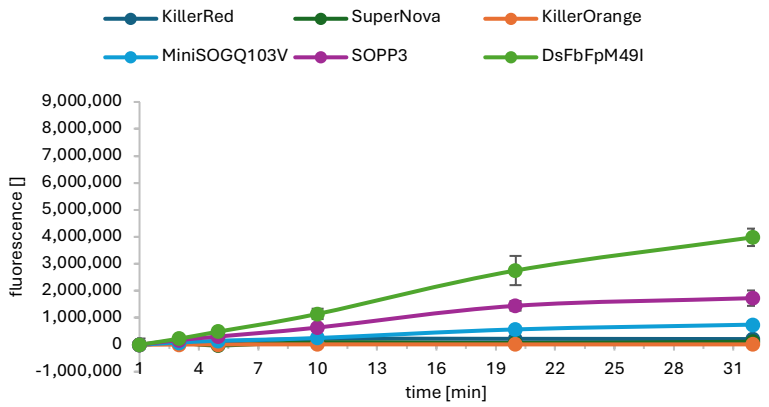

Figure 45| Results of the Amplex Red assay for the detection of H_2O_2. LOV proteins showed higher H_2O_2 production than GFP-like proteins, DsFbFpM49I showed the highest H_2O_2 production. 0.2 U/mL HRP and 0.05 mM Amplex Red were used. PSPs were adjusted to absorption of 0.02 at their absorption maximum (ex 450 nm for LOV proteins and KillerOrange and ex 595 nm for KillerRed and SuperNova) in 50 mM NaPi pH 7.2, in a total volume of 100 µL. It was illuminated with Megaman Helix daylight lamp (1.02 mW/cm^2). The increase in fluorescence was measured at ex 550 nm / em 595 nm, and corrected by the average fluorescence of the untreated reaction mixture and by the autoxidation of the assay reagent, values are mean ± σ for n = 3.

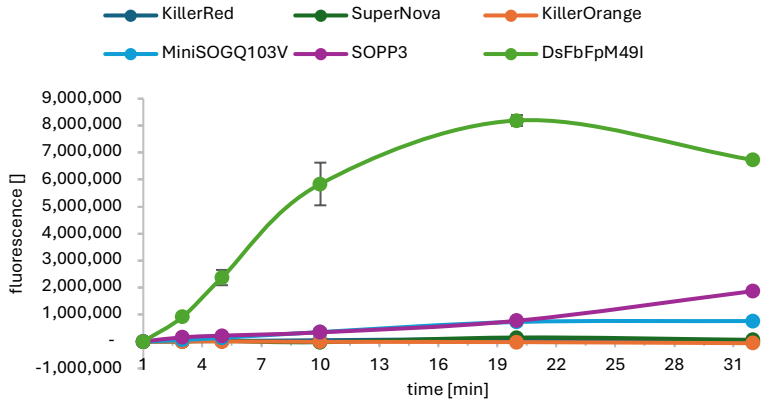

Figure 46| Results of the Amplex Red assay for the detection of H_2O_2 and $O_2^{\bullet-}$. LOV proteins showed higher H_2O_2 and $O_2^{\bullet-}$ production than GFP-like proteins, DsFbFpM49I showed the highest H_2O_2 and $O_2^{\bullet-}$ production. 0.2 U/mL HRP, 2 U/mL SOD, and 0.05 mM Amplex Red were used. PSPs were adjusted to absorption of 0.02 at their absorption maximum (ex 450 nm for LOV proteins and KillerOrange and ex 595 nm for KillerRed and SuperNova) in 50 mM NaPi pH 7.2, in a total volume of 100 µL. It was illuminated with Megaman Helix daylight lamp (1.02 mW/cm^2). The increase in fluorescence was measured at ex 550 nm / em 595 nm, and corrected by the average fluorescence of the untreated reaction mixture and by the autoxidation of the assay reagent, values are mean ± σ for n = 3.

To make quantitative statements, calibrations with H_2O_2 were done for both assays (Figure 47). Results showed that H_2O_2 and $O_2^{\bullet-}$ concentrations approximately range up to 4 µM (DsfbfpM49I) in the first 0.5 hour. It is important to mention that these absolute values are hardly comparable to values obtained in other studies. The setup of the experiment must be the same. Different protein or reagent concentrations, light conditions, calibration parameters, or detection parameters influence the outcome of the assay. During the assays, there was also a lot of variation between calibration curves which were done with different working solutions. This could be attributed to pipetting errors in this very low concentration range. Consequently, absolute H_2O_2 concentrations were not fully comparable between the different PSPs. To make a better comparison between all PSPs for both H_2O_2 and superoxide measurement, it would be advantageous to measure both assays and both calibration curves (one time in presence and one time in absence of SOD) on the same day with the same working solution. Nevertheless, the results were mostly comparable with previous literature. However, in one study, SOPP3 was reported to show higher H_2O_2 production levels than DsFbFpM49I.[93] The results presented in this work results clearly show the opposite behavior.

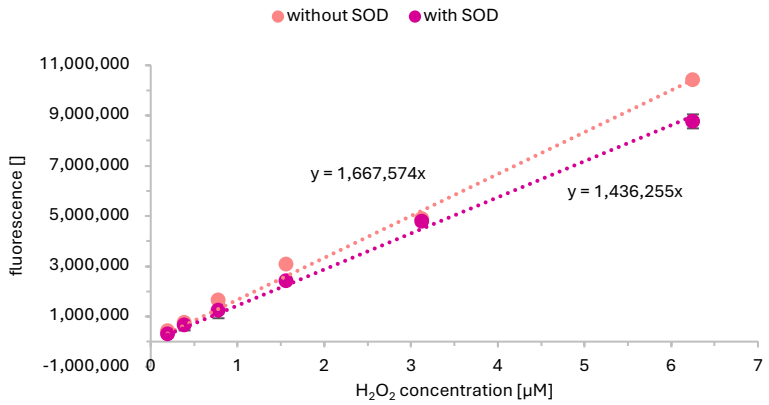

Figure 47| Calibration curve for the Amplex Red assay. Samples with known concentrations of H_2O_2 (0.20 µM, 0.39 µM, 0.78 µM, 1.56 µM, 3.13 µM, 6.25 µM) were prepared one time in the absence and one time in the presence of SOD. 0.2 U/mL HRP and 0.05 mM Amplex Red were used, without or with the addition of 2 U/mL SOD, in 50 mM NaPi pH 7.2, in a total volume of 100 µL. The increase in fluorescence was measured at ex 550 nm / em 595 nm, and corrected by the average fluorescence of the working solution without H_2O_2, values are mean ± σ for n = 3.

3.3.2.1.1 Quenching effect

The product of the Amplex Red assay resorufin emits fluorescence at 587. This interferes with the absorption spectra of SuperNova and KillerRed, which leads to a possible quenching of the fluorescence emitted by resorufin, and therefore to a weakening of the detected signal. To evaluate the quenching effect, known concentrations of H_2O_2 were measured via Amplex Red assay with or without the addition of KillerRed or SuperNova into the reaction mixture. Then, the measured fluorescence intensities were compared (Figure 48). Lower fluorescence intensities were observed in samples containing KillerRed or SuperNova when the H_2O_2 concentration rose above 0.5 µM. This indicates a quenching of the fluorescence of resorufin after this specific H_2O_2 concentration.

However, as this H_2O_2 concentration was never exceeded during the H_2O_2 or $O_2^{\bullet-}$ assay, it can be assumed that this quenching effect did not have any consequences on the results. For other applications with higher H_2O_2 concentrations, the detection method should be changed (for example dihydroethidium bleaching).[97]

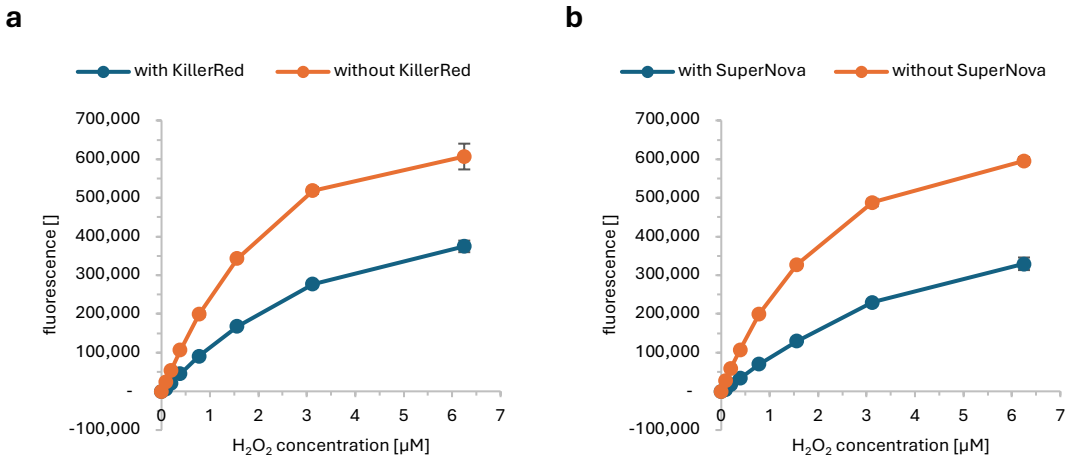

Figure 48| Quenching effect of KillerRed and SuperNova. Samples with known concentrations of H_2O_2 (0.20 µM, 0.39 µM, 0.78 µM, 1.56 µM, 3.13 µM, 6.25 µM) were prepared with or without the addition of KillerRed (**a**) or SuperNova (**b**), respectively. When the H_2O_2 concentration rose above 0.5 µM, a quenching effect was visible. 0.2 U/mL HRP and 0.05 mM Amplex Red were used in 50 mM NaPi pH 7.2, in a total volume of 100 µL. The increase in fluorescence was measured at ex 550 nm / em 595 nm, and corrected by the average fluorescence of the working solution without H_2O_2, values are mean ± σ for n = 3.

3.3.2.1.2 pH stability measurements

For further characterization of the PSPs and to explore the possibility of combining PSP-catalyzed ROS production with a conventional Fe^{2+}-catalyzed Fenton reaction in an acidic milieu, the stability of the proteins at different pH values was tested. Phosphate-citrate buffers with pH 4, 5, 6, 7, and 8 were prepared by mixing 0.2 M Na_2HPO_4 with 0.1 M citric acid and adjusting the pH value using a pH meter. LOV proteins were incubated for 30 min in these phosphate-citrate buffers. Fluorescence intensities of the PSPs after incubation at the different pH values were measured (chapter 6.8.1). Then, Amplex Red and HRP were added, the samples were illuminated for 10 min and the formation of H_2O_2 was determined by fluorescence measurement. For each pH value, a separate calibration curve was measured (to consider a change in the activity of HRP and the differences in fluorescence behavior of resorufin at different pH values, Figure 49). These calibration curves were used for the quantification of H_2O_2 production by the LOV proteins at different pH values. Results indicate that the LOV proteins were still active in a slightly acidic milieu around pH 5-6 (Figure 50). However, at pH 5 there was already less H_2O_2 production, and at pH 4 no H_2O_2 production could be observed.

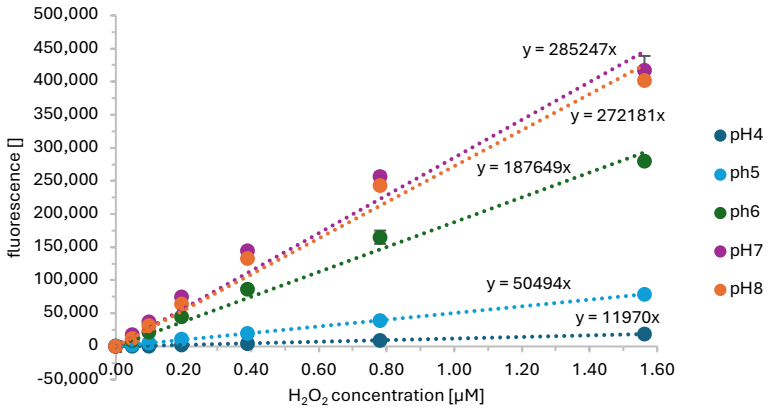

Figure 49| Calibration curves for the Amplex Red assay at different pH values. Samples with known concentrations of H_2O_2 (0.20 µM, 0.39 µM, 0.78 µM, 1.56 µM) were prepared in the pH-adjusted phosphate-citrate buffer. 0.2 U/mL HRP and 0.05 mM Amplex Red were used in the respective phosphate-citrate buffer, in a total volume of 100 µL. The increase in fluorescence was measured at ex 550 nm / em 595 nm and corrected by the average fluorescence of the working solution, values are mean ± σ for n = 3.

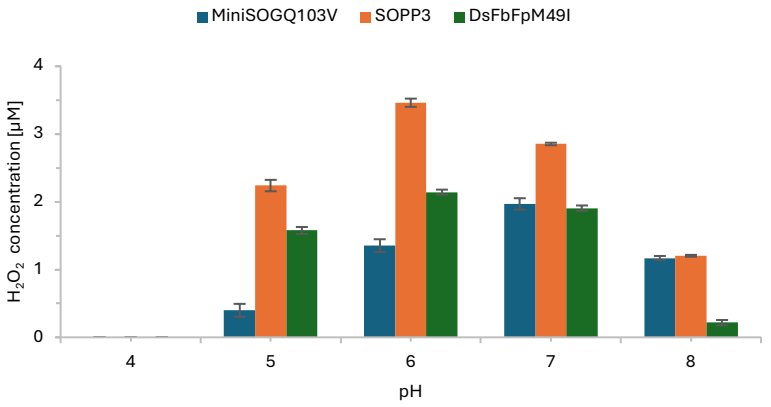

Figure 50| H_2O_2 production by LOV proteins at different pH values. H_2O_2 concentrations were calculated according to H_2O_2 calibration curves at different pH values. 0.2 U/mL HRP and 0.05 mM Amplex Red were used in the respective phosphate-citrate buffer, in a total volume of 100 µL. The increase in fluorescence was measured at ex 550 nm / em 595 nm and corrected by the average fluorescence of the untreated reaction mixture and by the autoxidation of the assay reagent, values are mean ± σ for n = 3.

3.3.2.2 Quantification of $^1O_2$ production

The Singlet Oxygen Sensor Green (SOSG) assay is based on the ability of the compound SOSG to react specifically with singlet oxygen $^1O_2$ to form a fluorescent product (Scheme 4). In the non-fluorescent SOSG, the fluorescence is quenched through intramolecular electron transfer. Upon reaction with $^1O_2$, the SOSG-endoperoxide (SOSG-EP) is formed. The intramolecular electron transfer is stopped and the molecule can emit green fluorescence.[186] This makes the relative quantification of $^1O_2$ possible. An absolute quantification is not possible, because a calibration with $^1O_2$ cannot be conducted. There are some doubts regarding the selectivity of the assay. Some studies suggest that SOSG

can partially react with other ROS.[187] However, this was not made the subject of discussion in this thesis.

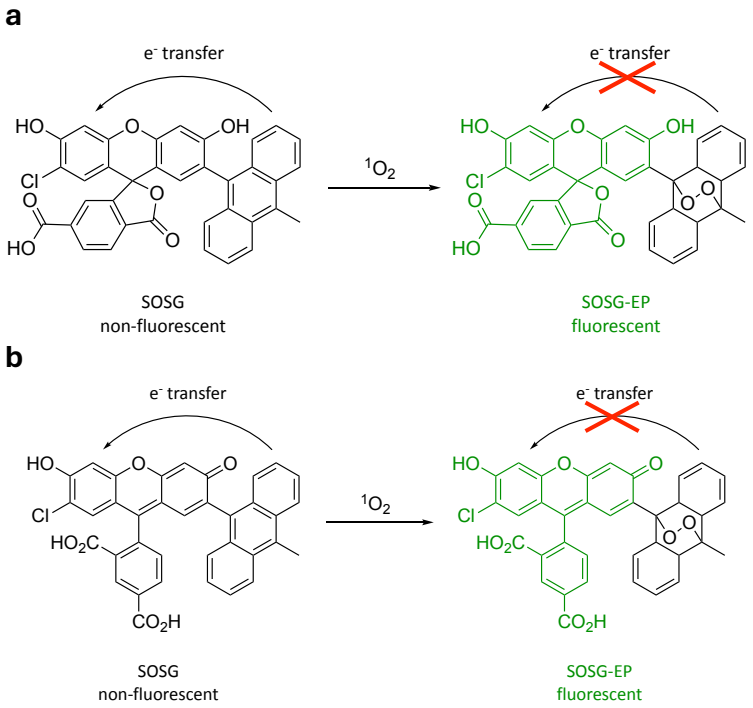

Scheme 4| The SOSG assay. $^1O_2$ reacts with the reagent SOSG to form the SOSG-endoperoxide. Before reaction with $^1O_2$, internal electron transfer quenches the fluorescence of chromophore structure. After the formation of the endoperoxide, electron transfer is not possible anymore and the chromophore structure is fluorescent (highlighted in green). **a**, The structure of SOSG by Molecular Probes, Inc.[187,188] **b**, The structure of SOSG by Lumiprobe GmbH.[189]

In initial trials during the development of the assay, a drop in fluorescence due to the assumed overoxidation/degradation of the fluorescent assay product could be observed. Therefore, assay conditions, primarily the light intensity and reagent concentration, were optimized.

As described for the Amplex Red assay in the previous chapter (chapter 3.3.2.1), dark controls were done (Figure 51). Moreover, the autoxidation of SOSG by light was measured. A slight increase in fluorescence could be observed (Figure 52). Another aspect that must be mentioned is, that the absorption and fluorescence of the PSP KillerOrange and the assay reagent SOSG overlap, which could lead to a lower sensitivity of the assay for KillerOrange. There must be paid attention to the correction of the results by the fluorescence of KillerOrange itself.

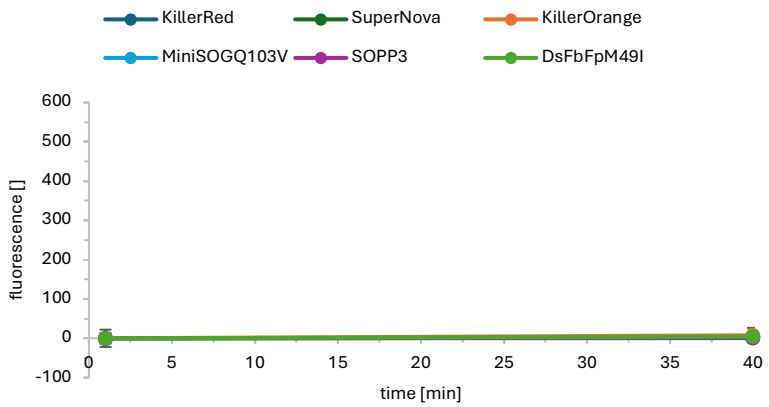

Figure 51| Dark controls for the SOSG assay for $^1O_2$ detection. Reaction mixtures with the respective PSPs were incubated in the dark. Almost no rise in fluorescence was observed. 1 µM SOSG was used. PSPs were adjusted to absorption of 0.02 at their absorption maximum (ex 450 nm for LOV proteins and KillerOrange and ex 595 nm for KillerRed and SuperNova) in 50 mM NaPi pH 7.2, in a total volume of 100 µL. The increase in fluorescence was measured at ex 510 nm / em 530 nm and corrected by the average fluorescence of the initial mixture, values are mean ± σ for n = 3.

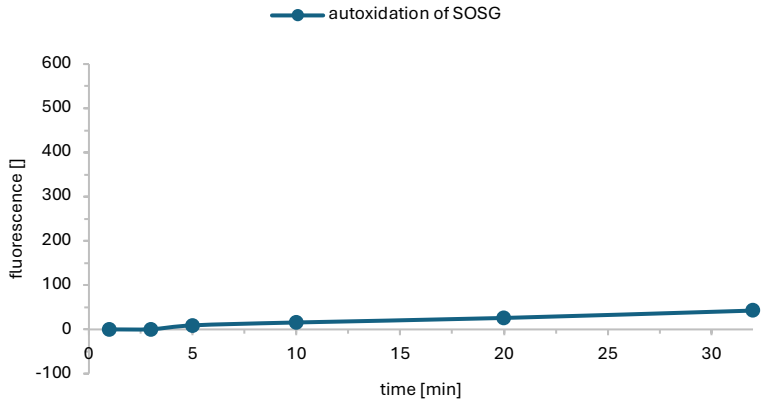

Figure 52| Autoxidation of SOSG by light. Only a slight increase in fluorescence signal was observed. 1 µM SOSG was used in 50 mM NaPi pH 7.2, in a total volume of 100 µL. It was illuminated with Megaman Helix daylight lamp (1.02 mW/cm^2). The increase in fluorescence was measured at ex 510 nm / em 530 nm and corrected by the average fluorescence of the initial mixture, values are mean ± σ for n = 3.

As already observed in the Amplex Red assay for H_2O_2 and $O_2^{\bullet-}$ detection, the LOV proteins produce significantly higher $^1O_2$ levels than the GFP-like proteins (Figure 53). Here, the LOV protein SOPP3 showed slightly higher $^1O_2$ production than the other two LOV proteins. In previous studies, LOV proteins have also been reported to produce higher levels of $^1O_2$ than GFP-family proteins.[77,97] However, in most of these studies, $^1O_2$ is directly measured via its phosphorescence at 1275 nm.

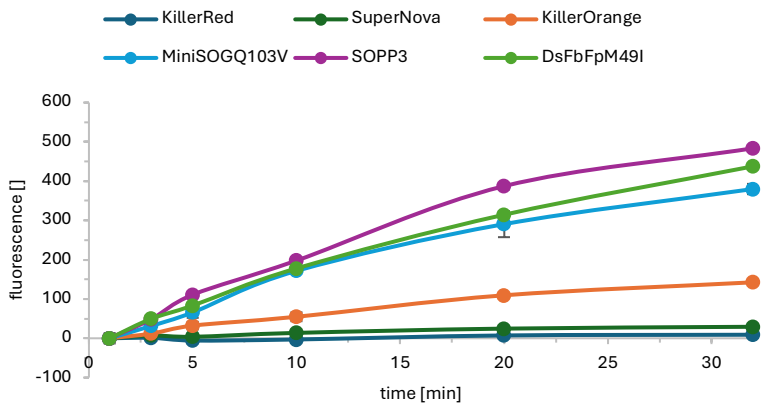

Figure 53| Results of the SOSG assay for the detection of $^1O_2$. LOV proteins show higher $^1O_2$ production than GFP-like proteins. 1 µM SOSG, was used. PSPs were adjusted to absorption of 0.02 at their absorption maximum (ex 450 nm for LOV proteins and KillerOrange and ex 595 nm for KillerRed and SuperNova) in 50 mM NaPi pH 7.2, in a total volume of 100 µL. It was illuminated with Megaman Helix daylight lamp (1.02 mW/cm^2). The increase in fluorescence was measured at ex 510 nm / em 530 nm and corrected by the average fluorescence of the untreated reaction mixture and by the autoxidation of the assay reagent, values are mean ± σ for n = 3.

3.3.2.3 Quantification of HO• production

As elucidated in the chapter 1.2, hydroxyl radical HO• is the most reactive oxygen species towards the attack of covalent C-H or C-C bonds. Hydroxyl radical (HO•), hypochlorite ($^-$OCl), peroxynitrite anions (ONOO$^-$), or peroxy radical (ROO•) are classified as highly reactive oxygen species (hROS). The assay reagent aminophenyl fluorescein (APF) reacts specifically with hROS resulting in the formation of fluorescein (Scheme 5).[190] Fluorescein can be detected fluorometrically and correlated to the hROS concentration. As in the SOSG assay for $^1O_2$ detection, a HO•-calibration for this assay is not possible, because of the short half-life of HO•.

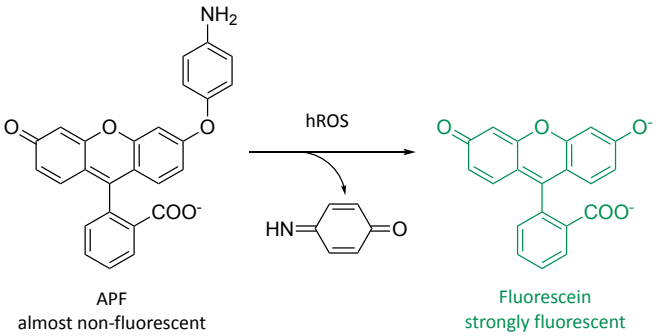

Scheme 5| The APF assay. Highly reactive oxygen species (hROS) react with APF and form the fluorescent product Fluorescein (highlighted in green).

Also, for this assay, dark controls were done (Figure 54). Moreover, the autoxidation of APF by light was measured. A slight increase in fluorescence could be observed (Figure 55).

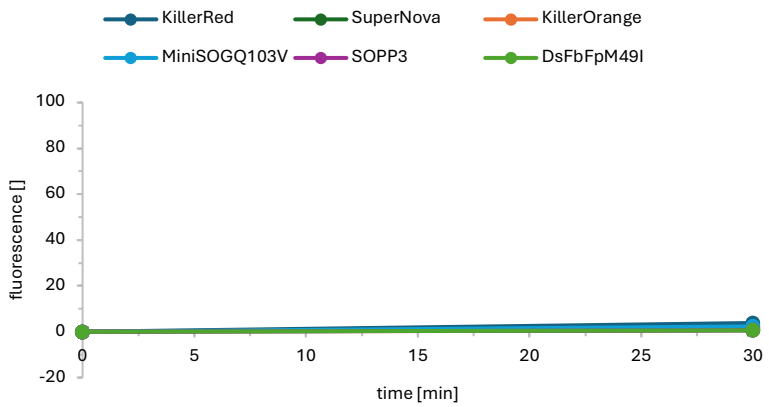

Figure 54| Dark controls for the APF assay for HO• detection. Reaction mixtures with the respective PSPs were incubated in the dark. Almost no rise in fluorescence was observed. 5 µM APF was used. PSPs were adjusted to absorption of 0.02 at their absorption maximum (ex 450 nm for LOV proteins and KillerOrange and ex 595 nm for KillerRed and SuperNova) in 50 mM NaPi pH 7.2, in a total volume of 100 µL. The increase in fluorescence was measured at ex 495 nm / em 515 nm and corrected by the average fluorescence of the initial mixture, values are mean ± σ for n = 3.

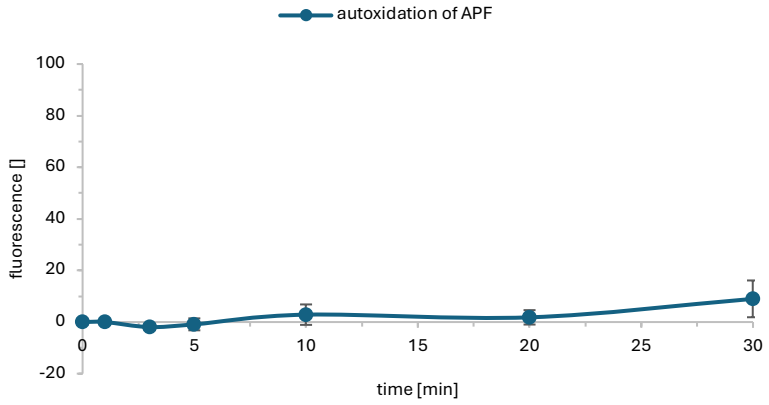

Figure 55| Autoxidation of APF by light. A slight increase in fluorescence signal was observed. 5 µM APF was used in 50 mM NaPi pH 7.2, in a total volume of 100 µL. It was illuminated with Megaman Helix daylight lamp (1.02 mW/cm^2). The increase in fluorescence was measured at 495 nm / em 515 nm and corrected by the average fluorescence of the initial mixture, values are mean ± σ for n = 3.

Following the previous trend, the LOV proteins produced significantly higher HO• levels than the GFP-like proteins (Figure 56). The LOV protein SOPP3 showed higher HO• production than the other two LOV proteins. GFP-like proteins (KillerRed, SuperNova, and KillerOrange) did not show any detectable HO• production.

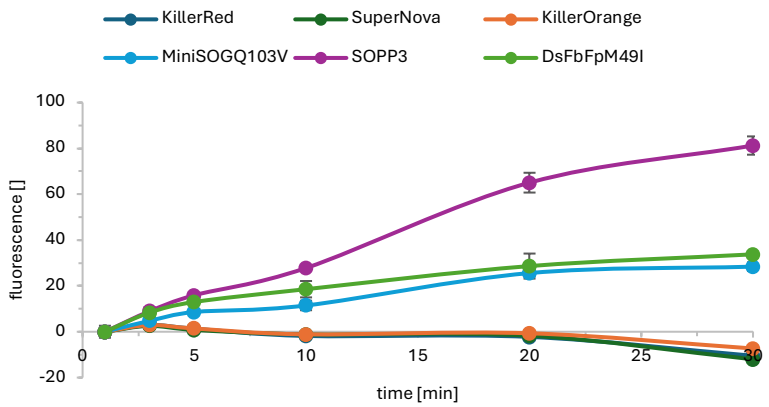

Figure 56| Results of the APF assay for the detection of HO•. LOV proteins showed HO• production, whereas with GFP-like proteins no HO• formation could be detected. 5 µM APF was used. PSPs were adjusted to absorption of 0.02 at their absorption maximum (ex 450 nm for LOV proteins and KillerOrange and ex 595 nm for KillerRed and SuperNova) in 50 mM NaPi pH 7.2, in a total volume of 100 µL. It was illuminated with Megaman Helix daylight lamp (1.02 mW/cm^2). The increase in fluorescence was measured at 495 nm / em 515 nm and corrected by the average fluorescence of the untreated reaction mixture and by the autoxidation of the assay reagent, values are mean ± σ for n = 3.

3.3.2.4 Add-on to the quantification of ROS production

It was not completely clear during the initial trials which LOV PSP (MiniSOGQ103V, SOPP3, DsFbFpM49I) should be used for the assembly of fusion proteins. Therefore, three different fusion proteins with the conformation PSP-linker-mHGF1-linker-PSP-6xHis (design, assembly, and protein production of fusion proteins are described in chapters 3.5, 3.6, and 3.7) were analyzed via SOSG and APF assay. Protein samples were normalized to their molar concentration, as opposed to normalization by absorption during the characterization of the original proteins. The results agreed with the characterization of the original proteins. The fusion protein containing DsFbFpM49I produced the highest amounts of ROS, while the fusion protein containing MiniSOGQ103V produced comparable or lower amounts of ROS than the fusion protein containing SOPP3 (Figure 57). Therefore, the assembly of fusion proteins was continued with only two PSPs, SOPP3 and DsFbFpM49I.

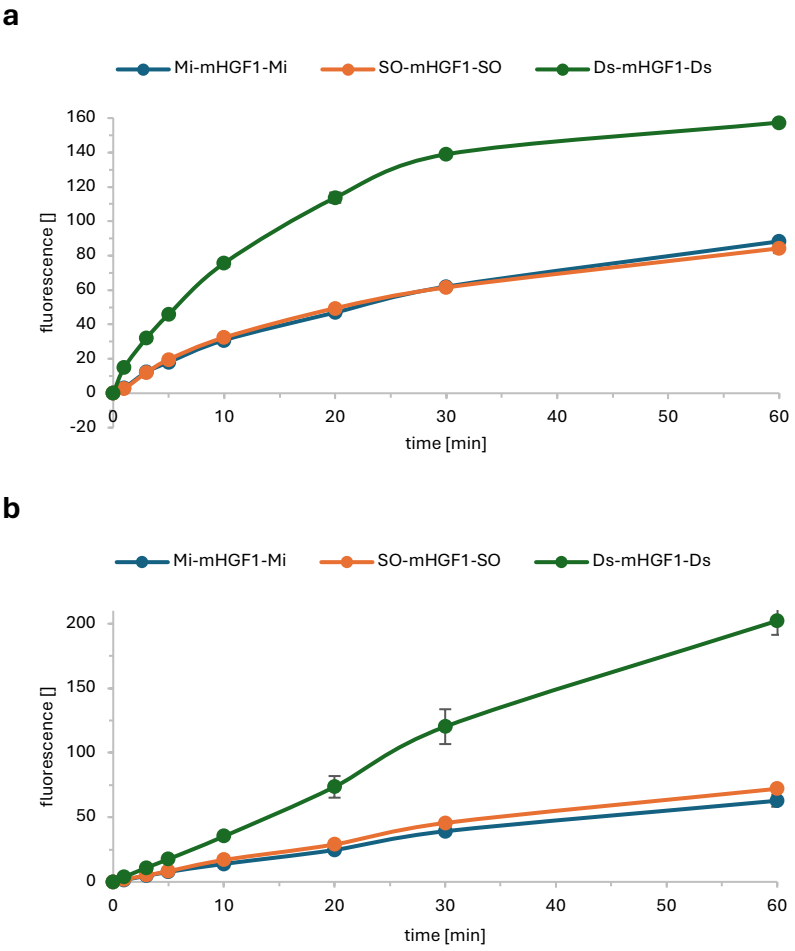

Figure 57|Analysis of $^1O_2$ and HO$^\bullet$ production by fusion proteins with the conformation LOV-linker-mHGF1-linker-LOV-6xHis. Samples were incubated for 0, 1, 3, 5, 10, 20, 30, and 60 min. Protein samples were adjusted to 5 µM protein concentration in 50 mM NaPi buffer, in a total volume of 100 µL. It was illuminated with Eurolite IP FL-30 SMD blue, IP65 (0.9 mW/cm^2). It was corrected by the average fluorescence of the untreated reaction mixture, values are mean ± σ for n = 3. Mi = MiniSOQ103V, SO = SOPP3, Ds = DsFbFpM49I. **a**, SOSG assay for analysis of $^1O_2$ production. 2 µM SOSG reagent was used.[189] The increase in fluorescence was measured at ex 510 nm / em 530 nm. **b**, APF assay for analysis of HO$^\bullet$ production. 20 µM APF reagent was used. The increase in fluorescence was measured at ex 495 nm / em 515 nm.

3.4 Attempts to establish a model reaction for PE degradation

Because of the difficulties that arose during the analysis of polymer degradation (as described in chapter 3.11), there was an attempt to establish a model reaction for PE degradation. The model reaction should be based on short-chain alkanes, which can be analyzed by nuclear magnetic resonance (NMR). The short-chain alkanes *n*-heptane and *n*-dodecane were used. First, to establish a positive control reaction for oxidative degradation of these short-chain alkanes, the Fenton reaction was conducted. As explained in chapter 1.1.2.2, during the Fenton reaction, $HO^{\bullet}$ is produced which then can oxidize the alkane. Incubation of *n*-heptane with Fenton's reagent (0.2 M *n*-heptane, 15 % (ω/ω) H_2O_2, 10 mM $FeSO_4$, in Milli-Q H_2O, pH 5, 2 h) and analysis by NMR after extraction of the reaction solution with $CDCl_3$ showed that there is a very small amount of oxidative degradation of the alkane (Figure 58). However, when the same experiment was conducted with the longer chain alkane, *n*-dodecane, no signals indicating degradation were observed in the NMR. These results suggested that probably solubility was the limiting factor, as n-dodecane is completely insoluble in H_2O, whereas *n*-heptane still shows some marginal solubility (0.0003 % at 20 °C).[191]

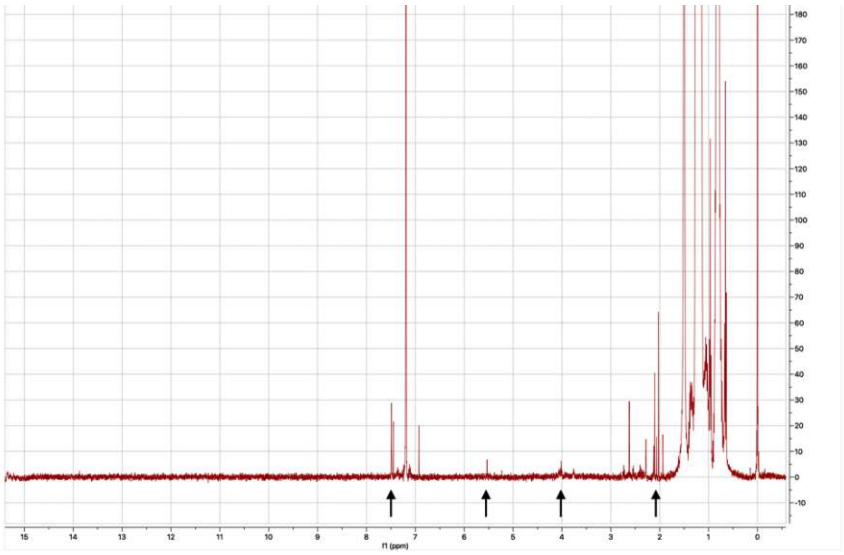

Figure 58| ^{1}H NMR (200 MHz, $CDCl_3$) spectrum of *n*-heptane treated with Fenton's reagent. 0.2 M *n*-heptane were incubated with 15 % (ω/ω) H_2O_2 and 10 mM $FeSO_4$ in Milli-Q H_2O, at pH 5, for 2 h. Potential degradation signals are indicated with black arrows.

In the previous chapter 3.3.2, it was shown that the LOV proteins produce $HO^{\bullet}$. Therefore, attempts were made to conduct the experiment in the presence of a LOV protein instead of the Fenton's reagent. Thus, *n*-heptane was illuminated in the presence of the LOV protein SOPP3 (0.4 mM *n*-heptane, 1.19 mM SOPP3, stirring with 450 rpm, 3.9 mW/cm^2, 21 h). A control experiment was conducted as well, where the aqueous *n*-heptane solution was incubated under the same conditions. Analysis by NMR after extraction of the reaction solution with $CDCl_3$ showed that potential degradation signals indicating the formation of hydroxyl groups were visible in the range of 4.5-3.5 ppm (Figure 59, a). These are more prominent in the reaction with the protein SOPP3 than in the light control reaction without protein. However, the difference was not significant. As suggested previously, the solubility of the alkane in H_2O and the short half-life of the $HO^{\bullet}$ radical

were presumed to be the limiting factors for the success of the degradation reaction, either by the Fenton's reagent or by the LOV protein. One approach to tackle this problem was the addition of a surfactant to enhance the solubility of *n*-heptane. Therefore, 0.5 % (v/v) Tween20 was added to the *n*-heptane degradation reaction by the LOV protein SOPP3. However, it became apparent that the signals for the surfactant interfered with potential *n*-heptane degradation signals, making the interpretation of the NMR spectra impossible. Alternatively, 1-heptanol was used instead of *n*-heptane SOPP3 (0.4 mM 1-heptane, 0.23 mM SOPP3, stirring with 450 rpm, 3.9 mW/cm^2, 21 h). An additional control experiment was conducted with the protein SOPP3 but without illumination. Solubility was not significantly improved. However, some degradation signals indicating the formation of aldehyde groups (9.75 ppm) and hydroxyl or alkene groups (4.65 ppm) could only be detected in the experiment with protein and light illumination (Figure 59, b). However, again the difference was not considered significant. Finally, sodium 1-heptanesulfonate which is a surfactant itself, was used as substrate. The reaction was conducted in D_2O and analyzed by NMR after protein precipitation and separation of the protein. However, because the aqueous phase was analyzed, signals from glycerol which was used for protein storage interfered with potential *n*-heptane degradation signals.

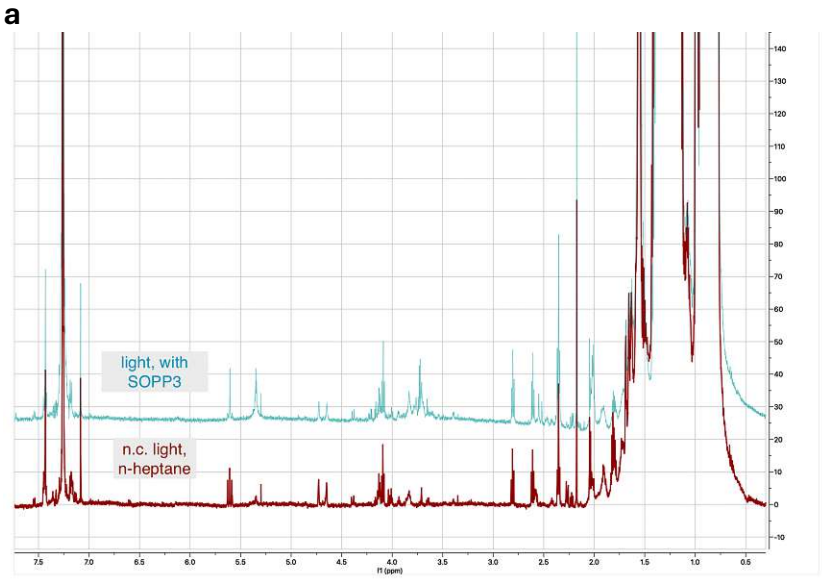

Figure 59| ^{1}H NMR spectra of *n*-heptane or 1-heptanol treated with LOV protein SOPP3. a, 0.4 M *n*-heptane was incubated with 1.19 mM SOPP3 in Milli-Q H_2O while stirring (450 rpm) and illuminating (3.9 mW/cm^2) for 21h. The NMR spectrum (200 MHz, $CDCl_3$) shows the reaction with protein SOPP3 in cyan and the light control experiment without protein in brown. Some additional potential degradation signals are visible in the range of 4.5-3.5 ppm.

b

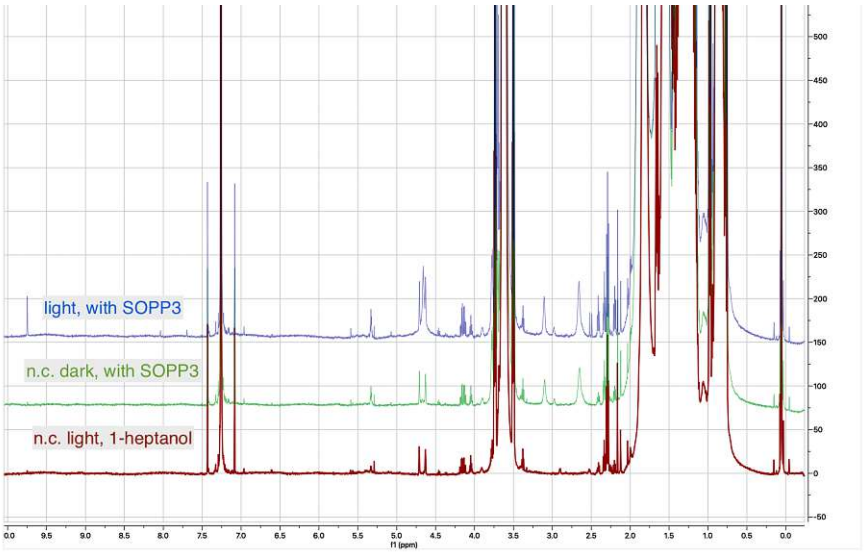

Figure 59| continued. b, 0.4 M 1-heptanol was incubated with 0.23 mM SOPP3 in Milli-Q H_2O while stirring (450 rpm) and illuminating (3.9 mW/cm^2) for 20h. The NMR spectrum (600 MHz, $CDCl_3$) shows the reaction with protein SOPP3 in blue, a dark control experiment with protein in green, and the light control experiment without protein in brown. Some potential degradation signals are visible at 9.75 and 4.65 ppm.

Another approach was the combination of the PSPs, which are potent H_2O_2 producers, with Fe^{2+} to mimic a Fenton's reagent. However, a problem arose due to the stability of the proteins in an acidic milieu. The protein precipitated in an acidic milieu or after the addition of $FeSO_4$ which also resulted in a slightly acidic milieu. An attempt was made to circumvent this problem by conducting the reaction in a buffered system, however, the acidic milieu was necessary for the progress of the Fenton reaction, because of the instability of the Fe^{2+} ion at higher pH.

Overall, several attempts were conducted to detect degradation of the model substrate *n*-heptane. Even though degradation of *n*-heptane by Fenton's reagent could be observed via NMR, no significant signals could be observed for degradation attempts with the LOV proteins. The interpretation of the obtained results was very difficult. The primary problem for all attempts was the incompatibility of the solubility of the alkane and the protein. This made finding a suitable substrate very difficult. These experiments underlined the hypothesis that the limiting factor for oxidative polyolefin degradation is the proximity of hydrophilic protein and hydrophobic polyolefin.

3.5 Design of plasmids for cloning – fusion proteins with hydrophobins

Next, hydrophobic elements, which should improve adsorption to a hydrophobic polyolefin surface, were attached to the ROS-generating PSPs by molecular cloning. After the results obtained during the assay for quantification of ROS production (chapter 3.3.2), it became clear that the LOV proteins showed much higher activity than the GFP-like PSPs. Moreover, MiniSOGQ103V showed the lowest ROS production of the three LOV proteins. Therefore, it was decided to continue only with the LOV proteins SOPP3 and DsFbFpM49I. Initially, there were created some fusion proteins containing MiniSOGQ103V, however, for clarity, this is not mentioned here (chapter 3.3.2.4).

Hydrophobins were chosen for the creation of fusion proteins consisting of PSP (LOV protein) and hydrophobin (as described in the chapter 1.4). The chosen hydrophobins were the following:

- mHGF1 (cysteine → serine mutant) – derived from *Grifola frondosa*
- HFB1 – derived from *Trichoderma reesei*
- HFB2 – derived from *Trichoderma reesei*

Genetic sequences of the proteins were codon optimized for production in *E. coli* using online tools for codon optimization.[175,176] Then, the company Twist Bioscience was chosen for the DNA synthesis of the genes of interest. There was no intention to express the hydrophobins in their original form before the fusion to the PSPs. Therefore, the cloning vector ptwistamphighcopy (from Twist Bioscience) was chosen as a vector for storage and a template for cloning.

The expression vector pET29b(+) with the T7 expression system for high-yield production in E. *coli* BL21(DE3) was chosen for all fusion proteins. A rigid linker (with the amino acid sequence AEAAAKEAAAKEAAAKA) was used for the connection of PSP and hydrophobin.[192] A C-terminal 6 x His tag was included for purification via immobilized metal affinity chromatography (IMAC).

Initially, the plan was to develop fusion proteins with all three hydrophobins in two different conformations. Moreover, it was decided to just add a small hydrophobic element next to the PSP. As a hydrophobic element, there was chosen a α-helix (LA)12.[193,194] The structures of all planned constructs are shown in Figure 60, a. Due to difficulties in expression (chapter 3.7), 2 more conformations were developed. In one conformation, the hydrophobin and the PSP genetic sequences were switched, so that the 6 x His tag was located next to the PSP. The second conformation was the insertion of a flexible linker (with the amino acid sequence GGGGSGGGGS) between the fusion protein and the 6 x His tag (Figure 60, b).[192] An exemplary plasmid map of a fusion protein showing the organization of the respective genetic fragments is shown in Figure 61. Libraries of all fusion proteins and all genetic sequences are listed in chapters 6.1 and 6.2.

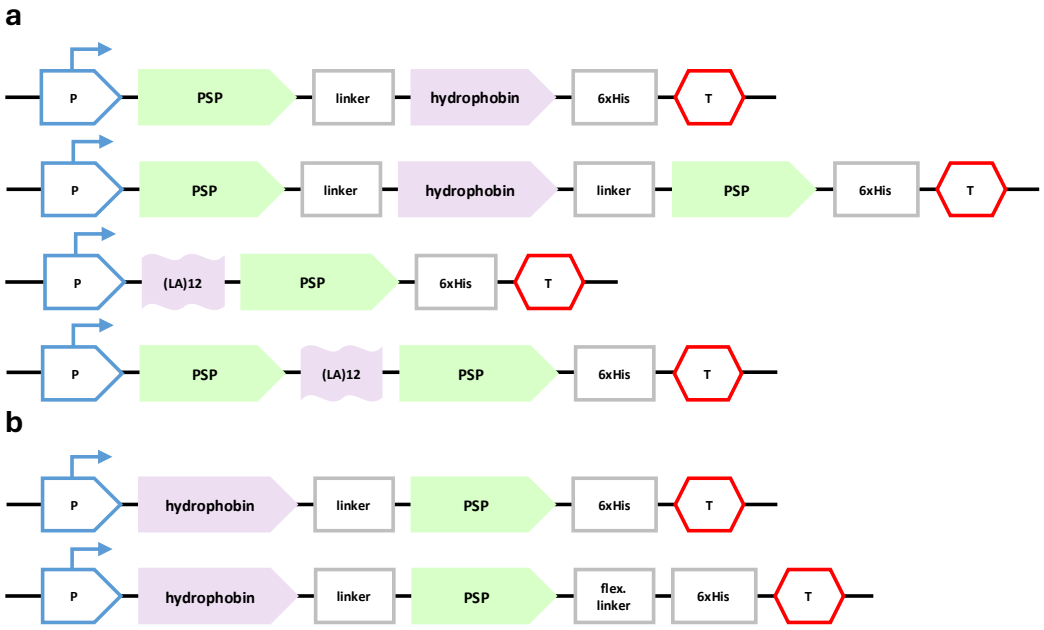

Figure 60| Design of the genetic constructs for fusion protein production. The designs show different concepts of genetic constructs for the combination of a PSP (LOV protein) with a hydrophobin or a short hydrophobic α-helix (LA)12. P = promoter, PSP = photosensitizing protein, linker = rigid linker AEAAAKEAAAKEAAAKA, hydrophobin = mHGF1, HFB1 or HFB2, (LA)12 = helix, 6xHis = tag for purification via IMAC, flex. linker = flexible linker GGGGSGGGGS, T = terminator. **a**, Initially planned constructs. **b**, Additional constructs.

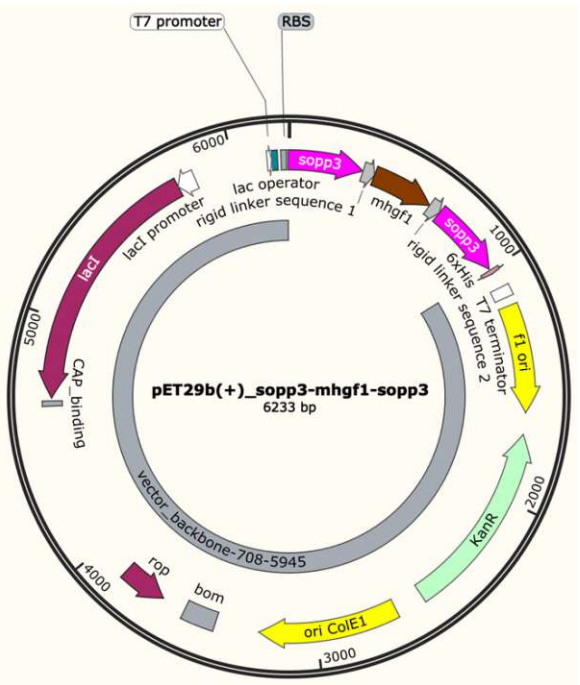

Figure 61| An exemplary plasmid map of the genetic construct for the expression of the fusion protein SOPP3-mHGF1-SOPP3. The pET29b(+) vector contains the gene encoding the fusion protein SOPP3-mHGF1-SOPP3, a 6 x His tag embedded in a T7 expression cassette (lac inhibitor (lacI) with lacI promoter, T7 promoter, lac operator, ribosome binding site (RBS) and T7 terminator). Other relevant genetic elements are the kanamycin resistance (KanR) and a high-copy-number ColE1 origin of replication.

3.6 Assembly of fusion protein constructs

For the assembly of the respective genetic constructs in the expression vector, molecular cloning was done. In practice, this was achieved by the assembly of two DNA fragments: the plasmid backbone and an insert. Genetic fragments with overlapping DNA overhangs were generated by PCR. After gel electrophoresis, followed by gel extraction and purification of the fragments, the constructs were assembled by NEBuilder HiFi DNA Assembly (Gibson isothermal assembly).[195] The Gibson isothermal assembly is a widely used cloning method, which is a single-reaction approach with few preparation steps and reagents for the parallel assembly of multiple DNA molecules.[196] In the assembly step, three enzymes are combined, namely a T5 exonuclease, which chews back 5' ends, a DNA polymerase which then extends the 3' ends, and in the last step a Taq DNA ligase for sealing the nicks (Figure 62). The enzymes are simultaneously active and do not compete with each other. The incubation at 50 °C helps to resolve secondary DNA structures which would interfere with the success of the assembly. Important factors for the success of the assembly are the length and the sequence of the overlapping regions. Short overlapping regions or homologous sequences may complicate the assembly substantially.

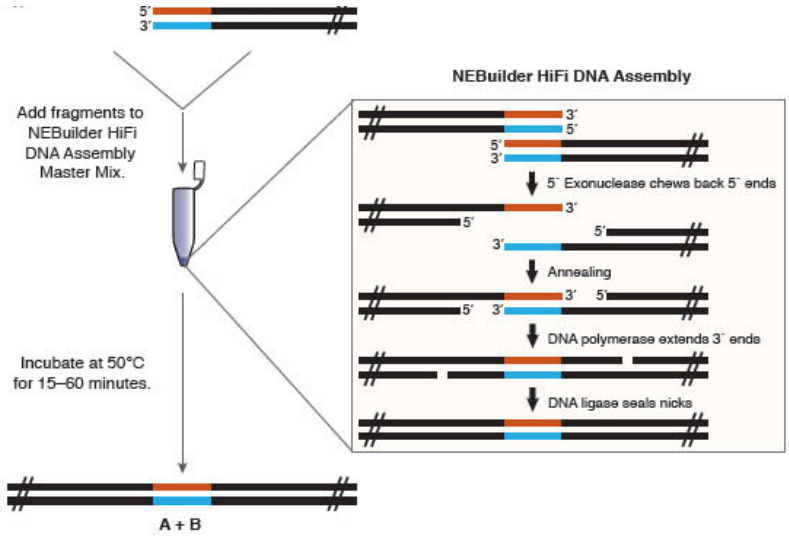

Figure 62| Illustration of the NEB HiFi DNA assembly method (Gibson isothermal assembly). The figure is adapted from www.neb-online.de. [197]

The constructs containing the hydrophobic α-helix (LA)12 were not generated by the assembly of two DNA fragments but by a Q5® site-directed mutagenesis. The DNA fragment for the (LA)12 helix was inserted into the respective plasmid by respective mutagenesis primers in a PCR reaction and the mutagenesis protocol was completed by sealing the ends in a Kinase, Ligase, and DpnI (KLD) treatment (Figure 63).[198]

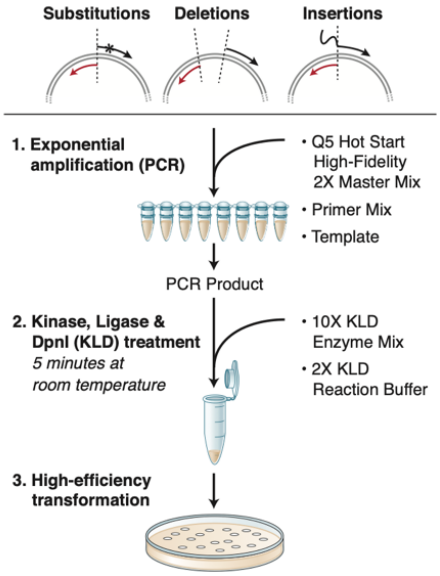

Figure 63| Illustration of the Q5® site-directed mutagenesis method. The figure is adapted from www.neb.com.[198]

After NEB HiFi DNA assembly or Q5® site-directed mutagenesis, the obtained assembled plasmid DNA was transformed in an *E. coli* cloning strain (*E. coli* Top 10). If the assembly was successful, the correct gene sequence was verified by colony PCR and sequencing. Only then, the plasmid was transformed in the *E. coli* expression strain (*E. coli* BL21(DE3)). Some assemblies had to be repeated, when transformation did not yield any colonies, or wrong positives were obtained because of problems with contamination.

The cloning protocol is described in chapter 5.12. All primers, parameters for molecular cloning, and analyses by gel electrophoresis are shown in chapter 6.

3.7 Protein production analysis of fusion proteins

Production of the fusion proteins was conducted in *E. coli* BL21(DE3), and an autoinduction protocol using media containing the inducer α-lactose, was followed.[178] Cultures were harvested and protein purification was done via IMAC. For Verification of the production of correct proteins, sodium dodecyl sulfate polyacrylamide gel electrophoresis (SDS-PAGE) was done.

Fusion proteins containing PSP and hydrophobin in a 1:1 ratio (PSP-linker-hydrophobin-6xHis) showed only a slight or no correct band after purification and analysis via SDS-PAGE. The first assumption was that the binding of the fusion protein to the Ni Sepharose™ column for purification via IMAC was not efficient. It was speculated that this was the case because of a hidden 6 x His tag. One way to approach this suspected problem, was the addition of a flexible linker in between the 6 x His tag and the hydrophobin, to create space and make the 6 x His tag accessible (PSP-linker-hydrophobin-flexlinker-6xHis). As a flexible linker, there was used the amino acid sequence GGGGSGGGGS. However, this approach was discarded as it did not show any expression. A second approach was to change the conformation by switching the location of the PSP and the hydrophobin, putting the 6 x His tag next to the PSP, where it may be more accessible (hydrophobin-linker-PSP-6xHis). After the comparison of the two original conformation PSP-linker-hydrophobin-6xHis with the new conformation hydrophobin-linker-protein-6xHis, it became clear that the change of position did not improve the outcome. However, it could be concluded that only constructs containing the hydrophobin mHGF1 in both conformations showed much better yield and purity after purifications than the constructs with the other two hydrophobins HFB1 and HFB2 (Figure 64).

a

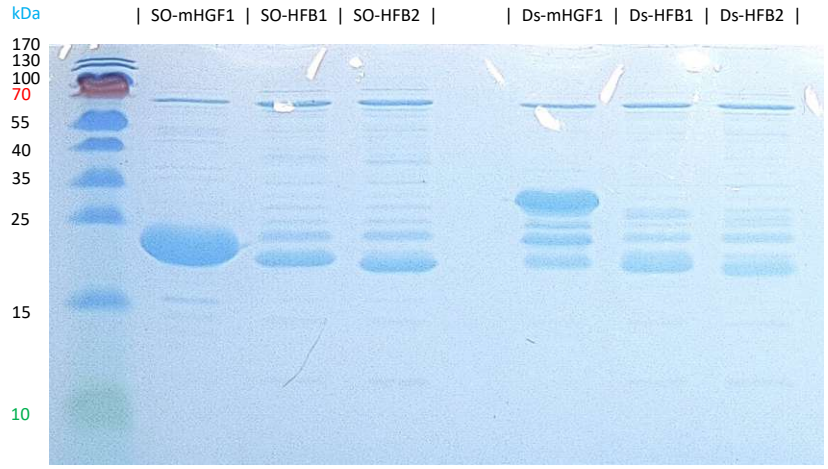

b

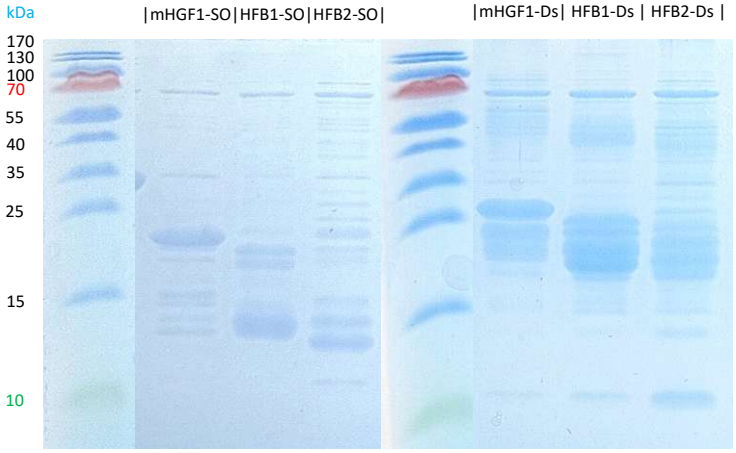

c

Protein	Size [kDa]
SO-mHGF1	23.2
SO-HFB1	22.2
SO-HFB2	21.9
Ds-mHGF1	26.9
Ds-HFB1	25.9
Ds-HFB2	25.5

d

Protein	Size [kDa]
mHGF1-SO	23.2
HFB1-SO	22.2
HFB2-SO	21.9
mHGF1-Ds	26.9
HFB1-Ds	25.9
HFB2-Ds	25.5

Figure 64| SDS-PAGE of fusion proteins PSP-linker-hydrophobin-6xHis and hydrophobin-linker-PSP-6xHis. Protein content was normalized to 5 µg protein per lane, and a 17.5 % acrylamide gel was used. SO = SOPP3, Ds = DsFbFpM49I. **a**, Only SO-mHGF1 and Ds-mHGF1 show a strong band with the expected size. **b**, Only mHGF1-SO and mHGF1-Ds show a strong band with the expected size. **c** & **d**, The expected molecular weight (size) of the fusion proteins.

To elucidate the cause for the poor yield of the fusion proteins containing the hydrophobins HFB1 and HFB2, soluble and insoluble fractions of the expressing cultures were compared. Bands for constructs PSP-linker-HFB1/HFB2-6xHis were visible in the insoluble fraction. However, there was almost no soluble expression of these constructs. That is why purification via IMAC led to very low protein yields. Constructs HFB1/HFB2-linker-PSP-6xHis did not show any detectable expression (Figure 65).

a

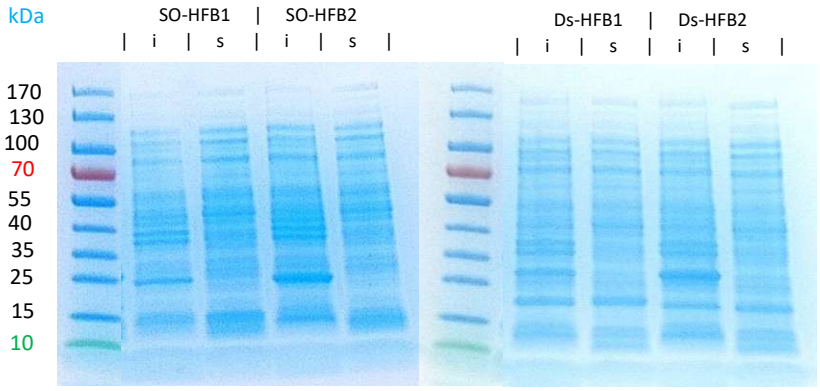

c

Protein	Size [kDa]
SO-HFB1	22.2
SO-HFB2	21.9
Ds-HFB1	25.9
Ds-HFB2	25.5

b

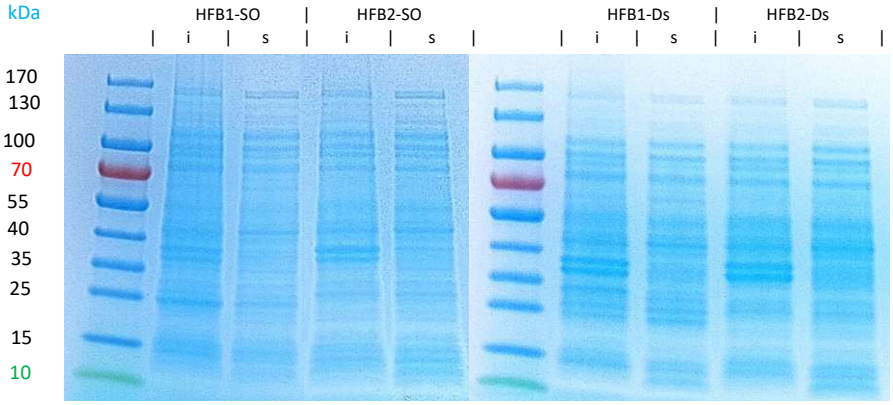

d

Protein	Size [kDa]
HFB1-SO	22.2
HFB2-SO	21.9
HFB1-Ds	25.9
HFB2-Ds	25.5

Figure 65| SDS-PAGE of the insoluble and soluble fractions of fusion proteins PSP-linker-HFB1/HFB2-6xHis and HFB1/HFB2-linker-PSP-6xHis. Protein content was normalized to 5 µg protein per lane, and a 17.5 % acrylamide gel was used. SO = SOPP3, Ds = DsFbFpM49I, i = insoluble, s =soluble. **a**, The correct band is visible in the insoluble fraction, however, not in the soluble fraction. **b**, No detectable expression is observed. **c** & **d**, The expected molecular weight (size) of the fusion proteins.

Constructs containing the hydrophobic α-helix (LA)12 next to the PSP in a 1:1 ratio ((LA)12-PSP) did not show expression. Constructs with PSP and (LA)12 in a 2:1 ratio (PSP-(LA)12-PSP) showed expression, however, the band was only visible in the insoluble fraction and no soluble expression was observed. Therefore, no purification was possible for these constructs (Figure 66).

a

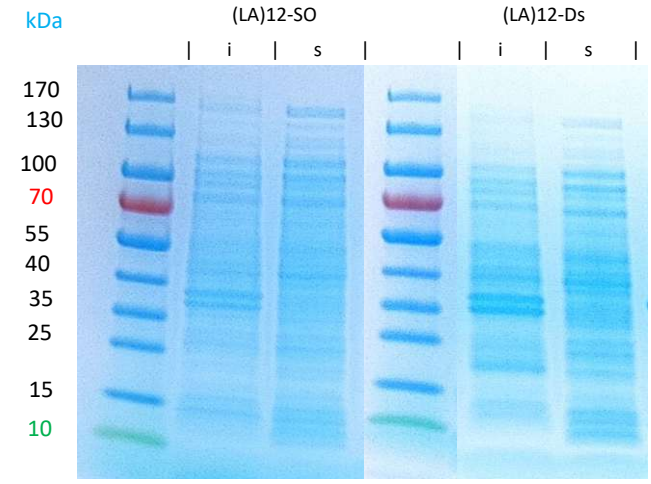

c

Protein	Size [kDa]
(LA)12-SO	15.6
(LA)12-Ds	19.3

b

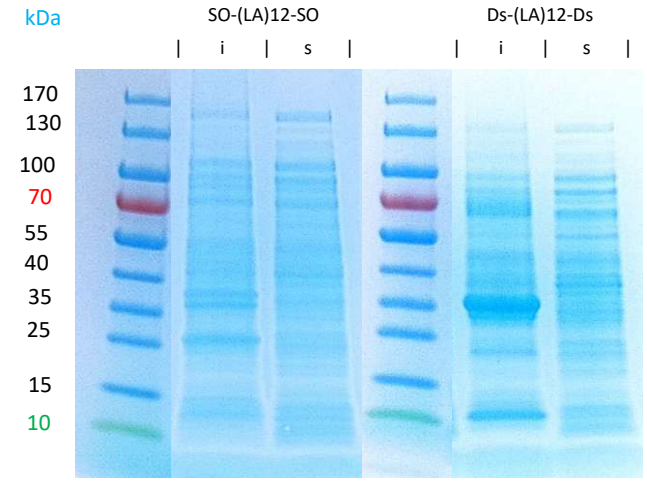

d

Protein	Size [kDa]
SO-(LA)12-SO	27.8
Ds-(LA)12-Ds	35.1

Figure 66| SDS-PAGE of constructs containing the hydrophobic α-helix (LA)12. Protein content was normalized to 5 µg protein per lane, and a 17.5 % acrylamide gel was used. SO = SOPP3, Ds = DsFbFpM49I, i = insoluble, s =soluble. **a**, No detectable expression is observed. **b**, The correct band is visible in the insoluble fraction, however, not in the soluble fraction. **c** & **d**, The expected molecular weight (size) of the fusion proteins.

Fusion proteins containing PSP and hydrophobin in a 2:1 ratio (PSP-linker-hydrophobin-linker-PSP-6xHis) showed good expression and good yields after purification. An overview of all proteins that were successfully expressed and purified is shown in Figure 67.

a

c

Protein	Size [kDa]
SO	13.2
SO-mHGF1-SO	36.7
SO-HFB1-SO	35.7
SO-HFB2-SO	35.4
mHGF1-SO	23.2
SO-mHGF1	23.2

b

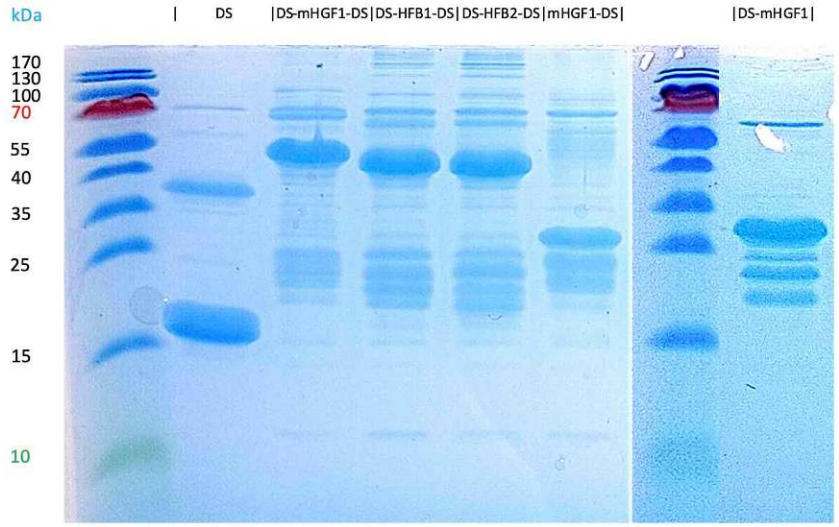

d

Protein	Size [kDa]
SO	13.2
SO-mHGF1-SO	36.7
SO-HFB1-SO	35.7
SO-HFB2-SO	35.4
mHGF1-SO	23.2
SO-mHGF1	23.2

Figure 67| SDS-PAGE of the fusion proteins that were successfully expressed and purified. Protein content was normalized to 5 µg protein per lane, and a 17.5 % acrylamide gel was used. SO = SOPP3, Ds = DsFbFpM49I. **a**, Bands with the expected size are visible for all for all successfully produced constructs containing SOPP3. **b**, Bands with the expected size are visible for all successfully produced constructs containing DsFbFpM49I. **c** & **d**, The expected molecular weight (size) of the fusion proteins.

3.8 Characterization of selected fusion proteins

After analysis of protein production, it was decided to continue with the 10 fusion proteins which showed good expression and good yields after purification. The two PSPs DsFbFpM49I and SOPP3 and the three hydrophobins mHGF1, HFB1, and HFB2 were combined either in a 1:1 or a 2:1 stoichiometry. In total 10 different fusion proteins and the two original proteins SOPP3 and DsFbFPM49I were characterized (Table 3).

Table 3: Fusion proteins

Fusion proteins with PSP SOPP3	SOPP3
	SOPP3-linker-mHGF1-linker-SOPP3-6xHis
	SOPP3-linker-HFB1-linker-SOPP3-6xHis
	SOPP3-linker-HFB2-linker-SOPP3-6xHis
	mHGF1-linker-SOPP3-6xHis
	SOPP3-linker-mHGF1-6xHis
Fusion proteins with PSP DsFbFpM49I	DsFbFpM49I
	DsfbfpM49I-linker-mHGF1-linker-DsfbfpM49I-6xHis
	DsfbfpM49I-linker-HFB1-linker-DsfbfpM49I-6xHis
	DsfbfpM49I-linker-HFB2-linker-DsfbfpM49I-6xHis
	mHGF1-linker-DsfbfpM49I-6xHis
	DsfbfpM49I-linker-mHGF1-6xHis

The final 12 fusion proteins were characterized regarding their spectroscopic and ROS-producing properties. Therefore, absorption and fluorescence spectra were recorded, assays for the detection of all ROS (H_2O_2, $O_2^{\bullet-}$, $^1O_2$, $HO^{\bullet}$) were conducted and finally, the decrease in dissolved O_2 was measured via O_2 sensor measurements.

Initially, proteins were normalized via absorption at 450 nm (chapter 3.3) as described in the literature.[77,93] However, repetitive measurements showed low reproducibility. Because low protein concentration showed very low absorption, fluctuations due to pipetting, etc. had a big impact and therefore resulted in low reliability. Therefore, all proteins were normalized by molarity, with respect to their chromophore content. This means that 1 mol of a fusion protein containing PSP and hydrophobin in a 2:1 ratio equals 2 mol of a fusion protein containing PSP and hydrophobin in a 1:1 ratio. The molar concentration was elucidated by measurement of protein mass concentration via BCA assay. To minimize pipetting error, measurement was done in duplicates of triplicates. Then the protein content was converted to molarity using the molecular weight of the respective fusion protein.

3.8.1 Spectroscopic characterization

After verification of protein production, the question arose, if the fusion proteins still show the same spectral properties as the original PSP. It was not clear if the fusion to a hydrophobin could change the structure significantly and influence/impede fluorescence. Measurement of absorption spectra showed that fusion proteins had the

same absorption maxima as the respective original protein. Absorption maximum for SOPP3 and all SOPP3-based fusion proteins was at approx. 438 nm (Figure 68, a). Absorption maximum for DsfbfpM49I and DsfbfpM49I-based fusion proteins was at approx. 448 nm (Figure 68, b). The chromophore FMN was measured as well, and the absorption maximum was determined at approx. 446 nm (Figure 68, c).

For the measurement of fluorescence spectra, fusion proteins were excited at their absorption maximum. From these measurements, fluorescence maxima were determined. The fluorescence maximum for SOPP3 and all SOPP3-based fusion proteins was at approx. 505 nm (Figure 68, d). The fluorescence maximum for DsfbfpM49I and DsfbfpM49I-based fusion proteins was at approx. 509 nm (Figure 68, e). The chromophore FMN was measured as well, and the fluorescence maximum was determined at approx. 531 nm (Figure 68, f).

Interestingly, the fusion to the hydrophobin mHGF1 in the conformation mHGF1-linker-PSP led to higher absorption and fluorescence. It must be mentioned that small differences in absorption or fluorescence behavior could arise due to pipetting mistakes during normalization (BCA assay), however, the conformation mHGF1-linker-PSP showed a significant trend towards higher absorption and fluorescence for both PSPs (Figure 68).

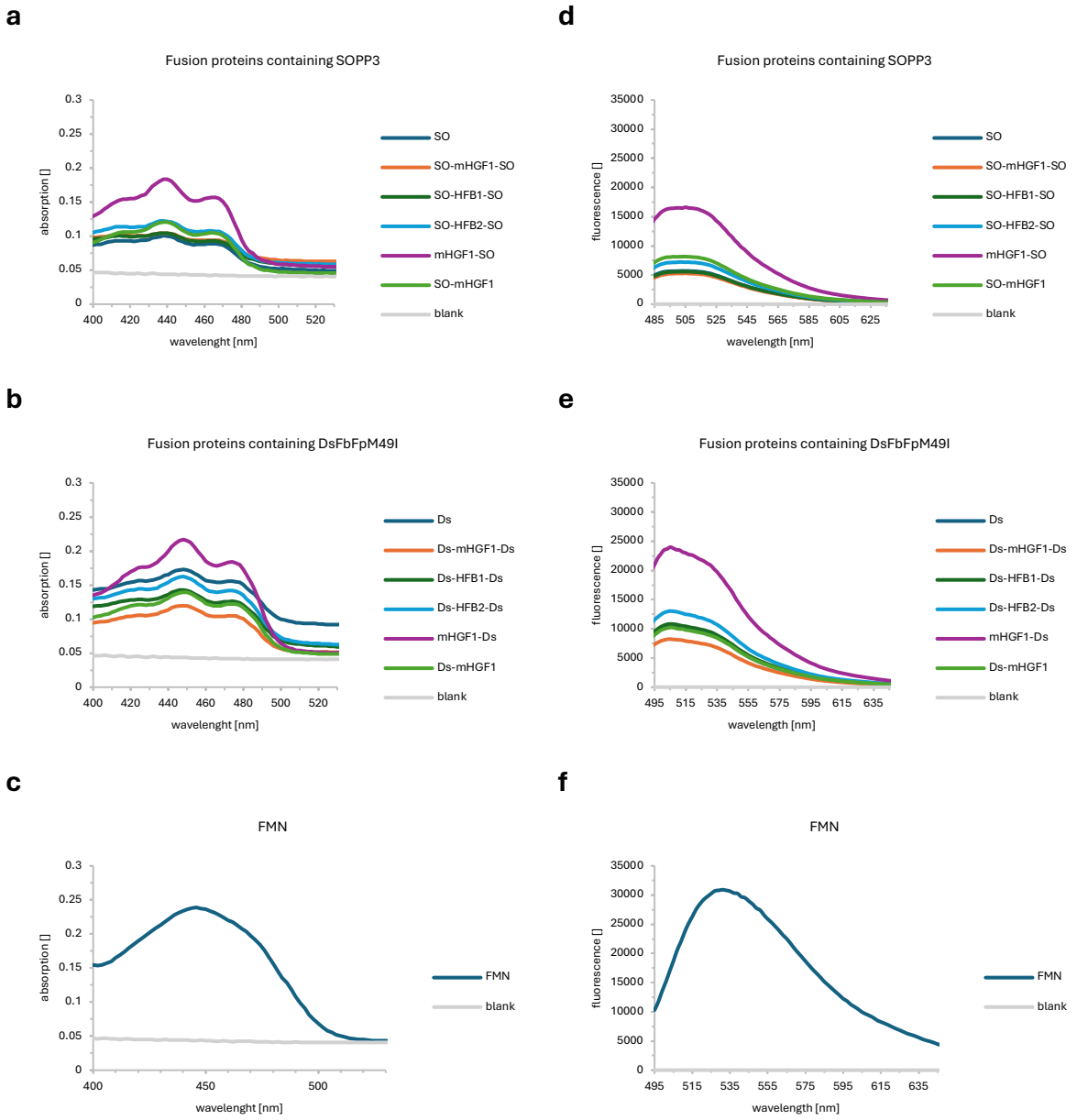

Figure 68| Absorption and fluorescence emission spectra of all fusion proteins and FMN. Proteins were normalized to a chromophore concentration of 50 µM, protein solutions were prepared in Milli-Q H_2O in a final volume of 100 µL. The chromophore FMN was measured as well. As a blank, Milli-Q H_2O was measured. SO = SOPP3, Ds = DsFbFpM49I. **a**, Absorption spectra of fusion proteins containing the protein SOPP3. **b**, Absorption spectra of fusion proteins containing the protein DsFbFpM49I. **c**, Absorption spectrum of FMN. **d**, Fluorescence spectra of fusion proteins containing the protein SOPP3. **e**, Fluorescence spectra of fusion proteins containing the protein DsFbFpM49I. **f**, Fluorescence spectrum of FMN.

Then, absorption and fluorescence measurements were used as a tool for determining the stability of the fusion proteins towards blue light, as photobleaching would play a significant role during polymer degradation. Therefore, samples were incubated under blue light (16.4 mW/cm^2). Absorption and fluorescence spectra were measured after different periods of illumination time (0 min, 30 min, 60 min, 90 min). Fusion proteins containing the protein SOPP3 showed almost complete photobleaching already after 30 min of illumination time. Meanwhile, fusion proteins containing protein DsFbFpM49I

showed better stability towards blue light, where after 30 min there was still absorption/fluorescence detectable. The chromophore FMN was analyzed as well and showed complete photobleaching already after 30 min illumination time (
Figure 69, Figure 70, Figure 71, Figure 72, Figure 73, Figure 74). Furthermore, an experiment was conducted on a bigger scale to analyze the degradation of FMN during photobleaching (chapter 6.7).

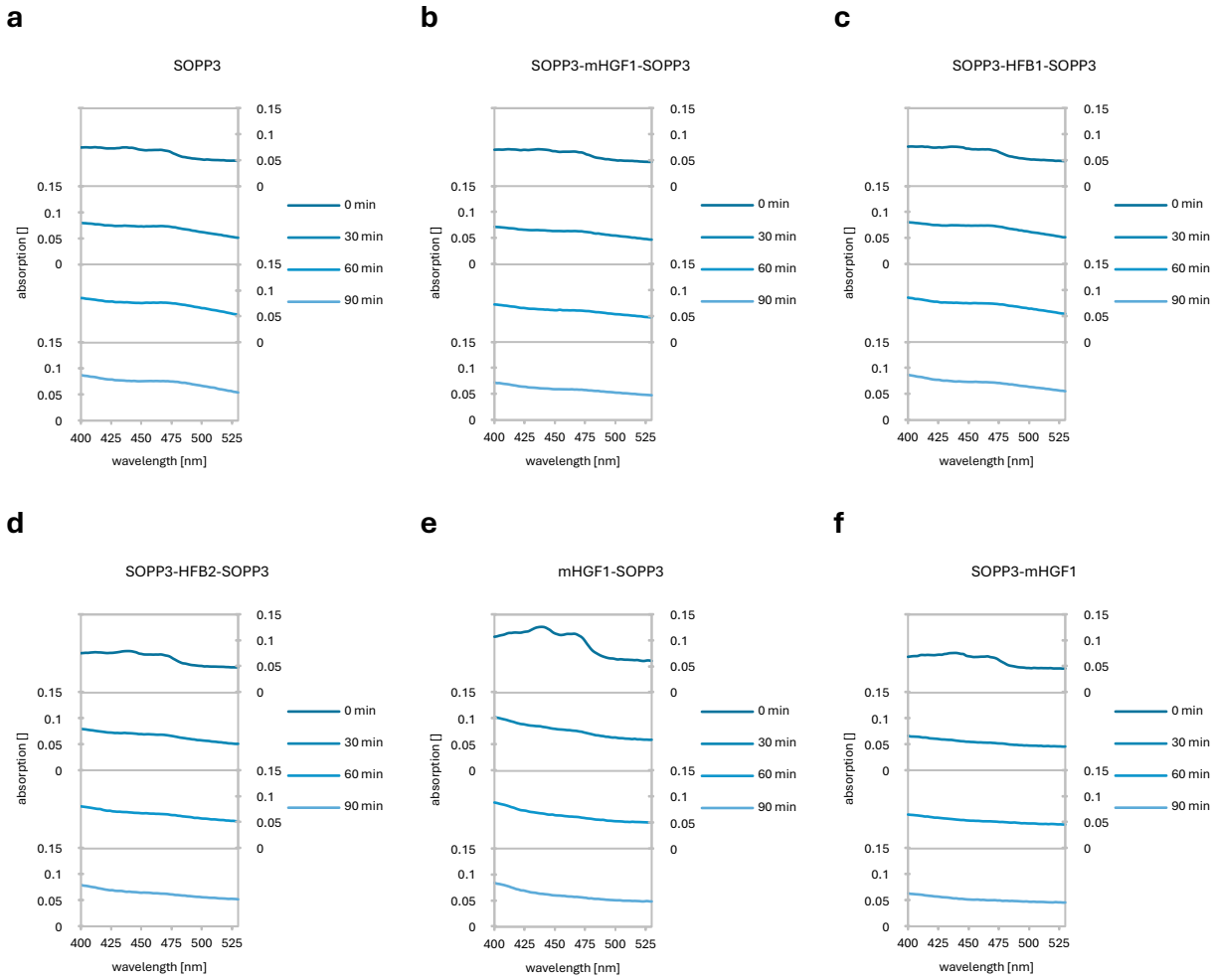

Figure 69| Stability towards blue light - absorption spectra of the fusion proteins containing SOPP3 after different periods of illumination. Absorption spectra were measured after 0 min, 30 min, 60 min, and 90 min. It was illuminated under blue light (16.4 mW/cm^2). Proteins were normalized to a chromophore concentration of 50 µM, protein solutions were prepared in Milli-Q H_2O in a final volume of 100 µL. As a blank, Milli-Q H_2O was measured. For better visibility, spectra are displayed in a stacked arrangement. **a**, SOPP3. **b**, SOPP3-mHGF1-SOPP3. **c**, SOPP3-HFB1-SOPP3. **d**, SOPP3-HFB2-SOPP3. **e**, mHGF1-SOPP3. **f**, SOPP3-mHGF1.

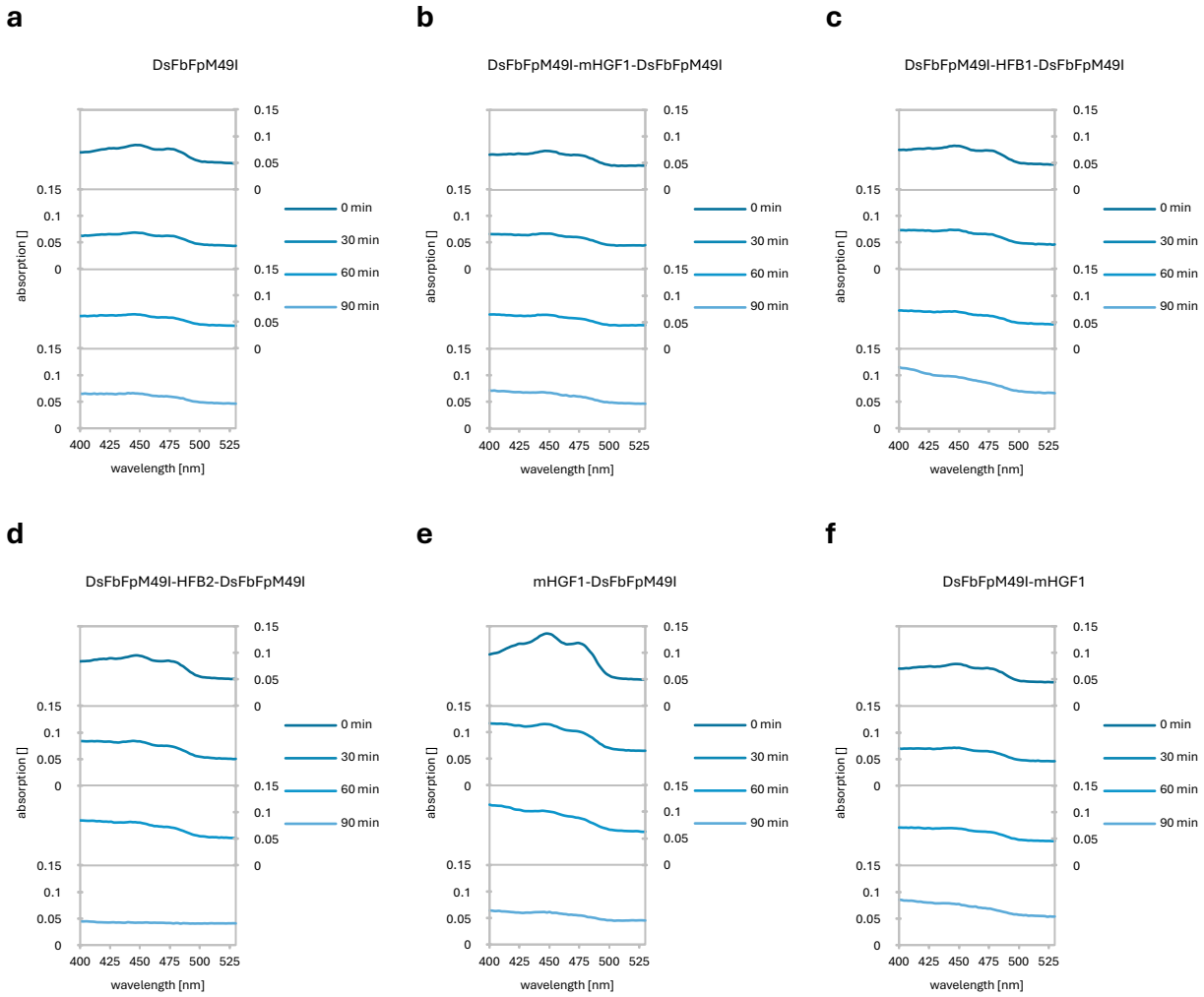

Figure 70| Stability towards blue light - absorption spectra of the fusion proteins containing DsFbFpM49I after different periods of illumination. Absorption spectra were measured after 0 min, 30 min, 60 min, and 90 min. It was illuminated under blue light (16.4 mW/cm^2). Proteins were normalized to a chromophore concentration of 50 µM, protein solutions were prepared in Milli-Q H_2O in a final volume of 100 µL. As a blank, Milli-Q H_2O was measured. For better visibility, spectra are displayed in a stacked arrangement. **a**, DsFbFpM49I. **b**, DsFbFpM49I-mHGF1-DsFbFpM49I. **c**, DsFbFpM49I-HFB1-DsFbFpM49I. **d**, DsFbFpM49I-HFB2-DsFbFpM49I. **e**, mHGF1-DsFbFpM49I. **f**, DsFbFpM49I-mHGF1.

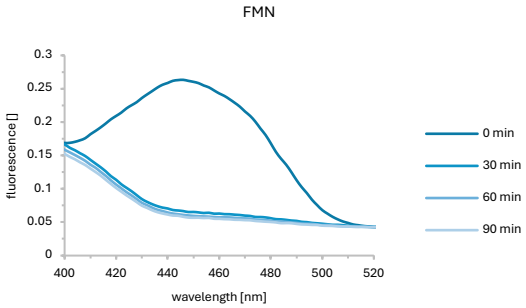

Figure 71| Stability towards blue light - absorption spectrum of FMN after different periods of illumination. Absorption spectra were measured after 0 min, 30 min, 60 min, and 90 min. It was illuminated under blue light (16.4 mW/cm^2). FMN was normalized to 50 µM, the solution was prepared in Milli-Q H_2O in a final volume of 100 µL. As a blank, Milli-Q H_2O was measured.

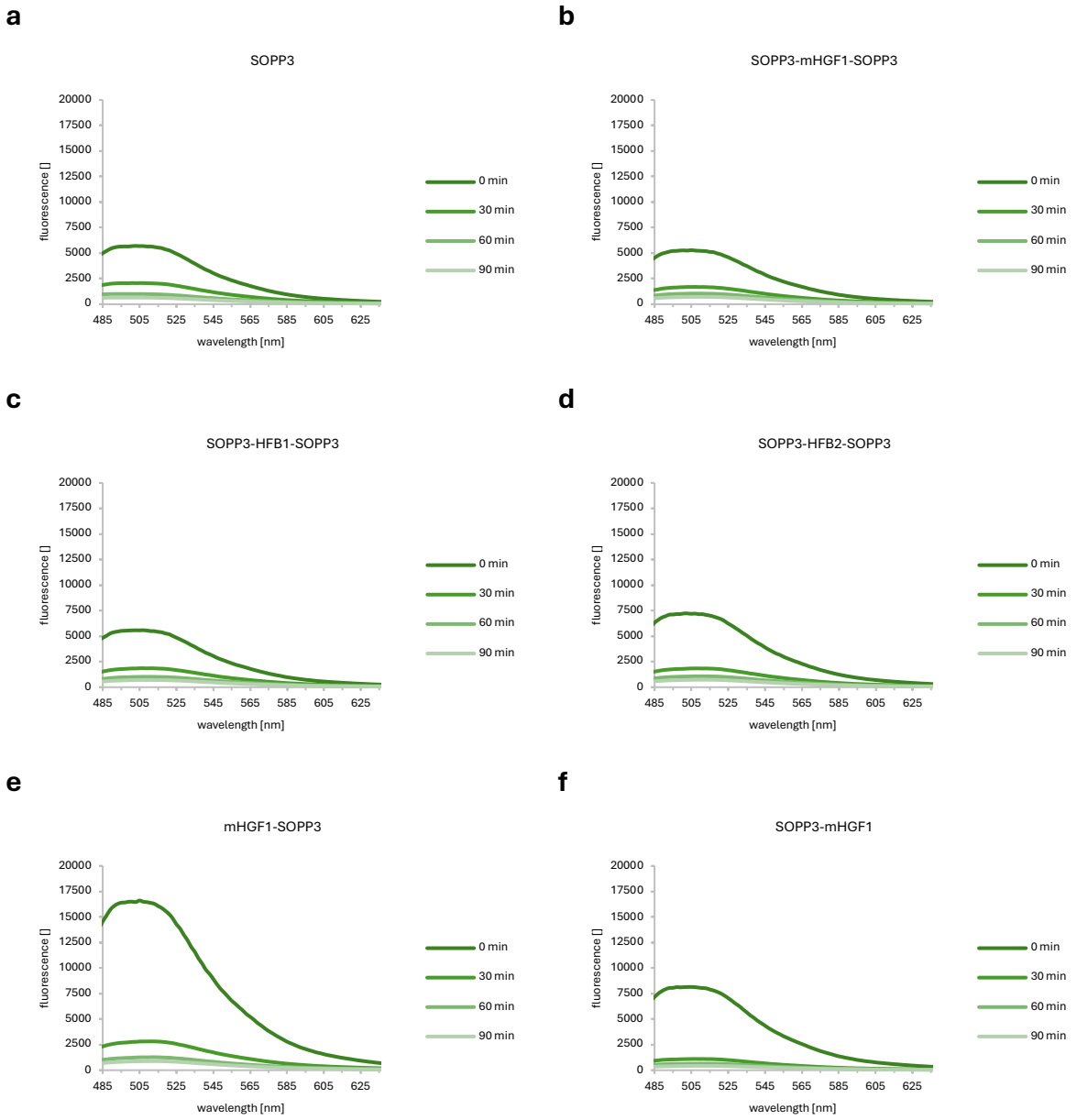

Figure 72| Stability towards blue light - fluorescence emission spectra of the fusion proteins containing SOPP3 after different periods of illumination. Fluorescence spectra were measured after 0 min, 30 min, 60 min, and 90 min. It was illuminated under blue light (16.4 mW/cm^2). Proteins were normalized to a chromophore concentration of 50 µM, protein solutions were prepared in Milli-Q H_2O in a final volume of 100 µL. As a blank, Milli-Q H_2O was measured. **a**, SOPP3. **b**, SOPP3-mHGF1-SOPP3. **c**, SOPP3-HFB1-SOPP3. **d**, SOPP3-HFB2-SOPP3. **e**, mHGF1-SOPP3. **f**, SOPP3-mHGF1.

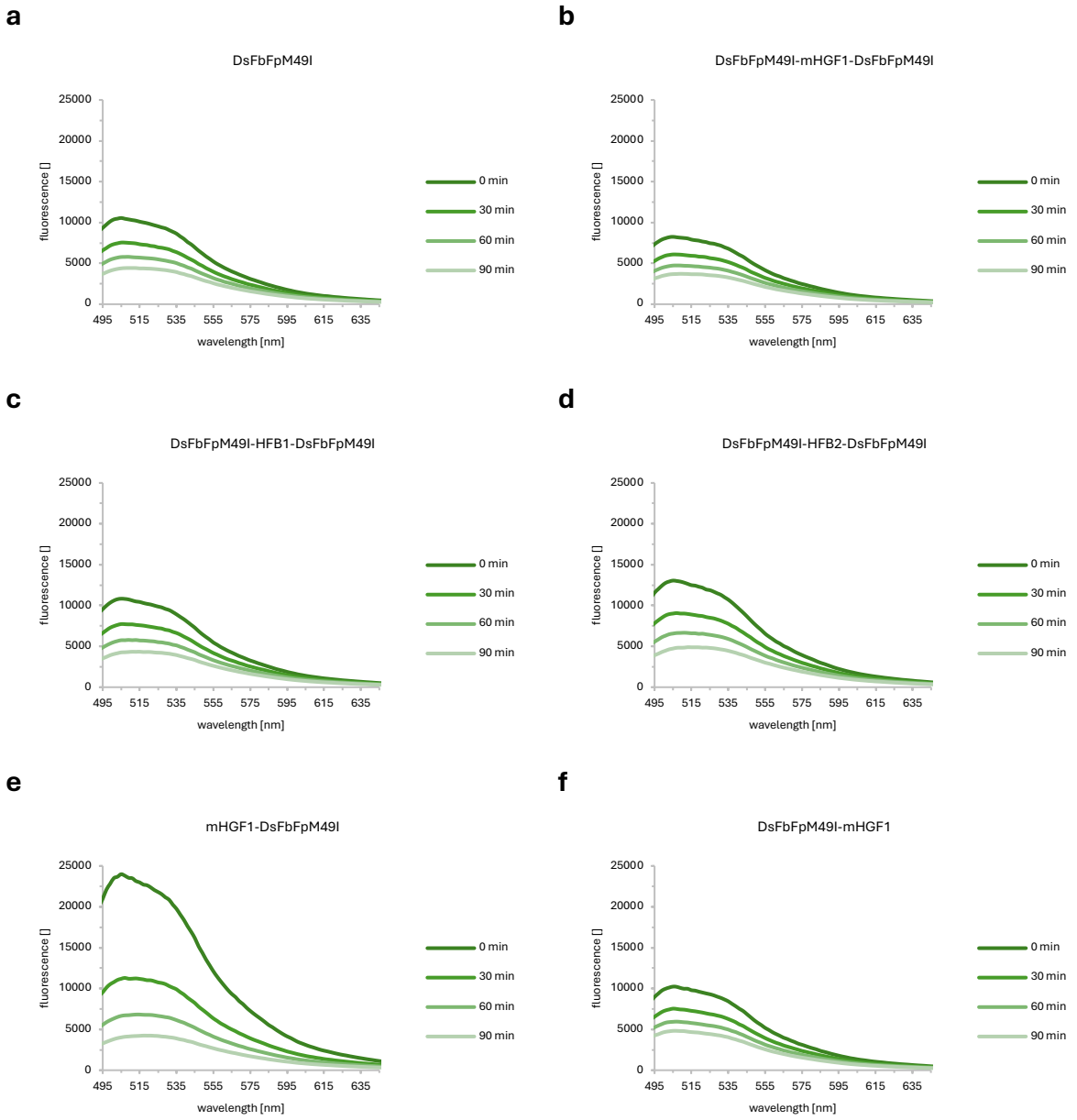

Figure 73| Stability towards blue light - fluorescence emission spectra of the fusion proteins containing DsFbFpM49I after different periods of illumination. Fluorescence spectra were measured after 0 min, 30 min, 60 min, and 90 min. It was illuminated under blue light (16.4 mW/cm^2). Proteins were normalized to a chromophore concentration of 50 µM, protein solutions were prepared in Milli-Q H_2O in a final volume of 100 µL. As a blank, Milli-Q H_2O was measured. **a**, DsFbFpM49I. **b**, DsFbFpM49I-mHGF1-DsFbFpM49I. **c**, DsFbFpM49I-HFB1-DsFbFpM49I. **d**, DsFbFpM49I-HFB2-DsFbFpM49I. **e**, mHGF1-DsFbFpM49I. **f**, DsFbFpM49I-mHGF1.

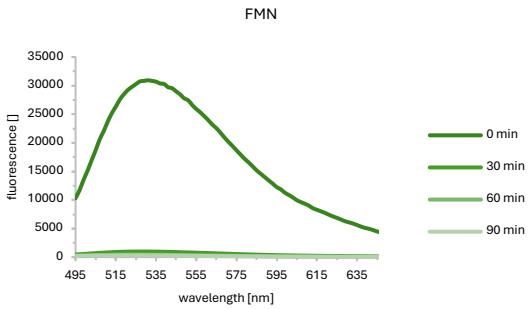

Figure 74| Stability towards blue light - fluorescence emission spectrum of FMN after different periods of illumination. Fluorescence spectra were measured after 0 min, 30 min, 60 min, and 90 min. It was illuminated under blue light (16.4 mW/cm^2). FMN was normalized to 50 µM, the solution was prepared in Milli-Q H_2O in a final volume of 100 µL. As a blank, Milli-Q H_2O was measured.

It was also tested if there was regeneration of absorption or fluorescence after photobleaching and recovery in the dark. Therefore, samples were incubated under blue light (16.4 mW/cm^2) for 30 min and then left in the dark for 1 h. There was no regeneration of absorption or fluorescence (Figure 75, Figure 76).

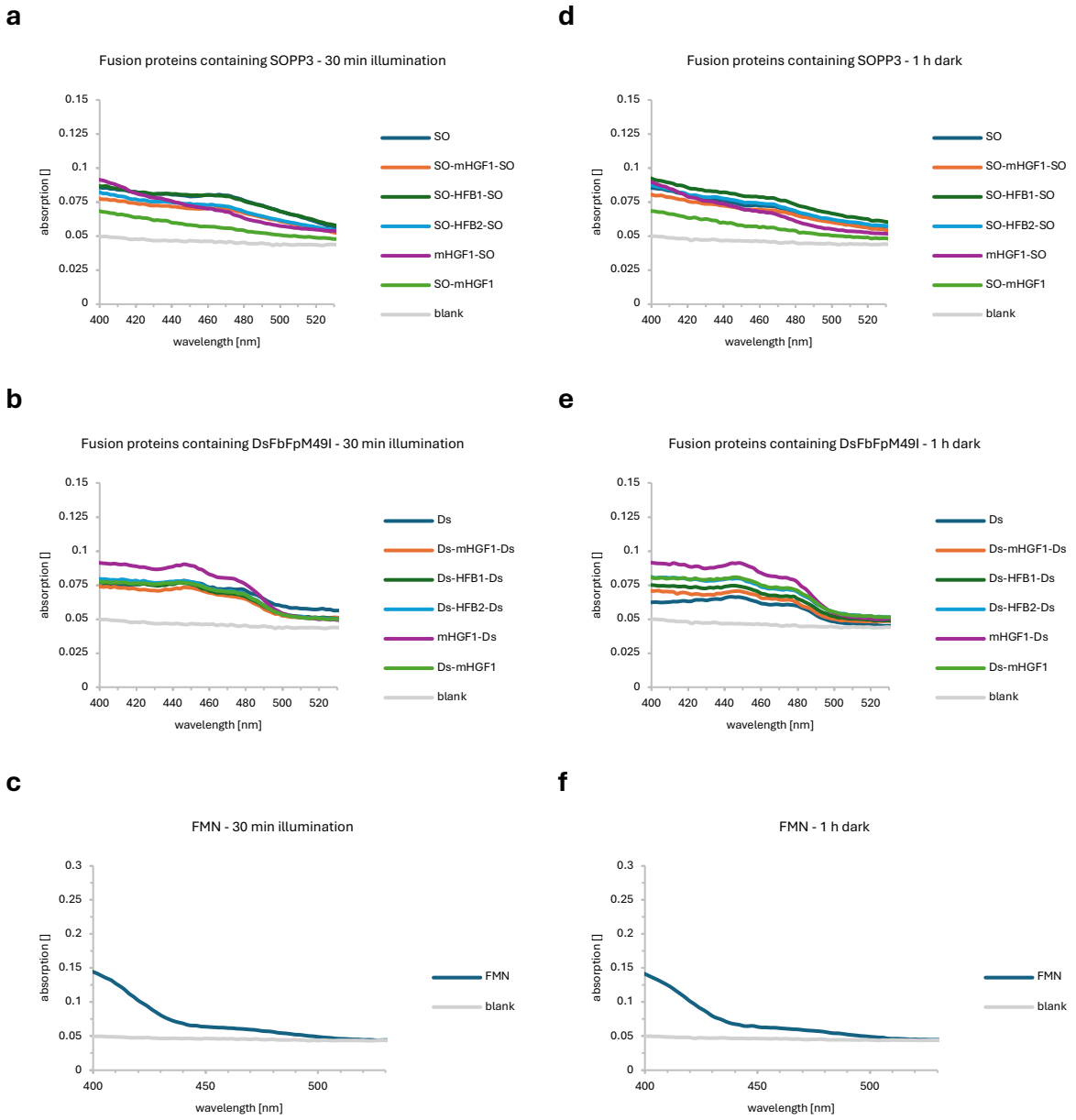

Figure 75| Regeneration of fusion proteins after photobleaching - absorption spectra after 30 min of illumination and 1 h of regeneration in the dark. It was illuminated under blue light (16.4 mW/cm^2). Proteins were normalized to a chromophore concentration of 50 µM, protein solutions were prepared in Milli-Q H_2O in a final volume of 100 µL. The chromophore FMN was measured as well. As a blank, Milli-Q H_2O was measured. SO = SOPP3, Ds = DsFbFpM49I. **a**, Fusion proteins containing the LOV protein SOPP3 after 30 min of illumination. **b**, Fusion proteins containing the LOV protein DsFbFpM49I after 30 min of illumination. **c**, FMN after 30 min of illumination. **d**, Fusion proteins containing the LOV protein SOPP3 after 1 h regeneration in the dark. **e**, Fusion proteins containing the LOV protein DsFbFpM49I after 1 h regeneration in the dark. **f**, FMN after 1 h regeneration in the dark.

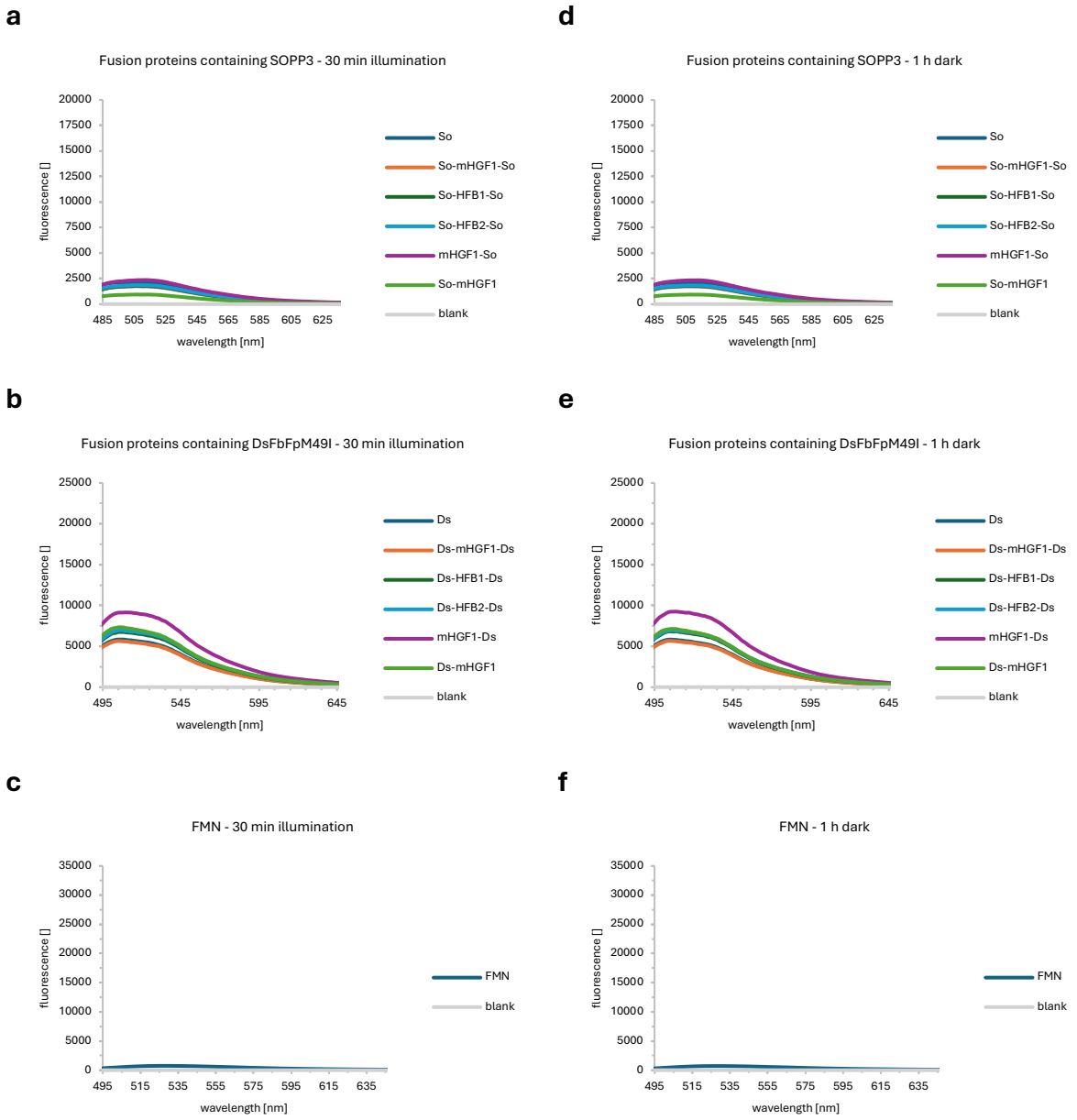

Figure 76| Regeneration of fusion proteins after photobleaching - fluorescence emission spectra after 30 min of illumination and 1 h of regeneration in the dark. It was illuminated under blue light (16.4 mW/cm^2). Proteins were normalized to a chromophore concentration of 50 µM, protein solutions were prepared in Milli-Q H_2O in a final volume of 100 µL. The chromophore FMN was measured as well. As a blank, Milli-Q H_2O was measured. SO = SOPP3, Ds = DsFbFpM49I. **a**, Fusion proteins containing the LOV protein SOPP3 after 30 min of illumination. **b**, Fusion proteins containing the LOV protein DsFbFpM49I after 30 min of illumination. **c**, FMN after 30 min of illumination. **d**, Fusion proteins containing the LOV protein SOPP3 after 1 h regeneration in the dark. **e**, Fusion proteins containing the LOV protein DsFbFpM49I after 1 h regeneration in the dark. **f**, FMN after 1 h regeneration in the dark.

It can be concluded that absorption and fluorescence properties remained consistent with the original PSPs. Moreover, fusion with hydrophobin mHGF1 enhanced both absorption and fluorescence significantly. Stability tests using blue light exposure revealed that proteins with SOPP3 photobleached almost completely within 30 minutes, while those containing DsFbFpM49I showed greater resistance to photobleaching. The

chromophore FMN also exhibited rapid photobleaching without recovery in the dark. These findings highlight the varying stability of the proteins when exposed to light, which is a crucial factor for light-driven applications. As an outlook, to gain further knowledge about protein stability, differential scanning calorimetry or circular dichroism measurements could be conducted for the determination of the melting temperatures of all fusion protein constructs.

3.8.2 Quantification of reactive oxygen species production

For all assays, a daylight lamp was used for illumination (Megaman Helix, 0.9 mW/cm^2), if not stated otherwise. Conditions for the three ROS-specific assays were adopted from chapter 3.3.2. However, fusion proteins were normalized by molar concentration instead of normalization by absorption as used in chapter 3.3. Some changes/improvements regarding assay reagent concentration or light intensity were made. All fusion proteins were analyzed by all three ROS-specific assays.

3.8.2.1 Quantification of H_2O_2 and $O_2^{\bullet-}$ production

The Amplex Red assay was used for quantification of H_2O_2 and $O_2^{\bullet-}$ production (chapter 3.3.2.1). As mentioned previously, the autoxidation of Amplex Red is substantial. In an aqueous solution, the reagent undergoes oxidation and is very sensitive to light. Therefore, a working solution should always be prepared shortly before use and measurements should be conducted concurrently on the same day.

Measurements for the Amplex Red assay were conducted after 0, 2, 5, and 10 min. After 10 min, the assay exceeded the linear range under the used assay conditions. The results for the detection of H_2O_2 (no addition of the enzyme SOD) showed that fusion proteins mHGF1-DsFbFpM49I and DsFbFpM49I-mHGF1 produced the highest amounts of H_2O_2 (Figure 77). The results for the detection of H_2O_2 and $O_2^{\bullet-}$ (addition of the enzyme SOD) showed that fusion protein mHGF1-DSFbFpM49I produced the highest amounts of these ROS (Figure 78).

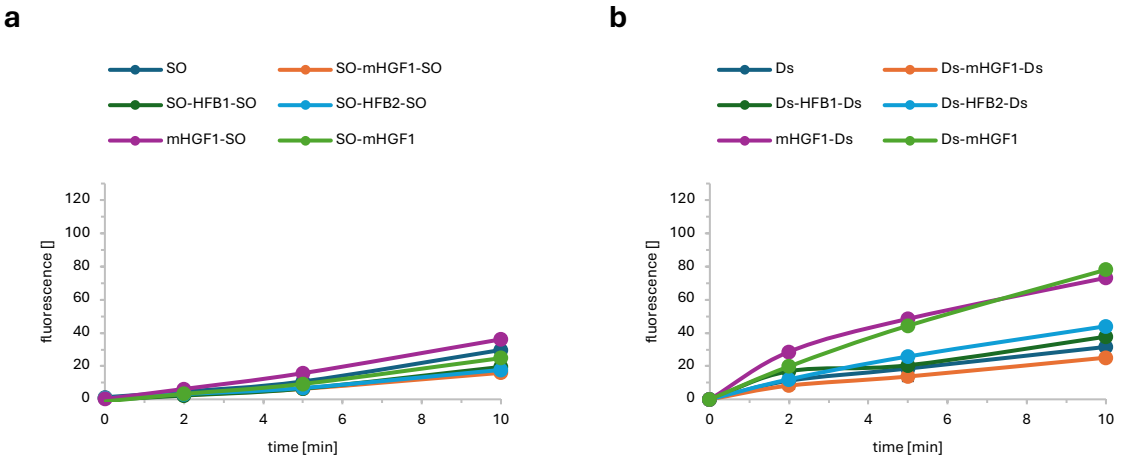

Figure 77| Results of the Amplex Red assay for the detection of H_2O_2 (light intensity 0.9 mW/cm²). Fusion proteins mHGF1-Ds and Ds-mHGF1 show the highest H_2O_2 production. Samples were incubated for 0, 2, 5, and 10 min. 0.2 U/mL HRP, and 0.1 mM Amplex Red were used. Samples were adjusted to 1 µM chromophore concentration in Milli-Q H_2O, in a total volume of 100 µL. It was illuminated with Megaman Helix daylight lamp (0.9 mW/cm²). The increase in fluorescence was measured at ex 550 nm / em 585 nm. It was corrected by the average fluorescence of the untreated reaction mixture and by the autoxidation of the assay reagent, values are mean ± σ for n = 3. SO = SOPP3, Ds = DsFbFpM49I. **a**, Fusion proteins containing SOPP3. **b**, Fusion proteins containing DsFbFpM49I.

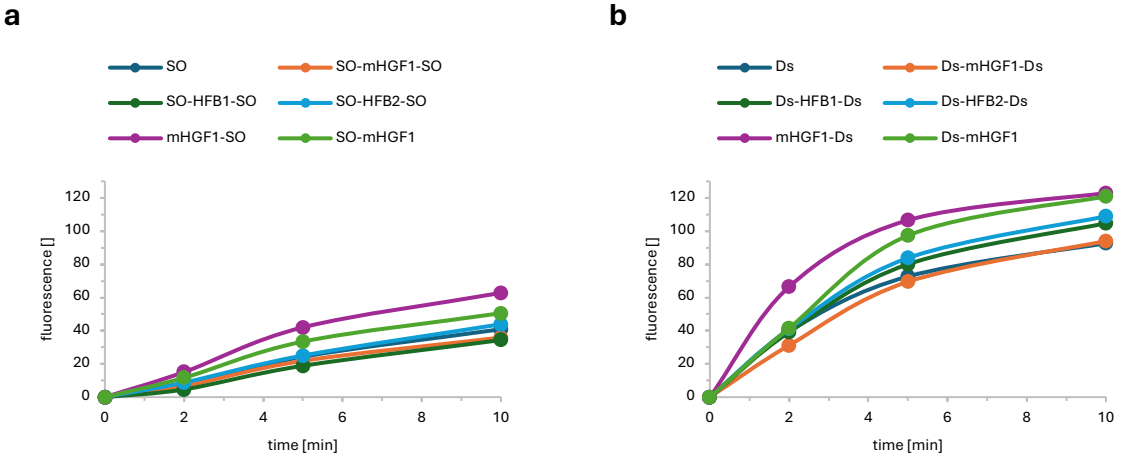

Figure 78| Results of the Amplex Red assay for the detection of H_2O_2 and $O_2^{\bullet-}$ (light intensity 0.9 mW/cm²). Fusion protein mHGF1-Ds shows the highest H_2O_2 and $O_2^{\bullet-}$ production. Samples were incubated for 0, 2, 5, and 10 min. 0.2 U/mL HRP, 2 U/mL SOD, 0.1 mM Amplex Red were used. Samples were adjusted to 1 µM chromophore concentration in Milli-Q H_2O, in a total volume of 100 µL. It was illuminated with Megaman Helix daylight lamp (0.9 mW/cm²). The increase in fluorescence was measured at ex 550 nm / em 585 nm. It was corrected by the average fluorescence of the untreated reaction mixture and by the autoxidation of the assay reagent, values are mean ± σ for n = 3. SO = SOPP3, Ds = DsFbFpM49I. **a**, Fusion proteins containing SOPP3. **b**, Fusion proteins containing DsFbFpM49I.

The assay was also conducted with lower light intensity (SciRobotics Pickolo, 0.3 mW/cm²) by a pipetting robot (Tecan liquid handler). With this lower light intensity, the linear range of the assay was improved. Measurements were conducted after 0, 2, 5, 10,

20, 30, and 90 min (Figure 79, Figure 80). The results showed a similar trend as the initial setup with higher light intensity (0.9 mW/cm^2).

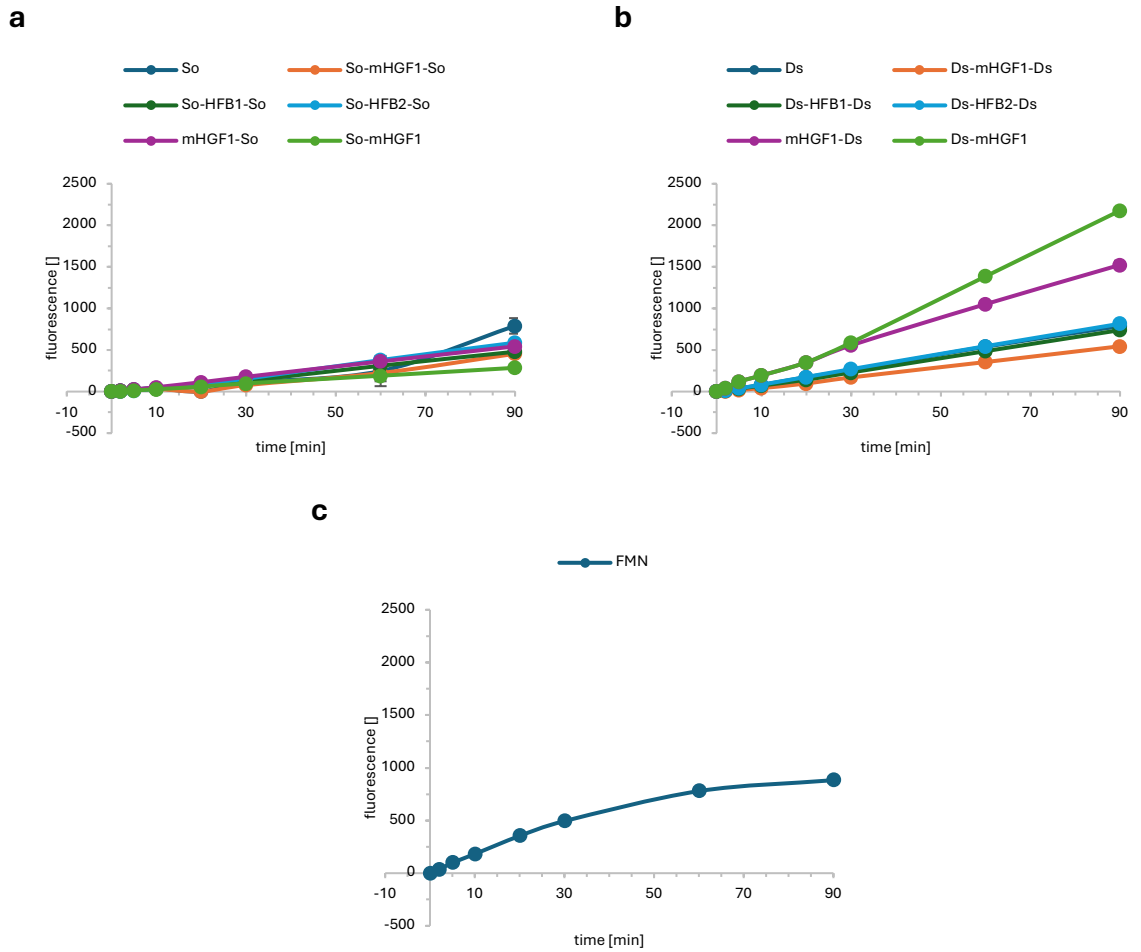

Figure 79| Results of the Amplex Red assay for the detection of H_2O_2 (light intensity 0.3 mW/cm^2). Fusion proteins mHGF1-Ds and Ds-mHGF1 show the highest H_2O_2 production. Samples were incubated for 0, 2, 5 10, 20, 30, 60, and 90 min. H_2O_2 production by the chromophore FMN was also analyzed. 0.2 U/mL HRP and 0.1 mM Amplex Red were used. Samples were adjusted to 1 µM chromophore concentration in Milli-Q H_2O, in a total volume of 100 µL. It was illuminated with Megaman Helix daylight lamp (0.3 mW/cm^2). For this experiment, measurements were conducted with the microplate reader Spark® Multimode, Tecan. The increase in fluorescence was measured at ex 550 nm / em 585 nm. It was corrected by the average fluorescence of the untreated reaction mixture and by the autoxidation of the assay reagent, values are mean ± σ for n = 3. SO = SOPP3, Ds = DsFbFpM49I. **a**, Fusion proteins containing SOPP3. **b**, Fusion proteins containing DsFbFpM49I. **c**, FMN.

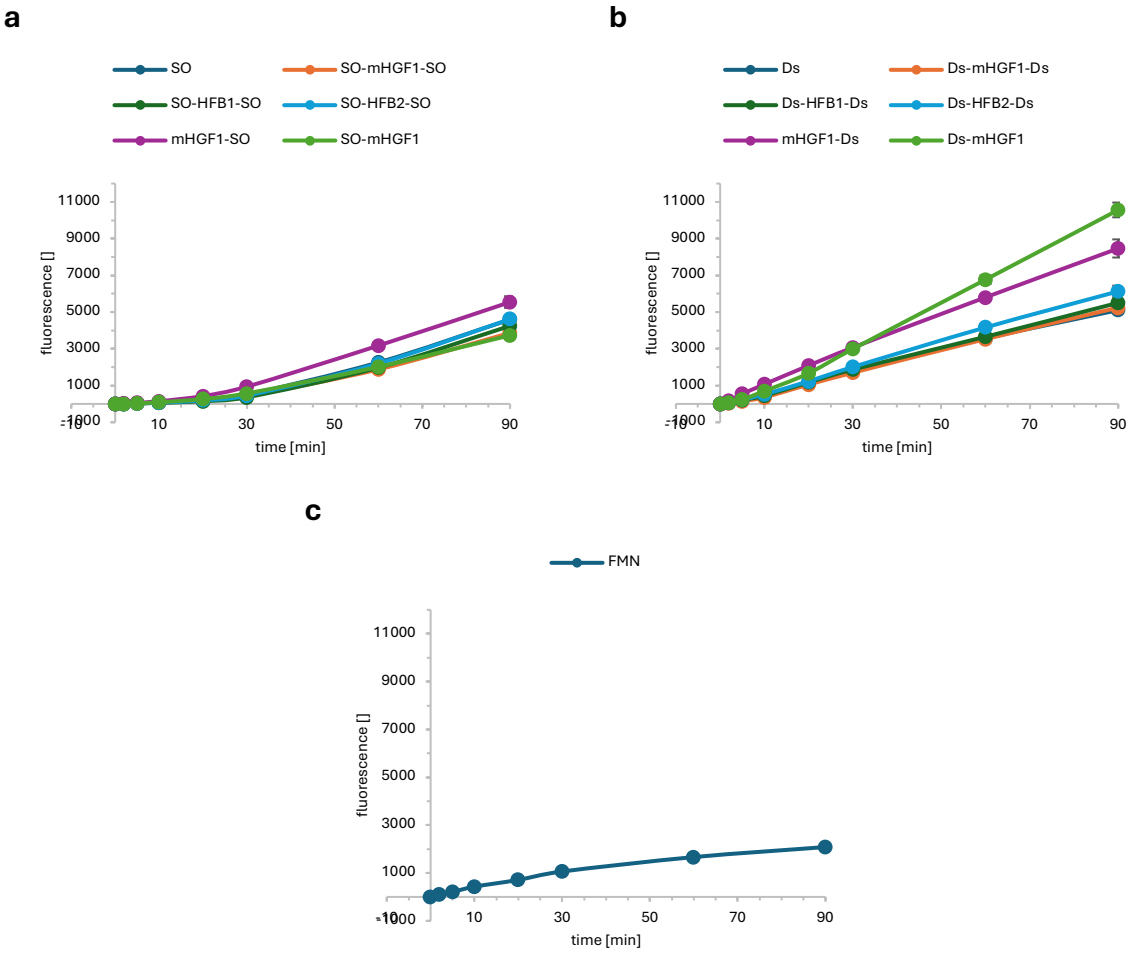

Figure 80| Results of the Amplex Red assay for the detection of H_2O_2 and $O_2^{\bullet-}$ (light intensity 0.3 mW/cm²). Fusion proteins mHGF1-Ds and Ds-mHGF1 show highest H_2O_2 and $O_2^{\bullet-}$ production. Samples were incubated for 0, 2, 5 10, 20, 30, 60, and 90 min. H_2O_2 and $O_2^{\bullet-}$ production by the chromophore FMN was also analyzed. 0.2 U/mL HRP, 2 U/mL SOD, 0.1 mM Amplex Red were used. Samples were adjusted to 1 µM chromophore concentration in Milli-Q H_2O, in a total volume of 100 µL. It was illuminated with Megaman Helix daylight lamp (0.3 mW/cm²). For this experiment, measurements were conducted with the microplate reader Spark® Multimode, Tecan. The increase in fluorescence was measured at ex 550 nm / em 585 nm. It was corrected by the average fluorescence of the untreated reaction mixture and by the autoxidation of the assay reagent, values are mean ± σ for n = 3. SO = SOPP3, Ds = DsFbFpM49I. **a**, Fusion proteins containing SOPP3. **b**, Fusion proteins containing DsFbFpM49I. **c**, FMN.

To make quantitative statements, calibrations with H_2O_2 were done for both assays, without SOD or with SOD (as described in chapter 3.3.2.1, Figure 81). New calibration curves were always prepared for each freshly prepared working solution. Results show that H_2O_2 and $O_2^{\bullet-}$ concentrations approximately range up to 2 µM in the first 10 min (using light intensity 0.9 mW/cm², Table 4).

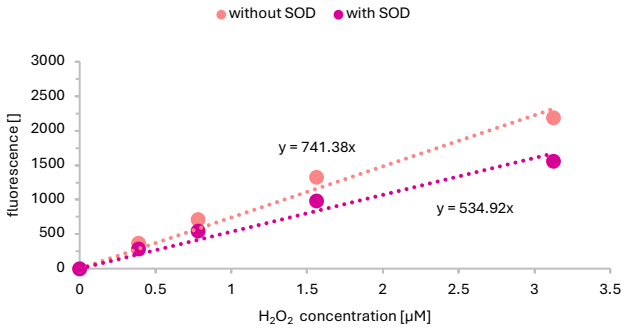

Figure 81| Calibration curve for the Amplex Red assay. Samples with known concentrations of H_2O_2 (0.20 µM, 0.39 µM, 0.78 µM, 1.56 µM, 3.13 µM) were prepared one time in the absence and one time in the presence of SOD. 0.2 U/mL HRP and 0.1 mM Amplex Red were used, without or with the addition of 2 U/mL SOD, in Milli-Q H2O, in a total volume of 100 µL. For this experiment, measurements were conducted with the microplate reader Spark® Multimode, Tecan. The increase in fluorescence was measured at ex 550 nm / em 585 nm and corrected by the average fluorescence of the working solution without H_2O_2, values are mean ± σ for n = 3.

Table 4: H_2O_2 and $O_2^{\bullet-}$ concentrations after 10 min of illumination (light intensity 0.3 mW/cm²)

Fusion protein[a]	H_2O_2 [µM]	H_2O_2 and $O_2^{\bullet-}$ [µM]
SO	0.05	0.11
SO-mHGF1-SO	0.04	0.06
SO-HFB1-SO	0.05	0.10
SO-HFB2-SO	0.05	0.11
mHGF1-SO	0.07	0.26
SO-mHGF1	0.04	0.26
Ds	0.15	0.93
Ds-mHGF1-Ds	0.12	0.67
Ds-HFB1-Ds	0.11	0.83
Ds-HFB2-Ds	0.12	0.97
mHGF1-Ds	0.27	2.0
Ds-mHGF1	0.17	1.31

[a] SO = SOPP3, Ds = DsFbFpM49I

3.8.2.2 Quantification of $^1O_2$ production

The Singlet Oxygen Sensor Green SOSG assay was used to detect $^1O_2$ generation (chapter 3.3.2.2). After initial trials with low protein concentrations, as in the Amplex assay for H_2O_2 and $O_2^{\bullet-}$ detection (1 µM), no significant rise in fluorescence was observed. The assay showed better results when higher protein concentrations (4 µM) were used. Light intensity was set to 0.9 mW/ cm². Measurements were conducted after 0, 2, 5, 10, 30, 60 and 90 min. The results indicate that all fusion proteins, containing the protein SOPP3 as well as DsFbFpM49I showed approx. the same amount of $^1O_2$ production. The two fusion proteins mHGF1-DsFbFpM49I and mHGF1-SOPP3 produced the highest amount of $^1O_2$ (Figure 82).

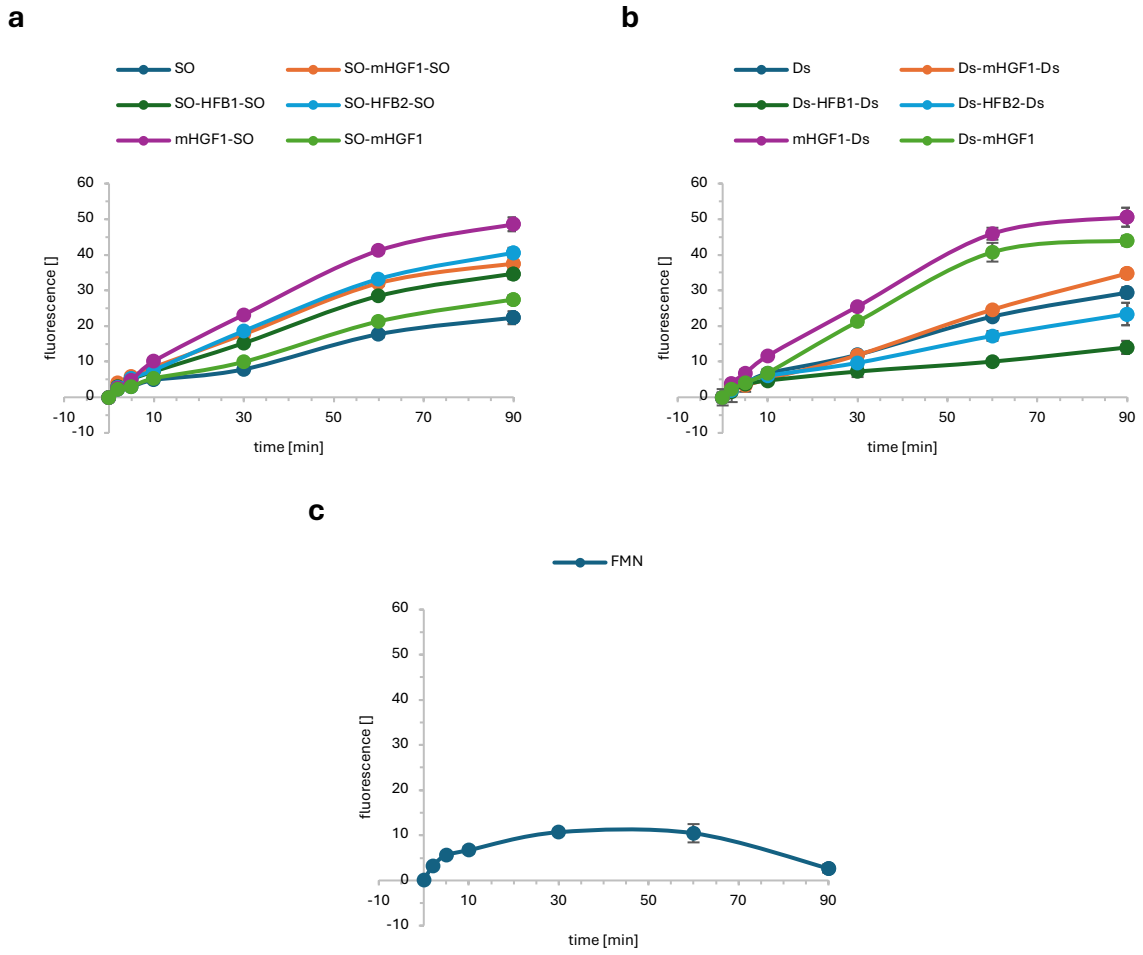

Figure 82| Results of the SOSG assay for the detection of $^1O_2$. Fusion proteins mHGF1-SO and mHGF1-Ds show highest $^1O_2$ production. Samples were incubated for 0, 2, 5, 10, 30, 60 and 90 min. $^1O_2$ production by the chromophore FMN was also analyzed. 5 µM SOSG reagent was used.[189] Samples were adjusted to 4 µM chromophore concentration in Milli-Q H_2O, in a total volume of 100 µL. It was illuminated with Megaman Helix daylight lamp (0.9 mW/cm^2). The increase in fluorescence was measured at ex 510 nm / em 530 nm. It was corrected by the average fluorescence of the untreated reaction mixture and by the autoxidation of the assay reagent, values are mean ± σ for n = 3. SO = SOPP3, Ds = DsFbFpM49I. **a**, Fusion proteins containing SOPP3. **b**, Fusion proteins containing DsFbFpM49I. **c**, FMN.

The assay was also conducted with lower protein concentration (1 µM chromophore concentration) and light intensity (0.3 mW/cm^2) by a pipetting robot (Tecan liquid handler). However, under these conditions, the $^1O_2$ production by the protein samples did not exceed the autoxidation of the reagent SOSG itself. Therefore, it was concluded that higher protein concentrations and higher light intensity were necessary to see significant $^1O_2$ production by the proteins.

3.8.2.3 *Quantification of HO• production*

The Aminophenyl fluorescein (APF) assay was used for the detection of HO• formation. Protein samples were normalized to 4 µM chromophore concentration. Measurements were conducted after 0, 2, 5, 10, 30, 60 and 90 min. As already observed in the Amplex assay for H_2O_2 and $O_2^{\bullet-}$ detection (chapter 3.3.2.3), the fusion proteins containing DsFbFpM49I produced tendentially higher HO• levels than the fusion proteins containing SOPP3. In particular, the fusion protein mHGF1-Ds produced by far the highest amount of HO•. There was a big difference to all other constructs (Figure 83).

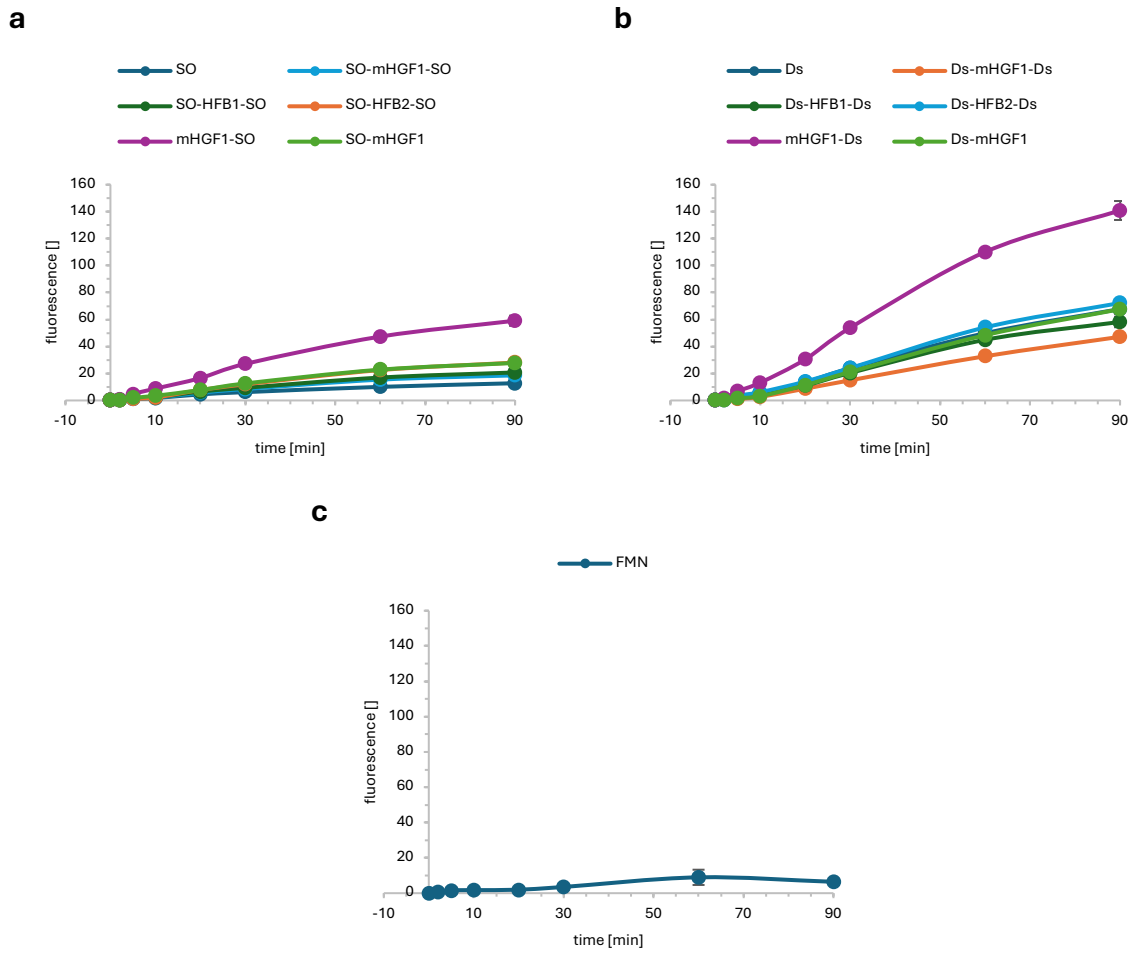

Figure 83| Results of the APF assay for the detection of HO•. Fusion protein mHGF1-Ds shows the highest HO• production. Samples were incubated for 0, 2, 5, 10, 30, 60 and 90 min. HO• production by the chromophore FMN was also analyzed. 15 µM APF reagent was used. Samples were adjusted to 4 µM chromophore concentration in Milli-Q H_2O, in a total volume of 100 µL. It was illuminated with Megaman Helix daylight lamp (0.9 mW/cm^2). The increase in fluorescence was measured at ex 495 nm / em 515 nm. It was corrected by the average fluorescence of the untreated reaction mixture and by the autoxidation of the assay reagent, values are mean ± σ for n = 3. SO = SOPP3, Ds = DsFbFpM49I. **a**, Fusion proteins containing SOPP3. **b**, Fusion proteins containing DsFbFpM49I. **c**, FMN.

The assay was also conducted with lower protein concentration (1 µM chromophore concentration) and light intensity (0.3 mW/cm^2) by a pipetting robot (Tecan liquid handler). Measurements were conducted after 0, 2, 5, 10, 20, 30, and 90 min (Figure 84).

Comparable results were obtained as with the initial setup with higher protein concentration and higher light intensity.

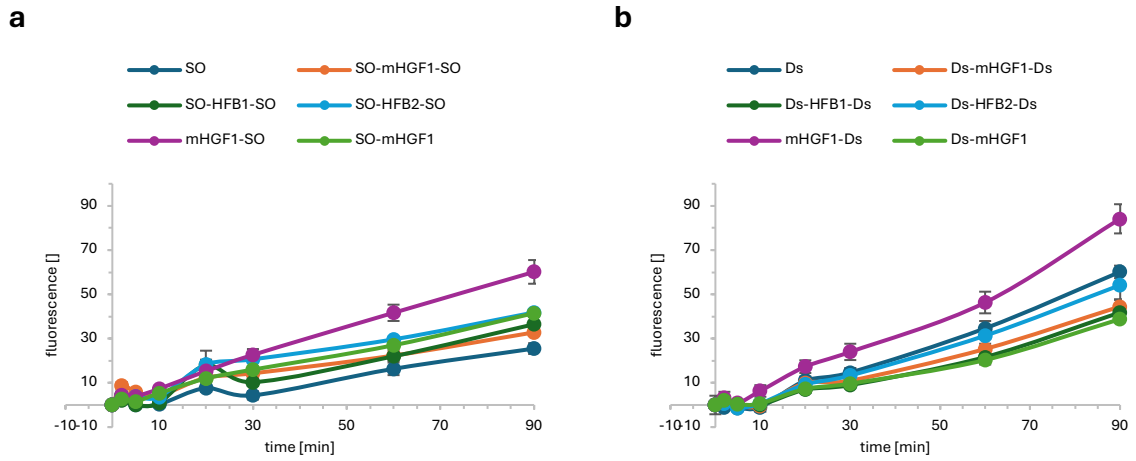

Figure 84| Results of the APF assay for the detection of HO•. Fusion protein mHGF1-Ds shows the highest HO• production. Samples were incubated for 0, 2, 5, 10, 30, 60 and 90 min. 15 µM APF reagent was used. Samples were adjusted to 1 µM chromophore concentration in Milli-Q H_2O, in a total volume of 100 µL. It was illuminated with Megaman Helix daylight lamp (0.3 mW/cm^2). The increase in fluorescence was measured at ex 495 nm / em 515 nm. It was corrected by the average fluorescence of the untreated reaction mixture and by the autoxidation of the assay reagent, values are mean ± σ for n = 3. SO = SOPP3, Ds = DsFbFpM49I. **a**, Fusion proteins containing SOPP3. **b**, Fusion proteins containing DsFbFpM49I.

3.8.2.4 Discussion

When comparing the three ROS-specific assays, first, it should be mentioned that the best conditions are different for each assay. However, it can be concluded that the light intensity and the protein concentration are the decisive factors for the outcome of the respective assay. In this regard, the Amplex Red assay for H_2O_2 and $O_2^{\bullet-}$ detection differed from the other two assays. For the Amplex Red assay, low protein concentrations (1 µM) and very low light intensities (0.3 mW/cm^2) showed already good results, and the linear range of the assay was not exceeded under these circumstances. With higher light intensity (0.9 mW/cm^2), the assay could also be conducted, however, it exceeded the linear range after 10 min illumination time. Regarding the SOSG assay for $^1O_2$ detection, a higher protein concentration (4 µM) and light intensity (0.9 mW/cm^2) were necessary to yield detectable $^1O_2$ formation. For the APF for HO• detection, both settings showed comparable results.

For all assays, the chromophore FMN was also measured. However, results of FMN measurements need to be taken with caution, as errors/fluctuations can occur during weighing of small FMN amounts and during pipetting for the preparation of dilutions (for a concentration of 1 µM or 4 µM).

Regarding the outcome of the assays, interestingly, the fusion of the PSPs to the hydrophobin mHGF1 in a 1:1 ratio (mHGF1-SOPP3 or mHGF1-DsFbFpM49I) improved

the production of all three ROS. Moreover, regarding H_2O_2, $O_2^{\bullet-}$ and $HO^{\bullet}$ production, fusion proteins containing the protein DsFbFpM49I clearly showed higher activity. Regarding $^1O_2$ production, fusion proteins containing SOPP3 or DsFbFpM49I showed similar results.

Therefore, it can be concluded that the PSP DsFbFpM49I is more active towards a type-I photosensitizing mechanism than the PSP SOPP3. This leads to a higher $HO^{\bullet}$ production, which is the most reactive species towards the attack of covalent C-H or C-C bonds. The conclusion can be drawn, that the fusion protein containing DsFbFpM49I in the conformation mHGF1-DsFbFpM49I will be the best candidate for an application in PE degradation.

3.8.3 Oxygen consumption

The PSPs need oxygen to produce ROS. Therefore, the idea arose to measure dissolved oxygen and observe if there is a drop in oxygen concentration due to ROS production if a PSP is present and is illuminated. To achieve this, an oxygen sensor (PyroScience) was used. It consists of a fiber-optic sensor which is coated with an indicator (REDFLASH), which shows luminescence when excited with red light. Oxygen quenches this luminescence of the indicator and therefore, the luminescence intensity can be correlated to the oxygen concentration. It is important to mention, that initial oxygen measurements were conducted before determining the strongest ROS producers (chapter 3.8.2). Therefore, initial measurements were conducted with fusion proteins containing the PSP SOPP3.

First, a selected fusion protein (SOPP3-mHGF1-SOPP3) was illuminated with a light intensity of 7.0 mW/cm^2 and the concentration of dissolved oxygen was measured. A decrease in oxygen concentration could be observed, which stopped after approx. 40 min (Figure 85, a). To confirm the correlation between oxygen concentration and ROS production, an APF assay for the detection of $HO^{\bullet}$ was conducted under the same conditions. The result of the assay shows the same behavior. A rise in $HO^{\bullet}$ production which stops after approx. 40 min was observed (Figure 85, b). Therefore, it can be assumed that the protein stops producing ROS after a specific illumination time, presumably because of photobleaching (photodegradation). Oxygen consumption (= ROS production) therefore depends on the time of illumination. This result agrees with the findings during spectroscopic characterization (chapter 3.8.1).

When the selected fusion protein was illuminated with a lower light intensity than before (2.5 mW/cm^2), a slower drop in oxygen concentration could be observed. On the other hand, if the protein concentration was raised to 9 µM instead of 3 µM, a much faster drop in oxygen concentration was observed. This leads to the conclusion, that oxygen consumption (= ROS production) depends on light intensity as well as protein concentration (Figure 85, c).

With the knowledge that a PSP is only active for a given illumination time, presumably due to photobleaching, an experiment was conducted to find out if the addition of non-

illuminated PSP would lead to a new drop in oxygen concentration (= ROS production). For this experiment, the protein (mHGF1-SOPP3) was illuminated with even higher light intensity (16.4 mW/cm^2) and therefore, the decrease in oxygen concentration already stopped after 30 min, followed by a slow rise in oxygen concentration due to the dissolution of oxygen from the gaseous phase in the reaction vial. Then, the same amount of protein was added. A drop in oxygen concentration similar to the previous one could be observed, leading to the conclusion that ROS production can be recovered in the same reaction vessel by the addition of new protein solution (Figure 85, d).

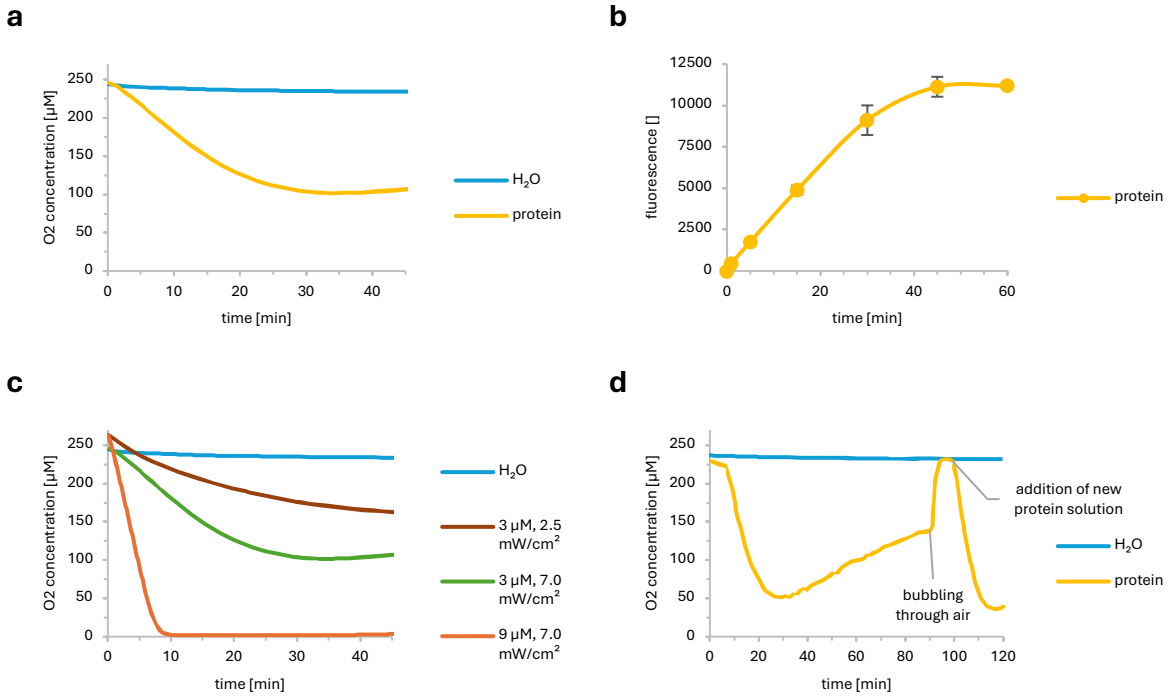

Figure 85| Measurement of oxygen consumption under different experimental conditions. a, Fusion protein SOPP3-mHGF1-SOPP3 (3 µM) was illuminated (7.0 mW/cm^2), and a drop in oxygen concentration was observed until approx. 40 min. **b**, The APF assay for the detection of HO$^\bullet$ was conducted with fusion protein SOPP3-mHGF1-SOPP3 (2.5 µM protein, 15 µM APF in Milli-Q H_2O, in a total volume of 100 µL) under the same conditions (7.0 mW/cm^2). A rise in HO$^\bullet$ production was observed for approx. 40 min. The increase in fluorescence was measured at ex 495 nm / em 515 nm. It was corrected by the average fluorescence of the untreated reaction mixture and by the autoxidation of the assay reagent, values are mean ± σ for n = 3. **c**, Different concentrations of fusion protein SOPP3-mHGF1-SOPP3 (3 and 9 µM) were illuminated using different light intensities (2.5 and 7.0 mW/cm^2). The decrease in oxygen concentration depends on protein concentration as well as light intensity. **d**, Fusion protein mHGF1-SOPP3 (2.5 µM) was illuminated with high light intensity (16.4 mW/cm^2). A drop in oxygen concentration was observed until approx. 30 min. After the addition of the same amount of non-illuminated protein, the same drop in oxygen concentration was observed.

Moreover, all fusion proteins were normalized to 2.5 µM chromophore concentration, and the decrease in oxygen concentration during light illumination (16.4 mW/cm^2) was measured. The chromophore FMN was measured under the same conditions. Measurements were done in triplicates with the same oxygen sensor. The measurements showed that the chromophore FMN behaves differently than the fusion proteins. No observable drop in oxygen concentration was observed (Figure 86, a). When comparing

fusion proteins containing either the PSP SOPP3 or the PSP DsFbFpM49I, differences could be observed. Fusion proteins containing SOPP3 showed a faster drop in oxygen concentration which stopped after approx. 30 min (Figure 86, b). Meanwhile, fusion proteins containing DsFbFpM49I showed a slower drop in concentration which stopped after approx. 80-90 min (Figure 86, c). This finding agrees with the results obtained during spectroscopic characterization (chapter 3.8.1). Unexpectedly, the fusion protein DsFbFpM49I-mHGF1 showed a much bigger drop in oxygen concentration than the other fusion proteins containing DsFbFpM49I (Figure 86, d).

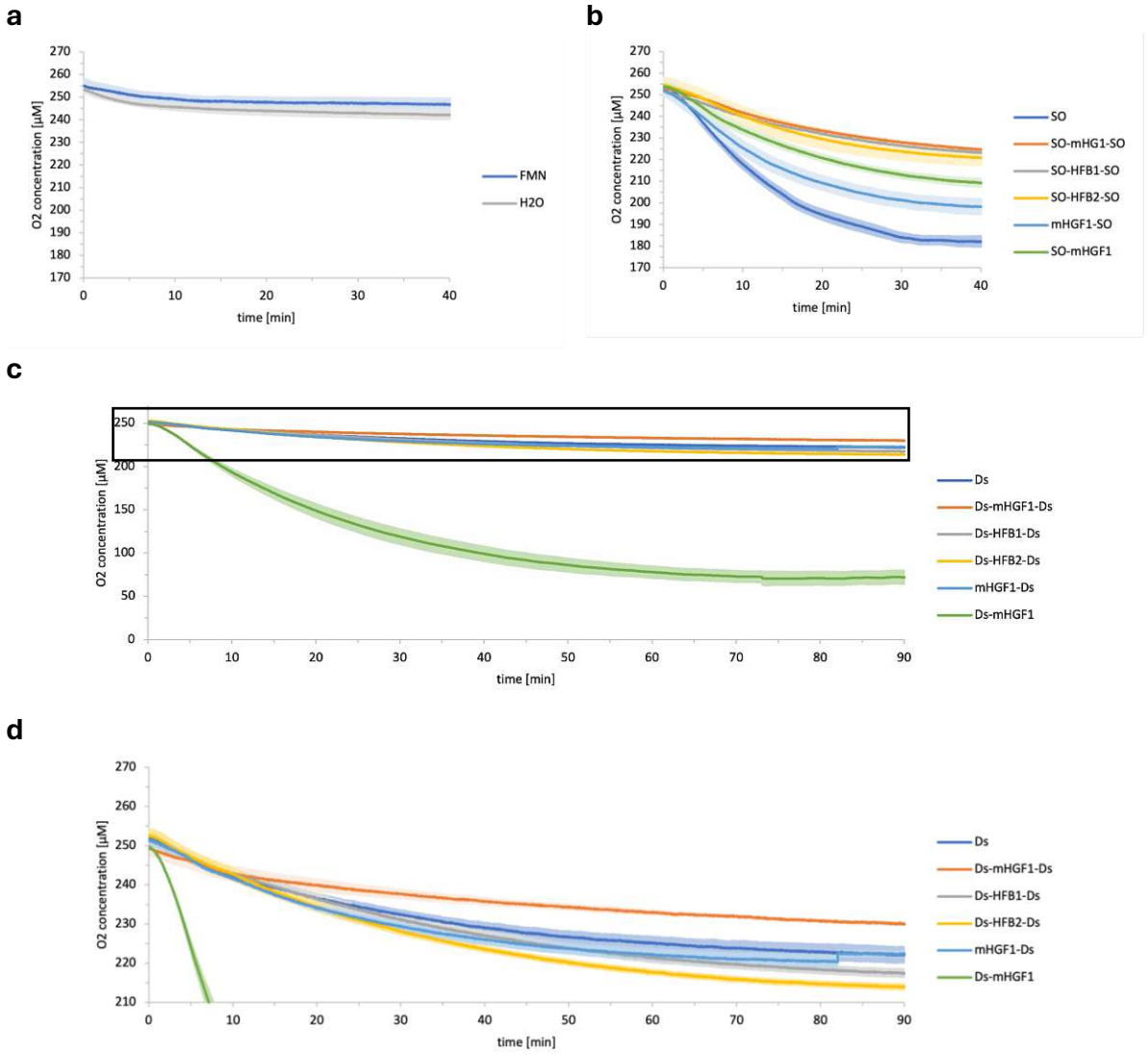

Figure 86| Measurement of oxygen consumption of all fusion proteins. Samples were normalized to 2.5 µM chromophore concentration, and it was illuminated with a light intensity of 16.4 mW/cm^2. Values are mean ± σ for n = 3. SO = SOPP3, Ds = DsFbFpM49I. **a**, FMN. No drop in oxygen concentration was observed. **b**, Fusion proteins containing SOPP3. A drop in oxygen concentration was observed until approx. 30 min. **c**, Fusion proteins containing DsFbFpM49. A drop in oxygen concentration was observed until approx. 80-90 min. **d**, Close-up view of the highlighted area in c. The fusion protein Ds-mHGF1 shows a big drop in oxygen concentration.

There is a correlation between the results obtained during spectroscopic characterization (chapter 3.8.1), characterization of ROS production (chapter 3.8.2), and the oxygen measurements, determining stability (= ROS production activity) of the proteins during blue light illumination. However, there are discrepancies between the quantification of ROS production and the oxygen measurements regarding the amount of consumed oxygen. The oxygen consumption by the different fusion proteins does not reflect all the trends observed during the quantification of ROS production (chapter 3.8.2). Especially, the proteins SOPP3 (Figure 86, b) and Ds-mHGF1 (Figure 86, c) show an exceptional oxygen-consuming behavior. However, it can be concluded that the trend from the quantification of H_2O_2 production is followed (Figure 79), where the proteins SOPP3 and Ds-mHGF1 show the highest H_2O_2 production. Therefore, most of the oxygen is likely consumed in the formation of H_2O_2. Moreover, it can be argued that there was used a much higher light intensity during oxygen measurements than during the assay for quantification of H_2O_2 production (due to the different sensitivities of the detection methods). This could lead to enhanced differences among the different proteins. Nevertheless, it can be concluded that oxygen measurements rather serve as a tool for the qualitative analysis of protein stability/activity, than the quantitative comparison of ROS production by different proteins.

3.9 Analysis of the interaction between fusion protein and polymer

After the determination of the fusion proteins with the highest ROS producing activity and characterization of their behavior when illuminated with blue light, it had to be analyzed if the linkage to the hydrophobin would serve as an “anchor” for the attachment of the protein to the hydrophobic polymer surface (Figure 87). The aim was to show that fusion proteins containing the hydrophobin show stronger adsorption than the original PSP. Moreover, a method for the quantitative desorption of the protein should be developed, as it would simplify the analysis of polymer degradation in subsequent degradation experiments.

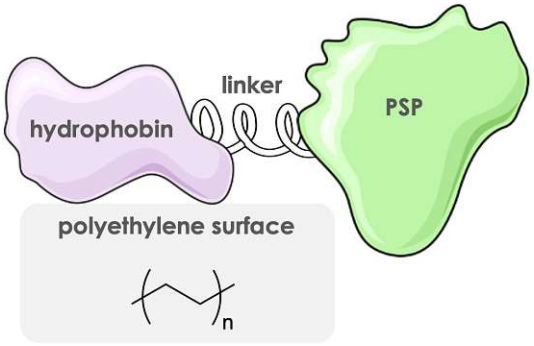

Figure 87| Adsorption of the fusion protein to a hydrophobic polymer (polyethylene) surface. In the schematic representation, the linked hydrophobin leads to an attachment of the fusion protein to the PE surface.

3.9.1 Generation of a smooth polymer surface: spin coating

For a reliable analysis of the polymer surface by several surface analysis techniques (water contact angle measurements (WCA), surface plasmon resonance (SPR), and atomic force microscopy (AFM)), it was necessary to generate a smooth polyolefin surface. Because commercially obtained samples show roughness or impurity due to processing or shipping, a method for the coating of a thin and smooth polymer layer had to be developed. Moreover, for SPR measurements (chapter 3.9.3.4), a very thin (<50 nm) PE layer was needed. According to the literature, several possibilities to generate a smooth PE surface exist. The core principle for all methods is that PE is dissolved in a solvent (e.g., in hot toluene) and applied on a clean and flat surface by different means. The most common coating methods are spin coating, drop casting, or dip coating.[146,199] In the first attempts, drop casting and dip coating showed irregular coatings, due to non-uniform evaporation of the solvent toluene. However, spin coating showed uniform coating. The principle of spin coating is depicted in Figure 88.

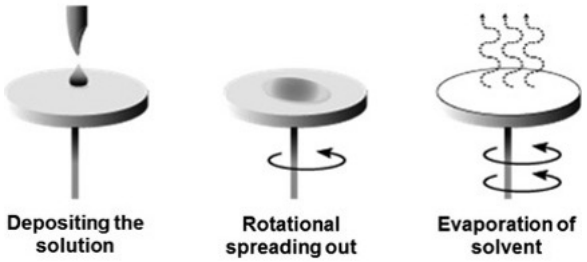

Figure 88| The principle of spin coating. The solution containing the dissolved polymer is deposited on the flat substrate. Then, rotation enables an even spreading out of the deposited solution while the solvent evaporates, and the polymer remains as a thin layer on the substrate. The figure was adapted from Amokrane et al.[200]

For spin coating, low density polyethylene (LDPE) was dissolved in 90 °C hot toluene and applied to the preheated substrate. For SPR experiments, SPR gold sensor slides were spin coated, for other purposes, either glass slides or silicon (Si) pieces were spin coated. A thorough washing protocol was followed to ensure that the respective substrate was clean prior to spin coating. Different concentrations of LDPE and different spin speeds were tried. Finally, it became apparent that the temperature of the substrate during spin coating was the decisive factor, indicating the importance of preheating the substrate before the deposition of the hot solution.

For the expansion of the application of this research, other polymers apart from PE should be used for the analysis of protein-polymer interaction. The polymers polystyrene (PS), polypropylene (PP), polylactic acid (PLA), and polyvinyl chloride (PVC) were used for spin coating, however, the latter two (PLA and PVC) were not analyzed further due to time reasons. For spin coating of PS, the same conditions as for spin coating of PE were used. However, for spin coating of PP, a different solvent and temperature had to be used (*p*-xylene, 125 °C).

3.9.2 Analysis of the pristine polymer surface

The thickness of the spin coated PE on Si was analyzed by ellipsometry (Figure 89). Therefore, 1 x 1 cm Si pieces spin coated with or 1 wt. % LDPE were used. Three samples were measured on at least 5 positions and results showed a thickness of 104.4 ± 5.4 nm.

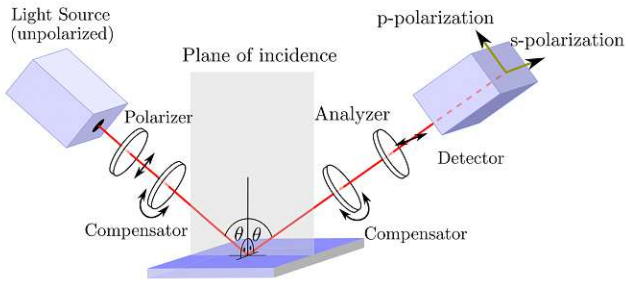

Figure 89| Conventional configuration of an ellipsometer. The figure was adapted from Beyerer et al.[201]

For the analysis of pristine PE, different surface analysis methods were developed. Either commercial PE foil or the spin coated PE on Si samples were analyzed by water contact

angle measurement (WCA), attenuated total reflectance Fourier transform infrared spectroscopy (ATR-FTIR), and X-ray photoelectron spectroscopy (XPS), surface plasmon resonance (SPR) and atomic force microscopy (AFM).

First, WCA measurements were conducted with commercial PE foil. However, due to high fluctuations of the obtained values, it became clear, that a completely smooth surface is needed for reliable WCA measurements. Therefore, subsequent measurements were conducted with spin coated PE. The different substrates glass, SPR gold sensor slide, and Si were analyzed by WCA after spin coating with PE (Table 5). The WCA of the spin coated PE surface was 102-103 °. Because the handling of Si pieces for spin coating was easier than glass slides, further experiments were conducted with spin coated PE on Si, and glass was discarded as a substrate.

Table 5: WCA measurements of spin coated PE on different substrates

Substrate	uncoated	PE coated
Glass slide	22 °	102 °
SPR gold sensor slide	64 °	103 °
Si piece	15 °	102 °

For ATR-FTIR measurements, it was not possible to measure spin coated Si wafer pieces. Si leads to distorted spectra due to the high refractive index of the element. Therefore, for ATR-FTIR analysis the best option was to use commercial PE foil. An ATR-FTIR spectrum thereof is shown in Figure 90.

a

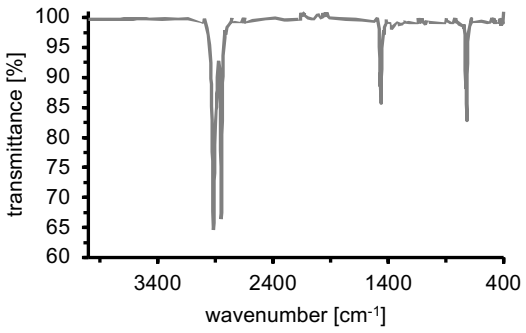

b

Mode of vibration	Wavenumber [cm^{-1}]
CH_2 stretch	2917/2848
CH_2 bending	1465/1462
CH_3 bending	1375
wagging deformation	1368/1351
twisting deformation	1300
CH_2 rocking	729/720

Figure 90| ATR-FTIR analysis of pristine PE foil. a, ATR-FTIR spectrum. **b**, Absorption bands assigned to the respective vibrations in PE.

XPS measurements could be conducted with both, spin coated PE on Si samples, as well as commercial PE foil. An XPS spectrum of PE is shown in the next chapter 3.9.3.3. For SPR measurements, spin coated PE (0.5 wt. % LDPE) on SPR gold sensor slides were used. Fitting of the PE layer thickness was done, and results indicated a thickness of approx. 30 nm. This was suitable for further SPR measurements. Moreover, spin coated PE on Si samples were analyzed by AFM. The topography of the surface was analyzed in imaging mode. The surface roughness and the texture of the PE layer could be analyzed (Figure 91).

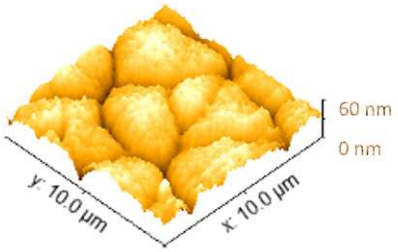

Figure 91| Imaging of spin coated PE on Si by AFM. A 10 x 10 µm section was analyzed. The surface showed a grain-like structure with a height of approx. 60 nm.

3.9.3 Analysis of the adsorption of fusion proteins to the polymer surface

After generating the polymer surface, it could be analyzed if the fusion proteins adsorb better to the surface than the original PSPs. The important question arose, which surface analysis techniques would be best for the analysis of the interaction between the protein and the polymer surface? The best techniques for this application resulted to be WCA, ATR-FTIR, and XPS.

Most experiments regarding the analysis of protein adsorption and desorption were conducted before identifying the most effective ROS producers (chapter 3.8). Therefore, most experiments were carried out using fusion proteins containing the PSP SOPP3.

3.9.3.1 WCA (Water Contact Angle measurement)

As mentioned in the previous chapter 3.9.2, initial WCA measurements were conducted with commercial PE foil instead of spin coated samples. For adsorption experiments, the purified protein solution (3 µM) was added to approximately 1.5 x 1.5 cm PE foil samples. The surfaces were incubated with the respective protein solution and then washed and dried. Water contact angle measurements were performed in triplicates. For the first trials, the PSP SOPP3 and the fusion protein SOPP3-mHGF1 were used. As anticipated, the WCA after incubation with the fusion protein was significantly smaller than the WCA after incubation with the original protein SOPP3 (Table 6). This indicates that the former shows stronger adsorption to the hydrophobic polymer surface, leading to a higher change in WCA. There was also conducted an experiment to analyze the adsorption of these two proteins to a gold surface which showed a similar trend (chapter 16.8.3).

However, it became clear, that a smooth surface is needed for reliable measurements. The PE foil made the measurement of WCA difficult due to tilted or uneven surface characteristics. Measurements were not reproducible. Thicker PE samples or PE foil attached to an even glass surface by double-sided tape also led to unreliable results. It was concluded that also surface irregularities like scratches, roughness, or grease led to high variation in measured WCA. Therefore, the PE samples prepared by spin coating offered a solution to these problems, as they offered a completely even and clean surface. When the adsorption experiment was repeated with spin coated PE on Si samples, more reliable results were obtained and a higher change in WCA was observed (Table 6).

Table 6: WCA of PE foil or PE on Si after incubation with protein solutions[a]

	Control Buffer	SO	SO-mHGF1	BSA
PE foil[b]	96.3 ± 0.8 °	87.9 ± 1.0 °	75.1 ± 1.8 °	
PE on Si[c]	102.9 ± 1.3 °	79.0 ± 1.0 °	67.1 ± 1.8 °	75.9 ± 1.3 °

[a] WCA measurements were performed on different areas of the sample surfaces, values are mean ± σ for n = 3. SO = SOPP3.
[b] PE foil was used, 800 µL of 3 µM protein sample was added and incubated at room temperature for 0.5 h, then washed with 25 mL NaPi buffer and dried with an argon stream.
[c] Spin coated PE on Si was used, 800 µl of 3 µM protein sample was added and incubated at room temperature for 2 h, then washed with 25 mL Milli-Q water and dried with an argon stream.

Moreover, the experiment was aimed to be expanded to other polymers than PE. Again, initially, there were used commercially available polymer samples. PP foil and a PS plate were used. After a cleaning protocol, the samples were treated as described in the previous experiment, however, a lower protein concentration was used (0.5 µM). Also, the adsorption to spin coated PE on Si samples was analyzed again. As observed for PE, for the other two polymer samples, the trend could be observed that the fusion protein had a bigger influence on the WCA than the original protein, indicating stronger adsorption of the fusion protein (Table 7). Furthermore, a higher protein concentration of the fusion protein mHGF1-SOPP3 (9 µM) was tested on PP foil. If the protein concentration was too high, a smaller WCA change was observed (72.4 ± 0.5 ° instead of 68.0 ± 0.4°, Table 7). This could potentially be explained by the self-association of the protein. During these experiments, mostly, reproducible results were obtained. However, difficulties arose again because of irregularities (uneven or damaged surfaces) in the commercial PP and PS samples.

Table 7: WCA of PE on Si, PP foil, and PS plate after incubation with protein solutions[a]

	Control	SO	mHGF1-SO
PE on Si	101.2 ± 1.1 °	87.0 ± 0.4 °	77.0 ± 0.4 °
PP foil	103.6 ± 0.3 °	79.1 ± 0.2 °	68.0 ± 0.4 °
PS plate	83.1 ± 0.4 °	63.6 ± 0.2 °	57.8 ± 0.9 °

[a] 0.5 µM protein sample was added and incubated at room temperature for 0.5 h, then washed with Milli-Q water and dried with synthetic air. WCA measurements were performed on different areas of the sample surfaces, values are mean ± σ for n = 3. SO = SOPP3.

It became clear that spin coating would be the best option to provide a smooth and clean polymer surface and thereby generate comparable, reliable results for all 3 polymers. After establishing the protocol for spin coating of PE, PP, and PS (previous chapter 3.9.1), the final conditions for the experimental setup were optimized. WCA was measured on the three polymer surfaces after incubation with the original PSPs SOPP3 or DsFbFpM49I and all their fusion proteins. Moreover, two controls (H_2O and a solution of the free chromophore FMN) were conducted. Results show that all fusion proteins containing a hydrophobin as a hydrophobic “anchor” show higher adsorption affinity than the original PSPs (Table 8, Table 9).

Table 8: WCA measurements of PSP SOPP3 and all its fusion proteins[a]

	Control H_2O	Control FMN	SO	SO-mHGF1-SO	SO-HFB1-SO	SO-HFB2-SO	mHGF1-SO	SO-mHGF1
PE	103.0 ± 0.7 °	103.7 ± 0.5 °	82.9 ± 0.2 °	73.8 ± 0.5 °	74.8 ± 0.2 °	74.6 ± 0.3 °	72.6 ± 0.1 °	79.9 ± 1.1 °
PP	103.9 ± 0.5 °	105.1 ± 0.4 °	76.2 ± 0.8 °	69.0 ± 0.2 °	69.6 ± 0.2 °	68.8 ± 0.2 °	69.8 ± 0.2 °	75.6 ± 1.0 °
PS	96.3 ± 0.0 °	95.7 ± 1.0 °	71.3 ± 0.9 °	69.4 ± 0.2 °	68.5 ± 0.5 °	65.9 ± 0.4 °	66.6 ± 0.4 °	68.8 ± 0.2 °

[a] Conditions: The surface was incubated with 2 µM protein solution for 30 minutes, then washed with H_2O and dried (with compressed air and at 50 °C for 10 minutes). WCA measurements were performed on different areas of the sample surfaces, values are mean ± σ for n = 3. SO = SOPP3.

Table 9: WCA measurements of LOV protein DsFbFpM49I and all its fusion proteins[a]

	Control H_2O	Control FMN	Ds	Ds-mHGF1-Ds	Ds-HFB1-Ds	Ds-HFB2-Ds	mHGF1-Ds	Ds-mHGF1
PE	103.0 ± 0.7 °	103.7 ± 0.5 °	92.3 ± 0.9 °	75.9 ± 0.5 °	81.6 ± 0.5	74.9 ± 1.0 °	76.4 ± 0.2 °	71.7 ± 0.4 °
PP	103.9 ± 0.5 °	105.1 ± 0.4 °	95.9 ± 0.7 °	76.8 ± 0.6 °	75.7 ± 0.9 °	72.3 ± 0.7 °	72.7 ± 0.5 °	71.5 ± 0.1 °
PS	96.3 ± 0.0 °	95.7 ± 1.0 °	74.5 ± 0.3 °	73.5 ± 0.4 °	74.2 ± 1.2 °	72.8 ± 0.4 °	69.9 ± 0.4 °	64.7 ± 0.5 °

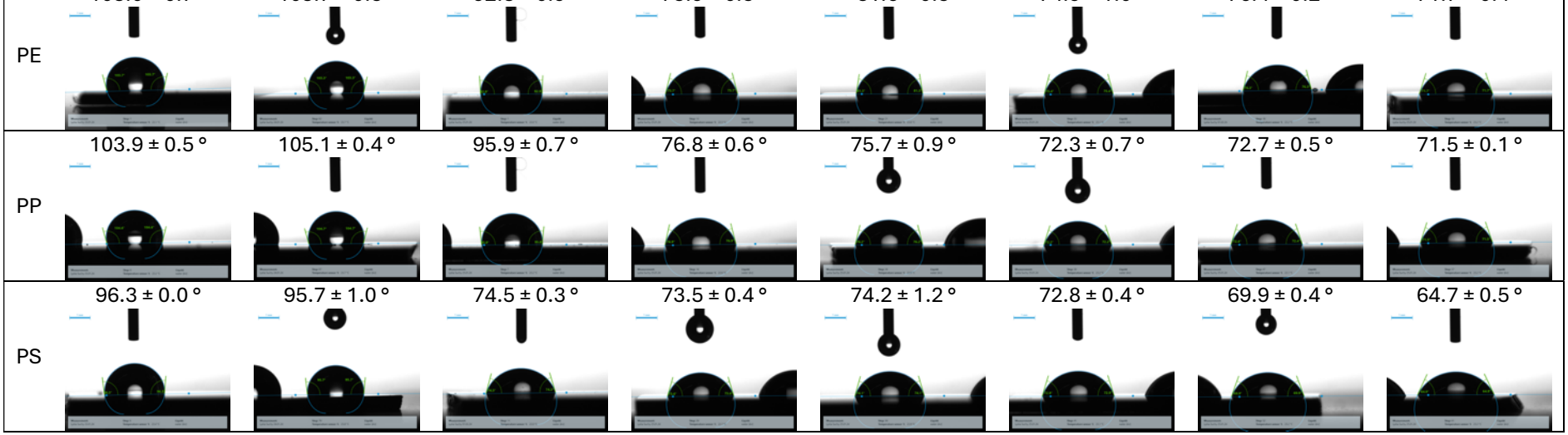

[a] Conditions: The surface was incubated with 2 µM protein solution for 30 minutes, then washed with H_2O and dried (with compressed air and at 50 °C for 10 minutes). WCA measurements were performed on different areas of the sample surfaces, values are mean ± σ for n = 3. Ds = DsFbFpM49I.

3.9.3.2 *ATR-FTIR (Attenuated Total Reflectance Fourier Transform InfraRed Spectroscopy)*

The adsorption of protein to the polymer surface was analyzed by ATR-FTIR. Therefore, commercial PE and PP foils were used. Amide bonds in a peptide or protein show characteristic bands in the IR (Table 10). A comparison of the original PSP SOPP3 and fusion protein mHGF1-SOPP3 is shown in Figure 92. PE as well as PP foils were analyzed. Results obtained by this analysis method agreed with WCA measurements. Fusion proteins containing a hydrophobin show higher adsorption affinity than the original LOV proteins. However, ATR-FTIR is a semiquantitative analysis method, and therefore, only qualitative statements can be made.

Table 10: Characteristic IR-bands for amide bonds in a peptide/protein

Peptide/protein signal	Mode of vibration	Wavenumber [cm^{-1}]
Amide A	N-H stretch	3400-3200
Amide I	C=O stretch	1680-1620
Amide II	N-H bend, C-N stretch	1550-1500

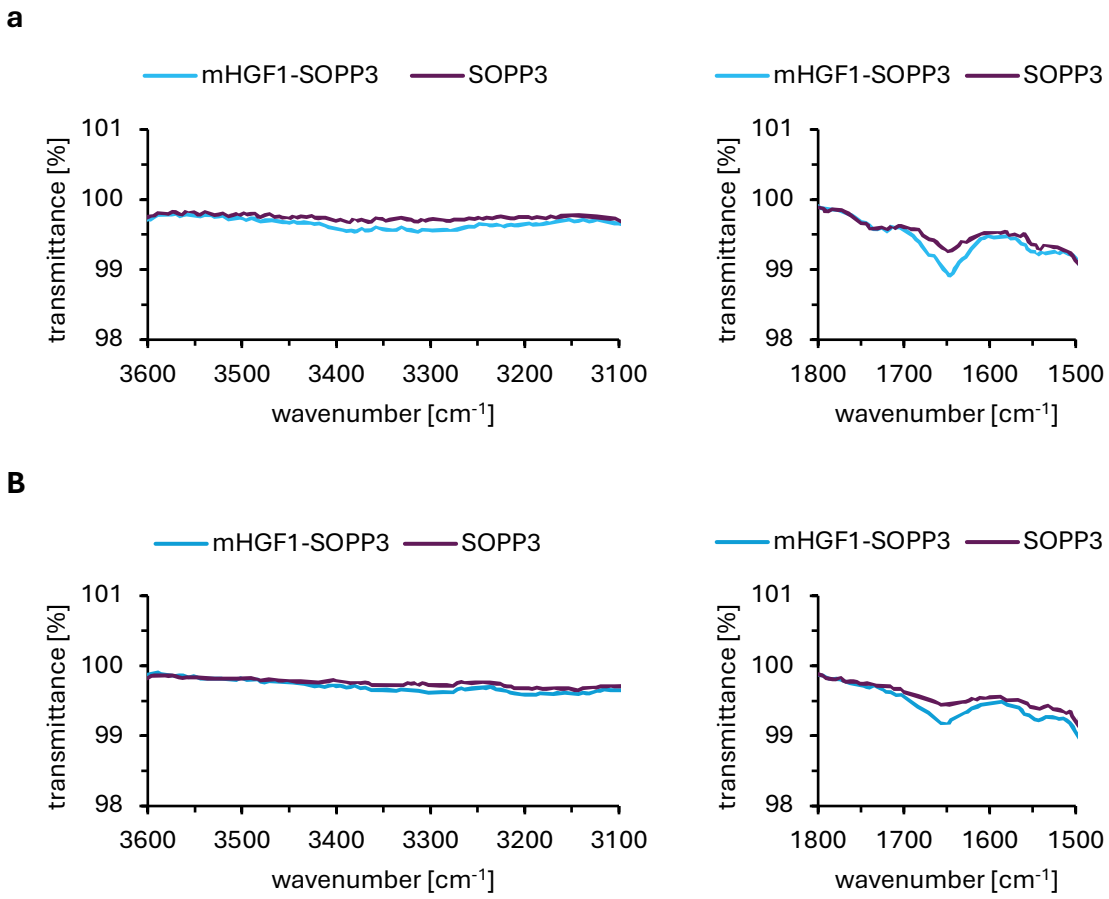

Figure 92| Adsorption behavior of SOPP3 and mHGF1-SOPP3. ATR-FTIR magnified and superimposed spectra of adsorbed SOPP3 and the fusion protein mHGF1-SOPP3 showing the characteristic bands for amide bonds in a peptide or protein. It was incubated with 1 µM protein for 30 min, then washed with H_2O and dried (with compressed air and at 50 °C for 10 minutes). **a**, Adsorption to PE foil. **b**, Adsorption to PP foil.

3.9.3.3 XPS (X-Ray Photoelectron Spectroscopy)

It was tested if XPS would be a suitable method for the analysis of the adsorption of the protein to the polymer surface. Therefore, spin coated PE on Si (1 wt. %) was used. It was incubated with the fusion protein SOPP3-mHGF1-SOPP3 (3 µM) and compared to a control (Figure 93). Table 11 and Table 12 show detailed spectra analysis, indicating the elemental and functional group composition of the two samples.

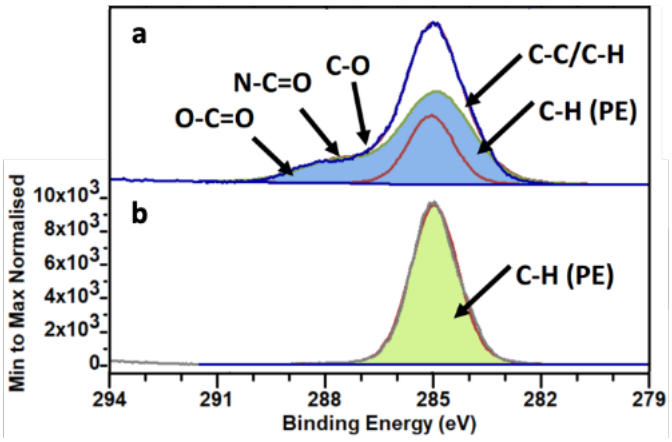

Figure 93| XPS detail spectra (C1s) of PE adsorbed fusion protein SO-mHGF1-SO (a) and comparison to the PE control (b). All spectra have been normalized to their strongest signal.

Table 11: Fusion protein adsorbed to PE

Element [at%]				
C	N	O	Si	
81.2	8.2	8.8	1.8	
Component [at%]				
C-C/C-H	C-O	N-C=O	O-C=O	PE
56.8	1.4	12.5	1.0	28.2

Table 12: PE control

Element [at%]				
C	N	O	Si	
99.5		0.5		
Component [at%]				
C-C/C-H	C-O	N-C=O	O-C=O	PE
				100

3.9.3.4 SPR (Surface Plasmon Resonance)

SPR was expected to be a promising method for real-time analysis of fusion protein adsorption. For SPR experiments, spin coated PE (0.5 wt. % LDPE) on SPR gold sensor slides were used (Figure 94). The adsorption of fusion protein SOPP3-mHGF1-SOPP3 to spin coated PE on SPR gold sensor slide was analyzed. Results show an increase in the SPR signal, which indicates the adsorption of the protein to the PE surface. The amount of adsorbed protein was calculated through the SPR signal increase (Figure 94).

However, this method could not verify anything apart from the adsorption of the protein to the PE surface. The original LOV protein SOPP3 and different fusion proteins were measured under the same conditions. All show approximately the same amount of adsorption, and no desorption of the proteins was observed. According to the instrument specifications, the buffer flow had to be slow and could not exceed 1 mL/min slow buffer flow. Presumably, a different setting for better washing would be necessary for the

desorption. Therefore, SPR did not represent a suitable method for the comparison of different fusion proteins.

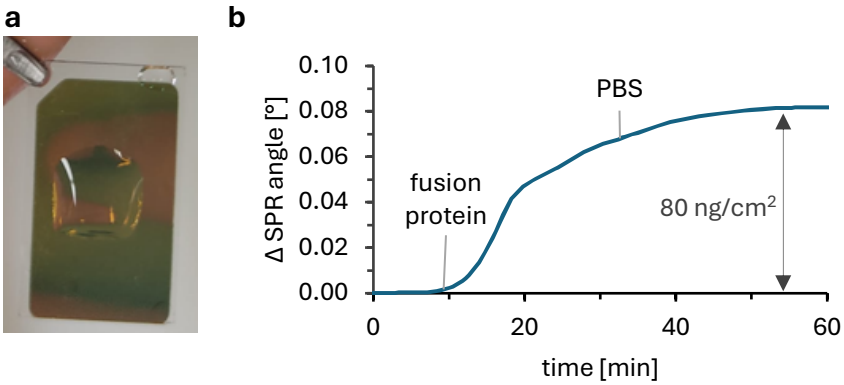

Figure 94| Analysis of adsorption of fusion protein SOPP3-mHGF1-SOPP3 to PE by SPR. a, A spin coated PE (0.5 wt. % LDPE) on SPR gold sensor slide showing the area that is coated with the sample solution. **b**, The protein solution (1 µM, in PBS buffer) was injected for 20 min with a flow rate of 10 µL/min onto the spin coated PE on SPR gold sensor slide. After 20 min, it was switched to PBS buffer. The SPR angle indicates a surface coverage of 80 ng/cm^2.

3.9.3.5 AFM (Atomic Force Microscopy)

AFM was used not only for the analysis of the spin coated PE layer (chapter 3.9.1) but also for the analysis of the adsorption of the protein to the PE surface. 1 wt. % spin coated PE on Si was incubated with 9 µM protein solution under blue light (7.0 mW/cm^2) for 20 h.* The fusion protein SOPP3-mHGF1-SOPP3 was compared to the original PSP SOPP3 or the protein BSA as a control. AFM imaging showed a different behavior of the original LOV protein SOPP3 and the hydrophobin-containing fusion protein (Figure 95). Results showed that the fusion protein showed some kind of agglomeration during denaturation and evaporation of the solvent, while the original LOV protein SOP33 did not show this behavior.

* This experiment was conducted before the analysis of protein stability (chapter 3.8). Therefore, the experiment could have been conducted for a shorter period because of the photobleaching of the PSP (chapter 3.8.1).

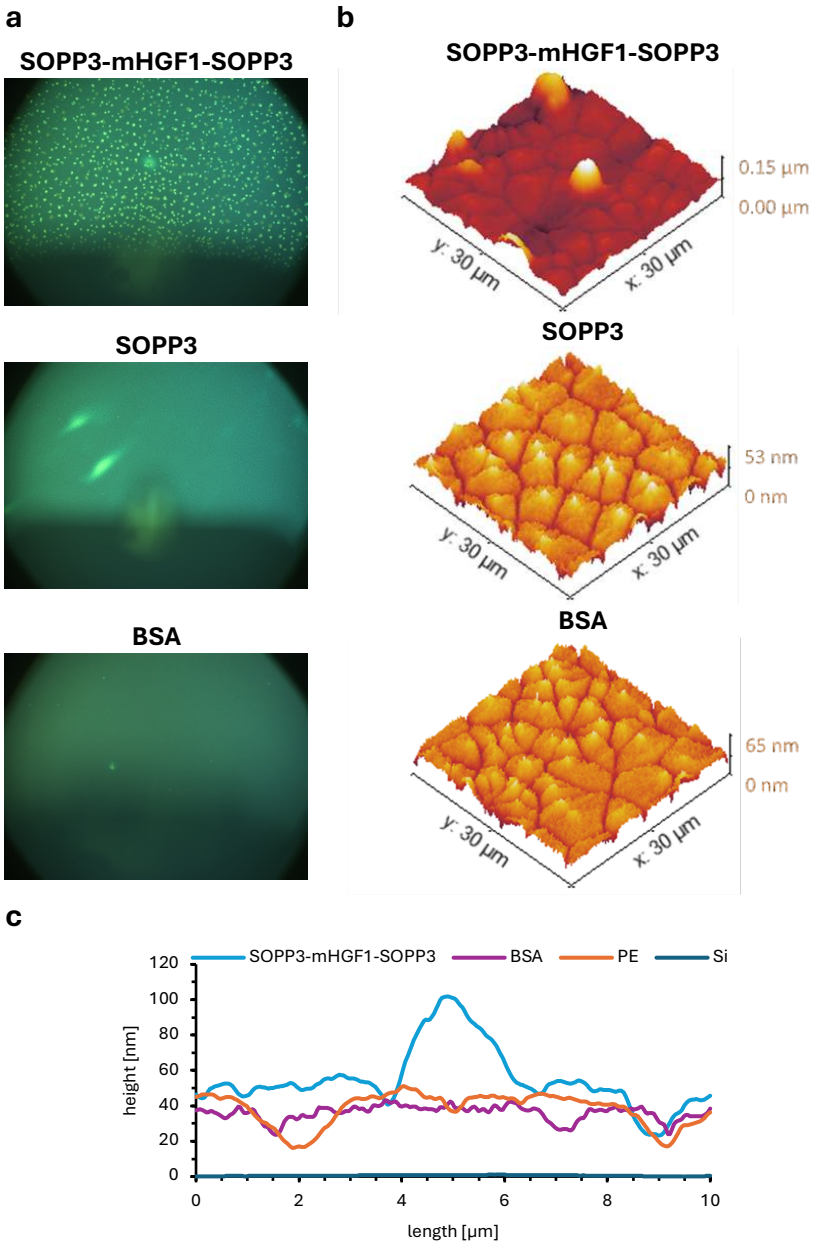

Figure 95| Analysis of protein adsorption to PE by AFM. a, Microscope images of PE samples incubated SOPP3-mHGF1-SOPP3, SOPP3, or BSA. **b**, AFM imaging results of PE samples incubated with SOPP3-mHGF1-SOPP3, SOPP3, or BSA. **c**, Comparison of the height profile of samples SOPP3-mHGF1-SOPP3 and BSA to PE and the uncoated Si surface.

3.9.4 Analysis of the desorption of fusion proteins from the polymer surface

A method for the quantitative desorption of the adsorbed fusion protein should be developed. Firstly, this would simplify the detection of polymer degradation by surface analysis methods in subsequent degradation experiments. Secondly, the desorption of the inactive protein after 30 min of illumination would be necessary, so that the surface can be covered with new active protein. Therefore, different experimental conditions for

the desorption of protein from the PE surface were investigated. Different conditions (EtOH, ethylene glycol, DMSO, EtOAc, AcOH, Tween 20) were tested.

First desorption experiments were conducted and analyzed by WCA. It is presumed that an increase in WCA (which indicates an increase in hydrophobicity) means that the protein desorbs from the surface exposing the hydrophobic PE surface. Therefore, spin coated PE on Si samples were incubated for 0.5 h with the protein solution (fusion protein SOPP3-mHGF1-SOPP3 or control BSA). The samples were not illuminated with light. After measurement of WCA, samples were incubated with the surfactant Tween 20. This did not lead to any change in WCA, indicating no desorption. Repetition of the experiment, where samples were incubated for 0.7 h with 50 % (v/v) EtOH, led to a small change in WCA (Table 13). Interestingly, the BSA control showed a bigger change in WCA, indicating a more efficient desorption of BSA than the fusion protein SOPP3-mHGF1-SOPP3.

The experiment was repeated with a solution that consisted of 50 % (v/v) ethylene glycol and 0.5 % (ω/v) SDS (Table 14). After incubation for 0.5 h and 1.5 h a change in WCA can be observed, however, this change is similar for both the fusion protein SOPP3-mHGF1-SOPP3 and the BSA control. This indicates more efficient desorption under these conditions. However, results from WCA did suggest incomplete desorption.

Table 13: WCA measurements - desorption with 50 % (v/v) EtOH

	Protein solution (3 µM) 0.5 h	50 % (v/v) EtOH 0.7 h
BSA	81.2 ± 0.3 °	94.6 ± 1.0 °
SO-mHGF1-SO	74.5 ± 1.6 °	79.5 ± 1.5 °

Table 14: WCA measurements - desorption with 50 % (v/v) ethylene glycol and 0.5 % (ω/v) SDS [a]

	Protein solution (1 µM) 0.5 h	50 % (v/v) ethylene glycol & 0.5 % (ω/v) SDS 0.5 h	50 % (v/v) ethylene glycol & 0.5 % (ω/v) SDS 1.5 h
BSA	75.4 °	83.0 °	86.2 °
SO-mHGF1-SO	70.7 °	84.6 °	88.7 °

[a] not measured in triplicates

Additionally, SPR was used for the in-situ analysis of desorption with different solvents. Apart from the solvent DMSO, the two previously employed solutions were analyzed: 50% (v/v) EtOH and a solution containing 50 % (v/v) ethylene glycol and 0.5 % (ω/v) SDS. Desorption by the solvent DMSO was analyzed for fusion protein SOPP3-mHGF1-SOPP3. With this solvent, the signal went back to the baseline. However, DMSO led to a tailing of the signal, complicating SPR measurements (Figure 96, a). Other experiments were conducted not only with the fusion protein SOPP3-mHGF1-SOPP3, but also with the original PSP SOPP3 and a BSA control. With 50% (v/v) EtOH, the signal did not go back to the baseline for any of the three proteins (Figure 96, b). This indicated that there was no

desorption which contradicted WCA measurements. However, an explanation could be that for WCA measurements, samples were incubated with the solvent for a longer period. With 50 % (v/v) ethylene glycol and 0.5 % (ω/v) SDS, the signal went back to the baseline for all three proteins (Figure 96, c). This was an indicator that the protein got washed off using this solution which agreed with WCA measurements. However, all experiments were done without illumination of the adsorbed protein.

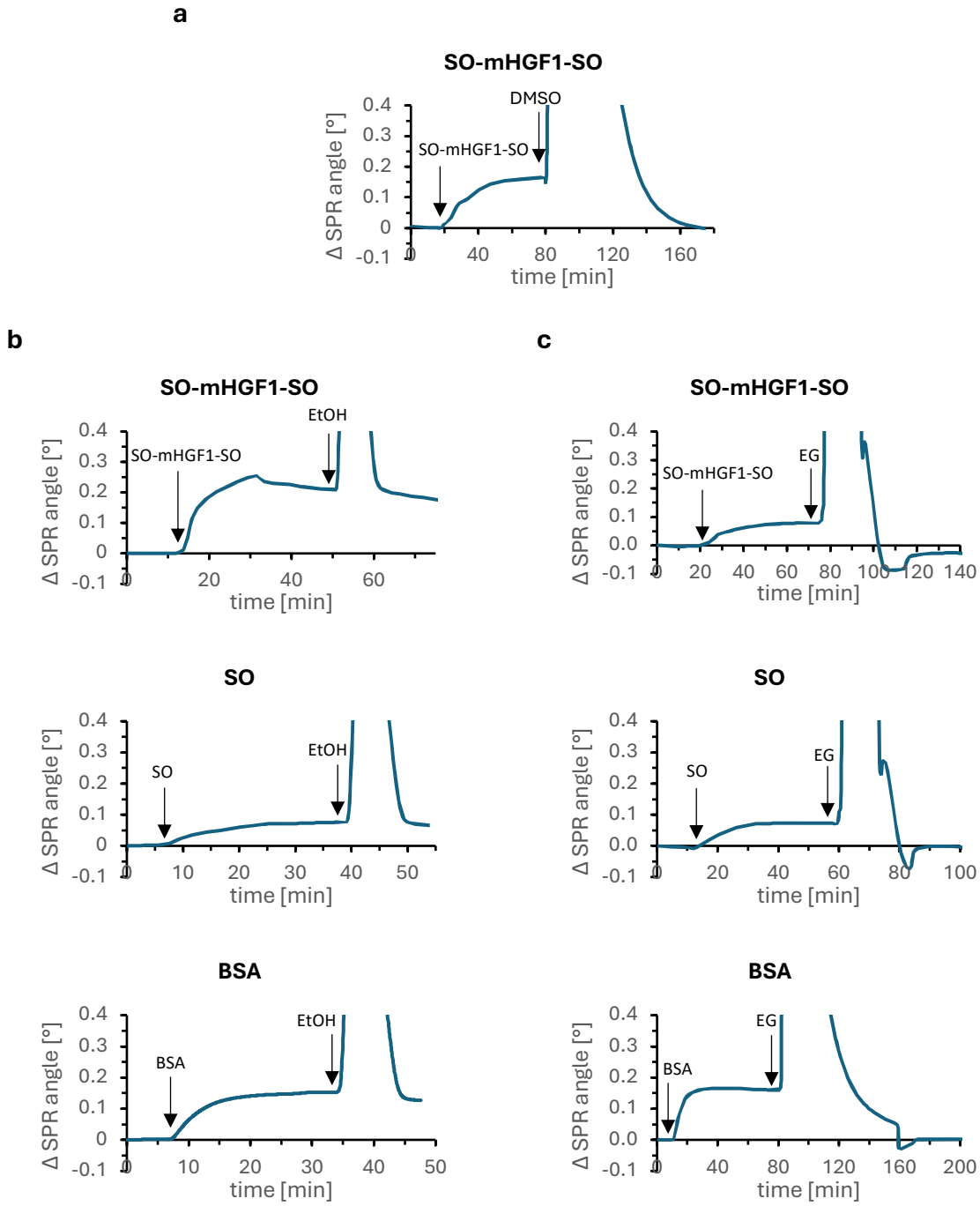

Figure 96| SPR analysis of protein desorption under different conditions. SO = SOPP3. **a**, 6 µM SOPP3-mHGF1-SOPP3, DMSO = 30 % (v/v) DMSO, 10 µL/min, L4 785 nm. **b**, 3 µM protein (SOPP3-mHGF1-SOPP3, SOPP3 or BSA), EtOH = 50 % (v/v) EtOH, 10 µL/min, L2 785 nm. **c**, 1 µM protein (SOPP3-mHGF1-SOPP3 or SOPP3) or 3 µM protein (BSA), EG = 50 % (v/v) ethylene glycol and 0.5 % (ω/v) SDS, 10 µL/min, L4 785 nm.

Another approach for the analysis of desorption was the measurement of ATR-FTIR. This was done by analyzing the change of characteristic bands for amide bonds (Table 15). Therefore, commercial PE foil was incubated for 1 h with 9 µM mHGF1-SOPP3 solution and then incubated for 1 h with either 50 % (v/v) EtOH, 50 % (v/v) ethylene glycol and 0.5 % (ω/v) SDS or 10 % (ω/v) SDS. Results obtained by WCA and SPR could be verified. A small decrease of the protein signals on the PE surface could be observed for 50 % (v/v) EtOH. Better desorption could be observed with 50 % (v/v) ethylene glycol and 0.5 % (ω/v) SDS or 10 % (ω/v) SDS. However almost complete removal of the signals could only be observed when incubated with 10 % (ω/v) SDS (Figure 97).

Table 15: Characteristic IR-bands for amide bonds in a peptide/protein

Peptide/protein signal	Mode of vibration	Wavenumber [cm^{-1}]
Amide A	N-H stretch	3400-3200
Amide I	C=O stretch	1680-1620
Amide II	N-H bend, C-N stretch	1550-1500

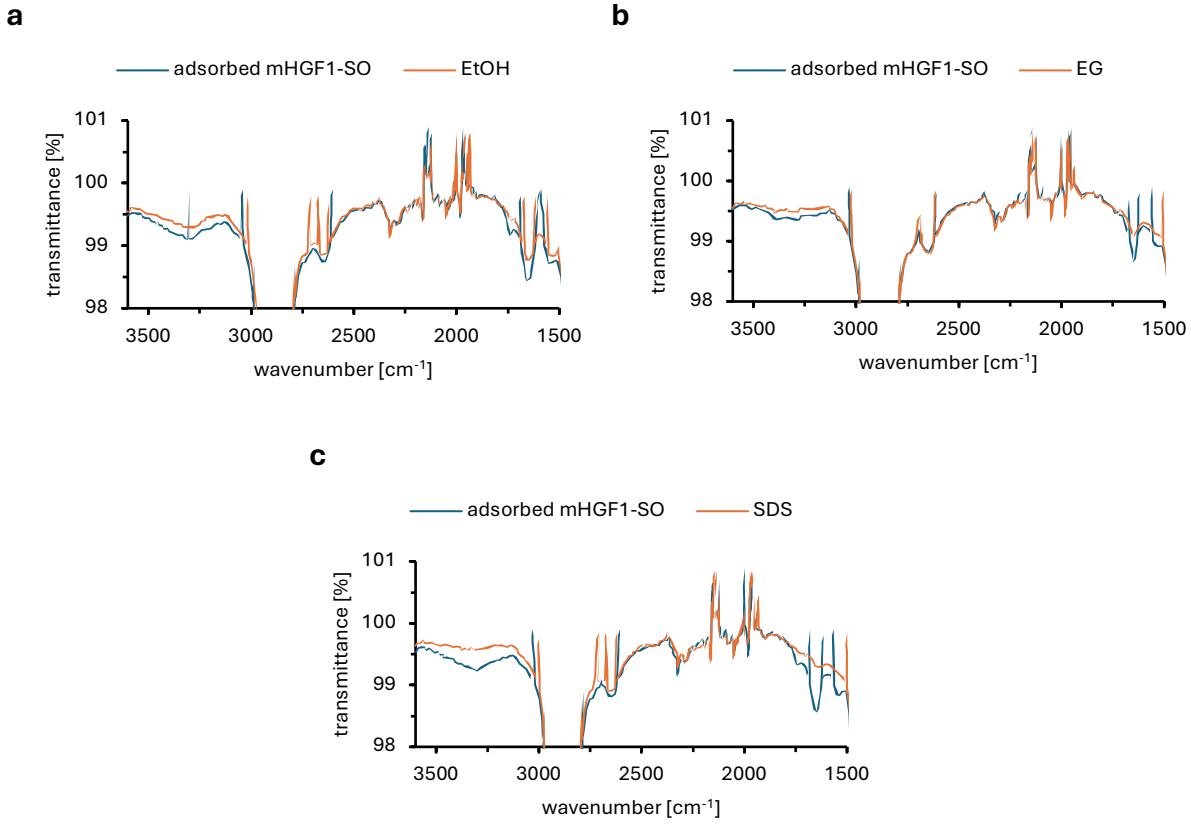

Figure 97| ATR-FTIR analysis of desorption under different conditions. ATR-FTIR magnified and superimposed spectra of adsorbed mHGF1-SOPP3 on commercial PE foil showing the characteristic bands for amide bonds. The sample was incubated with 9 µM protein solution for 1 h, then washed with H_2O, dried, and measured. SO = SOPP3. It was incubated with 50 % (v/v) EtOH (**a**), 50 % (v/v) ethylene glycol, and 0.5 % (ω/v) SDS (**b**) or 10 % (ω/v) SDS at 95 °C (**c**) for 1 h, washed with H_2O, dried and measured.

However, for PE degradation experiments, samples had to be illuminated with light. Therefore, protein desorption should also be tested after light illumination. The experiment was conducted with 9 µM fusion protein mHGF1-SOPP3 which was added to commercial PE foil and incubated for 1 h under blue light (7.0 mW/cm^2). Apart from previously employed EtOH and ethylene glycol solutions, EtOAc, DMSO, AcOH, and protease (1 wt. %) were tested for desorption of the protein from the illuminated sample and analyzed by ATR-FTIR. No difference was observed. When the sample was rinsed with 10 % (ω/v) SDS solution or incubated with the same solution at 95 °C for 5 min, a decrease of the protein signals on the PE surface could be observed. When incubating with the SDS solution at 95 °C for 1 h, quantitative desorption of the protein from the surface could be observed (Figure 98). It can be concluded, that the protein presumably precipitates/denatures during illumination with light (agreeing with results in chapter 3.8), therefore, these different conditions (10 % (ω/v) SDS, 95 °C) were necessary for the solubilization and thereby desorption of the protein.

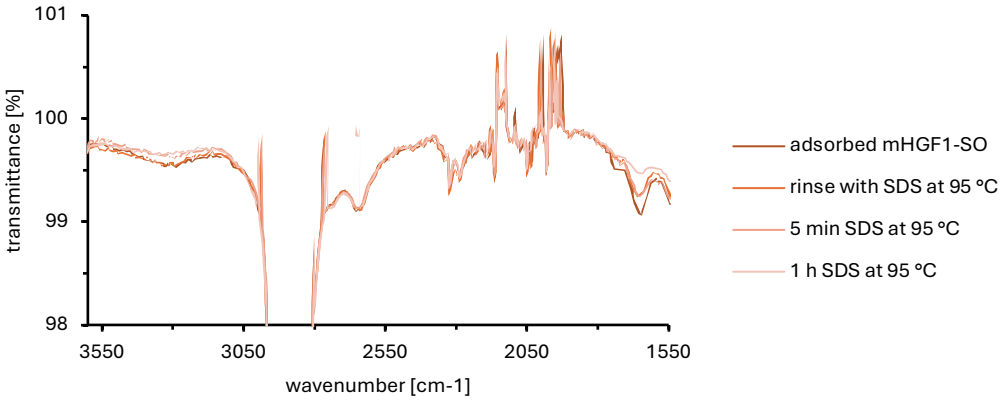

Figure 98| ATR-FTIR analysis of desorption with 10 % (ω/v) SDS after illumination. ATR-FTIR magnified and superimposed spectra of adsorbed mHGF1-SOPP3 on commercial PE foil showing the characteristic bands for amide bonds. The sample was incubated for 1 h with 9 µM fusion protein mHGF1-SOPP3 under blue light (7.0 mW/cm^2), washed with H_2O, dried, and measured. The sample was rinsed with 10 % (ω/v) SDS at 95 °C, incubated with 10 % (ω/v) SDS at 95 °C for 5 min and finally for 1 h, washed with H_2O, dried and measured. SO = SOPP3.

3.10 Quantification of HO• production on the polymer surface

After the first degradation experiments which did not show any positive results (chapter 3.11.2), an important question came up. Can the HO• production be verified directly on the PE surface, or is the protein still not close enough, so that HO• cannot reach the PE surface and are quenched before reaching the surface? Immediate proximity was necessary so that HO• could be generated in situ and reach the surface. The idea came up to expand the APF assay for quantification of HO• production (chapter 3.3.2.3) to analyze the HO• production directly on the PE Surface. Therefore, the assay reagent APF was incorporated into a polyethylene layer for the detection of HO• formation in situ. PE was dissolved in the presence of the reagent APF in toluene and drop cast into the wells of a 96-well plate. Then, the drop casted wells were incubated with either a solution containing the highest HO•-producing fusion protein (mHGF1-DsFbFpM49I, chapter 3.8.2.3) or a solution containing only the dissolved chromophore FMN (20 µM chromophore concentration). For the generation of HO• by the fusion protein or by FMN, it was illuminated for different periods (16.4 mW/cm^2). This was done either with or without the removal of the respective solution. The increase in fluorescence due to the conversion of APF to strongly fluorescent assay product fluorescein by HO• was measured (Figure 99). Incubation with the FMN solution did not lead to any increase in fluorescence in either option, suggesting the necessity of the protein scaffold for the in situ generation of HO• (Figure 99). While the experiment without the removal of the protein solution (Figure 99, a) did not show any rise in fluorescence, the experiment with the removal of the protein solution (Figure 99, b) showed an increase in fluorescence, implying HO• production on the PE surface. Therefore, it can be concluded that HO• can reach the surface, but only after removal of excess aqueous solution leaving only the adsorbed protein. The excess aqueous solution prevents HO• radicals from reaching the PE surface.

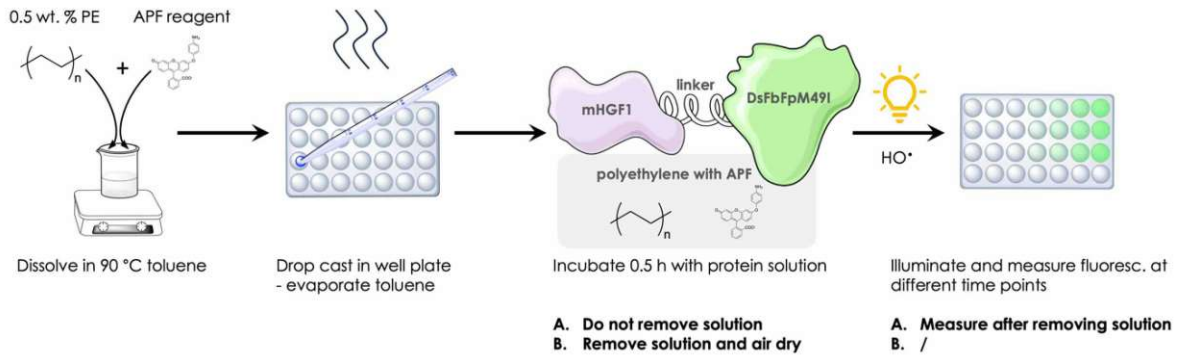

Figure 99| Quantification of HO• production on the PE surface by the fusion protein mHGF1-DsFbFpM49I.

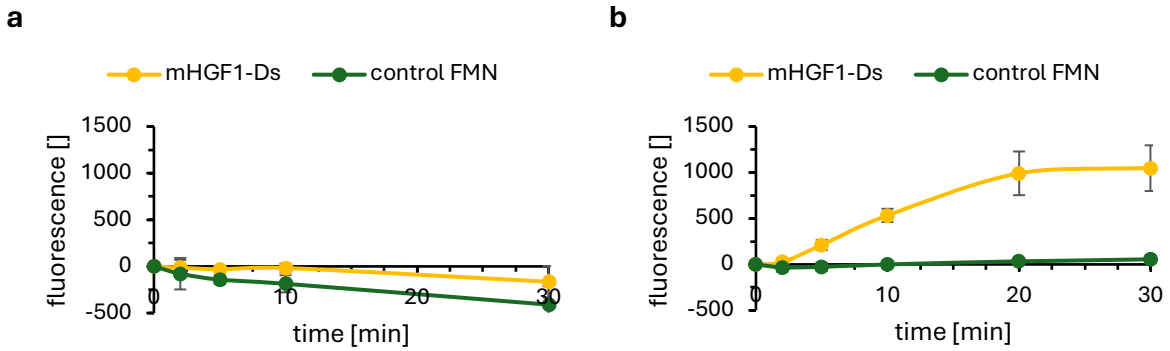

Figure 99| continued. The assay was either conducted without the removal of sample solution (**a**) or with the removal of sample solution before illumination (**b**). It was incubated with 90 µl of protein samples normalized to 20 µM chromophore concentration under white light (0.9 mW/cm^2), values are mean ± σ for n = 3. Ds = DsFbFpM49I.

An attempt was conducted to compare the results obtained by the fusion protein mHGF1-DsFbFpM49I to the Fenton reaction to see if HO• formation is in a similar range. When incubated with 10 mM $FeSO_4$ and 15 % H_2O_2, a similar rise in fluorescence could be observed as in the previous experiment with the fusion protein (Figure 100). This result would imply that incubation with the fusion protein should theoretically lead to a comparable surface oxidation as incubation with Fenton's reagent. However, these results should be taken with caution. Inhomogeneous coverage of the hydrophobic surface during the Fenton reaction due to the exothermic nature of the reaction (bubble formation) led to a high variance in the results.

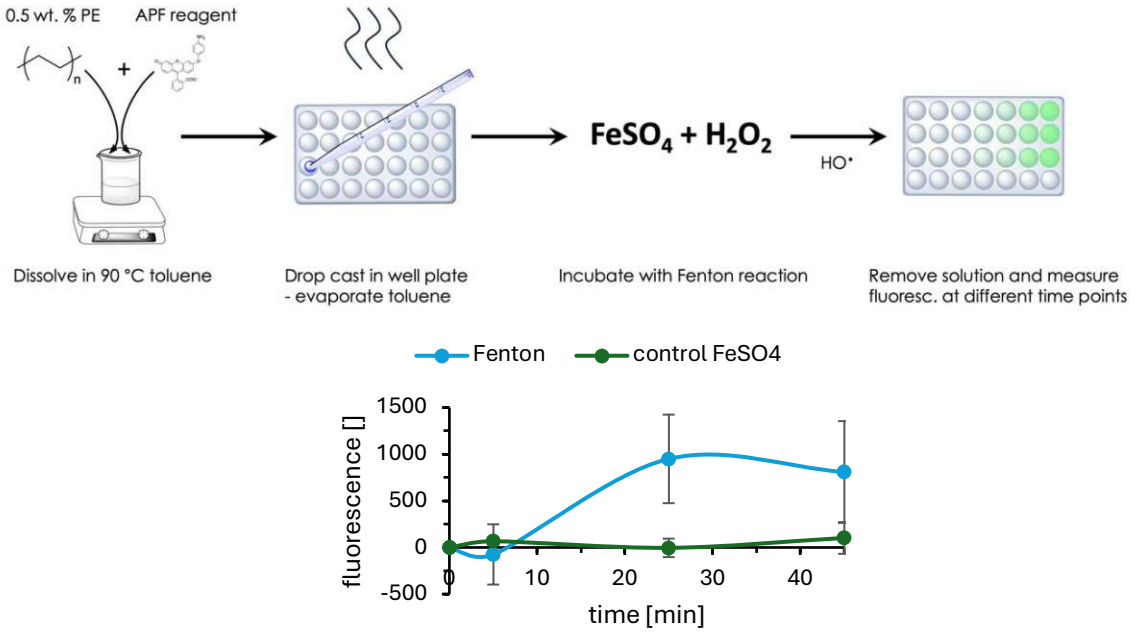

Figure 100| Quantification of HO• production on the PE surface by Fenton reaction. It was incubated with 90 µl of 10 mM $FeSO_4$ and 15 % H_2O_2, values are mean ± σ for n = 3.

3.11 Polyolefin degradation

After the establishment of surface analysis methods, the last problem that had to be addressed was the analysis of oxidative degradation on the PE surface. Oxidation of a PE surface, leading to different functional groups on the inert PE surface (Scheme 6), should be analyzed by the surface analysis methods ATR-FTIR, XPS, and laser induced breakdown spectroscopy (LIBS) (chapter 3.11.3). However, the experimental setup employing a protein makes analysis complicated. As mentioned previously, quantitative desorption of the protein would simplify PE-degradation analysis. This is the case because the signals for oxygen or the functional groups O-H/C=C/C=O, which are decisive for PE degradation, overlap with the same signals coming from the adsorbed protein during analysis. Therefore, desorption of adsorbed protein before analysis is crucial.

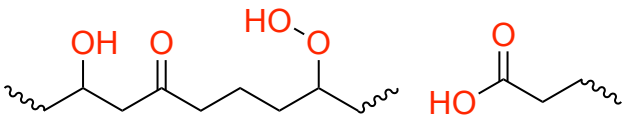

Scheme 6| Scheme of expected functional groups generated during PE oxidative degradation.

3.11.1 Positive control – Fenton reaction

To verify the detectability of an oxidized PE surface, a positive control was conducted. This was implemented by incubating a sample of commercial PE foil with Fenton's reagent. Initially, the reaction was conducted in glass vials (conditions: 10 mM $FeSO_4$, 15 % H_2O_2, in Milli-Q H_2O, pH adjusted to approx. 3 with 2 M HCl). In the first trial, only one reaction was conducted for approx. 1 h. The second trial was conducted for 3 days exchanging the Fenton's reagent every hour. Doing so, the analysis by ATR-FTIR showed a rise in signal in regions characteristic for O-H and C-O regions. However, through XPS analysis, Si-OH, Si-CH_3, and Si-O-Si could be detected. It became clear that the signals in the ATR-FTIR spectrum corresponded to signals from Silicium (Si-OH at < 3000 cm^{-1} and Si-O at approx. 1100 cm^{-1}, chapters 6.8.4 and 6.8.5).

A new trial for PE degradation by Fenton's reagent was done in a hydrothermal reactor (Figure 101), adapting a protocol from Hu et al.[42] Therefore, 4 mM $FeSO_4$, 200 mM H_2O_2 (=approx. 1 %), and 200 mM HCl were incubated for 5 h at 140 °C in a hydrothermal reactor. The remaining PE pieces were washed with 2 M HCl, and H_2O, dried, and analyzed by ATR-FTIR, and XPS (chapters 6.8.4 and 6.8.5).

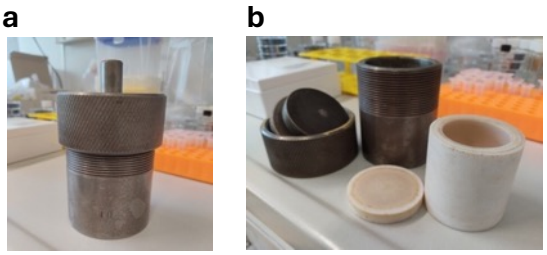

Figure 101| Hydrothermal reactor used for PE degradation by Fenton's reagent. a, The closed hydrothermal reactor. **b**, The open hydrothermal reactor with PTFE liner.

A different approach for PE degradation by Fenton's reagent was the incubation of the PE sample with Fenton's reagent (10 mM $FeSO_4$, 15 % H_2O_2, 10 mM HCl) in a PTFE container at rt (Figure 102). The idea was to conduct the experiment for a long time and regularly add new Fenton's reagent. After 42 h reaction time, exchanging the Fenton's reagent each hour, the PE piece was washed with Milli-Q H_2O, dried, and analyzed by ATR-FTIR, LIBS, and XPS (chapter 3.11.3).

Figure 102| PE degradation by Fenton's reagent in a PTFE container at rt.

3.11.2 Incubation with the selected fusion protein and negative control

First attempts for protein-mediated PE degradation were made during SPR measurements, to analyze PE degradation in situ (chapter 3.9.3.4). The SPR flow cell was coupled to a light source via a fiber bundle and the PE coated SPR gold sensor slide was illuminated with blue light while charging with the fusion protein solution (6 µM SOPP3-mHGF1-SOPP3). However, due to the limited stability of the LOV protein (chapters 3.8.1 and 3.8.3), this setup would require frequent adsorption and desorption of the denatured protein. This would require a complex and long experimental setup, which exceeded the capacities of the instrument. Therefore, the focus was switched to different experimental setups.

Trials were conducted the protein solution was added on top of spin coated PE on Si and it was illuminated with blue light (7.0 mW/cm^2). First, it was incubated with 3 µM fusion protein SOPP3-mHGF1-SOPP3 for 20 h, without exchanging the protein solution. In the next trial, it was incubated with higher concentrated SOPP3-mHGF1-SOPP3 (9 µM) and shaking (150 rpm) for approx. 9 h, but this time exchanging the protein solution every 3 hours. In both cases, XPS measurements showed complete removal of oxygen after a few sputter cycles, suggesting no covalent bond between the surface and oxygen, hence no oxidation of the surface (chapter 6.8.5).

After oxygen sensor measurements (chapter 3.8.3), it became clear that the protein is only active for a short time (less than 1 h). Therefore, a better setup for degradation experiments should be tested. For an automated exchange of protein solution, the idea came up to establish a flow setup. Therefore, a flow cell was made using two glass slides and a rubber septum. A pump with pressure control and a flow regulator with micro tubing was used. The flow regulator was necessary to adjust the flow according to pressure changes. It was important to illuminate only the flow chamber and protect e.g., tubing from light to prevent denaturation of protein and consequent clogging. A commercial PE foil sample was incubated for 16 days with 1 µM fusion protein mHGF1-SOPP3 under blue light (7.0 mW/cm^2). The flow was set to 80 µL/min for 1 min within a cycle of 13.3 min (1 min flow, 12.3 min no flow) resulting in the addition of 80 µl every 13.3 min. After the determination of the best candidate for PE degradation by APF assay for quantification of HO$^\bullet$ production (see chapter 3.8.2.3), the fusion protein mHGF1-DsFbFpM49I was used for further degradation experiments. A control experiment was conducted. Therefore, a PE sample was incubated with Milli-Q H_2O under the same conditions. XPS measurements showed that oxygen was still present after a few sputter cycles, suggesting a covalent bond between the surface and oxygen and therefore some surface oxidation. However, also the negative control showed functionalization with oxygen. No significant difference between the protein samples and the negative control could be observed. Therefore, it was concluded, that the oxidation of the surface was only mediated by blue light illumination (chapters 6.8.4 and 6.8.5).

The next setup for PE degradation was developed including a washing step with 10 % (ω/v) SDS at 95 °C. The desorption with SDS was necessary for the removal of adsorbed photobleached and thus inactive protein before the addition of new protein solution (Figure 103, a). Therefore, a commercial PE foil sample was incubated with a 1 µM solution of the selected fusion protein mHGF1-DsFbFpM49I for 0.5 h. Subsequently, it was illuminated under blue light (16.4 mW/cm^2) for 0.5 h or 1 h. To remove adsorbed protein, the PE sample was washed for 4 min with 10 % (ω/v) SDS at 95 °C and it was rinsed with Milli-Q H_2O. All steps were repeated, leading to a total reaction time of 148 h (Figure 103, b). A negative control with H_2O was conducted under the same conditions.

Following the results obtained during the analysis of HO$^\bullet$ production on the PE surface (chapter 3.10), an improved experimental setup for protein-mediated PE degradation was developed. Under the experimental conditions used, HO$^\bullet$ was produced for 20 min. Moreover, the excess solution was removed before blue light illumination, because HO$^\bullet$ production on the PE surface could only be observed with the adsorbed protein after removing the excess solution. Therefore, a PE sample was incubated with a 1 µM solution of the selected fusion protein mHGF1-DsFbFpM49I for 20 min. After removal of the solution, it was illuminated under blue light (16.4 mW/cm^2) for 20 min. Then, the sample was incubated with 10 % SDS at 95 °C and it was rinsed with H_2O. The experiment was incubated for the same time as the positive control by Fenton's reagent (chapter 3.11.1). Therefore, all steps were repeated, leading to a total illumination time of 42 h (Figure 103, c). A negative control with H_2O was conducted under the same conditions.

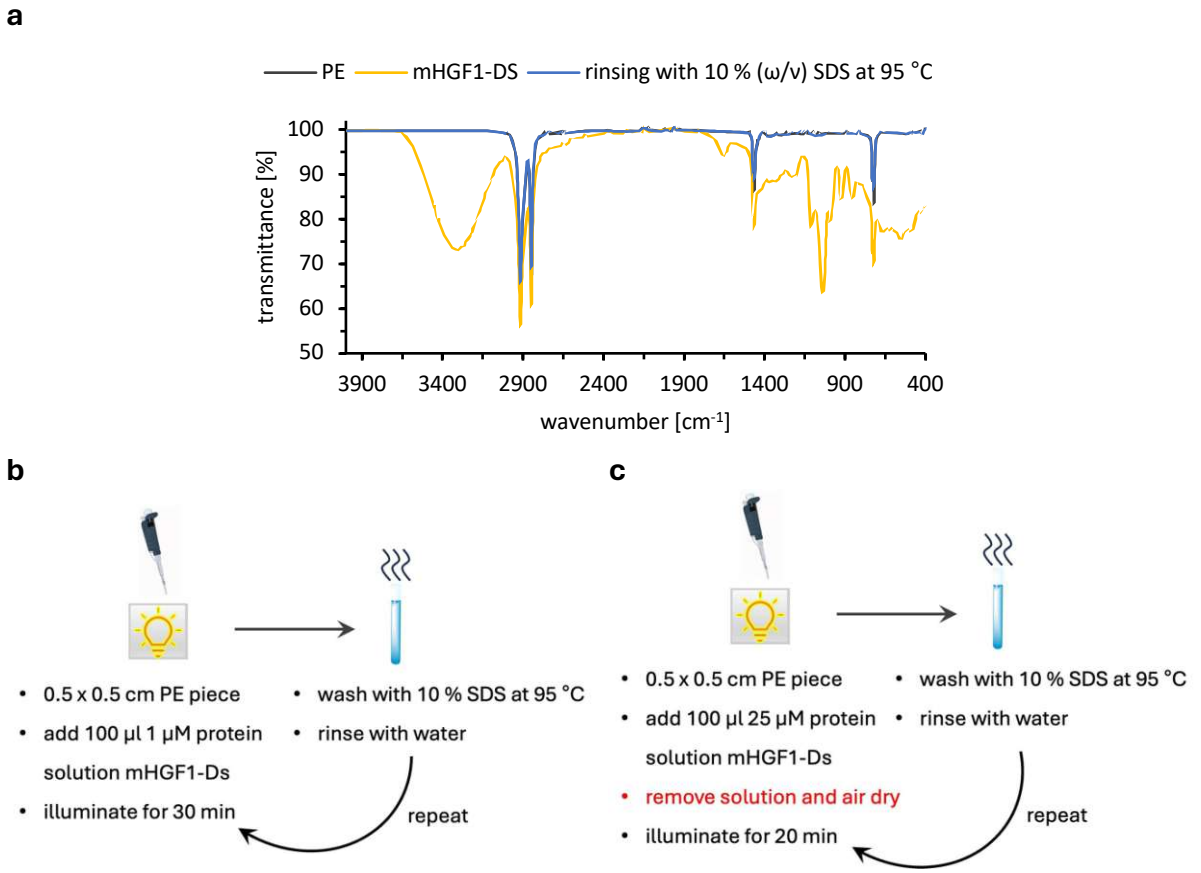

Figure 103| Design of the PE-degradation experiment with fusion protein mHGF1-DsFbFpM49I. a, ATR-FTIR analysis of desorption of mHGF1-DsFbFpM49I with 10 % (ω/v) SDS at 95 °C. **b**, The PE sample was incubated for 0.5 h or 1 h with 1 µM protein solution (100 µL) while illuminating with blue light (16.4 mW/cm^2). Subsequently, to remove the adsorbed protein, the PE piece was washed for 3 min in 10 % (ω/v) SDS at 95 °C. It was rinsed with Milli-Q H_2O and dried with compressed air. All steps were repeated. In total, the sample was illuminated for approx. 148 h. **c**, The PE sample was incubated for 10 min with 25 µM protein solution (100 µL) in the dark. Then, the solution was removed and dried with compressed air. It was illuminated for 20 min (16.4 mW/cm^2). Subsequently, to remove the adsorbed protein, the PE piece was washed for 3 min in 10 % (ω/v) SDS at 95 °C. It was rinsed with Milli-Q H_2O and dried with compressed air. All steps were repeated. In total, the sample was illuminated for approx. 42 h.

3.11.3 Analysis by ATR-FTIR, LIBS, and XPS

In this chapter, the focus lies on the last two degradation experiments with fusion protein mHGF1-DsFbFpM49I (chapter 3.11.2, Figure 103) and their comparison to the positive control (Fenton reaction, chapter 3.11.1). Characteristic IR bands for functional groups generated during oxidative PE degradation are summarized in Table 16.

The positive control (with Fenton's reagent) showed significant oxygen-functionalization during ATR-FTIR analysis (Figure 104). Analysis of the protein-mediated degradation experiment using the fusion protein in solution shows no significant difference between the negative control and the protein-mediated reaction (Figure 104, a). Regarding the last protein-mediated degradation experiment using adsorbed fusion protein for PE

degradation, ATR-FTIR analysis could show some signal in the area for O-H/C=O/C-O, while the negative control showed less signal in these areas (Figure 104, b).

Table 16: Characteristic IR-bands for functional groups generated during oxidative PE degradation

Functional group	Mode of vibration	Wavenumber [cm^{-1}]
Alcohol	O-H stretch	3600-3200
Carbonyl	C=O stretch	1870-1650
Alkene	C=C stretch	1670-1600
Alcohol, ether, ester, anhydride, acetal	C-O stretch	1300-1020

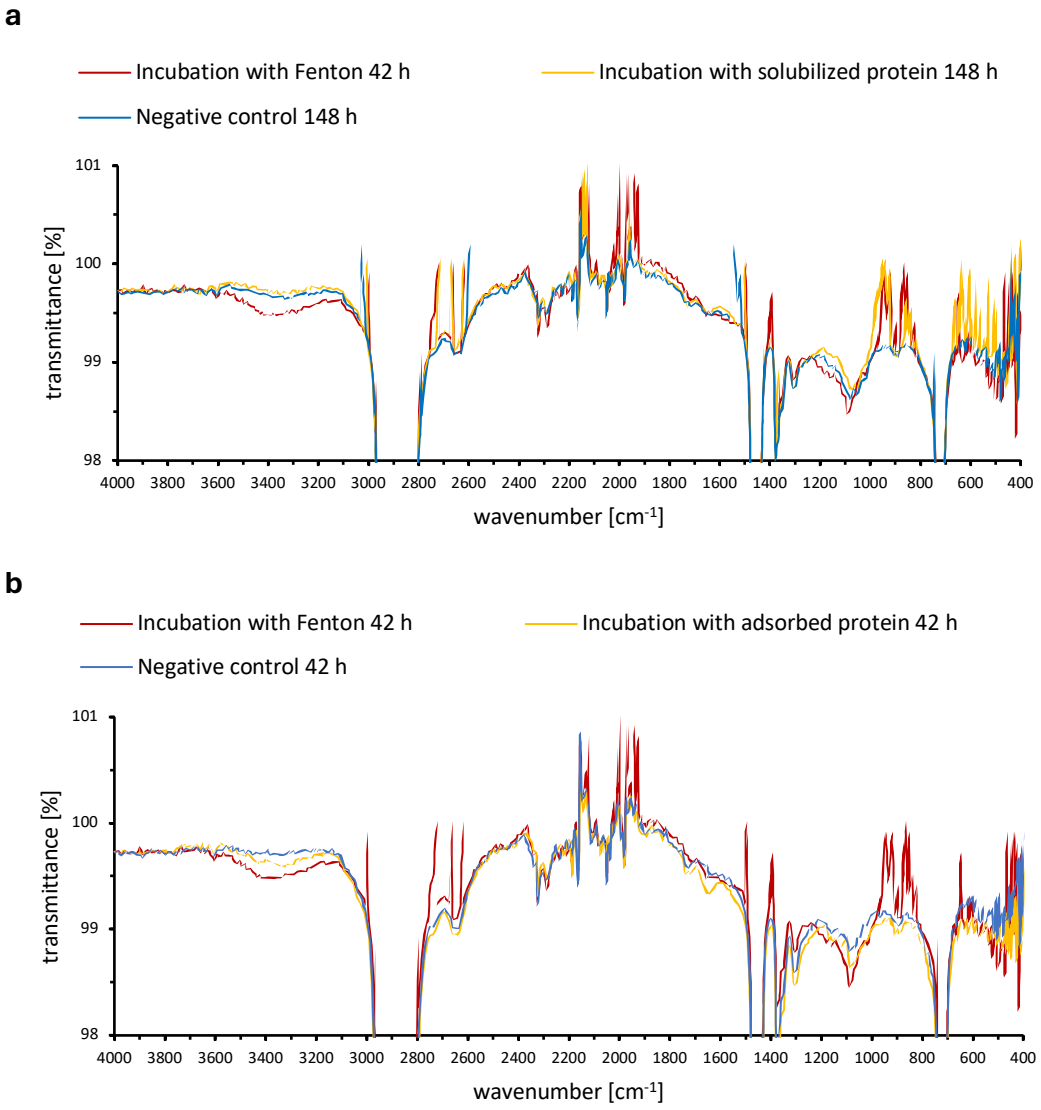

Figure 104| ATR-FTIR analysis of PE degradation. PE-Degradation by Fenton Reaction 10 mM Fe^{2+} & 15 % H_2O_2, exchanging solution each hour, in total 42 h. **a**, PE-Degradation by protein in solution, in total 148 h, a negative control was conducted with Milli-Q H_2O under the same experimental conditions. **b**, PE-Degradation by adsorbed protein, in total 42 h, a negative control was conducted with Milli-Q H_2O under the same experimental conditions.

LIBS measurements (a semiquantitative method that can be used for the detection of oxygen) could validate the results obtained in ATR-FTIR measurement. However, it did show, that oxidation is only on the surface and did not go deeper into the material (Figure 105). However, a disadvantage of this method is that N is not detectable. Moreover, the measurement of oxygen on the surface did not necessarily indicate surface oxidation.

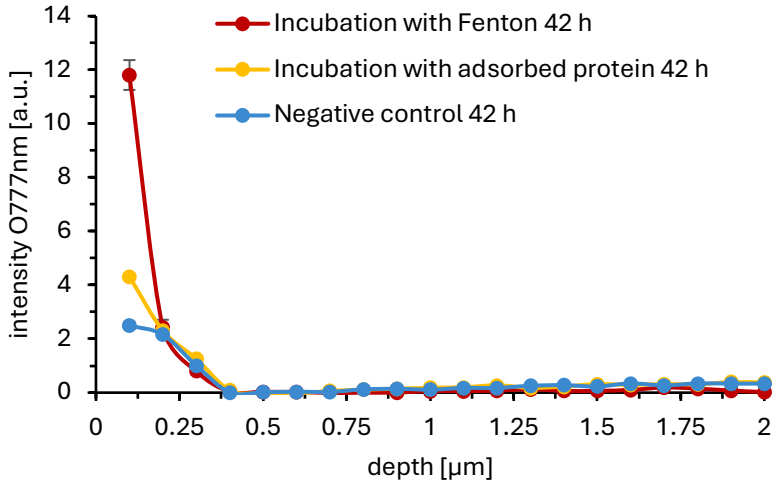

Figure 105| LIBS analysis of PE degradation. PE-Degradation by Fenton Reaction 10 mM Fe^{2+} & 15 % H_2O_2, exchanging solution each hour, in total 42 h. PE-Degradation by adsorbed protein, in total 42 h, a negative control was conducted with Milli-Q H_2O under the same experimental conditions.

Oxygen on the PE surface can be derived from protein. Signals for O-H/C=O/C-O which are decisive for PE degradation overlap with the same signals coming from the adsorbed protein. This represents a difficulty in the detection of surface oxidation. Therefore, XPS depth profiles were analyzed using an Ar gas cluster ion gun, which can remove loosely bound material from the surface. The last 5 sputter cycles before the fastest GCIB setting, after removal of loosely bound material, were compared. The positive control (with Fenton's reagent) showed significant oxygen functionalization (Figure 106, a). While for the protein-mediated degradation experiment using the fusion protein in solution, no difference to the negative control was observed (Figure 106, b), a difference in surface-bound oxygen between the incubation with adsorbed protein and the negative control could be detected (Figure 106, c). The comparison of the first sputter cycle of the fastest GCIB setting (which already can remove covalently bound material) is shown in chapter 6.8.5, Figure 139. Also with this setting, there is still oxygen present in the protein-mediated degradation experiment, while the negative control does not show any traces of oxygen anymore.

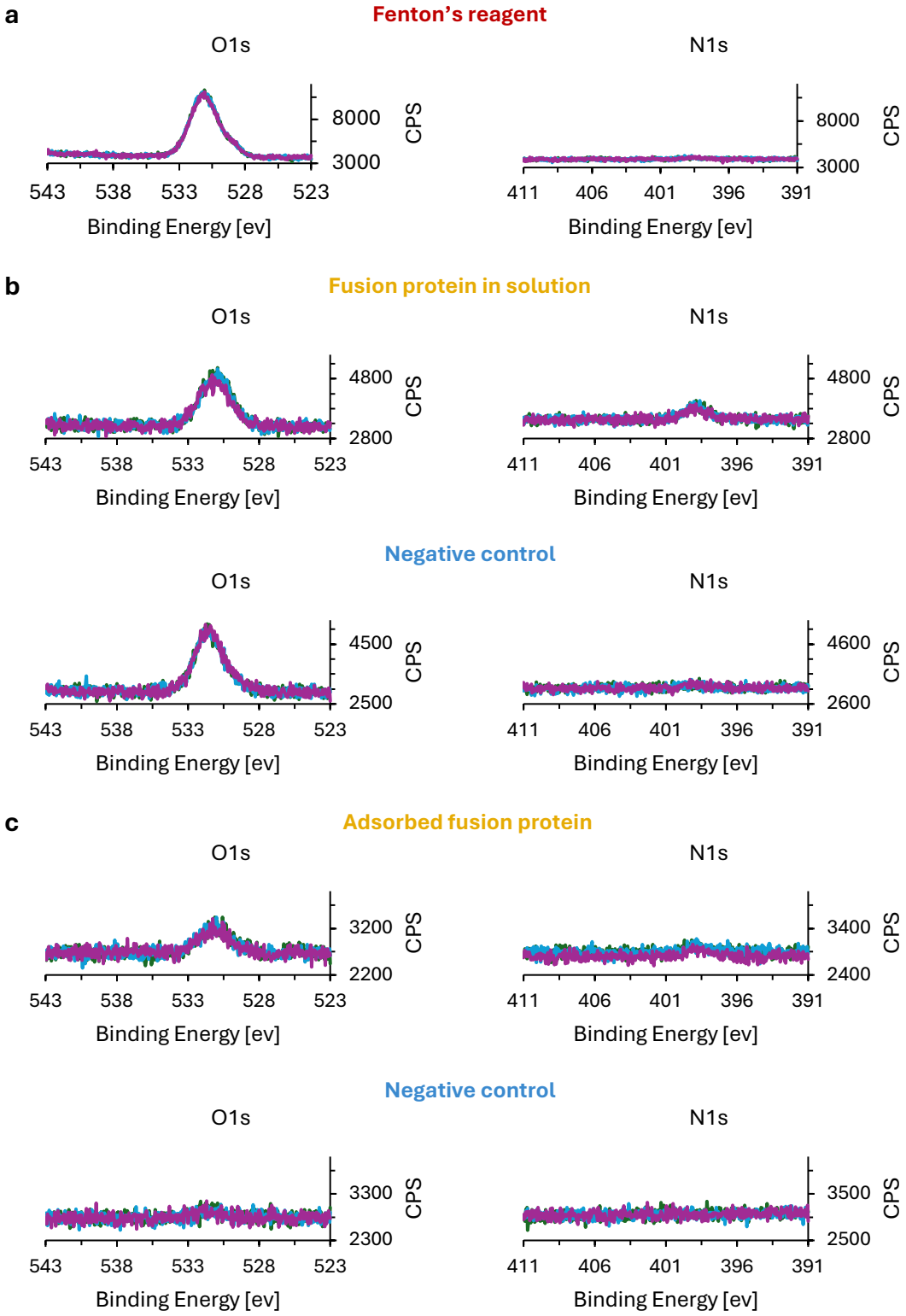

Figure 106| XPS analysis of PE degradation (detail spectra of the O1s and N1s regions). After the removal of loosely bound material by an Ar gas cluster ion gun, the last three sputter cycles before the fastest gas cluster ion beam setting are depicted. **a**, Incubation with Fenton's reagent for 42 h in a PTFE container (Lys1, 0224). **b**, Incubation with fusion protein mHGF1-DsFbFpM49I in solution for 148 h, illumination with blue light (16.4 mW/cm^2) (Lys6, 0224). Negative control (Lys7, 0224). **c**, Incubation with adsorbed fusion protein mHGF1-DsFbFpM49I for 42 h, illumination with blue light (16.4 mW/cm^2) (Lys8, 0724). Negative control (Lys9, 0724).

To ensure that treatment with 10 % (ω/v) SDS at 95 °C did not remove the oxygen from to PE surface, a control experiment was conducted. The positive control sample, which was treated with Fenton's reagent and showed significant surface oxidation, was incubated in 10 % (ω/v) SDS at 95 °C for 15 min. Then, the XPS measurement was repeated. Again, the last 5 sputter cycles before the fastest GCIB setting, after removal of loosely bound material, were compared (Figure 107). Oxygen was still present after Incubation. Therefore, it can be concluded that treatment with SDS did not remove the surface oxidation.

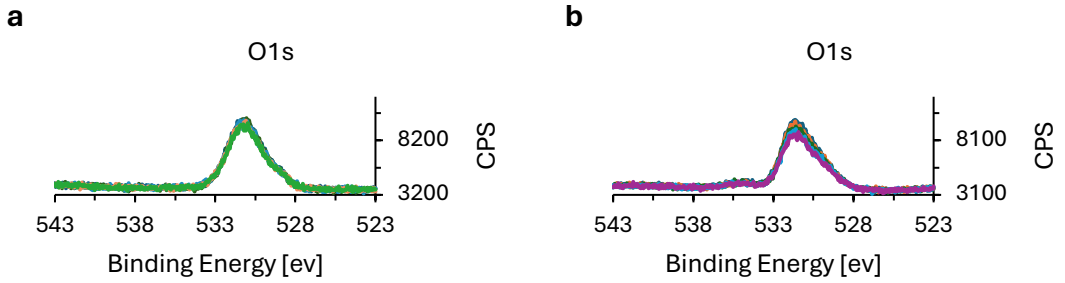

Figure 107| XPS analysis of PE incubated with Fenton's reagent. a, Before treatment with 10 % (ω/v) SDS at 95 °C. **b**, After treatment with 10 % (ω/v) SDS at 95 °C.

Moreover, to show the impact of different sputter conditions, the C1s XPS spectrum of pure PE is shown in Figure 108. While, initial sputter conditions do not influence the PE surface, during final monoatomic Ar sputtering conditions a decrease in C1s can be observed. Therefore, it can be concluded that soft sputter conditions only remove loosely bound (adsorbed) material, while monoatomic Ar sputtering damages the PE surface and therefore can break also covalently bound material.

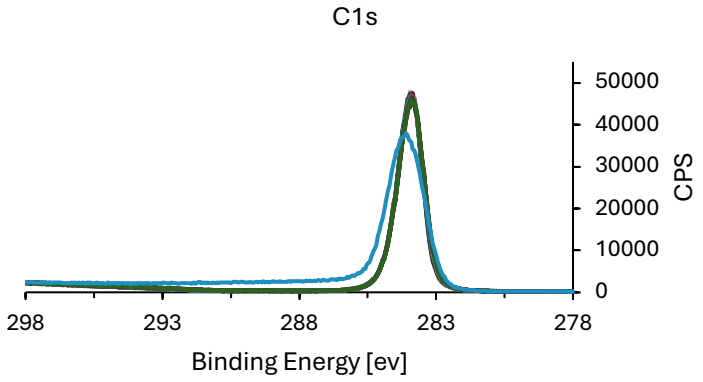

Figure 108| XPS analysis of pristine PE showing C1s. XPS spectra after initial soft sputter conditions by an Ar gas cluster ion gun and after final monoatomic Ar sputtering are depicted. Only with monoatomic Ar sputtering conditions (light blue line), the pristine PE surface can be damaged resulting in a decreased signal for C1s.

4 Conclusion

In this work, a new approach for protein-mediated polymer degradation was developed. Not only protein design and production, but also the development of surface analysis methods for the analysis of the interaction between the protein and the polymer and its degradation, was conducted and is described in this thesis. Therefore, this thesis describes a multidisciplinary work. For the accomplishment of the objective, the disciplines micro-/molecular biology, polymer/material chemistry, and analytical chemistry had to be combined. However, this work represents the first attempt to develop a polymer-degrading catalyst based on ROS producing proteins. It was conducted with a focus on the discipline micro-/molecular biology. Therefore, this work serves as a basis for further interdisciplinary cooperation.

Different photosensitizing proteins (PSPs) were selected, based on their ROS-producing activity reported in literature. After the production and purification of the PSPs, the first challenge arose during the quantification of ROS production. Assays for the detection of different ROS were established and the highest ROS producer was determined. However, it must be mentioned that some factors introduce variability and uncertainty into the outcome of assay measurements. First, the normalization of proteins represents a variable. It requires the precise measurement of protein concentration and requires the same degree of purity of protein solutions. Really small amounts were used to set up the reaction mixture of the assay, which led to a high variability. Moreover, it must be considered that highly reactive ROS can react unpredictably with all surroundings, assay reagents, assay products, buffer components, or other proteins.

To model PE degradation, several attempts were made to detect *n*-heptane degradation. While Fenton's reagent successfully degraded *n*-heptane (as shown by NMR), no significant results were observed with LOV proteins. The main challenge was the incompatible solubility of the alkane and the protein. These experiments highlighted that the key issue in oxidative polyolefin degradation is the proximity of the hydrophilic protein to the hydrophobic polyolefin.

Then, fusion proteins consisting of PSP and hydrophobin were generated. Therefore, genetic constructs were generated by molecular cloning. During expression, difficulties arose due to the insoluble expression of some fusion protein constructs. It became clear that some hydrophobins complicated soluble expression in *E. coli*. Differences were observed between different hydrophobins. Moreover, the conformation played a role in successful expression. The introduction of an artificial hydrophobic moiety (α-helix (LA)12) only yielded insoluble expression. However, 10 different fusion proteins could be successfully produced in *E. coli* and purified.

Fusion proteins were characterized regarding their ROS-producing activity using the established ROS-specific assays. It can be concluded that fusion proteins containing the PSP DsFbFpM49I are more active towards a type-I photosensitizing mechanism than those containing the PSP SOPP3. Interestingly, the fusion of the PSP DsFbFpM49I to the hydrophobin mHGF1 in a 1:1 ratio (mHGF1-DsFbFpM49I) improved the production of all

ROS, including hydroxyl radical HO•, which is the most reactive species towards the attack of covalent C-H or C-C bonds.

Absorption and fluorescence measurements were used as a tool for determining the stability of the fusion proteins towards blue light. The obtained findings correlated with oxygen measurements. The fusion proteins undergo photobleaching already after a short time when they are illuminated with blue light. This is a decisive factor in the planning of degradation experiments. It could be shown that fusion proteins containing the PSP SOPP3 undergo faster photobleaching than fusion proteins containing DsFbFpM49I. Oxygen measurements could be linked to ROS production. Therefore, the decrease in ROS production could be linked directly to photobleaching. Moreover, it was shown that oxygen consumption, and therefore ROS generation, was dependent on the concentration of the protein solution and the light intensity.

The next challenge was the analysis of the adsorption of the protein to a PE surface. Also, desorption was analyzed, as it was necessary for the analysis of PE oxidation. The establishment of methods for surface analysis proved to be the most challenging part of this work. During the development of surface analysis methods, it became apparent that a smooth PE surface was necessary. A spin coating protocol for the generation of such a surface was developed. It was shown that fusion proteins containing the hydrophobin improve adsorption to different hydrophobic polymer surfaces. The most fitting method for this purpose proved to be WCA measurement. Moreover, a protocol for the desorption of the photobleached/denatured protein from a polymer surface was developed using 10 % (ω/v) SDS. For the analysis of protein desorption, ATR-FTIR measurement was the method of choice.

After the first unsuccessful attempts for protein-mediated PE degradation, an assay was developed to analyze the protein's activity directly on the PE surface. Therefore, the APF assay for quantification of HO• production was incorporated into a PE layer. The assay was conducted with either solubilized protein or with a layer of adsorbed protein. The production of HO• directly on the PE surface by the adsorbed fusion protein could be proven, while incubation with solubilized protein did not show HO• production.

The last challenge was the reaction setup and subsequent analysis of PE degradation. The best analysis techniques for this objective proved to be ATR-FTIR, LIBS, and XPS. A positive control was prepared using Fenton's reagent for PE degradation. Analysis showed surface oxidation and could be used as a template for comparison to protein-mediated PE degradation experiments. The positive control (with Fenton's reagent) showed significant oxygen-functionalization during ATR-FTIR as well as XPS depth profile analysis. Several attempts for protein-mediated PE degradation were conducted with different reaction setups. Finally, following the results obtained during the analysis of HO• production on the PE surface, an improved experimental setup for protein-mediated PE degradation was developed which was conducted with adsorbed fusion protein mHGF1-DsFbFpM49I and consisted of iterative adsorption, light illumination, and desorption steps. Analysis of the protein-mediated degradation experiment by ATR-FTIR measurement could show some signal in the area for O-H/C=O/C-O, while the negative control showed less signal in these areas. LIBS measurement could show that oxidation

took place only on the surface and did not go deeper into the material. This was also true for the positive control. During XPS depth profile analysis a difference in surface-bound oxygen between the incubation with adsorbed protein and the negative control could be detected, suggesting surface oxidation by the protein.

It must be mentioned that it is very difficult to analyze the outermost surface layer of any polymer. There are examples of many surface analysis techniques in the literature. However, results should be taken with caution as they are prone to errors and comparability is very difficult due to the many variable parameters. In this research, the focus was put on the analysis of the formation of new functional groups on a PE surface. As previously mentioned, the overlap of protein signals with degradation signals represents a difficulty in the detection of surface oxidation. However, a possibility that cannot be ruled out is that the protein not only adsorbs but could also react with the PE surface forming covalent bonds. Looking at the results obtained during this thesis, there is a hint, that the protein oxidizes the PE surface. However, to verify the real impact, an extension of the research project for more extensive degradation and complementary analysis (e.g., molecular weight measurement (gel permeation chromatography, gravimetric analysis, thickness or imaging measurements (ellipsometry, profilometry, AFM or electron microscopy (EM)) of longer degradation experiments would be necessary.

This work represents a completely new approach for protein-based PE degradation. To our knowledge, no comparable study has been done before. This novelty represents a big challenge for the development of a reaction setup and the establishment of analysis methods. Nevertheless, the positive aspects of this scientific approach are worth attention. Only oxygen, light, and an aqueous environment are necessary for the biocatalyst. A possible outlook would be the incorporation of the proteins into the genome of microorganisms. By secretion, they could be released into their environment. Thus, production could take place locally in e.g. waste management facilities. Expression would only require nutrients for the microorganism. After production, only oxygen and light would be necessary to start the degradation of the polymer waste.

5 Material and methods

All glassware, media, and other solutions that were used during the cultivation of *E. coli* were sterilized before use by autoclaving (220 °C until elevated pressure, then 120 °C, 20 min; WMF Pressure Cooker Cromargan Stainless Steel) or by filtration (sterile syringe filter, 0.22 µm cellulose acetate, VWR International GmbH). Milli-Q H_2O was used for the dilution of protein solutions and all surface analytical techniques.

5.1 Stock solutions

Table 17: Antibiotic stock solutions[a]

Antibiotic	Stock conc. [mg/mL]	Working conc. [µg/mL]
Ampicillin (Amp) in dH_2O	100	100
Chloramphenicol (Cam) in abs. EtOH	34	34
Kanamycin (Kan) in dH_2O	50	50

[a] Solutions were sterilized by filtration and stored at -20 °C

Table 18: Other stock solutions

Compound	Stock conc.	Working conc.
PMSF in abs. *i*PrOH	0.1 M	0.1 mM
Glycerol in dH_2O[a]	60 % (v/v)	30 % (v/v)

[a] Autoclaved before use

5.2 Media

Table 19: Composition of bacterial media

LB-Miller medium (400 mL)[a]	SOC medium (400 mL)[b]
4 g bacto-peptone	8 g bacto-tryptone
2 g yeast extract	2 g yeast extract
4 g NaCl	0.076 g KCl
	3.6 mL 40 % (ω/v) glucose[c]
	4 mL 1 M $MgCl_2$[c]

[a] Filled up to 400 mL dH_2O and autoclaved

[b] Before the addition of glucose and $MgCl_2$, it was adjusted to pH 7, filled up to 392.4 mL, and autoclaved.

[c] Sterilized by filtration separately and added under sterile conditions

Table 20: Bacterial autoinduction media

LB-0.8G (400 mL)[a]	LB-5052 (400 mL)[a]	20 x NPS (400 mL)[b]	50 x 5052 (250 mL)[c]
4.0 g bacto-peptone	4.0 g bacto-peptone	26.4 g $(NH_4)_2SO_4$	62.5 g glycerol
2.0 g yeast extract	2.0 g yeast extract	54.4 g KH_2PO_4	6.25 g glucose
4.0 g NaCl	4.0 g NaCl	56.8 g Na_2HPO_4	25.0 g α-lactose
0.4 mL 1M $MgSO_4$[d]	0.4 mL 1M $MgSO_4$[d]		
8 mL 40 % (ω/v) glucose[e]	8 mL 50 x 5052		
20 mL 20 x NPS	20 mL 20 x NPS		

[a] After the addition of bacto-peptone, yeast extract, and NaCl, it was filled up to 371.6 mL dH_2O and autoclaved
[b] Filled up to 400 mL dH_2O and autoclaved
[c] Filled up to 250 mL dH_2O and sterilized by filtration
[d] Autoclaved separately and added under sterile conditions
[e] Sterilized by filtration separately and added under sterile conditions

Table 21: Composition of LB-agar plates

LB-Agar (400 mL)[a]
4 g bacto-peptone
2 g yeast extract
4 g NaCl
6 g Agar No. 1

[a] Filled up to 400 mL dH_2O and autoclaved; after cooling down to approximately 50 °C, the respective antibiotic was added, and the plates were poured (in standard petri dishes, 94 x 16 mm).

5.3 Buffers and other solutions

Table 22: Composition of standard buffers

50 x TAE Buffer	50 mM NaPi buffer (1 L, pH 7.2)[b]	50 mM NaPi buffer containing 25 % (v/v) glycerol (1 L, pH 7.2)[b]
2 M Tris	33.3 mM Na_2HPO_4 (4.73 g)	33.3 mM Na_2HPO_4 (4.73 g)
5.71 % (v/v) acetic acid	16.7 mM NaH_2PO_4 (2 g)	16.7 mM NaH_2PO_4 (2 g)
50 mM EDTA[a]		25 % (v/v) glycerol (250 mL)

[a] From 0.5 M stock solution adjusted to pH 8 with NaOH
[b] pH was adjusted with 2 M HCl or NaOH

Table 23: Composition of buffers for the preparation of RbCl competent cells

RF1 buffer (200 mL, pH 5.8)[a]	RF2 buffer (100 mL, pH 6.8)[a]
100 mM RbCl (2.42 g)	10 mM RbCl (0.12 g)
50 mM $MnCl_2$ (1.258 g)	10 mM MOPS (0.21 g)
30 mM KOAc (0.589 g)	7.5 mM $CaCl_2 \cdot 2\ H_2O$ (0.11 g)
10 mM $CaCl_2 \cdot 2\ H_2O$ (0.294 g)	15 % (ω/v) glycerol (15 g)
15 % (ω/v) glycerol (30 g)	

[a] pH was adjusted by the addition of 0.2 M acetic acid or 1 M NaOH and it was sterilized by filtration

Table 24: Composition of buffers for IMAC

Equilibration buffer (1 L, pH 7.2)[a]	Elution buffer (1 L, pH 7.2)[a]	Stripping buffer (100 mL, pH 7.5)
25 mM Na_2HPO_4 (3.55 g)	25 mM Na_2HPO_4 (3.55 g)	50 mM Tris (0.606 g)
25 mM NaH_2PO_4 (3 g)	25 mM NaH_2PO_4 (3 g)	50 mM EDTA (20 mL)[b]
0.3 M NaCl (17.53 g)	0.3 M NaCl (17.53 g)	0.5 M NaCl (2.92 g)
10 % (v/v) glycerol (100 mL)	10 % (v/v) glycerol (100 mL)	
30 mM imidazole (2.04 g)	0.4 M imidazole (27.2 g)	

[a] pH was adjusted with 2 M HCl or NaOH

[b] From 0.5 M stock solution adjusted to pH 8 with NaOH

Table 25: Composition of reagents for SDS-PAGE

30 % (ω/v) Acrylamide (100 mL)[a]	10 % (ω/v) APS (10 mL)[b]	0.5 % (ω/v) Bromopehnol blue (10 mL)[c]	10 % (ω/v) SDS (10 mL)[c]
29.2 g acrylamide	1 g APS	50 mg bromophenol blue	1 g SDS
0.8 g N',N'-bis-methylene acrylamide			

[a] After dissolving in 100 mL dH_2O, the solution was filtered into a container with dark glass and kept in the dark at 4 °C

[b] Dissolved in dH_2O, dispensed in 1 mL aliquots, and stored at -20 °C

[c] Dissolved in dH_2O and stored at rt

Table 26: Composition of buffers for SDS-PAGE

10 x SDS running buffer (1 L)	Resolving Gel Buffer (250 mL, pH 8.8)[a]	Stacking Gel Buffer (250 mL, pH 6.8)[a]	Sample Buffer (20 mL)[b]
30.3 g Tris	46.2 g Tris (1.5 M)	15.15 g Tris (0.5 M)	5 mL stacking gel buffer
144 g glycine	10 mL 10 % (ω/v) SDS stock	10 mL 10 % (ω/v) SDS stock	7.8 mL 10 % SDS (final conc. 4 % (ω/v))
10 g SDS			1.2 mL dH_2O
			4 mL glycerol (final conc. 20 % (ω/v))
			2 mL ß-mercaptoethanol

[a] After the addition of SDS, it was filled up to approximately 200 mL, and the pH was adjusted with 2 M or concentrated HCl; then it was filled up to 250 mL and solutions were sterilized

[b] Store at 4 °C without adding ß-mercaptoethanol, add 10 % v/v ß-mercaptoethanol before use

5.4 Cultivation of bacteria

5.4.1 Overnight culture

There was picked a colony from an LB-agar plate (using a pipette tip) and grown in 10 mL LB-Miller medium in a 50 mL falcon tube (supplemented with respective antibiotic). It was incubated at 37 °C for 12-24 h (180 rpm; InforsHT Multitron Standard).

5.4.2 Preparation of cryostocks

For each *E. coli* strain, cryostocks were prepared and stored at -80 °C. Therefore, 0.5 mL 60 % (v/v) glycerol + 0.5 mL overnight culture were combined and stored in a cryogenic vial.

5.4.3 Cultivation on LB-agar plates (recovery of bacteria from cryostock)

While keeping cryostocks on ice, there was used an inoculation loop to take up some cell material and streak it by the four-quadrant streak method on an LB-agar plate (with the respective antibiotic). The plates were incubated upside down at 37 °C (INCU-line VWR International GmbH) for 12-24 h. Plates were stored in the dark at 4 °C.

5.5 Preparation of chemically competent (RbCl) *E. coli* cells

All steps were carried out on ice and under sterile conditions if applicable. A single colony of the respective *E. coli* strain was incubated in LB-Miller medium (4 mL) at 37 °C with shaking (200 rpm, InforsHT Multitron Standard) for approximately 12 h. An LB-Miller main culture (100 mL) was inoculated with 1 % (v/v) of the overnight culture (1 mL) and grown to an OD_{590} of approximately 0.35. Cells were harvested by centrifugation (4000 x g, 4 °C, 10 min, Sigma Laboratory Centrifuge 6K15 or 3K30) and resuspended in RF1 buffer (20 mL = 1/5 volume of the main culture). Cells were incubated for 15 min, centrifuged, and resuspended in RF2 buffer (4 mL = 1/5 volume of the RF1 suspension). Cells were divided into aliquots (100 µL, in 1.5 mL Eppendorf tubes), snap-frozen in liquid nitrogen, and stored at -80 °C.

5.6 Transformation of chemically competent (RbCl) *E. coli* cells

An aliquot (100 µL) of chemically competent (RbCl) cells was thawed on ice. 1 µL of plasmid DNA (with a concentration of 50–100 ng/µL) or 5 µL of KLD mix were added to the competent cells. Cells were incubated on ice for 1 h. The heat shock was performed at 42 °C for 45 sec (Biometra TS1 Thermoshaker Analytik Jena) and cells were put on ice for 2 min. 0.5 mL prewarmed SOC medium was added for recovery and cells were incubated at 37 °C with shaking (650 rpm, Biometra TS1 Thermoshaker Analytik Jena) for 1 h. Subsequently, 50 µL were plated on one half of a pre-warmed LB agar plate supplemented with the appropriate antibiotic and the rest was centrifuged (7000 rpm, 1 min) to obtain a higher cell density. The supernatant was discarded, cells were resuspended and plated on the other half of the plate. Plates were incubated upside down at 37 °C for 12–24 h (INCU-line VWR International GmbH).

5.7 Plasmid DNA isolation and quantification

The GeneJET Plasmid Miniprep Kit by Thermo Scientific was used following the enclosed instructions. 4 x. 1.9 mL (= 7.6 mL) of a respective overnight culture were pelleted in four centrifugation steps (16162 x g, 1 min, Sigma Tabletop Centrifuge 1-14) in 2 mL Eppendorf tubes. The pellets were resuspended in 250 µL of Resuspension Solution (stored at 4 °C) by vortexing and pipetting. 250 µL of Lysis Solution were added, it was mixed by inverting 4-6 times and incubated for 5 min. 350 µL of Neutralization Solution were added, it was mixed by inverting 4-6 times and subsequently centrifuged (16162 x g, 10 min). Afterward, the supernatant was transferred to a GeneJET spin column by decanting or pipetting with caution. The column was centrifuged (16162 x g, 1 min) and the flow-through was discarded. Two consecutive washing steps with 500 µL of Wash Solution, (16162 x g, 1 min) were performed. The flow-through was discarded and the empty column was centrifuged (16162 x g, 2 min). The column was transferred into a clean 1.5 mL Eppendorf tube and placed into a heat block (approximately 50 °C, Grant Instruments BTA Dry Block Heating System) for evaporation of residual EtOH. Pre-warmed 35 µL nuclease-free water was added to the center of the purification column, it

was incubated for at least 5 min, and it was centrifuged (16162 x g, 2 min). The purified plasmid-DNA was quantified by NanoQuant (NanoQuant Plate™, Spark® Multimode Microplate Reader, Tecan) or NanoDrop (NanoDrop™ OneC Microvolume UV-Vis Spectrophotometer, Thermo Scientific) in the measurement mode "dsDNA" using 1.5 µL of the sample. Afterward, the purification columns were discarded, and the samples were stored at -20 °C.

5.8 Verification of DNA by sequencing

Plasmid DNA samples were prepared for sequencing (480-1200 ng DNA in 12 µL, + 3 µL sequencing primer = 15 µL in total). Primers were added immediately from 10 µM stock solutions or chosen from a standard primer list.

5.9 Dilution of primers

Primers (obtained from Sigma-Aldrich) were centrifuged at max. speed 1 min and diluted in nuclease-free water for 100 µM. After vortexing, they were diluted in nuclease-free water for 10 µM and stored at -20 °C.

5.10 Colony PCR

For colony PCR, Opti Taq DNA Polymerase was used (5 U/µL, OptiTaq DNA Polymerase EURx). The following PCR reaction mix was prepared on ice:

Table 27: Colony PCR reaction mix

Component	Amount [µL]
Primer *fwd* (10 µM)	0.125
Primer *rev* (10 µM)	0.125
dNTP mix (2 mM)	0.5
10 x Buffer C (EURx)	0.5
$MgCl_2$ (25 mM)	0.2
DMSO	0.1
Nuclease-free water	3.4
Opti Taq DNA Polymerase 5 U/µL	0.05

After adding the polymerase, 5 µL of the master mix were aliquoted into pre-cooled PCR tubes. Usually, five colonies were picked with a 10 µL pipette tip from an agar plate. Each clone was streaked onto a separate agar plate for later use. Then, the pipette tip was put into the PCR tube containing the master mix, incubated for at least 10 sec, and pipetted up and down. As positive controls, there were done PCR reactions of one colony of a previously verified plasmid and of a purified plasmid (diluted to approximately 1 ng/µL). The PCR samples were spun down and the PCR program was performed under the following temperature conditions (Biometra TAdvanced Twin Analytik Jena):

Table 28: Temperature program

PCR Step	Temperature [°C]	Time	Number of Cycles
Initial Denaturation	95	5 min	1
Denaturation	95	30 sec	
Annealing	50-72[a]	30 sec	30
Extension	72	1 min/kb	
Final Extension	72	7 min	1
Hold	4	indefinite	

[a] 5°C below T_m of the primer with the lowest T_m

The PCR reactions were analyzed on a 1 % (ω/v) agarose gel.

5.11 Gel electrophoresis

If not noted otherwise, 1 % (ω/v) agarose gel was prepared. Agarose (1.8 or 0.6 g) was resolved in TAE buffer (180 or 60 mL) for approximately 5 min in the microwave. SYBR Safe gel stain (18 or 6 µL, SYBR® Safe DNA gel stain; S33102, Thermo Scientific) was added and the gel was poured. The electrophoresis chamber was filled with TAE buffer, the gel was positioned and loaded. Therefore, the DNA-containing mixture was previously combined 5:1 with purple 6 x purple DNA gel loading dye (B7024S, NEB). Samples from colony PCR were loaded directly, without the addition of purple DNA gel loading dye. DNA marker (6 µL, GeneRulerTM 1 kb DNA Ladder; SM01313, Thermo Scientific) was loaded. The electrophoresis was run at 120 V for 30-45 min. For preparative purposes, the gel electrophoresis was run at 90 V for 70-90 min. A picture was made visualizing DNA fragments in UV light (UVP UVsolo touch, Analytik Jena).

5.12 Molecular cloning - NEBuilder® HiFi DNA assembly

5.12.1 Primer design

The online NEBuilder assembly tool from New England Biolabs Inc. was used to assemble the desired plasmid harboring the target gene *in silico*.[202] Primer pairs for amplification of the backbone as well as the target insert were designed manually. Primers were chosen to have approximately 20 bp annealing to the DNA sequencing to be amplified and to have more than 30 bp overlapping overhangs for DNA assembly. Primers had terminal GC pairs and the GC content was kept below 60 %. All used primers are summarized in chapter 6.3.

5.12.2 PCR amplification of target DNA fragments

Target inserts and backbone were both generated by PCR using Q5 High-Fidelity DNA Polymerase (M0491, NEB). Recommendations from NEB were followed.[198] The following

reaction mix was prepared on ice:

Table 29: PCR reaction mix (50 µL volume)

Component	Amount [µL]	Final Concentration
Primer *fwd* (10 µM)	2.5	0.5 µM
Primer *rev* (10 µM)	2.5	0.5 µM
Template DNA (~1 ng/µL)	1	~1 ng/50 µL
dNTP mix (2 mM)	5	200 µM
5 x Q5 Reaction Buffer	10	1 x
Optional: 5X Q5 High GC Enhancer[a]	10	1 x
Nuclease-free water	28.5/18.5	-
Q5 High-Fidelity DNA Polymerase (2 U/µL)	0.5	0.02 U/µL

[a] Q5 High GC Enhancer was used for the amplification of the backbone as it can improve the reaction performance of difficult targets, like GC-rich templates or those with secondary structures.

First, the primer and template DNA solutions were pipetted into pre-cooled PCR tubes (6 µL). After adding Q5 High-Fidelity DNA Polymerase to the reaction master mix, 44 µL of the mix were aliquoted into the PCR tubes. The PCR samples were spun down and the PCR program was performed under the following temperature conditions (Biometra TAdvanced Twin Analytik Jena):

Table 30: Temperature program

PCR Step	Temperature [°C]	Time	Number of Cycles
Initial Denaturation	98 °C	30 sec	1
Denaturation Annealing Extension	98°C Ta_1 50-72 °C[a] 72 °C	10 sec 30 sec 30-45 sec/kb[b]	10
Denaturation Annealing Extension	98°C Ta_2 50-72 °C[a] 72 °C	10 sec 30 sec 30-45 sec/kb[b]	20
Final Extension	72 °C	2 min	1
Hold	4 °C		1

[a] Annealing temperature was calculated according to NEB Tm calculator[203]

[b] 30 sec were used for the amplification of target inserts and 45 sec were used for the amplification of backbone

The PCR reactions were analyzed on a 1 % (ω/v) agarose gel as described in chapter 5.11.

5.12.3 Gel purification of PCR-amplified DNA fragments

The target DNA band was visualized by exposure to UV light (UV Transilluminator 2000 Bio-Rad) and excised. For purification the GeneJET gel extraction kit from Thermo Scientific) was used following the enclosed instructions. An equal volume of binding buffer was added to the gel slices and the resulting gel mixtures were incubated at 50 °C for 10 min until the gel was dissolved. The solubilized gel solution was transferred to the GeneJET purification column, centrifuged (16162 x g, 1 min, Sigma Tabletop Centrifuge 1-14) and the flow-through discarded. An additional binding step (application of 100 µL additional binding buffer to the column and centrifugation) was done if the purified DNA subsequently was used for sequencing. Two consecutive washing steps with 700 µL and 500 µL of wash solution, (16162 x g, 1 min) were performed. The flow-through was discarded and the empty column was centrifuged (16162 x g, 2 min). The column was transferred into a clean 1.5 mL Eppendorf tube and placed into a heat block (approximately 50 °C, Grant Instruments BTA Dry Block Heating System) for evaporation of residual EtOH. Pre-warmed 35 µL nuclease-free water was added to the center of the purification column, it was incubated for 10 min, and it was centrifuged (16162 x g, 2 min). The purified plasmid-DNA was quantified by NanoDrop® (NanoDrop™ OneC Microvolume UV-Vis Spectrophotometer, Thermo Scientific) in the measurement mode “dsDNA” using 1.5 µL of the sample. Afterward, the purification columns were discarded, and the samples were stored at -20 °C.

5.12.4 Assembly

For the assembly of the backbone with the target insert, recommendations from NEBuilder HiFi DNA assembly reaction protocol were followed.[195] The amount of backbone was set to 100 ng and the molar ratio of 1:10 backbone to insert resulted in the best assembly efficiency. DNA-containing solutions were diluted for better pipetting if necessary and the following mix was prepared:

Table 31: Assembly reaction mix

Component	Amount
Backbone DNA	100 ng = 0.02 pmol
Target insert DNA	0.2 pmol
Nuclease-free water	fill up to 10 µL
NEBuilder HiFi DNA assembly master mix	10 µL

The assembly reaction mix was prepared in pre-cooled PCR tubes. If necessary, there was also prepared a positive control:

Table 32: Positive control reaction mix

Component	Amount
NEBuilder positive control	10 µL
NEBuilder HiFi DNA assembly master mix	10 µL

For best assembly efficiency, samples were incubated at 50 °C in the thermocycler (Biometra TAdvanced Twin Analytik Jena) for 3 h.

5.12.5 Chemical transformation and verification

10 µL of the assembly reaction mix were used directly for the transformation in chemically competent (RbCl) *E. coli* Top 10 cells as described in chapter 5.6. 5 transformants from each plate were picked and amplification of the insert DNA was analyzed by colony PCR and subsequent gel electrophoresis as described in chapters 5.10 and 5.11. The plasmid DNA of positive clones was isolated from the corresponding colonies and verified by sequencing as described in chapter 5.8.

5.13 Molecular cloning – Q5® site-directed mutagenesis

For the insertion of a (LA)12 alpha helix next to the photosensitizer protein, Q5® site-directed mutagenesis (Q5® Site-Directed Mutagenesis Kit, New England Biolabs Inc.) was done. Mutagenesis primers were designed by the online tool NEBaseChanger®.[204]

5.13.1 Step 1: Exponential amplification

The whole plasmid was exponentially amplified by PCR reaction using the respective mutagenesis primers.

Table 33: PCR reaction mix

Component	Amount [µL]	Final Concentration
Primer *fwd* (10 µM)	2.5	0.5 µM
Primer *rev* (10 µM)	2.5	0.5 µM
Template DNA (1 pg - 1 ng)	1	< 1.000 ng
dNTP mix (2 mM)	5	200 µM
5 x Q5 Reaction Buffer	10	1 x
5 x Q5 High GC Enhancer	10	1 x
Nuclease-Free Water	18.5	-
Q5 High-Fidelity DNA Polymerase (2 U/µL)	0.5	0.02 U/µL

Table 34: Temperature program

PCR Step	Temperature [°C]	Time	Number of Cycles
Initial Denaturation	98 °C	30 sec	1
Denaturation	98 °C	10 sec	
Annealing	56-57 °C	30 sec	25
Extension	72 °C	45 sec/kb	
Final Extension	72 °C	2 min	1
Hold	4 °C	indefinite	

[a] 5°C below T_m of the primer with the lowest T_m

5.13.2 Step 2: KLD reaction

In the 2nd step, the KLD reaction, intramolecular ligation, and template removal were performed in one step. It was mixed well by pipetting gently up and down and incubated for 5 min at rt.

Table 35: Reaction Mix for the KLD Reaction

Component	Amount [µL]	Final Concentration
PCR Product	1	-
2 x KLD Reaction Buffer	5	1 x
10 x KLD Enzyme Mix	1	1 x
Nuclease-free water	3	-

5.13.3 Step 3: Chemical transformation and verification

Immediately after performing the reaction, 5 µL of KLD reaction mix were transformed into chemically competent (RbCl) *E. coli* Top 10 cells as described in chapter 5.6. Transformants were picked, and amplification of the insert DNA was analyzed by colony PCR and subsequent gel electrophoresis as described in chapters 5.10 and 5.11. The plasmid DNA of positive clones was isolated from the corresponding colonies and verified by sequencing as described in chapter 5.8.

5.14 Protein production in E. coli BL21(DE3)

5.14.1 Cultivation in autoinduction media[178]

A preculture of the respective *E. coli* BL21(DE3) strain was grown in LB-0.8G (12 mL) supplemented with appropriate antibiotic in a 50 mL falcon tube for approximately 16 h (37 °C, 275 rpm, InforsHT Multitron Standard). The LB-5052 medium main culture (usually 200 mL in a 1 L baffled shake flask) supplemented with appropriate antibiotic

was inoculated with 0.2 % (v/v) of the preculture and grown for 4 h (37 °C, 150 rpm). Thereafter, protein production was performed for approximately 20 h (20 °C, 150 rpm).

5.15 Protein purification

5.15.1 Cell harvesting

All further steps were carried out at 4 °C to protect the protein against degradation. Cells were harvested by centrifugation (4 000 x g, 4 °C, 15 min, Sigma Laboratory Centrifuge 6K15 or 3K30). The cell pellet was resuspended (by pipetting and vortexing) in 1/10 volume of the main culture in Equilibration buffer and centrifuged. The pellet could be stored at -20 °C or processed further immediately.

5.15.2 Cell lysis

The washed pellet was resuspended in 1/10 volume of the main culture in Equilibration buffer. To the resulting cell suspension, 0.1 M PMSF was added to the standard working concentration of 0.1 mM before cell lysis. Afterward, cell lysis was done on ice by sonication (10 sec/min pulse for 9 min, 40 % amplitude, Bandelin Sonoplus HD4100, TS106 probe). The insoluble cell debris was removed by centrifugation (14 000 x g, 4 °C, 25 min, Sigma Laboratory Centrifuge 6K15 or 3K30). Immediately after centrifugation, the soluble cell free extract (CFE) was separated from the cell debris.

5.15.3 Purification by IMAC

The CFE was centrifuged (14 000 x g, 4 °C, 25 min, Sigma Laboratory Centrifuge 6K15 or 3K30) another time immediately before purification to remove residual debris. For purification, His-tag protein purification columns HisTrapTM FF prepacked Ni Sepharose™ columns (1 or 5 mL, Cytiva) were used.

Manual purification by IMAC	The precharged column was washed with 5 x column volume dH_2O and Equilibration buffer, respectively. The CFE was slowly loaded (approx. 3 mL/min) onto the column. The column was washed with 5 x column volume Equilibration Buffer. Elution was done with 5 x column volume Elution buffer. Fractions were collected in 2 mL tubes. The flow-through during sample loading and washing was collected and analyzed as well.

Automated purification by IMAC	Automated purification was conducted with the ÄKTA™ start system (Cytiva) according to the operating Instructions. A UV flow cell was used for detection while purification. A flow of 2 mL/min was used throughout the purification. The precharged column was washed with approx. 5 x column volume dH_2O and Equilibration buffer, respectively (until the stabilization of the baseline in the UV signal). The CFE was loaded onto the column. The column was washed with approx. 5 x column volume Equilibration Buffer (until the stabilization of the baseline in the UV signal). Elution was done in a 20 %/min gradient with Elution buffer. 3 mL fractions were collected with the Frac30 fraction collector. After elution, the column was washed with approx. 5 x column volumes Equilibration buffer before the loading of another CFE.

If verification was necessary, fractions were analyzed by SDS-PAGE, and eluates containing the target protein were pooled, buffer exchanged with NaPi buffer containing 25 % (v/v) glycerol and concentrated with a centrifugal membrane concentrator (Amicon Ultra-15, PLGC Ultracel-PL Membran, 10 kDa, Merck Millipore). Therefore, combined fractions were diluted with the same amount of NaPi buffer containing 25 % (v/v) glycerol in the concentrator and it was centrifuged (4000 x g, 10-30 min, Sigma Laboratory Centrifuge 6K15 or 3K30). The flow-through was discarded and the residual protein solution was diluted with buffer, and it was centrifuged under the same conditions. The last step was repeated. The buffer exchanged protein solution was stored at -20 °C. The concentrator was washed (1 x 0.5 M NaOH, 1 x 0.5 M AcOH, 1 x dH_2O), filled with 20 % (v/v) EtOH, and stored at 4 °C for further use.

After protein purification, the His-tag protein purification column was washed with 5 x column volume Equilibration buffer and dH_2O, respectively, and preserved in 20 % (v/v) EtOH. After five purifications, the column was stripped and recharged. Therefore, the column was purged with 5 x column volume dH_2O and Stripping buffer, respectively. The column was washed with 5 x column volume Equilibration buffer and dH_2O, respectively (the column was colorless after this step). Subsequently, the column was charged with 1 x column volume of 0.1 M $NiSO_4$ and incubated for 2 min. After incubation, the non-attached $NiSO_4$ was washed with 5 x column volume dH_2O and Equilibration buffer, respectively. The column was filled with 20 % (v/v) EtOH and stored at rt.

5.16 Determination of protein concentration

For the determination of the total protein concentration, protein samples were usually diluted 1:50 with dH_2O. During each assay, there was prepared a dH_2O blank as well and all samples were measured in triplicates (Bradford Assay) or duplicates of triplicates (BCA assay).[205]

Bradford assay	BCA (bicinchoninic acid) assay
5 µL of the diluted protein solutions were mixed with 200 µL of 1:5-diluted Bradford reagent (Bradford Dye Reagent, Ready-to-use solution, abcr GmbH) in 96-well plates (Greiner Bio-One, PS, U-bottom, clear) and incubated at rt for 15 min (protein solutions were pipetted first, and then the diluted Bradford reagent was added quickly). The absorbance was measured at 595 nm with a plate reader (Anthos Zenyth 3100) and the amount of protein was calculated by BSA calibration. The calibration was done for fresh Bradford reagents. In this regard, a dilution series of BSA (0-1 mg/mL) was prepared in dH_2O and measured in triplicates.	The Pierce™ BCA Protein Assay Kit (Thermo Scientific) was used, following the enclosed user guide. The working reagent was prepared by mixing 50 parts of BCA reagent A with 1 part of BCA reagent B. 25 µl of the diluted protein solutions were mixed with 200 µl of the working reagent in 96-well plates (Greiner Bio-One, PS, U-bottom, clear) and incubated at 37 °C for 30 min (protein solutions were pipetted first, and then the working reagent was added quickly). After cooling the plate for 5 min at rt, the absorbance was measured at 562 nm with a plate reader (Spark® Multimode Microplate Reader, Tecan) and the amount of protein was calculated by BSA calibration. The BSA calibration was conducted as described in the user guide.

5.17 Protein production analysis by SDS-PAGE (Sodium Dodecyl Sulfate Polyacrylamide Gel Electrophoresis)

Either precast gels (Mini-PROTEAN TGX Gels, 4-20 %, Bio-Rad) or self-made 12 % or 17.5 % (ω/v) polyacrylamide gels (0.75 mm or 1.5 mm thickness) were used for SDS-PAGE (the composition of self-made resolving and stacking gels is summarized in Table 36. After the addition of 10 % (ω/v) APS and TEMED the resolving gel was poured immediately. It was covered with *i*PrOH. After 20 min, the *i*PrOH was removed again and the stacking gel was prepared and immediately added on top.

Table 36: Preparation of resolving and stacking gels

Resolving gel (12 % (ω/v))[a]	Resolving gel (17.5 % (ω/v))[a]	Stacking gel[a]
3.2 mL dH_2O	1.5 mL dH_2O	2.2 mL dH_2O
2.5 mL resolving gel buffer	2.5 mL resolving gel buffer	1.3 mL stacking gel buffer
4.2 mL 30 % (ω/v) acrylamide[b]	5.9 mL 30 % (ω/v) acrylamide[b]	0.5 mL 30 % (ω/v) acrylamide[b]
50 µL 10 % (ω/v) APS	50 µL 10 % (ω/v) APS	30 µL bromophenol blue
8 µL TEMED	8 µL TEMED	25 µL 10 % (ω/v) APS
		8 µL TEMED

[a] Amounts account for the preparation of two gels
[b] Acrylamide was added with a sterile pipette

The protein samples were mixed with SDS-PAGE sample buffer 1:1 and denatured at 95 °C for 4 min (purified proteins and CFE) or 10 min (insoluble cell debris) before loading onto the gel (whole cell samples were mixed 1:4 and denatured at 95 °C for 10 min). For comparison between different gels, sample loading was normalized to 5 µg protein per lane or whole cell samples were normalized to OD_{590} = 3 and 20 µL loading volume. Prestained protein marker (5 µL, PageRuler™ Prestained Protein Ladder 26616, Thermo Scientific) was loaded onto each gel. Gel electrophoresis was performed in SDS-PAGE running buffer at 150 V (precast gels) or 80-120 V (self-made gels). Afterward, gels were stained according to a microwave staining procedure. Therefore, the stacking gel was carefully removed. The resolving gels were covered with dH_2O and incubated at 750 W in the microwave for 1 min. The gels were slightly shaken at rt for 2 min (PSU-10i Orbital Shaking Platform, Grant-bio) and then covered in fresh dH_2O, incubated at 500 W for 1 min, and once more shaken at rt for 2 min. After discarding the dH_2O, the gels were covered in a dying solution (Invitrogen™ SimplyBlue™ SafeStain, LC6065) and incubated at 350 W for 45 s. The gels were slightly shaken at rt for 5 min, the dying solution was removed, and the gels were washed in dH_2O with shaking for at least 10 min. At last, the gels were preserved in dH_2O overnight or over the weekend. A picture was made for documentation.

5.18 Characterization of fusion proteins

5.18.1 Spectroscopic characterization of fusion proteins

For the measurement of absorption and fluorescence spectra, proteins were normalized *via* BCA assay to a chromophore concentration of 50 µM in 100 µl (BCA assay). Spectra were measured in 96-well plates (Krystal Microplate, 96-well Black, Porvair) with a plate reader (Spark® Multimode Microplate Reader, Tecan). For analysis of the stability towards blue light, samples were incubated under blue light (Eurolite IP FL-30 SMD blue, IP65, 16.4 mW/cm²). Absorption and Fluorescence spectra were measured after 0.5 h, 1 h, 1.5 h, 2 h, 3 h and 4 h.

5.18.2 Quantification of ROS production

ROS-specific fluorescent assay reagents were used for the relative comparison of all fusion proteins regarding their ROS-producing activity. All measurements were conducted in 96-well plates (Greiner Bio-One, PS, F-bottom, white, Lumitrac, med. binding) with a plate reader (Fluorescence spectrometer PerkinElmer LS-55, 3 nm slit, low gain). A white light lamp (Megaman Helix daylight lamp, 0.9 mW/cm²) was used for illumination. Protein samples were normalized *via* BCA assay. Working solutions of the assay reagents were prepared immediately before the measurements and kept on ice in the dark. Both, protein sample (50 µL) and assay reagent (50 µL) were added successively, and then illuminated in a final volume of 100 µL for different periods. For each time point, there was measured a separate reaction mixture. Everything was pipetted in triplicates. The autoxidation of the respective assay reagent was subtracted

from all measurements. Furthermore, negative controls were incubated in the dark and measured after 60 min. All measurements of one ROS assay were carried out on the same day for better comparison.

5.18.2.1 Quantification of H_2O_2 and $O_2^{\bullet-}$ production

Protein samples were normalized to chromophore concentration 1 µM. 100 µM Amplex Red reagent (10-Acetyl-3,7-dihydroxyphenoxazine 98%, abcr GmbH; a 20 mM stock solution was prepared in DMSO on the same day) and 0.2 U/mL HRP (abcr GmbH) were used.[206] For quantification of superoxide production, additionally, there were added 2 U/mL SOD (Sigma Aldrich). The fluorescence was measured at an excitation wavelength of 550 nm and an emission wavelength of 585 nm. The following time points were measured: 0, 2, 5, and 10 min. For the determination of absolute H_2O_2 concentrations, the measured fluorescence intensities were compared to an H_2O_2 calibration curve. A calibration curve was generated by preparing samples of known H_2O_2 (3 wt. %, Thermo Scientific) concentrations (0 to 6.25 µM).

5.18.2.2 Quantification of $^1O_2$ production

Protein samples were normalized to chromophore concentration 4 µM. 5 µM SOSG reagent was used (Lumiprobe GmbH or Thermo Fisher Scientific; a 5 mM stock solution was prepared in MeOH and could be stored at -20 °C for further use).[207] The fluorescence was measured at excitation wavelength 510 nm and emission wavelength 530 nm. The following time points were measured: 0, 2, 5, 10, 30, 60, and 90 min.

5.18.2.3 Quantification of $HO^{\bullet}$ production

Protein samples were normalized to chromophore concentration 4 µM. 15 µM APF reagent was used (synthesized according to a developed in-house protocol by Clemens Cziegler[208], a 5 mM stock solution was prepared in DMF and could be stored at 4 °C for further use). The fluorescence was measured at an excitation wavelength of 495 nm and an emission wavelength of 515 nm. The following time points were measured: 0, 2, 5, 10, 30, 60, and 90 min.

5.18.3 O_2 consumption analysis

The decreasing concentration of dissolved oxygen due to ROS formation in a protein solution was measured with an oxygen sensor (FireSting-O2, PyroScience) with a robust fiber-optic sensor (OXROB10). For temperature compensation, an electrical temperature sensor (Pt100, TDIP15) was used. For the comparison of different fusion proteins, samples were normalized to a given chromophore concentration via BCA assay. Dilutions were prepared in Milli-Q H_2O in closed 1.5 mL glass vials with a rubber septum. The oxygen sensor and temperature sensor were immersed in the solution through the septum. Samples were illuminated using a blue light lamp (Eurolite IP FL-30 SMD blue, IP65).

5.19 Surface analysis

5.19.1 Spin coating for the preparation of a smooth polymer surface

5.19.1.1 Preparation of Si-wafer pieces or gold SPR sensor slides for spin coating

Si-wafer pieces were cut (approx. 1 x 1 cm) and washed before spin coating. They were rinsed with toluene, acetone, EtOH, and Milli-Q H_2O and blown dry with compressed air (Druckluftspray 67, 400 mL, CRC GmbH).[209]

Gold SPR sensor slides were cleaned by immersing in Piranha solution (three parts concentrated H_2SO_4 and one part 30 wt. % H_2O_2 solution) for 30 min, rinsing with Milli-Q H_2O, blowing dry with compressed air (Druckluftspray 67, 400 ml, CRC GmbH) and putting 10 min into a UV ozone cleaner (Ossila).[210,211] For the removal of PE from used SPR gold slides, the slide was incubated 2 x 20 min in toluene in an ultrasonic bath (VWR International GmbH) before all other steps.

5.19.1.2 Spin coating

Polymers (0.5 or 1 wt. %) were dissolved as described in Table 37 in a glass vial with a rubber septum. The spin coater chuck and the sample for spin coating were preheated with a heat gun for 6-8 sec. Immediately after covering the surface with the hot solution using a syringe, the spin coater was started, and it was spun at 2000 rpm for 90 sec.

Table 37: Conditions for the solution of different polymers

Polymer	Source	Solvent	Temperature [°C]
PE	low density, ≤ 400 micron, Thermo Scientific (powder)	toluene	90
PP	isotactic, average Mw 340 000, Sigma Aldrich (pellets)	*p*-xylene	125
PS	spheres 1-2 mm	toluene	90
PLA	3D printer filament, Maert	DCM	30
PVC	low molecular weight, Sigma Aldrich (powder)	THF	50

5.19.2 Ellipsometry

Ellipsometry was conducted for the determination of the width of the spin coated PE layer (1 wt. %). The ellipsometer (SE 500adv, SENTECH; software SE400AdvancedBASIC) was used using the following parameters: wavelength=633 nm, n=1.4998, k=0). The average of five measurements on three spin coated samples (15 measurements in total) was calculated.

5.19.3 SPR (Surface Plasmon Resonance)

Experiments were conducted using original gold SPR sensor slides (BioNavis) or PE spin coated sensor slides. SPR measurements were performed on an MP-SPR Navi™ 210A VASA instrument (BioNavis). The thickness of the polyethylene was elucidated using the program MP-SPR Navi™ LayerSolver™ (BioNavis). The average thickness was 30 nm, which proved to be suitable for further SPR measurements. Dulbecco's phosphate-buffered saline (PBS, Sigma Aldrich) was used as the running buffer. The protein sample solutions were injected for 20 min with a flow rate of 10 µL/min. The increase in the SPR signal indicated the adsorption of the protein to the polymer surface. The amount of adsorbed protein was calculated through the SPR signal increase (conversion factor: 1° = 10 000 RU = 1000 ng/cm^2 for 785 nm wavelength).

5.19.4 WCA (Water Contact Angle measurement)

For WCA measurements, spin coated Si-wafer pieces (LDPE, PP, PS) were used. The wettability of the polymer surfaces was analyzed by static contact angle measurements of 7 µl water droplets. Water contact angle measurements were performed using a Drop Shape Analyzer (Krüss DSA30) using the software Krüss Advance (using the fitting method Young Laplace). Purified protein (2 µM in Milli-Q H_2O) was added to the polymer surface. The sample was incubated at room temperature for 0.5 h, washed with Milli-Q H_2O, dried with compressed air (Druckluftspray 67, 400 mL, CRC GmbH) followed by a drying step at 50 °C for 10 min. WCA measurements were performed in triplicates on different areas of the sample surface.

5.19.5 ATR-FTIR (Attenuated Total Reflectance Fourier Transform InfraRed Spectroscopy)

For ATR-FTIR measurements, PE foil (Müllbeutel 5 l mit Tragegriff für Kosmetikeimer, Profissimo) or PP foil (Entsorgungsbeutel SEKUROKA aus PP, 40 µm, Carl ROTH) was used. Spin coated Si-wafer pieces could not be used because of the high refractive index of Si, which does not satisfy the total reflection requirements for ATR-FTIR. An ATR-FTIR spectrometer (Perkin Elmer UATR Two) was used in the range 4000 - 400 cm^{-1} at 1 cm^{-1} resolution over 4 scans.

5.19.6 XPS (X-Ray Photoelectron Spectroscopy)

All XPS measurements were conducted by the Analytical Instrumentation Center TU Wien. Either PE foil (Müllbeutel 5 l mit Tragegriff für Kosmetikeimer, Profissimo) or PE spin coated Si-wafer pieces were used.

All XPS measurements were conducted at the Analytical Instrumentation Center (AIC) TU Wien. All measurements were carried out on a PHI Versa Probe III-spectrometer

equipped with a monochromatic Al- Kα X-ray source and a hemispherical analyzer (acceptance angle: ±20°). Pass energies of 140/112 eV and 27/55 eV and step widths of 0.5 eV and 0.05 eV were used for survey and detail spectra, respectively. (Excitation energy: 1486.6 eV Beam energy and spot size: 25/50 W onto 100/200 µm; Mean electron take-off angle: 45° to sample surface normal; Base pressure: <7x10-10 mbar, Pressure during measurements: <1x10-8 mbar). Samples were mounted on non-conductive Teflon tape. Electronic and ionic charge compensation was used for all measurements (automatized as provided by PHI). The outermost surface layers were removed by using an Ar gas cluster ion gun (2.5/5/10 kV/20 kV, 10/20/30 nA/40 nA, 600 kPa partial pressure, 2x2 mm^2). Data analysis was performed using CASA XPS and Multipak software packages, employing transmission corrections, Shirley/Tougaard backgrounds[212,213], and Scofield sensitivity factors.[214]

5.19.7 LIBS (Laser Induced Breakdown Spectroscopy)

For LIBS measurement, an "imageGEO193^{LIBS}" laser ablation system from Elemental Scientific Lasers (Bozeman, MT, USA) operating at a wavelength of 193 nm, with a "TwoVol3" ablation chamber and a fiber mount capable of collecting the light that is emitted from the laser-induced plasma was used. The collected light was analyzed using a "Spectra HRS-750Pro" spectrometer equipped with a "PI-MAX- 4" ICCD camera, both from Teledyne Princeton Instruments (Acton, MA, USA). To measure the oxygen emission (triplet @ 777.3 nm), the ICCD spectrometer was operated with an entrance-slit width of 300 µm and an 1800 g mm^{-1} grating set to a center wavelength of 777 nm, providing a spectral resolution of 0.05 nm. The spectra were recorded with a gate delay of 0.1 µs, a gate width of 20 µs, and an intensifier gain of 20. The ICCD-LIBS data were acquired with "LightField®" (version 6.13, Teledyne Princeton Instruments). LIBS measurements were carried out by repeatedly measuring line scans (length of 1.8 mm) with non-overlapping shots 20 times at the same position. Resulting craters were analyzed using a profilometer (Dektak XT, Bruker Corporation, Billerica, United States of America) resulting in a total ablation depth of approx. 2 µm. For data evaluation, obtained LIBS spectra of each layer were averaged, and the standard deviation was calculated.

Table 38: LIBS measurement parameters

Laser fluence [J/cm^2]	2.4
Spot shape	Square
Spot size [µm]	100x100
Scan speed [µm/s]	5000
Repetition rate [Hz]	50
Atmosphere	He

5.19.8 AFM (Atomic Force Microscopy)

AFM measurements were conducted on a Cypher ES Environmental AFM (Oxford Instruments, Asylum Research) in imaging mode using the software Cypher 16.29.230 in

mode AC Air Topography. A Tap300-G tip (resonance frequency 300 kHz, force constant 40 N/m, BudgetSensors) was used. 1 wt. % PE spin coated Si-wafer pieces were mounted onto magnetic discs using double-sided tape. For the post-processing of imaging data, the software Gwyddion was used.

5.20 Quantification of $HO^{\bullet}$ production on the polymer surface

A 5 mM APF stock solution was prepared in dimethylformamide and stored at 4 °C. From this stock solution a 60 µM APF solution in toluene (99+%, Sigma Aldrich) containing 0.5 wt. % LDPE was prepared and heated up to 90 °C. 10 drops of the hot solution were applied in each well of a preheated 96 well plate (PS, 96 well, f-bottom, white, lumitrac, Greiner Bio-One) and the residual toluene evaporated for 40 min at 90 °C. Then, 90 µl of 20 µM sample solution were added to each well and incubated in the dark for 30 min. The solution was removed, and the wells were dried with compressed air (Druckluftspray 67, 400 mL, CRC GmbH). It was irradiated for different periods using white light (Megaman Helix daylight lamp, 0.9 mW/cm^2). The relative fluorescence change was measured using a fluorescence spectrometer (Spark® Multimode Microplate Reader, Tecan) with an excitation wavelength of 495 nm and an emission wavelength of 540 nm (gain 45, z-achsis 16613 (strongest fluorescence signal)).

5.21 Polyethylene degradation experiments

5.21.1 Degradation experiments with Fenton reaction

Reaction in hydrothermal reactor:
A thermal Fenton reaction was conducted in a 50 mL autoclave as described in literature.[42] In a reaction volume of 37. 5 mL, there were dissolved 4 mM $FeSO_4$, 200 mM H_2O_2, and 200 mM HCl. An approx. 1 x 1 cm PE piece (Müllbeutel 5 l mit Tragegriff für Kosmetikeimer, Profissimo) was added. The reaction was incubated for 5 h at 140 °C in an oven. After cooling down to rt, the remaining PE pieces were collected, washed with 2 M HCl and Milli-Q H_2O, and finally, dried.

Reaction in PTFE container:
A Fenton reaction at rt was conducted in a PTFE container. In a reaction volume of 1 mL, there were added 10 mM $FeSO_4$, 15 wt. % H_2O_2, and 10 mM HCl. An approx. 1 x 1 cm PE piece (Müllbeutel 5 l mit Tragegriff für Kosmetikeimer, Profissimo) was added and incubated for 1 h. The reaction was repeated with the same PE piece 42 times (in total approx. 42 h). Finally, the PE piece was washed with Milli-Q H_2O and dried.

5.21.2 Degradation experiments with protein

Long-term experiment with protein solution:
An approx. 0.5 x 0.5 cm PE piece (Müllbeutel 5 l mit Tragegriff für Kosmetikeimer, Profissimo) was used. One side of the PE piece was incubated for 30 min with 1 µM protein solution (100 µL) in the dark. Afterwards, it was illuminated for 30 min or 1 h using a blue light lamp (16.4 mW/cm^2, Eurolite IP FL-30 SMD blue, IP65). Subsequently, to remove the adsorbed protein, the PE piece was washed for 3 min in 10 % (ω/v) SDS at 95 °C. It was rinsed with Milli-Q H_2O and dried with compressed air (Druckluftspray 67, 400 mL, CRC GmbH). All steps were repeated (156 times with 30 min illumination and 70 times with 1 h illumination). In total, the sample was illuminated for approx. 148 h.

Long-term experiment with adsorbed protein:
An approx. 0.5 x 0.5 cm PE piece (Müllbeutel 5 l mit Tragegriff für Kosmetikeimer, Profissimo) was used. One side of the PE piece was incubated for 10 min with 25 µM protein solution (100 µL) in the dark. Then, the solution was removed and dried with compressed air (Druckluftspray 67, 400 mL, CRC GmbH). It was illuminated for 20 min using a blue light lamp (16.4 mW/cm^2, Eurolite IP FL-30 SMD blue, IP65). Subsequently, to remove the adsorbed protein, the PE piece was washed for 3 min in 10 % (ω/v) SDS at 95 °C. It was rinsed with Milli-Q H_2O and dried with compressed air (Druckluftspray 67, 400 mL, CRC GmbH). All steps were repeated (84 times). In total, the sample was illuminated for approx. 42 h.

6 Appendix

6.1 Protein library

Table 39: Original protein library

Protein	Primary host	Reference	Gene size [bp]	Protein size [aa]	Molecular mass [kDa]	λ Ex/Em [nm]
		Photosensitizer Proteins[a]				
KillerRed	*Anthomedusae sp*. DC-2005 (derived from the hydrozoan chromoprotein anm2CP)	FPbase ID: MSYZC	735	245	27.5	585/610[92]
KillerOrange	*Anthomedusae sp*. DC-2005 (mutant derived from KillerRed)	FPbase ID: 97MBQ	735	245	27.4	512/555[100]
SuperNova	*Anthomedusae sp*. DC-2005 (monomeric version derived from KillerRed)	FPbase ID: 6EEUG	735	245	27.4	579/610[98]
MiniSOGQ103V	*Arabidopsis thaliana (mutant derived from MiniSOG)*	FPbase ID: G4TXA	342	114	13.4	440/487[112]
SOPP3	*Arabidopsis thaliana (mutant derived from MiniSOG)*	FPbase ID: W4PW7	342	114	13.2	439/490[115]
DsFbFpM49I	*Dinoroseobacter shibae*	[109]	438	146	16.8	450/495[77]
		Hydrophobins[b]				
mHGF1	*Grifola frondosa* (cysteine → serine mutant for soluble expression in *E. coli*)	[140]	225	75	n.s.[c]	n.s.[d]
HFB1	*Trichoderma reesei*	UniProt ID: P52754	264	88	n.s.[c]	n.s.[d]
HFB2	*Trichoderma reesei*	UniProt ID: P79073	213	71	n.s.[c]	n.s.[d]

[a] Photosensitizer protein encoding genes were propagated on a pET29b(+) vector with a kanamycin resistance
[b] Hydrophobin encoding genes were propagated on a ptwistamphighcopy vector (from Twist Bioscience) with an ampicillin resistance
[c] Not expressed by itself; [d] Not fluorescent

Table 40: Fusion protein library

Protein[a]	Gene size [bp]	Protein size [aa]	Molecular mass [kDa]	λ Ex/Em [nm][d]
SuperNova-RL-mHGF1	1050	350	37.5	n.s.
MiniSOGQ103V-RL-mHGF1	657	219	23.4	n.s.
MiniSOGQ103V-RL-HFB1	618	206	22.4	n.s.
MiniSOGQ103V-RL-HFB2	606	202	22.1	n.s.
MiniSOGQ103V-RL-mHGF1-RL-MiniSOGQ103V	1023	341	37.1	n.s.
mHGF1-RL-MiniSOGQ103V	657	219	23.4	n.s.
MiniSOGQ103V-RL-mHGF1-FLHis[b]	687	229	24.1	n.s.
SOPP3-RL-mHGF1	657	219	23.2	438/505
SOPP3-RL-HFB1	618	206	22.2	n.s.
SOPP3-RL-HFB2	606	202	21.9	n.s.
SOPP3-RL-mHGF1-RL-SOPP3	1023	341	36.7	438/505
SOPP3-RL-HFB1-RL-SOPP3	984	328	35.7	438/505
SOPP3-RL-HFB2-RL-SOPP3	972	324	35.4	438/505
mHGF1-RL-SOPP3	657	219	23.2	438/505
HFB1-RL-SOPP3	618	206	22.2	n.s.
HFB2-RL-SOPP3	606	202	21.9	n.s.
SOPP3-RL-mHGF1-FLHis[b]	687	229	23.9	n.s.
(LA)12-SOPP3[c]	426	142	15.6	n.s.
SOPP3-(LA)12-SOPP3[c]	753	251	27.8	n.s.
DsFbFpM49I-RL-mHGF1	753	251	26.9	448/509
DsFbFpM49I-RL-HFB1	714	238	25.9	n.s.
DsFbFpM49I-RL-HFB2	702	234	25.5	n.s.
DsFbFpM49I-RL-mHGF1-RL-DsFbFpM49I	1215	405	44.0	448/509
DsFbFpM49I-RL-HFB1-RL-DsFbFpM49I	1176	392	43.0	448/509
DsFbFpM49I-RL-HFB2-RL-DsFbFpM49I	1164	388	42.6	448/509
mHGF1-RL-DsFbFpM49I	753	251	26.9	448/509
HFB1-RL-DsFbFpM49I	714	238	25.9	n.s.
HFB2-RL-DsFbFpM49I	702	234	25.5	n.s.
DsFbFpM49I-RL-mHGF1-FLHis[b]	783	261	27.5	n.s.
(LA)12-DsFbFpM49I[c]	522	174	19.3	n.s.
DsFbFpM49I-(LA)12-DsFbFpM49I[c]	945	315	35.1	n.s.

[a] RL = rigid linker with the aa sequence AEAAAKEAAAKEAAAKA

[b] FLHis = flexible linker with the aa sequence GGGGSGGGGS followed by a 6 x His tag

[c] (LA)12 is a short α-helix consisting of 12 repetitions of the aas LA followed by the short linker GGSG

[d] Values for fluorescence excitation and emission maxima are shown only for fusion proteins which could be produced and purified successfully and used for further characterization

6.2 Gene sequences

In the following, gene sequences are summarized. The start codon is highlighted in green, the stop codon in red, and a possible 6 x His tag in orange. The rigid linker sequences 1 and 2 (rl1 and rl2) are highlighted in grey and both encode the rigid linker with the amino acid sequence AEAAAKEAAAKEAAAKA. The flexible linker sequence (flhis) is highlighted in blue and encodes the flexible linker with the amino acid sequence GGGGSGGGGSLE followed by a 6 x His tag. The sequence for the short α-helix ((la)12) is highlighted in pink and encodes 12 repetitions of the amino acid sequence LA followed by a short linker with the amino acid sequence GGSG.

killerred (in pET29b(+)_killerred)

ATGGAAGGTGGCCCGGCACTGTTCCAGTCCGATATGACTTTTAAAATCTTTATTGATGGTGA
AGTGAACGGTCAGAAATTCACCATTGTTGCTGACGGTAGCTCTAAGTTCCCACACGGTGA
CTTCAACGTGCACGCTGTTTGCGAAACCGGTAAACTGCCGATGTCTTGGAAACCGATCTG
CCACCTGATCCAGTATGGTGAACCGTTTTTCGCGCGCTACCCGGATGGTATTTCCCACTTC
GCCCAGGAATGCTTCCCGGAAGGTCTGAGCATTGATCGTACCGTGCGCTTTGAGAACGAT
GGCACCATGACGAGCCATCACACCTATGAACTGGATGACACTTGCGTAGTTTCCCGTATC
ACTGTAAATTGCGACGGTTTCCAGCCTGATGGTCCTATCATGCGCGACCAGCTGGTGGAT
ATCCTGCCGAACGAAACCCACATGTTCCCGCACGGCCCGAACGCGGTTCGCCAGCTGG
CGTTCATTGGTTTTACCACTGCCGACGGCGGCCTGATGATGGGCCACTTCGATTCTAAAAT
GACTTTCAATGGTAGCCGTGCAATCGAAATCCCGGGCCCGCACTTCGTAACTATTATCAC
CAAACAGATGCGTGATACCAGCGACAAACGTGATCACGTTTGTCAGCGTGAAGTCGCATA
CGCGCACAGCGTTCCGCGTATCACGAGCGCCATTGGTTCTGACGAAGACCTCGAGCAC
CACCACCACCACCACTGA

killerorange (pET-29b(+)_killerorange)

ATGGAGTGTGGTCCGGCGCTGTTCCAGTCTGATATGACCTTCAAAATTTTCATCGATGGTGA
GGTGAACGGTCAGAAATTCACCATTGTTGCGGACGGTTCTAGCAAATTCCCACACGGTGA
CTTCAACGTACATGCGGTTTGCGAAACCGGTAAGCTGCCAATGTCCTGGAAGCCGATCTG
TCATCTGATCCAGTGGGGTGAACCGTTCTTTGCACGTTATCCGGATGGCATCTCTCATTTC
GCGCAGGAATGTTTCCCGGAAGGCCTGAGCATCGATCGTACTGTGCGCTTCGAAAACGA
CGGCACGATGACCTCCCACCACACTTACGAACTGTCTGATACCTGCGTGGTGTCCCGTAT
CACCGTTAATTGCGATGGCTTTCAGCCGGATGGCCCGATTATGCGTGACCAACTGGTGGA
CATCCTGCCGTCTGAAACCCACATGTTCCCGCACGGTCCTAACGCAGTACGTCAGCTGG
CGTTCATCGGTTTCACCACCGCTGACGGTGGCCTGATGATGGGCCATCTGGATTCCAAAA
TGACTTTCAACGGCTCCCGCGCTATCGAAATTCCAGGCCCGCACTTCGTGACCATTATTA
CCAAACAGATGCGTGACACCTCCGATAAACGTGACCACGTGTGTCAGCGCGAAGTTGCC
CACGCGCACTCTGTTCCGCGTATCACTAGCGCGATCGGCTCTGACCAAGACCTCGAGCA
CCACCACCACCACCACTGA

supernova (pET-29b(+)_supernova)

ATGGAAGTCGGTCCGGCGCTGTTCCAGAGCGATATGACCTTTAAGATCTTCATCGACGGC
GAAGTGAACGGCCAGAAATTCACCATCGTTGCAGACGGTTCCTCCAAATTTCCGCACGGT
GATTTTAATGTGCACGCGGTTTGCGAAACTGGCAAACTGCCGATGTCCTGGAAACCAATCT
GCCACCTGATTCAGTATGGCGAGCCGTTCTTCGCACGTTATCCTGACGGTATCAGCCACT
TTGCGCAGGAATGTTTCCCAGAAGGTCTGAGCATCGACCGTACCGTACGTTTCGAAAACG
ATGGCACCATGACCTCCCATCACACCTATGAACTGGACGATACCTGCGTTGTCAGCCGTA
TCACCGTGAACTGCGACGGTTTCCAGCCGGATGGCCCGATCATGCGTGACCAGCTGGTT
GACATCCTGCCGAGCGAAACCCATATGTTTCCGCATGGCCCAAACGCGGTTCGTCAGAC
CGCTACTATTGGTTTCACCACTGCTGATGGTGGTAAAATGATGGGTCACTTCGATTCTAAAA
TGACCTTCAATGGCTCTCGTGCGATCGAGATCCCGGGCCCGCACTTCGTCACTATCATTA
CCAAGCAGACCCGTGATACCTCCGATAAACGCGACCACGTTTGTCAGCGTGAAGTGGCT
TATGCGCACTCTGTTCCGCGTATTACTAGCGCGATCGGCAGCGACGAAGACCTCGAGCA
CCACCACCACCACCACTGA

minisogq103v (pET-29b(+)_minisogq103v)

ATGGAAAAAAGCTTTGTGATTACTGACCCGCGTCTGCCGGACAACCCTATCATCTTTGCGT
CCGACGGCTTCCTGGAACTGACCGAATACTCCCGTGAAGAAATCCTGGGTCGTAACGGC
CGCTTCCTGCAGGGTCCGGAAACTGACCAAGCAACCGTTCAGAAAATTCGTGACGCCAT
CCGTGATCAGCGTGAAATCACCGTTCAGCTGATTAACTATACCAAGTCCGGCAAAAAATTC
TGGAACCTGCTGCATCTGCAGCCGATGCGTGACCAGAAAGGCGAACTGCAGTACTTCATT
GGTGTGGTGCTGGACGGCCTCGAGCACCACCACCACCACCACTGA

sopp3 (pET-29b(+)_sopp3)

ATGGAAAAAAGCTTCGTTATCACCGACCCGCGTCTGCCGGACAACCCTATCATCTTCGCG
TCCGATGGCTTTCTGGAACTGACTGAATACTCTCGTGAGGAGATCCTGGGCCGCAACGGT
CGTTTCCTGCAGGGCCCGGAAACTGATCAGGCTACCGTTCAGAAAATCCGTGACGCAAT
CCGTGACCAGCGCGAAATCACTGTGCAGCTGATCAACTATACCAAAAGCGGCAAGAAGTT
CCTGAACCTGCTGAATCTGCAGCCGATTCGTGACCAGAAAGGTGAACTGCAAGCATTCAT
CGGCGTGGTTCTGGACGGTCTCGAGCACCACCACCACCACCACTGA

dsfbfpm49i (pET-29b(+)_dsfbfpm49i)

ATGCGTCGTCACTACCGTGATCTGATTCGTAACACCCCGATGCCAGACACTCCGCAAGAT
ATCGCCGATCTGCGTGCTCTGCTGGACGAAGACGAGGCCGAAATGAGCGTTGTTTTTTCT
GACCCGTCTCAGCCGGACAACCCGATCATCTACGTTTCCGACGCGTTCCTGGTACAGAC
TGGCTACACCCTGGAAGAAGTACTGGGTCGTAATGCTCGTTTCCTGCAAGGTCCGGACAC
CAACCCGCACGCAGTTGAAGCTATCCGCCAGGGTCTGAAGGCGGAGACCCGTTTCACC
ATTGATATCCTGAACTACCGCAAGGACGGCTCCGCTTTCGTTAACCGTCTGCGTATCCGTC
CTATCTATGATCCGGAAGGTAACCTGATGTTCTTCGCGGGCGCACAGAACCCGGTTCTCG
AGCACCACCACCACCACCACTGA

rl1-hgf1-rl2 (ptwistamphighcopy_rl1-hgf1-rl2)

GCAGAAGCAGCAGCTAAAGAAGCGGCAGCCAAGGAGGCTGCTGCAAAAGCGACTCCAG
TTCGCCGTCAGCAAAGCACCACTGGCCAGCTGCAGTCCAGCGAATCCACCAGCACCGC
CAACGACCCAGCAACTTCTGAACTGCTGGGCCTGATCGGTGTTGTTATTTCCGACGTCGAT
GCTCTGGTTGGTCTGACCTCTAGCCCGATCAGCGTTATCGGTGTTGGTTCCGGTAGCGCT
AGCACTGCGAACCCGGTTTCTTCCGACAGCAGCCCGATCGGTGGTCTGGTTTCCATCGG
CTCCGTTCCAGTTAACGTAGCTGAAGCTGCTGCAAAGGAGGCCGCCGCTAAAGAAGCCG
CAGCTAAAGCC

rl1-hfb1-rl2 (ptwistamphighcopy_rl1-hfb1-rl2)

GCAGAAGCAGCAGCTAAAGAAGCGGCAGCCAAGGAGGCTGCTGCAAAAGCGTCTAACG
GTAACGGTAACGTGTGCCCGCCTGGCCTGTTCTCTAACCCGCAGTGTTGTGCCACCCAG
GTACTGGGCCTGATTGGCCTGGACTGCAAGGTTCCGTCTCAGAATGTTTACGACGGCACG
GACTTCCGTAACGTTTGCGCTAAAACCGGTGCACAGCCACTGTGTTGTGTAGCCCCGGTT
GCTGGTCAGGCACTGCTGTGTCAGACTGCAGTTGGTGCGGCTGAAGCTGCTGCAAAGGA
GGCCGCCGCTAAAGAAGCCGCAGCTAAAGCC

rl1hfb2-rl2 (ptwistamphighcopy_rl1-hfb2-rl2)

GCAGAAGCAGCAGCTAAAGAAGCGGCAGCCAAGGAGGCTGCTGCAAAAGCGGCAGTCT
GTCCGACTGGTCTGTTCAGCAACCCGCTGTGCTGCGCAACCAACGTTCTGGATCTGATCG
GCGTTGACTGCAAAACCCCTACTATCGCGGTTGACACCGGCGCCATCTTCCAGGCTCAC
TGTGCGAGCAAAGGCTCCAAACCGCTGTGCTGTGTTGCGCCGGTAGCTGATCAGGCGCT
GCTGTGTCAGAAAGCTATTGGTACTTTTGCTGAAGCTGCTGCAAAGGAGGCCGCCGCTAA
AGAAGCCGCAGCTAAAGCC

supernova-rl1-mhgf1 (pET-29b(+)_supernova-rl1-mhgf1)

ATGGAAGTCGGTCCGGCGCTGTTCCAGAGCGATATGACCTTTAAGATCTTCATCGACGGC
GAAGTGAACGGCCAGAAATTCACCATCGTTGCAGACGGTTCCTCCAAATTTCCGCACGGT
GATTTTAATGTGCACGCGGTTTGCGAAACTGGCAAACTGCCGATGTCCTGGAAACCAATCT
GCCACCTGATTCAGTATGGCGAGCCGTTCTTCGCACGTTATCCTGACGGTATCAGCCACT
TTGCGCAGGAATGTTTCCCAGAAGGTCTGAGCATCGACCGTACCGTACGTTTCGAAAACG
ATGGCACCATGACCTCCCATCACACCTATGAACTGGACGATACCTGCGTTGTCAGCCGTA
TCACCGTGAACTGCGACGGTTTCCAGCCGGATGGCCCGATCATGCGTGACCAGCTGGTT
GACATCCTGCCGAGCGAAACCCATATGTTTCCGCATGGCCCAAACGCGGTTCGTCAGAC
CGCTACTATTGGTTTCACCACTGCTGATGGTGGTAAAATGATGGGTCACTTCGATTCTAAAA
TGACCTTCAATGGCTCTCGTGCGATCGAGATCCCGGGCCCGCACTTCGTCACTATCATTA
CCAAGCAGACCCGTGATACCTCCGATAAACGCGACCACGTTTGTCAGCGTGAAGTGGCT
TATGCGCACTCTGTTCCGCGTATTACTAGCGCGATCGGCAGCGACGAAGACGCAGAAGC
AGCAGCTAAAGAAGCGGCAGCCAAGGAGGCTGCTGCAAAAGCGACTCCAGTTCGCCGT
CAGCAAAGCACCACTGGCCAGCTGCAGTCCAGCGAATCCACCAGCACCGCCAACGAC
CCAGCAACTTCTGAACTGCTGGGCCTGATCGGTGTTGTTATTTCCGACGTCGATGCTCTGG
TTGGTCTGACCTCTAGCCCGATCAGCGTTATCGGTGTTGGTTCCGGTAGCGCTAGCACTG

CGAACCCGGTTTCTTCCGACAGCAGCCCGATCGGTGGTCTGGTTTCCATCGGCTCCGTT
CCAGTTAACGTACTCGAGCACCACCACCACCACCACTGA

minisogq103v-rl1-mhgf1 (pET-29b(+)_minisogq103v-rl1-mhgf1)

ATGGAAAAAAGCTTTGTGATTACTGACCCGCGTCTGCCGGACAACCCTATCATCTTTGCGT
CCGACGGCTTCCTGGAACTGACCGAATACTCCCGTGAAGAAATCCTGGGTCGTAACGGC
CGCTTCCTGCAGGGTCCGGAAACTGACCAAGCAACCGTTCAGAAAATTCGTGACGCCAT
CCGTGATCAGCGTGAAATCACCGTTCAGCTGATTAACTATACCAAGTCCGGCAAAAAATTC
TGGAACCTGCTGCATCTGCAGCCGATGCGTGACCAGAAAGGCGAACTGCAGTACTTCATT
GGTGTGGTGCTGGACGGCGCAGAAGCAGCAGCTAAAGAAGCGGCAGCCAAGGAGGCT
GCTGCAAAAGCGACTCCAGTTCGCCGTCAGCAAAGCACCACTGGCCAGCTGCAGTCCA
GCGAATCCACCAGCACCGCCAACGACCCAGCAACTTCTGAACTGCTGGGCCTGATCGG
TGTTGTTATTTCCGACGTCGATGCTCTGGTTGGTCTGACCTCTAGCCCGATCAGCGTTATC
GGTGTTGGTTCCGGTAGCGCTAGCACTGCGAACCCGGTTTCTTCCGACAGCAGCCCGAT
CGGTGGTCTGGTTTCCATCGGCTCCGTTCCAGTTAACGTACTCGAGCACCACCACCACC
ACCACTGA

minisogq103v-rl1-hfb1 (pET-29b(+)_minisogq103v-rl1-hfb1)

ATGGAAAAAAGCTTTGTGATTACTGACCCGCGTCTGCCGGACAACCCTATCATCTTTGCGT
CCGACGGCTTCCTGGAACTGACCGAATACTCCCGTGAAGAAATCCTGGGTCGTAACGGC
CGCTTCCTGCAGGGTCCGGAAACTGACCAAGCAACCGTTCAGAAAATTCGTGACGCCAT
CCGTGATCAGCGTGAAATCACCGTTCAGCTGATTAACTATACCAAGTCCGGCAAAAAATTC
TGGAACCTGCTGCATCTGCAGCCGATGCGTGACCAGAAAGGCGAACTGCAGTACTTCATT
GGTGTGGTGCTGGACGGCGCAGAAGCAGCAGCTAAAGAAGCGGCAGCCAAGGAGGCT
GCTGCAAAAGCGTCTAACGGTAACGGTAACGTGTGCCCGCCTGGCCTGTTCTCTAACCC
GCAGTGTTGTGCCACCCAGGTACTGGGCCTGATTGGCCTGGACTGCAAGGTTCCGTCTC
AGAATGTTTACGACGGCACGGACTTCCGTAACGTTTGCGCTAAAACCGGTGCACAGCCAC
TGTGTTGTGTAGCCCCGGTTGCTGGTCAGGCACTGCTGTGTCAGACTGCAGTTGGTGCGC
TCGAGCACCACCACCACCACCACTGA

minisogq103v-rl1-hfb2 (pET-29b(+)_minisogq103v-rl1-hfb2)

ATGGAAAAAAGCTTTGTGATTACTGACCCGCGTCTGCCGGACAACCCTATCATCTTTGCGT
CCGACGGCTTCCTGGAACTGACCGAATACTCCCGTGAAGAAATCCTGGGTCGTAACGGC
CGCTTCCTGCAGGGTCCGGAAACTGACCAAGCAACCGTTCAGAAAATTCGTGACGCCAT
CCGTGATCAGCGTGAAATCACCGTTCAGCTGATTAACTATACCAAGTCCGGCAAAAAATTC
TGGAACCTGCTGCATCTGCAGCCGATGCGTGACCAGAAAGGCGAACTGCAGTACTTCATT
GGTGTGGTGCTGGACGGCGCAGAAGCAGCAGCTAAAGAAGCGGCAGCCAAGGAGGCT
GCTGCAAAAGCGGCAGTCTGTCCGACTGGTCTGTTCAGCAACCCGCTGTGCTGCGCAAC
CAACGTTCTGGATCTGATCGGCGTTGACTGCAAAACCCCTACTATCGCGGTTGACACCGG
CGCCATCTTCCAGGCTCACTGTGCGAGCAAAGGCTCCAAACCGCTGTGCTGTGTTGCGC
CGGTAGCTGATCAGGCGCTGCTGTGTCAGAAAGCTATTGGTACTTTTCTCGAGCACCACC
ACCACCACCACTGA

minisogq103v-rl1-mhgf1-rl2-minisogq103v (pET-29b(+)_minisogq103v-rl1-mhgf1-rl2-minisogq103v)

ATGGAAAAAAGCTTTGTGATTACTGACCCGCGTCTGCCGGACAACCCTATCATCTTTGCGT
CCGACGGCTTCCTGGAACTGACCGAATACTCCCGTGAAGAAATCCTGGGTCGTAACGGC
CGCTTCCTGCAGGGTCCGGAAACTGACCAAGCAACCGTTCAGAAAATTCGTGACGCCAT
CCGTGATCAGCGTGAAATCACCGTTCAGCTGATTAACTATACCAAGTCCGGCAAAAAATTC
TGGAACCTGCTGCATCTGCAGCCGATGCGTGACCAGAAAGGCGAACTGCAGTACTTCATT
GGTGTGGTGCTGGACGGCGCAGAAGCAGCAGCTAAAGAAGCGGCAGCCAAGGAGGCT
GCTGCAAAAGCGACTCCAGTTCGCCGTCAGCAAAGCACCACTGGCCAGCTGCAGTCCA
GCGAATCCACCAGCACCGCCAACGACCCAGCAACTTCTGAACTGCTGGGCCTGATCGG
TGTTGTTATTTCCGACGTCGATGCTCTGGTTGGTCTGACCTCTAGCCCGATCAGCGTTATC
GGTGTTGGTTCCGGTAGCGCTAGCACTGCGAACCCGGTTTCTTCCGACAGCAGCCCGAT
CGGTGGTCTGGTTTCCATCGGCTCCGTTCCAGTTAACGTAGCTGAAGCTGCTGCAAAGGA
GGCCGCCGCTAAAGAAGCCGCAGCTAAAGCCGAAAAAAGCTTTGTGATTACTGACCCGC
GTCTGCCGGACAACCCTATCATCTTTGCGTCCGACGGCTTCCTGGAACTGACCGAATACT
CCCGTGAAGAAATCCTGGGTCGTAACGGCCGCTTCCTGCAGGGTCCGGAAACTGACCAA
GCAACCGTTCAGAAAATTCGTGACGCCATCCGTGATCAGCGTGAAATCACCGTTCAGCTG
ATTAACTATACCAAGTCCGGCAAAAAATTCTGGAACCTGCTGCATCTGCAGCCGATGCGTG
ACCAGAAAGGCGAACTGCAGTACTTCATTGGTGTGGTGCTGGACGGCCTCGAGCACCAC
CACCACCACCACTGA

mhgf1-rl2-minisogq103v (pET-29b(+)_mhgf1-rl2-minisogq103v)

ATGACTCCAGTTCGCCGTCAGCAAAGCACCACTGGCCAGCTGCAGTCCAGCGAATCCAC
CAGCACCGCCAACGACCCAGCAACTTCTGAACTGCTGGGCCTGATCGGTGTTGTTATTTC
CGACGTCGATGCTCTGGTTGGTCTGACCTCTAGCCCGATCAGCGTTATCGGTGTTGGTTC
CGGTAGCGCTAGCACTGCGAACCCGGTTTCTTCCGACAGCAGCCCGATCGGTGGTCTG
GTTTCCATCGGCTCCGTTCCAGTTAACGTAGCTGAAGCTGCTGCAAAGGAGGCCGCCGC
TAAAGAAGCCGCAGCTAAAGCCGAAAAAAGCTTTGTGATTACTGACCCGCGTCTGCCGGA
CAACCCTATCATCTTTGCGTCCGACGGCTTCCTGGAACTGACCGAATACTCCCGTGAAGA
AATCCTGGGTCGTAACGGCCGCTTCCTGCAGGGTCCGGAAACTGACCAAGCAACCGTTC
AGAAAATTCGTGACGCCATCCGTGATCAGCGTGAAATCACCGTTCAGCTGATTAACTATAC
CAAGTCCGGCAAAAAATTCTGGAACCTGCTGCATCTGCAGCCGATGCGTGACCAGAAAG
GCGAACTGCAGTACTTCATTGGTGTGGTGCTGGACGGCCTCGAGCACCACCACCACCAC
CACTGA

minisogq103v-rl1-mhgf1-flhis (pET-29b(+)_minisogq103v-rl1-mhgf1-flhis)

ATGGAAAAAAGCTTTGTGATTACTGACCCGCGTCTGCCGGACAACCCTATCATCTTTGCGT
CCGACGGCTTCCTGGAACTGACCGAATACTCCCGTGAAGAAATCCTGGGTCGTAACGGC
CGCTTCCTGCAGGGTCCGGAAACTGACCAAGCAACCGTTCAGAAAATTCGTGACGCCAT
CCGTGATCAGCGTGAAATCACCGTTCAGCTGATTAACTATACCAAGTCCGGCAAAAAATTC
TGGAACCTGCTGCATCTGCAGCCGATGCGTGACCAGAAAGGCGAACTGCAGTACTTCATT
GGTGTGGTGCTGGACGGCGCAGAAGCAGCAGCTAAAGAAGCGGCAGCCAAGGAGGCT
GCTGCAAAAGCGACTCCAGTTCGCCGTCAGCAAAGCACCACTGGCCAGCTGCAGTCCA
GCGAATCCACCAGCACCGCCAACGACCCAGCAACTTCTGAACTGCTGGGCCTGATCGG

TGTTGTTATTTCCGACGTCGATGCTCTGGTTGGTCTGACCTCTAGCCCGATCAGCGTTATC
GGTGTTGGTTCCGGTAGCGCTAGCACTGCGAACCCGGTTTCTTCCGACAGCAGCCCGAT
CGGTGGTCTGGTTTCCATCGGCTCCGTTCCAGTTAACGTAGGTGGCGGTGGGTCTGGCG
GTGGAGGTTCCCTCGAGCACCACCACCACCACCACTGA

sopp3-rl1-mhgf1 (pET-29b(+)_sopp3-rl1-mhgf1)

ATGGAAAAAAGCTTCGTTATCACCGACCCGCGTCTGCCGGACAACCCTATCATCTTCGCG
TCCGATGGCTTTCTGGAACTGACTGAATACTCTCGTGAGGAGATCCTGGGCCGCAACGGT
CGTTTCCTGCAGGGCCCGGAAACTGATCAGGCTACCGTTCAGAAAATCCGTGACGCAAT
CCGTGACCAGCGCGAAATCACTGTGCAGCTGATCAACTATACCAAAAGCGGCAAGAAGTT
CCTGAACCTGCTGAATCTGCAGCCGATTCGTGACCAGAAAGGTGAACTGCAAGCATTCAT
CGGCGTGGTTCTGGACGGTGCAGAAGCAGCAGCTAAAGAAGCGGCAGCCAAGGAGGCT
GCTGCAAAAGCGACTCCAGTTCGCCGTCAGCAAAGCACCACTGGCCAGCTGCAGTCCA
GCGAATCCACCAGCACCGCCAACGACCCAGCAACTTCTGAACTGCTGGGCCTGATCGG
TGTTGTTATTTCCGACGTCGATGCTCTGGTTGGTCTGACCTCTAGCCCGATCAGCGTTATC
GGTGTTGGTTCCGGTAGCGCTAGCACTGCGAACCCGGTTTCTTCCGACAGCAGCCCGAT
CGGTGGTCTGGTTTCCATCGGCTCCGTTCCAGTTAACGTACTCGAGCACCACCACCACC
ACCACTGA

sopp3-rl1-hfb1 (pET-29b(+)_sopp3-rl1-hfb1)

ATGGAAAAAAGCTTCGTTATCACCGACCCGCGTCTGCCGGACAACCCTATCATCTTCGCG
TCCGATGGCTTTCTGGAACTGACTGAATACTCTCGTGAGGAGATCCTGGGCCGCAACGGT
CGTTTCCTGCAGGGCCCGGAAACTGATCAGGCTACCGTTCAGAAAATCCGTGACGCAAT
CCGTGACCAGCGCGAAATCACTGTGCAGCTGATCAACTATACCAAAAGCGGCAAGAAGTT
CCTGAACCTGCTGAATCTGCAGCCGATTCGTGACCAGAAAGGTGAACTGCAAGCATTCAT
CGGCGTGGTTCTGGACGGTGCAGAAGCAGCAGCTAAAGAAGCGGCAGCCAAGGAGGCT
GCTGCAAAAGCGTCTAACGGTAACGGTAACGTGTGCCCGCCTGGCCTGTTCTCTAACCC
GCAGTGTTGTGCCACCCAGGTACTGGGCCTGATTGGCCTGGACTGCAAGGTTCCGTCTC
AGAATGTTTACGACGGCACGGACTTCCGTAACGTTTGCGCTAAAACCGGTGCACAGCCAC
TGTGTTGTGTAGCCCCGGTTGCTGGTCAGGCACTGCTGTGTCAGACTGCAGTTGGTGCGC
TCGAGCACCACCACCACCACCACTGA

sopp3-rl1-hfb2 (pET-29b(+)_sopp3-rl1-hfb2)

ATGGAAAAAAGCTTCGTTATCACCGACCCGCGTCTGCCGGACAACCCTATCATCTTCGCG
TCCGATGGCTTTCTGGAACTGACTGAATACTCTCGTGAGGAGATCCTGGGCCGCAACGGT
CGTTTCCTGCAGGGCCCGGAAACTGATCAGGCTACCGTTCAGAAAATCCGTGACGCAAT
CCGTGACCAGCGCGAAATCACTGTGCAGCTGATCAACTATACCAAAAGCGGCAAGAAGTT
CCTGAACCTGCTGAATCTGCAGCCGATTCGTGACCAGAAAGGTGAACTGCAAGCATTCAT
CGGCGTGGTTCTGGACGGTGCAGAAGCAGCAGCTAAAGAAGCGGCAGCCAAGGAGGCT
GCTGCAAAAGCGGCAGTCTGTCCGACTGGTCTGTTCAGCAACCCGCTGTGCTGCGCAAC
CAACGTTCTGGATCTGATCGGCGTTGACTGCAAAACCCCTACTATCGCGGTTGACACCGG
CGCCATCTTCCAGGCTCACTGTGCGAGCAAAGGCTCCAAACCGCTGTGCTGTGTTGCGC
CGGTAGCTGATCAGGCGCTGCTGTGTCAGAAAGCTATTGGTACTTTTCTCGAGCACCACC
ACCACCACCACTGA

sopp3-rl1-mhgf1-rl2-sopp3 (pET-29b(+)_sopp3-rl1-mhgf1-rl2-sopp3)

ATGGAAAAAAGCTTCGTTATCACCGACCCGCGTCTGCCGGACAACCCTATCATCTTCGCG
TCCGATGGCTTTCTGGAACTGACTGAATACTCTCGTGAGGAGATCCTGGGCCGCAACGGT
CGTTTCCTGCAGGGCCCGGAAACTGATCAGGCTACCGTTCAGAAAATCCGTGACGCAAT
CCGTGACCAGCGCGAAATCACTGTGCAGCTGATCAACTATACCAAAAGCGGCAAGAAGTT
CCTGAACCTGCTGAATCTGCAGCCGATTCGTGACCAGAAAGGTGAACTGCAAGCATTCAT
CGGCGTGGTTCTGGACGGTGCAGAAGCAGCAGCTAAAGAAGCGGCAGCCAAGGAGGCT
GCTGCAAAAGCGACTCCAGTTCGCCGTCAGCAAAGCACCACTGGCCAGCTGCAGTCCA
GCGAATCCACCAGCACCGCCAACGACCCAGCAACTTCTGAACTGCTGGGCCTGATCGG
TGTTGTTATTTCCGACGTCGATGCTCTGGTTGGTCTGACCTCTAGCCCGATCAGCGTTATC
GGTGTTGGTTCCGGTAGCGCTAGCACTGCGAACCCGGTTTCTTCCGACAGCAGCCCGAT
CGGTGGTCTGGTTTCCATCGGCTCCGTTCCAGTTAACGTAGCTGAAGCTGCTGCAAAGGA
GGCCGCCGCTAAAGAAGCCGCAGCTAAAGCCGAAAAAAGCTTCGTTATCACCGACCCG
CGTCTGCCGGACAACCCTATCATCTTCGCGTCCGATGGCTTTCTGGAACTGACTGAATACT
CTCGTGAGGAGATCCTGGGCCGCAACGGTCGTTTCCTGCAGGGCCCGGAAACTGATCA
GGCTACCGTTCAGAAAATCCGTGACGCAATCCGTGACCAGCGCGAAATCACTGTGCAGC
TGATCAACTATACCAAAAGCGGCAAGAAGTTCCTGAACCTGCTGAATCTGCAGCCGATTC
GTGACCAGAAAGGTGAACTGCAAGCATTCATCGGCGTGGTTCTGGACGGTCTCGAGCAC
CACCACCACCACCACTGA

sopp3-rl1-hfb1-rl2-sopp3 (pET-29b(+)_sopp3-rl1-hfb1-rl2-sopp3)

ATGGAAAAAAGCTTCGTTATCACCGACCCGCGTCTGCCGGACAACCCTATCATCTTCGCG
TCCGATGGCTTTCTGGAACTGACTGAATACTCTCGTGAGGAGATCCTGGGCCGCAACGGT
CGTTTCCTGCAGGGCCCGGAAACTGATCAGGCTACCGTTCAGAAAATCCGTGACGCAAT
CCGTGACCAGCGCGAAATCACTGTGCAGCTGATCAACTATACCAAAAGCGGCAAGAAGTT
CCTGAACCTGCTGAATCTGCAGCCGATTCGTGACCAGAAAGGTGAACTGCAAGCATTCAT
CGGCGTGGTTCTGGACGGTGCAGAAGCAGCAGCTAAAGAAGCGGCAGCCAAGGAGGCT
GCTGCAAAAGCGTCTAACGGTAACGGTAACGTGTGCCCGCCTGGCCTGTTCTCTAACCC
GCAGTGTTGTGCCACCCAGGTACTGGGCCTGATTGGCCTGGACTGCAAGGTTCCGTCTC
AGAATGTTTACGACGGCACGGACTTCCGTAACGTTTGCGCTAAAACCGGTGCACAGCCAC
TGTGTTGTGTAGCCCCGGTTGCTGGTCAGGCACTGCTGTGTCAGACTGCAGTTGGTGCGG
CTGAAGCTGCTGCAAAGGAGGCCGCCGCTAAAGAAGCCGCAGCTAAAGCCGAAAAAAG
CTTCGTTATCACCGACCCGCGTCTGCCGGACAACCCTATCATCTTCGCGTCCGATGGCTT
TCTGGAACTGACTGAATACTCTCGTGAGGAGATCCTGGGCCGCAACGGTCGTTTCCTGCA
GGGCCCGGAAACTGATCAGGCTACCGTTCAGAAAATCCGTGACGCAATCCGTGACCAGC
GCGAAATCACTGTGCAGCTGATCAACTATACCAAAAGCGGCAAGAAGTTCCTGAACCTGC
TGAATCTGCAGCCGATTCGTGACCAGAAAGGTGAACTGCAAGCATTCATCGGCGTGGTTC
TGGACGGTCTCGAGCACCACCACCACCACCACTGA

sopp3-rl1-hfb2-rl2-sopp3 (pET-29b(+)_sopp3-rl1-hfb2-rl2-sopp3)

ATGGAAAAAAGCTTCGTTATCACCGACCCGCGTCTGCCGGACAACCCTATCATCTTCGCG
TCCGATGGCTTTCTGGAACTGACTGAATACTCTCGTGAGGAGATCCTGGGCCGCAACGGT
CGTTTCCTGCAGGGCCCGGAAACTGATCAGGCTACCGTTCAGAAAATCCGTGACGCAAT
CCGTGACCAGCGCGAAATCACTGTGCAGCTGATCAACTATACCAAAAGCGGCAAGAAGTT

CCTGAACCTGCTGAATCTGCAGCCGATTCGTGACCAGAAAGGTGAACTGCAAGCATTCAT
CGGCGTGGTTCTGGACGGTGCAGAAGCAGCAGCTAAAGAAGCGGCAGCCAAGGAGGCT
GCTGCAAAAGCGGCAGTCTGTCCGACTGGTCTGTTCAGCAACCCGCTGTGCTGCGCAAC
CAACGTTCTGGATCTGATCGGCGTTGACTGCAAAACCCCTACTATCGCGGTTGACACCGG
CGCCATCTTCCAGGCTCACTGTGCGAGCAAAGGCTCCAAACCGCTGTGCTGTGTTGCGC
CGGTAGCTGATCAGGCGCTGCTGTGTCAGAAAGCTATTGGTACTTTTGCTGAAGCTGCTGC
AAAGGAGGCCGCCGCTAAAGAAGCCGCAGCTAAAGCCGAAAAAAGCTTCGTTATCACCG
ACCCGCGTCTGCCGGACAACCCTATCATCTTCGCGTCCGATGGCTTTCTGGAACTGACTG
AATACTCTCGTGAGGAGATCCTGGGCCGCAACGGTCGTTTCCTGCAGGGCCCGGAAACT
GATCAGGCTACCGTTCAGAAAATCCGTGACGCAATCCGTGACCAGCGCGAAATCACTGT
GCAGCTGATCAACTATACCAAAAGCGGCAAGAAGTTCCTGAACCTGCTGAATCTGCAGCC
GATTCGTGACCAGAAAGGTGAACTGCAAGCATTCATCGGCGTGGTTCTGGACGGTCTCGA
GCACCACCACCACCACCACTGA

mhgf1-rl2-sopp3 (pET-29b(+)_mhgf1-rl2-sopp3)

ATGACTCCAGTTCGCCGTCAGCAAAGCACCACTGGCCAGCTGCAGTCCAGCGAATCCAC
CAGCACCGCCAACGACCCAGCAACTTCTGAACTGCTGGGCCTGATCGGTGTTGTTATTTC
CGACGTCGATGCTCTGGTTGGTCTGACCTCTAGCCCGATCAGCGTTATCGGTGTTGGTTC
CGGTAGCGCTAGCACTGCGAACCCGGTTTCTTCCGACAGCAGCCCGATCGGTGGTCTG
GTTTCCATCGGCTCCGTTCCAGTTAACGTAGCTGAAGCTGCTGCAAAGGAGGCCGCCGC
TAAAGAAGCCGCAGCTAAAGCCGAAAAAAGCTTCGTTATCACCGACCCGCGTCTGCCGG
ACAACCCTATCATCTTCGCGTCCGATGGCTTTCTGGAACTGACTGAATACTCTCGTGAGGA
GATCCTGGGCCGCAACGGTCGTTTCCTGCAGGGCCCGGAAACTGATCAGGCTACCGTTC
AGAAAATCCGTGACGCAATCCGTGACCAGCGCGAAATCACTGTGCAGCTGATCAACTATA
CCAAAAGCGGCAAGAAGTTCCTGAACCTGCTGAATCTGCAGCCGATTCGTGACCAGAAA
GGTGAACTGCAAGCATTCATCGGCGTGGTTCTGGACGGTCTCGAGCACCACCACCACCA
CCACTGA

hfb1-rl2-sopp3 (pET-29b(+)_hfb1-rl2-sopp3)

ATGTCTAACGGTAACGGTAACGTGTGCCCGCCTGGCCTGTTCTCTAACCCGCAGTGTTGT
GCCACCCAGGTACTGGGCCTGATTGGCCTGGACTGCAAGGTTCCGTCTCAGAATGTTTAC
GACGGCACGGACTTCCGTAACGTTTGCGCTAAAACCGGTGCACAGCCACTGTGTTGTGTA
GCCCCGGTTGCTGGTCAGGCACTGCTGTGTCAGACTGCAGTTGGTGCGGCTGAAGCTGC
TGCAAAGGAGGCCGCCGCTAAAGAAGCCGCAGCTAAAGCCGAAAAAAGCTTCGTTATCA
CCGACCCGCGTCTGCCGGACAACCCTATCATCTTCGCGTCCGATGGCTTTCTGGAACTG
ACTGAATACTCTCGTGAGGAGATCCTGGGCCGCAACGGTCGTTTCCTGCAGGGCCCGGA
AACTGATCAGGCTACCGTTCAGAAAATCCGTGACGCAATCCGTGACCAGCGCGAAATCA
CTGTGCAGCTGATCAACTATACCAAAAGCGGCAAGAAGTTCCTGAACCTGCTGAATCTGC
AGCCGATTCGTGACCAGAAAGGTGAACTGCAAGCATTCATCGGCGTGGTTCTGGACGGT
CTCGAGCACCACCACCACCACCACTGA

hfb21-rl2-sopp3 (pET-29b(+)_hfb21-rl2-sopp3)

ATGGCAGTCTGTCCGACTGGTCTGTTCAGCAACCCGCTGTGCTGCGCAACCAACGTTCTG
GATCTGATCGGCGTTGACTGCAAAACCCCTACTATCGCGGTTGACACCGGCGCCATCTTC

CAGGCTCACTGTGCGAGCAAAGGCTCCAAACCGCTGTGCTGTGTTGCGCCGGTAGCTGA
TCAGGCGCTGCTGTGTCAGAAAGCTATTGGTACTTTTGCTGAAGCTGCTGCAAAGGAGGC
CGCCGCTAAAGAAGCCGCAGCTAAAGCCGAAAAAAGCTTCGTTATCACCGACCCGCGTC
TGCCGGACAACCCTATCATCTTCGCGTCCGATGGCTTTCTGGAACTGACTGAATACTCTCG
TGAGGAGATCCTGGGCCGCAACGGTCGTTTCCTGCAGGGCCCGGAAACTGATCAGGCTA
CCGTTCAGAAAATCCGTGACGCAATCCGTGACCAGCGCGAAATCACTGTGCAGCTGATC
AACTATACCAAAAGCGGCAAGAAGTTCCTGAACCTGCTGAATCTGCAGCCGATTCGTGAC
CAGAAAGGTGAACTGCAAGCATTCATCGGCGTGGTTCTGGACGGTCTCGAGCACCACCA
CCACCACCACTGA

sopp3-rl1-mhgf1-flhis (pET-29b(+)_sopp3-rl1-mhgf1-flhis)

ATGGAAAAAAGCTTCGTTATCACCGACCCGCGTCTGCCGGACAACCCTATCATCTTCGCG
TCCGATGGCTTTCTGGAACTGACTGAATACTCTCGTGAGGAGATCCTGGGCCGCAACGGT
CGTTTCCTGCAGGGCCCGGAAACTGATCAGGCTACCGTTCAGAAAATCCGTGACGCAAT
CCGTGACCAGCGCGAAATCACTGTGCAGCTGATCAACTATACCAAAAGCGGCAAGAAGTT
CCTGAACCTGCTGAATCTGCAGCCGATTCGTGACCAGAAAGGTGAACTGCAAGCATTCAT
CGGCGTGGTTCTGGACGGTGCAGAAGCAGCAGCTAAAGAAGCGGCAGCCAAGGAGGCT
GCTGCAAAAGCGACTCCAGTTCGCCGTCAGCAAAGCACCACTGGCCAGCTGCAGTCCA
GCGAATCCACCAGCACCGCCAACGACCCAGCAACTTCTGAACTGCTGGGCCTGATCGG
TGTTGTTATTTCCGACGTCGATGCTCTGGTTGGTCTGACCTCTAGCCCGATCAGCGTTATC
GGTGTTGGTTCCGGTAGCGCTAGCACTGCGAACCCGGTTTCTTCCGACAGCAGCCCGAT
CGGTGGTCTGGTTTCCATCGGCTCCGTTCCAGTTAACGTAGGTGGCGGTGGGTCTGGCG
GTGGAGGTTCCCTCGAGCACCACCACCACCACCACTGA

(la)12-sopp3 (pET-29b(+)_(la)12-sopp3)

ATGTTGGCTCTGGCGCTGGCACTCGCTCTGGCGTTAGCACTCGCTCTCGCACTGGCACT
GGCACTGGCATTGGCTGGCGGTTCTGGCGAAAAAAGCTTCGTTATCACCGACCCGCGTC
TGCCGGACAACCCTATCATCTTCGCGTCCGATGGCTTTCTGGAACTGACTGAATACTCTCG
TGAGGAGATCCTGGGCCGCAACGGTCGTTTCCTGCAGGGCCCGGAAACTGATCAGGCTA
CCGTTCAGAAAATCCGTGACGCAATCCGTGACCAGCGCGAAATCACTGTGCAGCTGATC
AACTATACCAAAAGCGGCAAGAAGTTCCTGAACCTGCTGAATCTGCAGCCGATTCGTGAC
CAGAAAGGTGAACTGCAAGCATTCATCGGCGTGGTTCTGGACGGTCTCGAGCACCACCA
CCACCACCACTGA

sopp3-(la)12-sopp3 (pET29b(+)_sopp3-(la)12-sopp3)

ATGGAAAAAAGCTTCGTTATCACCGACCCGCGTCTGCCGGACAACCCTATCATCTTCGCG
TCCGATGGCTTTCTGGAACTGACTGAATACTCTCGTGAGGAGATCCTGGGCCGCAACGGT
CGTTTCCTGCAGGGCCCGGAAACTGATCAGGCTACCGTTCAGAAAATCCGTGACGCAAT
CCGTGACCAGCGCGAAATCACTGTGCAGCTGATCAACTATACCAAAAGCGGCAAGAAGTT
CCTGAACCTGCTGAATCTGCAGCCGATTCGTGACCAGAAAGGTGAACTGCAAGCATTCAT
CGGCGTGGTTCTGGACGGTGGCGGTTCTGGCTTGGCTCTGGCGCTGGCACTCGCTCTG
GCGTTAGCACTCGCTCTCGCACTGGCACTGGCACTGGCATTGGCTGGCGGTTCTGGCGA
AAAAAGCTTCGTTATCACCGACCCGCGTCTGCCGGACAACCCTATCATCTTCGCGTCCGA
TGGCTTTCTGGAACTGACTGAATACTCTCGTGAGGAGATCCTGGGCCGCAACGGTCGTTT

CCTGCAGGGCCCGGAAACTGATCAGGCTACCGTTCAGAAAATCCGTGACGCAATCCGTG
ACCAGCGCGAAATCACTGTGCAGCTGATCAACTATACCAAAAGCGGCAAGAAGTTCCTGA
ACCTGCTGAATCTGCAGCCGATTCGTGACCAGAAAGGTGAACTGCAAGCATTCATCGGCG
TGGTTCTGGACGGTCTCGAGCACCACCACCACCACCACTGA

dsfbfpm49i-rl1-mhgf1 (pET-29b(+)_dsfbfpm49i-rl1-mhgf1)

ATGCGTCGTCACTACCGTGATCTGATTCGTAACACCCCGATGCCAGACACTCCGCAAGAT
ATCGCCGATCTGCGTGCTCTGCTGGACGAAGACGAGGCCGAAATGAGCGTTGTTTTTTCT
GACCCGTCTCAGCCGGACAACCCGATCATCTACGTTTCCGACGCGTTCCTGGTACAGAC
TGGCTACACCCTGGAAGAAGTACTGGGTCGTAATGCTCGTTTCCTGCAAGGTCCGGACAC
CAACCCGCACGCAGTTGAAGCTATCCGCCAGGGTCTGAAGGCGGAGACCCGTTTCACC
ATTGATATCCTGAACTACCGCAAGGACGGCTCCGCTTTCGTTAACCGTCTGCGTATCCGTC
CTATCTATGATCCGGAAGGTAACCTGATGTTCTTCGCGGGCGCACAGAACCCGGTTGCAG
AAGCAGCAGCTAAAGAAGCGGCAGCCAAGGAGGCTGCTGCAAAAGCGACTCCAGTTCG
CCGTCAGCAAAGCACCACTGGCCAGCTGCAGTCCAGCGAATCCACCAGCACCGCCAA
CGACCCAGCAACTTCTGAACTGCTGGGCCTGATCGGTGTTGTTATTTCCGACGTCGATGC
TCTGGTTGGTCTGACCTCTAGCCCGATCAGCGTTATCGGTGTTGGTTCCGGTAGCGCTAG
CACTGCGAACCCGGTTTCTTCCGACAGCAGCCCGATCGGTGGTCTGGTTTCCATCGGCT
CCGTTCCAGTTAACGTACTCGAGCACCACCACCACCACCACTGA

dsfbfpm49i-rl1-hfb1 (pET-29b(+)_dsfbfpm49i-rl1-hfb1)

ATGCGTCGTCACTACCGTGATCTGATTCGTAACACCCCGATGCCAGACACTCCGCAAGAT
ATCGCCGATCTGCGTGCTCTGCTGGACGAAGACGAGGCCGAAATGAGCGTTGTTTTTTCT
GACCCGTCTCAGCCGGACAACCCGATCATCTACGTTTCCGACGCGTTCCTGGTACAGAC
TGGCTACACCCTGGAAGAAGTACTGGGTCGTAATGCTCGTTTCCTGCAAGGTCCGGACAC
CAACCCGCACGCAGTTGAAGCTATCCGCCAGGGTCTGAAGGCGGAGACCCGTTTCACC
ATTGATATCCTGAACTACCGCAAGGACGGCTCCGCTTTCGTTAACCGTCTGCGTATCCGTC
CTATCTATGATCCGGAAGGTAACCTGATGTTCTTCGCGGGCGCACAGAACCCGGTTGCAG
AAGCAGCAGCTAAAGAAGCGGCAGCCAAGGAGGCTGCTGCAAAAGCGTCTAACGGTAA
CGGTAACGTGTGCCCGCCTGGCCTGTTCTCTAACCCGCAGTGTTGTGCCACCCAGGTAC
TGGGCCTGATTGGCCTGGACTGCAAGGTTCCGTCTCAGAATGTTTACGACGGCACGGACT
TCCGTAACGTTTGCGCTAAAACCGGTGCACAGCCACTGTGTTGTGTAGCCCCGGTTGCTG
GTCAGGCACTGCTGTGTCAGACTGCAGTTGGTGCGCTCGAGCACCACCACCACCACCA
CTGA

dsfbfpm49i-rl1-hfb2 (pET-29b(+)_dsfbfpm49i-rl1-hfb2)

ATGCGTCGTCACTACCGTGATCTGATTCGTAACACCCCGATGCCAGACACTCCGCAAGAT
ATCGCCGATCTGCGTGCTCTGCTGGACGAAGACGAGGCCGAAATGAGCGTTGTTTTTTCT
GACCCGTCTCAGCCGGACAACCCGATCATCTACGTTTCCGACGCGTTCCTGGTACAGAC
TGGCTACACCCTGGAAGAAGTACTGGGTCGTAATGCTCGTTTCCTGCAAGGTCCGGACAC
CAACCCGCACGCAGTTGAAGCTATCCGCCAGGGTCTGAAGGCGGAGACCCGTTTCACC
ATTGATATCCTGAACTACCGCAAGGACGGCTCCGCTTTCGTTAACCGTCTGCGTATCCGTC
CTATCTATGATCCGGAAGGTAACCTGATGTTCTTCGCGGGCGCACAGAACCCGGTTGCAG
AAGCAGCAGCTAAAGAAGCGGCAGCCAAGGAGGCTGCTGCAAAAGCGGCAGTCTGTCC

GACTGGTCTGTTCAGCAACCCGCTGTGCTGCGCAACCAACGTTCTGGATCTGATCGGCGT
TGACTGCAAAACCCCTACTATCGCGGTTGACACCGGCGCCATCTTCCAGGCTCACTGTG
CGAGCAAAGGCTCCAAACCGCTGTGCTGTGTTGCGCCGGTAGCTGATCAGGCGCTGCTG
TGTCAGAAAGCTATTGGTACTTTTCTCGAGCACCACCACCACCACCACTGA

dsfbfpm49i-rl1-mhgf1-rl2-dsfbfpm49i (pET-29b(+)_dsfbfpm49i-rl1-mhgf1-rl2-dsfbfpm49i)

ATGCGTCGTCACTACCGTGATCTGATTCGTAACACCCCGATGCCAGACACTCCGCAAGAT
ATCGCCGATCTGCGTGCTCTGCTGGACGAAGACGAGGCCGAAATGAGCGTTGTTTTTTCT
GACCCGTCTCAGCCGGACAACCCGATCATCTACGTTTCCGACGCGTTCCTGGTACAGAC
TGGCTACACCCTGGAAGAAGTACTGGGTCGTAATGCTCGTTTCCTGCAAGGTCCGGACAC
CAACCCGCACGCAGTTGAAGCTATCCGCCAGGGTCTGAAGGCGGAGACCCGTTTCACC
ATTGATATCCTGAACTACCGCAAGGACGGCTCCGCTTTCGTTAACCGTCTGCGTATCCGTC
CTATCTATGATCCGGAAGGTAACCTGATGTTCTTCGCGGGCGCACAGAACCCGGTTGCAG
AAGCAGCAGCTAAAGAAGCGGCAGCCAAGGAGGCTGCTGCAAAAGCGACTCCAGTTCG
CCGTCAGCAAAGCACCACTGGCCAGCTGCAGTCCAGCGAATCCACCAGCACCGCCAA
CGACCCAGCAACTTCTGAACTGCTGGGCCTGATCGGTGTTGTTATTTCCGACGTCGATGC
TCTGGTTGGTCTGACCTCTAGCCCGATCAGCGTTATCGGTGTTGGTTCCGGTAGCGCTAG
CACTGCGAACCCGGTTTCTTCCGACAGCAGCCCGATCGGTGGTCTGGTTTCCATCGGCT
CCGTTCCAGTTAACGTAGCTGAAGCTGCTGCAAAGGAGGCCGCCGCTAAAGAAGCCGCA
GCTAAAGCCCGTCGTCACTACCGTGATCTGATTCGTAACACCCCGATGCCAGACACTCC
GCAAGATATCGCCGATCTGCGTGCTCTGCTGGACGAAGACGAGGCCGAAATGAGCGTTG
TTTTTTCTGACCCGTCTCAGCCGGACAACCCGATCATCTACGTTTCCGACGCGTTCCTGGT
ACAGACTGGCTACACCCTGGAAGAAGTACTGGGTCGTAATGCTCGTTTCCTGCAAGGTCC
GGACACCAACCCGCACGCAGTTGAAGCTATCCGCCAGGGTCTGAAGGCGGAGACCCGT
TTCACCATTGATATCCTGAACTACCGCAAGGACGGCTCCGCTTTCGTTAACCGTCTGCGTA
TCCGTCCTATCTATGATCCGGAAGGTAACCTGATGTTCTTCGCGGGCGCACAGAACCCGG
TTCTCGAGCACCACCACCACCACCACTGA

dsfbfpm49i-rl1-hfb1-rl2-dsfbfpm49i (pET-29b(+)_dsfbfpm49i-rl1-hfb1-rl2-dsfbfpm49i)

ATGCGTCGTCACTACCGTGATCTGATTCGTAACACCCCGATGCCAGACACTCCGCAAGAT
ATCGCCGATCTGCGTGCTCTGCTGGACGAAGACGAGGCCGAAATGAGCGTTGTTTTTTCT
GACCCGTCTCAGCCGGACAACCCGATCATCTACGTTTCCGACGCGTTCCTGGTACAGAC
TGGCTACACCCTGGAAGAAGTACTGGGTCGTAATGCTCGTTTCCTGCAAGGTCCGGACAC
CAACCCGCACGCAGTTGAAGCTATCCGCCAGGGTCTGAAGGCGGAGACCCGTTTCACC
ATTGATATCCTGAACTACCGCAAGGACGGCTCCGCTTTCGTTAACCGTCTGCGTATCCGTC
CTATCTATGATCCGGAAGGTAACCTGATGTTCTTCGCGGGCGCACAGAACCCGGTTGCAG
AAGCAGCAGCTAAAGAAGCGGCAGCCAAGGAGGCTGCTGCAAAAGCGTCTAACGGTAA
CGGTAACGTGTGCCCGCCTGGCCTGTTCTCTAACCCGCAGTGTTGTGCCACCCAGGTAC
TGGGCCTGATTGGCCTGGACTGCAAGGTTCCGTCTCAGAATGTTTACGACGGCACGGACT
TCCGTAACGTTTGCGCTAAAACCGGTGCACAGCCACTGTGTTGTGTAGCCCCGGTTGCTG
GTCAGGCACTGCTGTGTCAGACTGCAGTTGGTGCGGCTGAAGCTGCTGCAAAGGAGGCC
GCCGCTAAAGAAGCCGCAGCTAAAGCCCGTCGTCACTACCGTGATCTGATTCGTAACAC
CCCGATGCCAGACACTCCGCAAGATATCGCCGATCTGCGTGCTCTGCTGGACGAAGAC

GAGGCCGAAATGAGCGTTGTTTTTTCTGACCCGTCTCAGCCGGACAACCCGATCATCTAC
GTTTCCGACGCGTTCCTGGTACAGACTGGCTACACCCTGGAAGAAGTACTGGGTCGTAAT
GCTCGTTTCCTGCAAGGTCCGGACACCAACCCGCACGCAGTTGAAGCTATCCGCCAGG
GTCTGAAGGCGGAGACCCGTTTCACCATTGATATCCTGAACTACCGCAAGGACGGCTCC
GCTTTCGTTAACCGTCTGCGTATCCGTCCTATCTATGATCCGGAAGGTAACCTGATGTTCTT
CGCGGGCGCACAGAACCCGGTTCTCGAGCACCACCACCACCACCACTGA

dsfbfpm49i-rl1-hfb2-rl2-dsfbfpm49i (pET-29b(+)_dsfbfpm49i-rl1-hfb2-rl2-dsfbfpm49i)

ATGCGTCGTCACTACCGTGATCTGATTCGTAACACCCCGATGCCAGACACTCCGCAAGAT
ATCGCCGATCTGCGTGCTCTGCTGGACGAAGACGAGGCCGAAATGAGCGTTGTTTTTTCT
GACCCGTCTCAGCCGGACAACCCGATCATCTACGTTTCCGACGCGTTCCTGGTACAGAC
TGGCTACACCCTGGAAGAAGTACTGGGTCGTAATGCTCGTTTCCTGCAAGGTCCGGACAC
CAACCCGCACGCAGTTGAAGCTATCCGCCAGGGTCTGAAGGCGGAGACCCGTTTCACC
ATTGATATCCTGAACTACCGCAAGGACGGCTCCGCTTTCGTTAACCGTCTGCGTATCCGTC
CTATCTATGATCCGGAAGGTAACCTGATGTTCTTCGCGGGCGCACAGAACCCGGTTGCAG
AAGCAGCAGCTAAAGAAGCGGCAGCCAAGGAGGCTGCTGCAAAAGCGGCAGTCTGTCC
GACTGGTCTGTTCAGCAACCCGCTGTGCTGCGCAACCAACGTTCTGGATCTGATCGGCGT
TGACTGCAAAACCCCTACTATCGCGGTTGACACCGGCGCCATCTTCCAGGCTCACTGTG
CGAGCAAAGGCTCCAAACCGCTGTGCTGTGTTGCGCCGGTAGCTGATCAGGCGCTGCTG
TGTCAGAAAGCTATTGGTACTTTTGCTGAAGCTGCTGCAAAGGAGGCCGCCGCTAAAGAA
GCCGCAGCTAAAGCCCGTCGTCACTACCGTGATCTGATTCGTAACACCCCGATGCCAGA
CACTCCGCAAGATATCGCCGATCTGCGTGCTCTGCTGGACGAAGACGAGGCCGAAATGA
GCGTTGTTTTTTCTGACCCGTCTCAGCCGGACAACCCGATCATCTACGTTTCCGACGCGTT
CCTGGTACAGACTGGCTACACCCTGGAAGAAGTACTGGGTCGTAATGCTCGTTTCCTGCA
AGGTCCGGACACCAACCCGCACGCAGTTGAAGCTATCCGCCAGGGTCTGAAGGCGGAG
ACCCGTTTCACCATTGATATCCTGAACTACCGCAAGGACGGCTCCGCTTTCGTTAACCGT
CTGCGTATCCGTCCTATCTATGATCCGGAAGGTAACCTGATGTTCTTCGCGGGCGCACAG
AACCCGGTTCTCGAGCACCACCACCACCACCACTGA

mhgf1-rl2-dsfbfpm49i (pET-29b(+)_mhgf1-rl2-dsfbfpm49i)

ATGACTCCAGTTCGCCGTCAGCAAAGCACCACTGGCCAGCTGCAGTCCAGCGAATCCAC
CAGCACCGCCAACGACCCAGCAACTTCTGAACTGCTGGGCCTGATCGGTGTTGTTATTTC
CGACGTCGATGCTCTGGTTGGTCTGACCTCTAGCCCGATCAGCGTTATCGGTGTTGGTTC
CGGTAGCGCTAGCACTGCGAACCCGGTTTCTTCCGACAGCAGCCCGATCGGTGGTCTG
GTTTCCATCGGCTCCGTTCCAGTTAACGTAGCTGAAGCTGCTGCAAAGGAGGCCGCCGC
TAAAGAAGCCGCAGCTAAAGCCCGTCGTCACTACCGTGATCTGATTCGTAACACCCCGAT
GCCAGACACTCCGCAAGATATCGCCGATCTGCGTGCTCTGCTGGACGAAGACGAGGCC
GAAATGAGCGTTGTTTTTTCTGACCCGTCTCAGCCGGACAACCCGATCATCTACGTTTCCG
ACGCGTTCCTGGTACAGACTGGCTACACCCTGGAAGAAGTACTGGGTCGTAATGCTCGTT
TCCTGCAAGGTCCGGACACCAACCCGCACGCAGTTGAAGCTATCCGCCAGGGTCTGAA
GGCGGAGACCCGTTTCACCATTGATATCCTGAACTACCGCAAGGACGGCTCCGCTTTCGT
TAACCGTCTGCGTATCCGTCCTATCTATGATCCGGAAGGTAACCTGATGTTCTTCGCGGGC
GCACAGAACCCGGTTCTCGAGCACCACCACCACCACCACTGA

hfb1-rl2-dsfbfpm49i (pET-29b(+)_hfb1-rl2-dsfbfpm49i)

ATGTCTAACGGTAACGGTAACGTGTGCCCGCCTGGCCTGTTCTCTAACCCGCAGTGTTGT
GCCACCCAGGTACTGGGCCTGATTGGCCTGGACTGCAAGGTTCCGTCTCAGAATGTTTAC
GACGGCACGGACTTCCGTAACGTTTGCGCTAAAACCGGTGCACAGCCACTGTGTTGTGTA
GCCCCGGTTGCTGGTCAGGCACTGCTGTGTCAGACTGCAGTTGGTGCGGCTGAAGCTGC
TGCAAAGGAGGCCGCCGCTAAAGAAGCCGCAGCTAAAGCCCGTCGTCACTACCGTGAT
CTGATTCGTAACACCCCGATGCCAGACACTCCGCAAGATATCGCCGATCTGCGTGCTCT
GCTGGACGAAGACGAGGCCGAAATGAGCGTTGTTTTTTCTGACCCGTCTCAGCCGGACA
ACCCGATCATCTACGTTTCCGACGCGTTCCTGGTACAGACTGGCTACACCCTGGAAGAAG
TACTGGGTCGTAATGCTCGTTTCCTGCAAGGTCCGGACACCAACCCGCACGCAGTTGAA
GCTATCCGCCAGGGTCTGAAGGCGGAGACCCGTTTCACCATTGATATCCTGAACTACCG
CAAGGACGGCTCCGCTTTCGTTAACCGTCTGCGTATCCGTCCTATCTATGATCCGGAAGG
TAACCTGATGTTCTTCGCGGGCGCACAGAACCCGGTTCTCGAGCACCACCACCACCACC
ACTGA

hfb2-rl2-dsfbfpm49i (pET-29b(+)_hfb2-rl2-dsfbfpm49i)

ATGGCAGTCTGTCCGACTGGTCTGTTCAGCAACCCGCTGTGCTGCGCAACCAACGTTCTG
GATCTGATCGGCGTTGACTGCAAAACCCCTACTATCGCGGTTGACACCGGCGCCATCTTC
CAGGCTCACTGTGCGAGCAAAGGCTCCAAACCGCTGTGCTGTGTTGCGCCGGTAGCTGA
TCAGGCGCTGCTGTGTCAGAAAGCTATTGGTACTTTTGCTGAAGCTGCTGCAAAGGAGGC
CGCCGCTAAAGAAGCCGCAGCTAAAGCCCGTCGTCACTACCGTGATCTGATTCGTAACA
CCCCGATGCCAGACACTCCGCAAGATATCGCCGATCTGCGTGCTCTGCTGGACGAAGA
CGAGGCCGAAATGAGCGTTGTTTTTTCTGACCCGTCTCAGCCGGACAACCCGATCATCTA
CGTTTCCGACGCGTTCCTGGTACAGACTGGCTACACCCTGGAAGAAGTACTGGGTCGTAA
TGCTCGTTTCCTGCAAGGTCCGGACACCAACCCGCACGCAGTTGAAGCTATCCGCCAGG
GTCTGAAGGCGGAGACCCGTTTCACCATTGATATCCTGAACTACCGCAAGGACGGCTCC
GCTTTCGTTAACCGTCTGCGTATCCGTCCTATCTATGATCCGGAAGGTAACCTGATGTTCTT
CGCGGGCGCACAGAACCCGGTTCTCGAGCACCACCACCACCACCACTGA

dsfbfpm49i-rl1-mhgf1-flhis (pET-29b(+)_dsfbfpm49i-rl1-mhgf1-flhis)

ATGCGTCGTCACTACCGTGATCTGATTCGTAACACCCCGATGCCAGACACTCCGCAAGAT
ATCGCCGATCTGCGTGCTCTGCTGGACGAAGACGAGGCCGAAATGAGCGTTGTTTTTTCT
GACCCGTCTCAGCCGGACAACCCGATCATCTACGTTTCCGACGCGTTCCTGGTACAGAC
TGGCTACACCCTGGAAGAAGTACTGGGTCGTAATGCTCGTTTCCTGCAAGGTCCGGACAC
CAACCCGCACGCAGTTGAAGCTATCCGCCAGGGTCTGAAGGCGGAGACCCGTTTCACC
ATTGATATCCTGAACTACCGCAAGGACGGCTCCGCTTTCGTTAACCGTCTGCGTATCCGTC
CTATCTATGATCCGGAAGGTAACCTGATGTTCTTCGCGGGCGCACAGAACCCGGTTGCAG
AAGCAGCAGCTAAAGAAGCGGCAGCCAAGGAGGCTGCTGCAAAAGCGACTCCAGTTCG
CCGTCAGCAAAGCACCACTGGCCAGCTGCAGTCCAGCGAATCCACCAGCACCGCCAA
CGACCCAGCAACTTCTGAACTGCTGGGCCTGATCGGTGTTGTTATTTCCGACGTCGATGC
TCTGGTTGGTCTGACCTCTAGCCCGATCAGCGTTATCGGTGTTGGTTCCGGTAGCGCTAG
CACTGCGAACCCGGTTTCTTCCGACAGCAGCCCGATCGGTGGTCTGGTTTCCATCGGCT
CCGTTCCAGTTAACGTAGGTGGCGGTGGGTCTGGCGGTGGAGGTTCCCTCGAGCACCAC
CACCACCACCACTGA

(la)12-dsfbfpm49i (pET29b(+)_(la)12-dsfbfpm49i49i)

ATGTTGGCTCTGGCGCTGGCACTCGCTCTGGCGTTAGCACTCGCTCTCGCACTGGCACT
GGCACTGGCATTGGCTGGCGGTTCTGGCCGTCGTCACTACCGTGATCTGATTCGTAACAC
CCCGATGCCAGACACTCCGCAAGATATCGCCGATCTGCGTGCTCTGCTGGACGAAGAC
GAGGCCGAAATGAGCGTTGTTTTTTCTGACCCGTCTCAGCCGGACAACCCGATCATCTAC
GTTTCCGACGCGTTCCTGGTACAGACTGGCTACACCCTGGAAGAAGTACTGGGTCGTAAT
GCTCGTTTCCTGCAAGGTCCGGACACCAACCCGCACGCAGTTGAAGCTATCCGCCAGG
GTCTGAAGGCGGAGACCCGTTTCACCATTGATATCCTGAACTACCGCAAGGACGGCTCC
GCTTTCGTTAACCGTCTGCGTATCCGTCCTATCTATGATCCGGAAGGTAACCTGATGTTCTT
CGCGGGCGCACAGAACCCGGTTCTCGAGCACCACCACCACCACCACTGA

dsfbfpm49i-(la)12-dsfbfpm49i (pET-29b(+)_dsfbfpm49i-(la)12-dsfbfpm49i)

ATGCGTCGTCACTACCGTGATCTGATTCGTAACACCCCGATGCCAGACACTCCGCAAGAT
ATCGCCGATCTGCGTGCTCTGCTGGACGAAGACGAGGCCGAAATGAGCGTTGTTTTTTCT
GACCCGTCTCAGCCGGACAACCCGATCATCTACGTTTCCGACGCGTTCCTGGTACAGAC
TGGCTACACCCTGGAAGAAGTACTGGGTCGTAATGCTCGTTTCCTGCAAGGTCCGGACAC
CAACCCGCACGCAGTTGAAGCTATCCGCCAGGGTCTGAAGGCGGAGACCCGTTTCACC
ATTGATATCCTGAACTACCGCAAGGACGGCTCCGCTTTCGTTAACCGTCTGCGTATCCGTC
CTATCTATGATCCGGAAGGTAACCTGATGTTCTTCGCGGGCGCACAGAACCCGGTTGGCG
GTTCTGGCTTGGCTCTGGCGCTGGCACTCGCTCTGGCGTTAGCACTCGCTCTCGCACTG
GCACTGGCACTGGCATTGGCTGGCGGTTCTGGCCGTCGTCACTACCGTGATCTGATTCGT
AACACCCCGATGCCAGACACTCCGCAAGATATCGCCGATCTGCGTGCTCTGCTGGACGA
AGACGAGGCCGAAATGAGCGTTGTTTTTTCTGACCCGTCTCAGCCGGACAACCCGATCAT
CTACGTTTCCGACGCGTTCCTGGTACAGACTGGCTACACCCTGGAAGAAGTACTGGGTCG
TAATGCTCGTTTCCTGCAAGGTCCGGACACCAACCCGCACGCAGTTGAAGCTATCCGCC
AGGGTCTGAAGGCGGAGACCCGTTTCACCATTGATATCCTGAACTACCGCAAGGACGGC
TCCGCTTTCGTTAACCGTCTGCGTATCCGTCCTATCTATGATCCGGAAGGTAACCTGATGTT
CTTCGCGGGCGCACAGAACCCGGTTCTCGAGCACCACCACCACCACCACTGA

6.3 List of primers

Table 41: Primers used in this work

Primers used for cloning		
Primer	Sequence	T_a [°C][a]
plysu020	GGAGATATACATATGACTCCAGTTCGCCGTCAG	68
plysu021	GTGGTGGTGCTCGAGTACGTTAACTGGAACGGAGCC	67
plysu022	GTTCCAGTTAACGTACTCGAGCACCACCAC	63
plysu023	CGGCGAACTGGAGTCATATGTATATCTCCTTCTTAAAGTTAAAC	59
plysu024	CCGCAGCTAAAGCCGAAGTCGGTCCGGC	63
plysu025	GCTGCTGCTTCTGCGTCTTCGTCGCTGCC	63
plysu026	GGCAGCGACGAAGACGCAGAAGCAGCAGCTAAAGAAG	66
plysu027	CAGCGCCGGACCGACTTCGGCTTTAGCTGCGGCTTCTT	69
plysu031	GCTGCTGCTTCTGCGCCGTCCAGCACC	64
plysu032	GTGGTGCTGGACGGCGCAGAAGCAGCAGCTAAAGAAG	66
plysu035	GCTGCTGCTTCTGCACCGTCCAGAACCACG	65
plysu036	GTGGTTCTGGACGGTGCAGAAGCAGCAGCTAAAGAAG	66
plysu039	GCTGCTGCTTCTGCAACCGGGTTCTGTGC	62
plysu040	GCACAGAACCCGGTTGCAGAAGCAGCAGCTAAAGAAG	66
plysu042	GAGATCCGGCTGCTAAC	62
plysu043	CAGCTTCCTTTCGGGC	64
plysu045	CAGCGCCGGACCGACTTCGGCTTTAGCTGCGG	60
plysu046	CAGACTGCAGTTGGTGCGCTCGAGCACCACCAC	63
plysu047	GTGGTGGTGCTCGAGCGCACCAACTGCAGTCTG	67
plysu048	GAAAGCTATTGGTACTTTTCTCGAGCACCACCAC	63
plysu049	GTGGTGGTGCTCGAGAAAAGTACCAATAGCTTTCTGACACAG	65
plysu050	CGGCTTCTTTAGCGGCGGCCTCCTTTGCAGCAGCTTCAGCTA CGTTAACTGGAACGGAG	61
plysu051	GCTGCGGCTTCTTTAGCG	67
plysu052	CTGCAAAGGAGGCCGCCGCTAAAGAAGCCGCAGCTAAAGCC GAAGTCGGTCCGGC	63
plysu053	CTGCAAAGGAGGCCGCCGCTAAAGAAGCCGCAGCTAAAGCC GAAAAAAGCTTTGTGATTACTGACC	62
plysu054	CTGCAAAGGAGGCCGCCGCTAAAGAAGCCGCAGCTAAAGCC GAAAAAAGCTTCGTTATCACCG	62
plysu055	CTGCAAAGGAGGCCGCCGCTAAAGAAGCCGCAGCTAAAGCC CGTCGTCACTACCGTG	62
plysu056	GGTGGCGGTGGGTCTGGCGGTGGAGGTTCCCTCGAGCACCA CCAC	63
plysu057	GGAACCTCCACCGCCAGACCCACCGCCACCTACGTTAACTG GAACGGAGCC	67
plysu058	CTCGAGGGAACCTCCACCGCCAGACCCACCGCCACCCGCA CCAACTGCAGTCTG	67
plysu059	CTCGAGGGAACCTCCACCGCCAGACCCACCGCCACCAAAAG TACCAATAGCTTTCTGACACAG	65

plysu060	CGGCTTCTTTAGCGGCGGCCTCCTTTGCAGCAGCTTCAGCCG CACCAACTGCAGTC	64
plysu061	CGGCTTCTTTAGCGGCGGCCTCCTTTGCAGCAGCTTCAGCAA AAGTACCAATAGCTTTCTGAC	60
plysu062	GGAGATATACATATGTCTAACGGTAACGGTAACGTGTG	67
plysu063	CCGTTACCGTTAGACATATGTATATCTCCTTCTTAAAGTTAAAC	59
plysu064	GGAGATATACATATGGCAGTCTGTCCGACTGG	68
plysu065	GTCGGACAGACTGCCATATGTATATCTCCTTCTTAAAGTTAAAC	61
plysu066[b]	CTCGCACTGGCACTGGCACTGGCATTGGCTGGCGGTTCTGGC GAAAAAAGCTTCGTTATCAC	57
plysu067[b]	AGCGAGTGCTAACGCCAGAGCGAGTGCCAGCGCCAGAGCCA ACATATGTATATCTCCTTCTTAAAG	57 or 56
plysu068[b]	CTCGCACTGGCACTGGCACTGGCATTGGCTGGCGGTTCTGGC CGTCGTCACTACCG	56
plysu069	TGGACGGTGGCGGTTCTGGCTTGGCTCTGGCGCTG	66
plysu070	CCAGAGCCAAGCCAGAACCGCCACCGTCCAGAACCACG	65
plysu071	ACCCGGTTGGCGGTTCTGGCTTGGCTCTGGCGCTG	66
plysu072	CCAGAGCCAAGCCAGAACCGCCAACCGGGTTCTGTGC	62
Primers used for colony PCR and/or sequencing		
Primer	Sequence	T_a [°C][c]
T7probis	TCCCGCGAAATTAATACG	46
T7terbis	AACCCCTCAAGACCCG	46
pET-up	ATGCGTCCGGCGTAG	n.s.[d]

[a] Q5 High-Fidelity DNA Polymerase was used, annealing temperature was calculated according to NEB Tm calculator[203]

[b] Primers were used for Q5® Site-Directed Mutagenesis

[c] Opti Taq DNA Polymerase was used for Colony PCR and therefore, the T_a was set 5 °C below the T_m of the primer with the lowest T_m

[d] Primer was used only for sequencing

6.4 Molecular cloning – specifications

The detailed procedures for cloning are described in chapters 5.12 and 5.13.

Table 42: Specifications for cloning

Construct	Backbone template	Primer *fwd*	Primer *rev*	Fragment length [bp]	Insert template	Primer *fwd*	Primer *rev*	Fragment length [bp]
pET-29b(+)_supernova-rl1-mhgf1	pET-29b(+)_supernova	plysu022	plysu025	5974	ptwistamphighcopy_rl1-hgf1-rl2	plysu026	plysu021	345
pET-29b(+)_minisogq103v-rl1-mhgf1	pET-29b(+)_minisogq103v	plysu022	plysu031	5581	ptwistamphighcopy_rl1-hgf1-rl2	plysu032	plysu021	345
pET-29b(+)_minisogq103v-rl1-hfb1	pET-29b(+)_minisogq103v	plysu046	plysu031	5584	ptwistamphighcopy_rl1-hfb1-rl2	plysu032	plysu047	306
pET-29b(+)_minisogq103v-rl1-hfb2	pET-29b(+)_minisogq103v	plysu048	plysu031	5585	ptwistamphighcopy_rl1-hfb2-rl2	plysu032	plysu049	294
pET-29b(+)_minisogq103v-rl1-mhgf1-rl2-minisogq103v	pET-29b(+)_minisogq103v-rl1-mhgf1	plysu042	plysu050	5882	pET-29b(+)_minisogq103v	plysu053	plysu043	417
pET-29b(+)_mhgf1-rl2-minisogq103v	pET-29b(+)_minisogq103v	plysu053	plysu023	5607	ptwistamphighcopy_rl1-hgf1-rl2	plysu020	plysu051	323
pET-29b(+)_minisogq103v-rl1-mhgf1-flhis	pET-29b(+)_minisogq103v	plysu056	plysu031	5596	ptwistamphighcopy_rl1-hgf1-rl2	plysu032	plysu057	360

pET-29b(+)_sopp3-rl1-mhgf1	pET-29b(+)_sopp3	plysu022	plysu035	5581	ptwistamphighcopy_rl1-hgf1-rl2	plysu036	plysu021	345
pET-29b(+)_sopp3-rl1-hfb1	pET-29b(+)_sopp3	plysu046	plysu035	5584	ptwistamphighcopy_rl1-hfb1-rl2	plysu036	plysu047	306
pET-29b(+)_sopp3-rl1-hfb2	pET-29b(+)_sopp3	plysu048	plysu035	5585	ptwistamphighcopy_rl1-hfb2-rl2	plysu036	plysu049	294
pET-29b(+)_sopp3-rl1-mhgf1-rl2-sopp3	pET-29b(+)_sopp3-rl1-mhgf1	plysu042	plysu050	5882	pET-29b(+)_sopp3	plysu054	plysu043	417
pET-29b(+)_sopp3-rl1-hfb1-rl2-sopp3	pET-29b(+)_sopp3-rl1-hfb1	plysu042	plysu060	5843	pET-29b(+)_sopp3	plysu054	plysu043	417
pET-29b(+)_sopp3-rl1-hfb2-rl2-sopp3	pET-29b(+)_sopp3-rl1-hfb2	plysu042	plysu061	5831	pET-29b(+)_sopp3	plysu054	plysu043	417
pET-29b(+)_mhgf1-rl2-sopp3	pET-29b(+)_sopp3	plysu054	plysu023	5607	ptwistamphighcopy_rl1-hgf1-rl2	plysu020	plysu051	323
pET-29b(+)_hfb1-rl2-sopp3	pET-29b(+)_sopp3	plysu054	plysu063	5607	ptwistamphighcopy_rl1-hfb1-rl2	plysu062	plysu051	284
pET-29b(+)_hfb2-rl2-sopp3	pET-29b(+)_sopp3	plysu054	plysu065	5607	ptwistamphighcopy_rl1-hfb2-rl2	plysu064	plysu051	272
pET-29b(+)_sopp3-rl1-mhgf1-flhis	pET-29b(+)_sopp3	plysu056	plysu035	5596	ptwistamphighcopy_rl1-hgf1-rl2	plysu036	plysu057	360
pET-29b(+)_(la)12-sopp3[a]	pET-29b(+)_SOPP3	plysu066	plysu067	5636	n.s.	n.s.	n.s.	n.s.
pET-29b(+)_sopp3-(la)12-sopp3	pET-29b(+)_SOPP3	plysu042	plysu070	5549	pET-29b(+)_(la)12-sopp3	plysu069	plysu043	480
pET-29b(+)_dsfbfpm49i-rl1-mhgf1	pET-29b(+)_dsfbfpm49i	plysu022	plysu039	5677	ptwistamphighcopy_rl1-hgf1-rl2	plysu040	plysu021	345
pET-29b(+)_dsfbfpm49i-rl1-hfb1	pET-29b(+)_dsfbfpm49i	plysu046	plysu039	5680	ptwistamphighcopy_rl1-hfb1-rl2	plysu040	plysu047	306
pET-29b(+)_dsfbfpm49i-rl1-hfb2	pET-29b(+)_dsfbfpm49i	plysu048	plysu039	5681	ptwistamphighcopy_rl1-hfb2-rl2	plysu040	plysu049	294

pET-29b(+)_dsfbfpm49i-rl1-mhgf1-rl2-dsfbfpm49i	pET-29b(+)_dsfbfpm49i-rl1-mhgf1	plysu042	plysu050	5978	pET-29b(+)_dsfbfpm49i	plysu055	plysu043	513
pET-29b(+)_dsfbfpm49i-rl1-hfb1-rl2-dsfbfpm49i	pET-29b(+)_dsfbfpm49i-rl1-hfb1	plysu042	plysu060	5939	pET-29b(+)_dsfbfpm49i	plysu055	plysu043	513
pET-29b(+)_dsfbfpm49i-rl1-hfb2-rl2-dsfbfpm49i	pET-29b(+)_dsfbfpm49i-rl1-hfb2	plysu042	plysu061	5927	pET-29b(+)_dsfbfpm49i	plysu055	plysu043	513
pET-29b(+)_mhgf1-rl2-dsfbfpm49i	pET-29b(+)_dsfbfpm49i	plysu055	plysu023	5703	ptwistamphighcopy_rl1-hgf1-rl2	plysu020	plysu051	323
pET-29b(+)_hfb1-rl2-dsfbfpm49i	pET-29b(+)_dsfbfpm49i	plysu055	plysu063	5703	ptwistamphighcopy_rl1-hfb1-rl2	plysu062	plysu051	284
pET-29b(+)_hfb2-rl2-dsfbfpm49i	pET-29b(+)_dsfbfpm49i	plysu055	plysu065	5703	ptwistamphighcopy_rl1-hfb2-rl2	plysu064	plysu051	272
pET-29b(+)_dsfbfpm49i-rl1-mhgf1-flhis	pET-29b(+)_dsfbfpm49i	plysu056	plysu039	5692	ptwistamphighcopy_rl1-hgf1-rl2	plysu040	plysu057	360
pET-29b(+)_(la)12-dsfbfpm49i49[a]	pET-29b(+)_DsfbfpM49I	plysu068	plysu067	5732	n.s.	n.s.	n.s.	n.s.
pET-29b(+)_dsfbfpm49i-(la)12-dsfbfpm49i	pET-29b(+)_DsfbfpM49I	plysu042	plysu072	5645	pET-29b(+)_(la)12-dsfbfpm49i49	plysu071	plysu043	576

[a] Generated by Q5® site-directed mutagenesis

6.5 Light intensity measurement

For the comparability of light intensities, light intensities of all used light sources were measured (Thorlabs Interactive Digital Source Meter PM100D, Model S3C10; S/N 120807; Sens 2.07289 mV/W) (Figure 109). A shortpass filter was used to compare the blue light proportion of the light sources, which is responsible for the excitation of the flavin-containing photosensitizer proteins (Knight Optical dichroic shortpass filter 490 nm, 50x50 mm, ItemCode: 490FDS50).

a

Eurolite IP FL-30 SMD blue, IP65	
Distance [cm]	Intensity [mW/cm²]
5	29.0
10	16.4
20	7.0
30	4.0
50	1.9
75	0.9

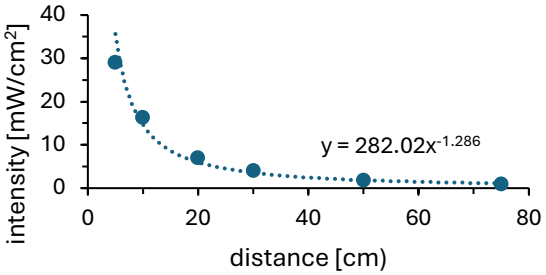

b

Megaman Helix daylight lamp	
Distance [cm]	Intensity [mW/cm²]
5	1.7
10	1.2
11.5	1.0
15	0.9
20	0.7
25	0.7
30	0.6

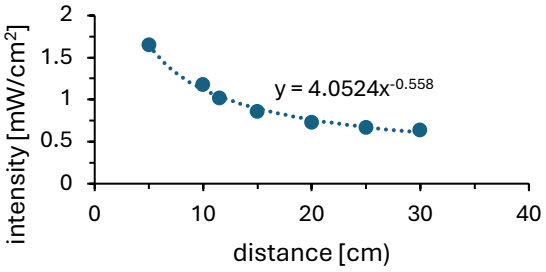

c

SciRobotics Pickolo	
Distance [cm]	Intensity [mW/cm²]
0	0.3

Figure 109|Light intensity of the different light sources at different distances. a, Eurolite IP FL-30 SMD blue, IP65 (blue light). **b**, Megaman Helix daylight lamp (white light). c, SciRobotics Pickolo (white light).

6.6 ABTS assay

Different control experiments were conducted to analyze which factors could interfere with the ABTS assay (Table 43).

Table 43: Control experiments for the ABTS assay

Control experiment	Description
Glycerol control	Glycerol is present in the PSP stocks. Therefore, approx. 25 % (v/v) glycerol was mixed to H_2O_2 before the addition of the working solution. The signal was compared to a control without glycerol. The addition of glycerol did not interfere with the assay.
Imidazole control	Imidazole is a component of the elution buffer for IMAC. Therefore, imidazole (200 mM) was mixed to H_2O_2 before the addition of the working solution. Imidazole did not interfere with the assay.
BSA protein control	BSA was used to determine the influence of proteins in general. Thus, BSA (0.65 mg/mL) was used instead of the PSP solution. BSA did not interfere with the assay.
Further purification of the PSPs	Another purification step for the PSPs was conducted. After IMAC, the isolated PSP solution was applied to a SEPHADEX column, to remove further impurities. There was no change in the assay outcome.
The amount of HRP and ABTS was increased	The working solution was changed**.** The activity of HRP was increased to 24 U/mL and the concentration of ABTS was increased to 4 mM. There was no change in the assay outcome.
H_2O_2 was added to the assay before and after illumination	The influence of the order of addition of the assay components was analyzed. First, H_2O_2 was pipetted to the PSP solution before the addition of the working solution and illumination. Second, H_2O_2 was added at the end, after the protein reacted with the working solution during illumination. The addition of H_2O_2 in the end led to an increase in fluorescence signal (the formed $ABTS^{\bullet+}$ could be detected). This led to the conclusion that most probably a photochemical process of the PSP interferes with the detection of $ABTS^{\bullet+}$.

6.7 FMN photobleaching experiment

To find out if Lumichrome was a degradation product during FMN photobleaching, there was conducted an experiment, where highly concentrated FMN was illuminated with the same light intensity for a long time (approx. 50 mM (34 mg/mL) FMN in D_2O, 72 h, blue light 16.4 mW/cm^2). After 72 h the color changed from orange to brown, which was partially insoluble in D_2O. An NMR was measured and compared to non-illuminated FMN. The FMN was detectable in traces and the signals were broadened, indicating degradation. Moreover, a sample was diluted and analyzed by HPLC-MS. A second peak was visible next to the FMN peak. The mass corresponded to Lumichrome (Figure 110).

a

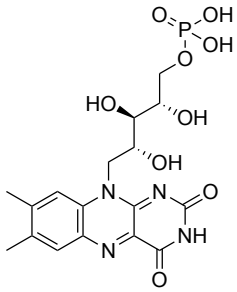

Flavin mononucleotide (FMN)
exact mass: 456.105 g/mol

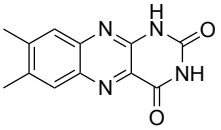

Lumichrome
exact mass: 242.080 g/mol

b

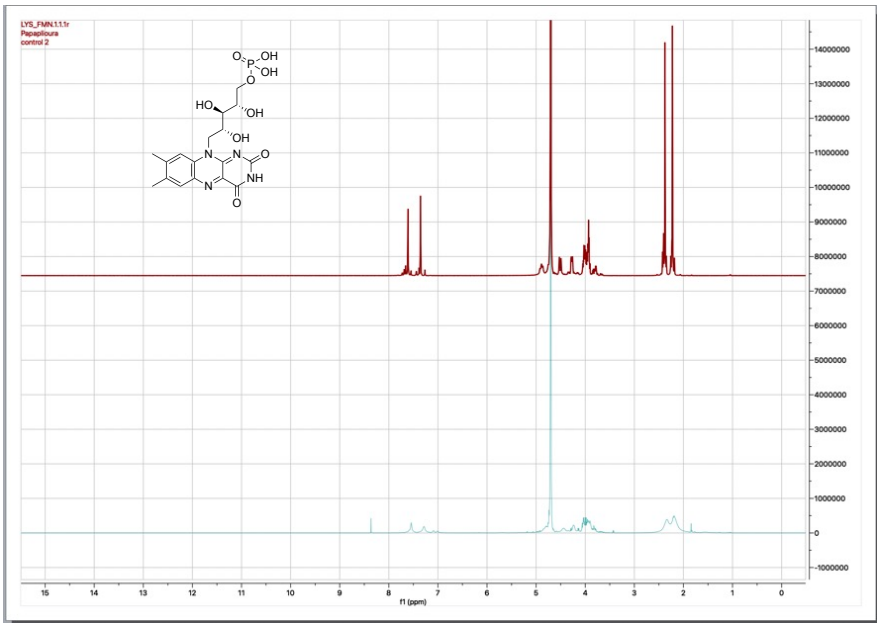

c

Control

After 72 h illumination

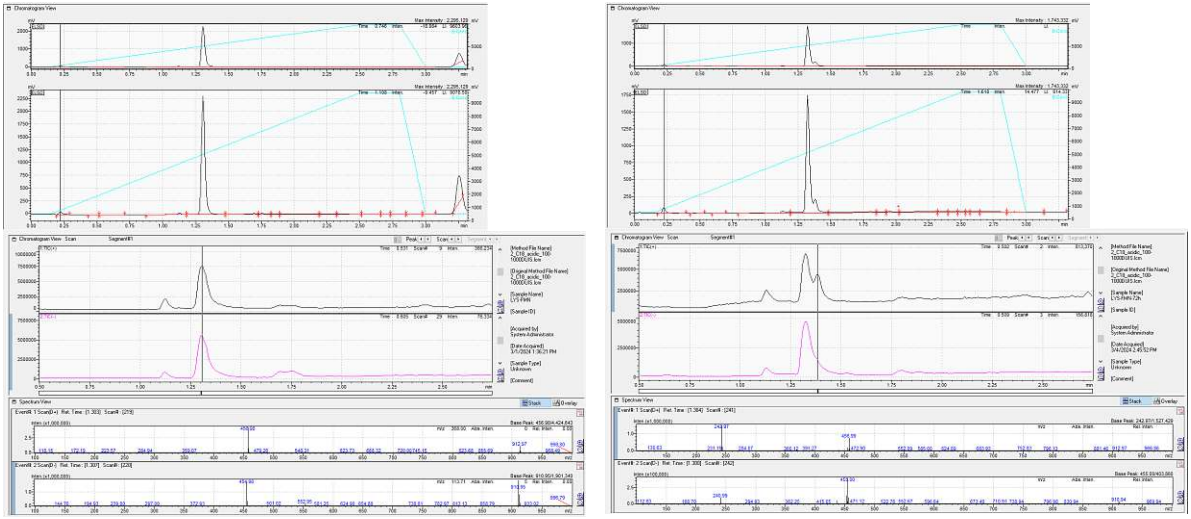

Figure 110|Photobleaching of FMN. a, Structural formulas, and exact masses of FMN and Lumichrome. **b**, ^{1}H NMR (200 MHz, $CDCl_3$) spectra of the FMN control (red) and the photobleached FMN after 72 h illumination (blue). **c**, HPLC-MS (Shimadzu Nexera X2 UHPLC system) traces of the FMN control (left) and the photobleached FMN after 72 h illumination (right).

6.8 Supplementary Figures

6.8.1 Fluorescence spectra

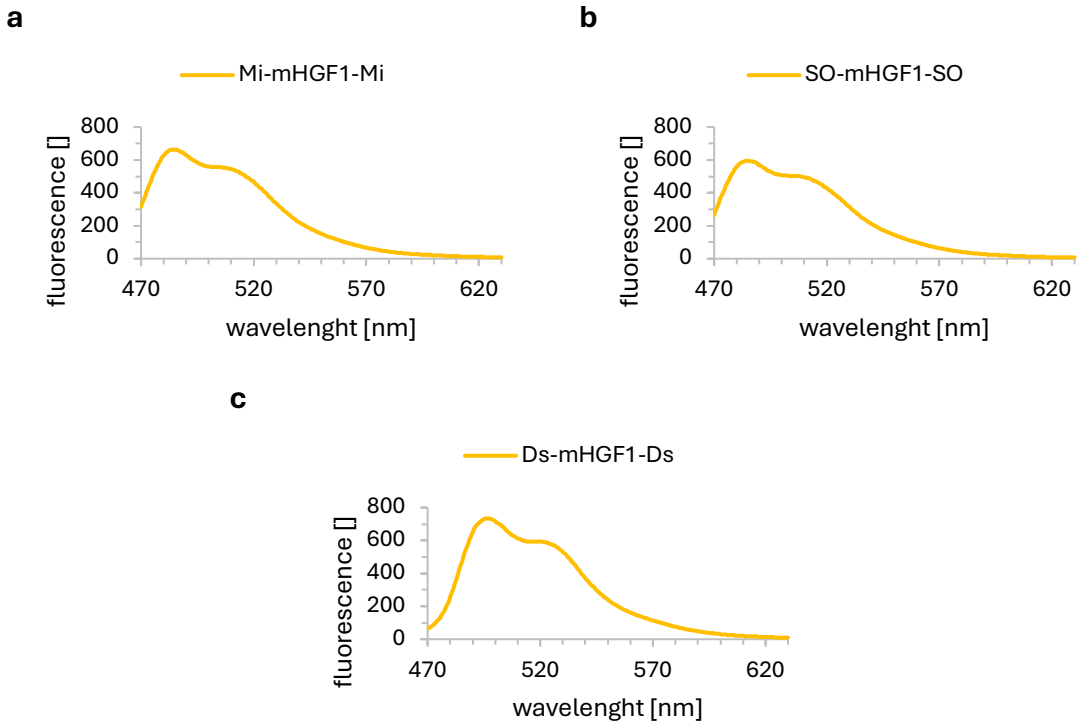

Figure 111|Fluorescence emission spectra of the fusion proteins with the conformation LOV-linker-mHGF1-linker-LOV-6xHis. 2 mM protein solutions were prepared in 50 mM NaPi buffer (pH 7.2) in a final volume of 100 µL. As a blank, the buffer was measured. Mi = MiniSOGQ103V, SO = SOPP3, Ds = DsFbFpM49I. **a**, Fluorescence spectrum of the fusion protein MiniSOGQ103V-mHGF1-MiniSOGQ103V. **b**, Fluorescence spectrum of the fusion protein SOPP3-mHGF1-SOPP3. **c**, Fluorescence spectrum of the fusion protein DsFbFpM49I-mHGF1-DsFbFpM49I.

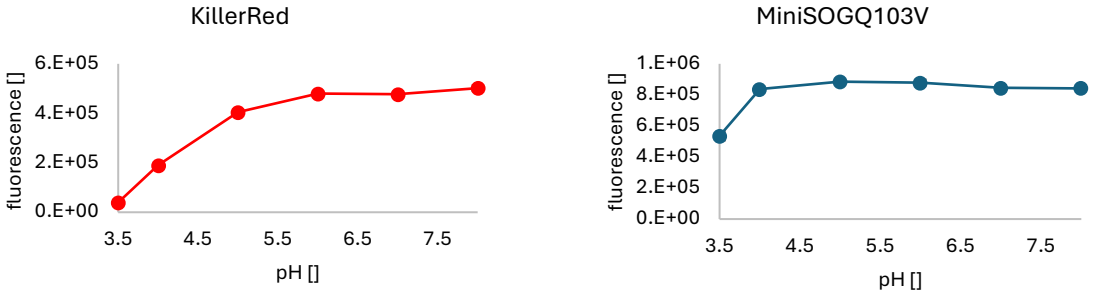

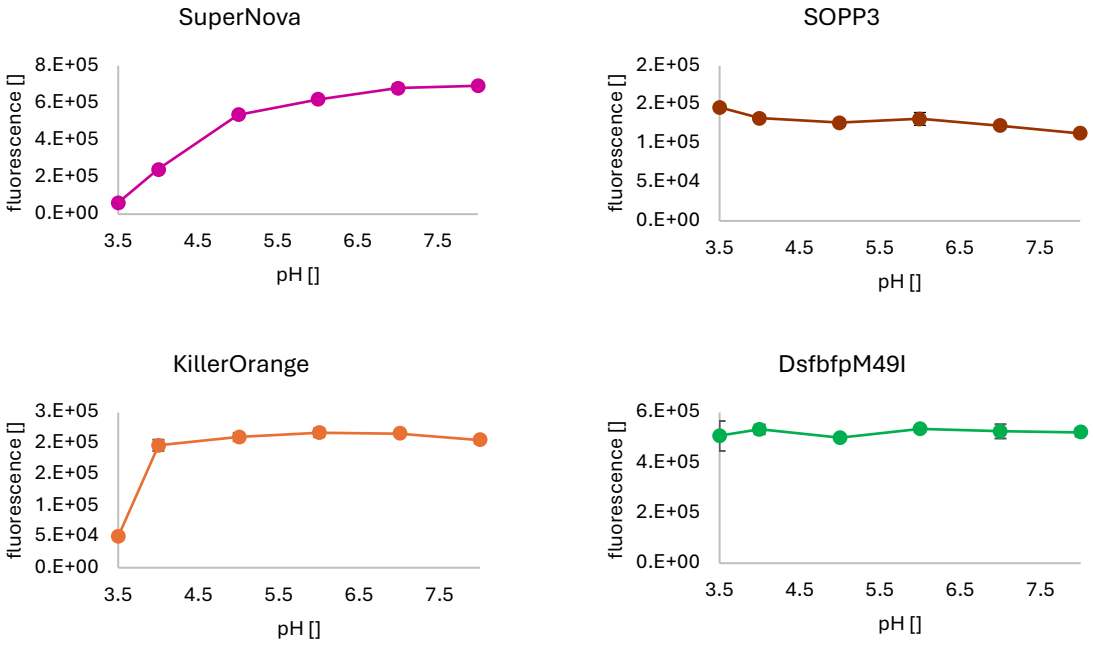

Figure 112| Fluorescence intensities of the PSPs after incubation for 30 min at different pH values. Phosphate-citrate buffers with the pH values 3.5-8 were prepared. Protein solutions were adjusted to an absorption of 0.02 in 100 µL in the different buffers. After incubation for 30 min in the respective buffer, fluorescence intensities of KillerRed and Supernova were measured at ex 540 nm / em 605 nm, KillerOrange at ex 500 nm / em 550 nm, and LOV proteins at ex 440 nm / em 490 nm, values are mean ± σ for n = 3.

6.8.2 Gel Electrophoresis

a

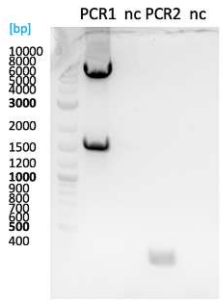

b

PCR	Expected length [bp]
1 backbone	5974
2 insert	345

Figure 113|Generation of insert and backbone for supernova-rl1-mhgf1. Gel electrophoresis of the PCR reactions (**a**) and expected lengths of the generated fragments (**b**) are depicted. Negative control (nc).

a

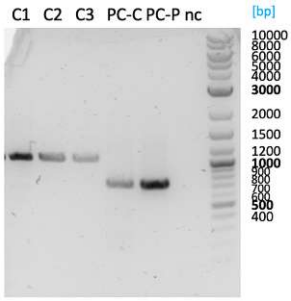

b

PCR	Expected length [bp]
C1-C2	1038
PC (supernova)	708

Figure 114|Colony PCR of supernova-rl1-mhgf1. Gel electrophoresis of the PCR reactions (**a**) and expected lengths of the generated fragments (**b**) are depicted. Colony (C), positive control colony (PC-C), positive control plasmid (PC-P), negative control (nc).

a

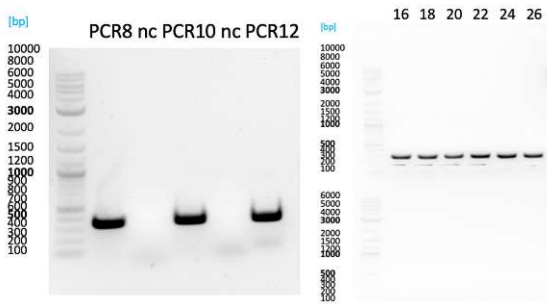

b

PCR	Expected length [bp]
8 (minisogq103v-rl1-mhgf1)	345
10 (sopp3-rl1-mhgf1)	345
12 (dsfbfpm49i-rl1-mhgf1)	345
15 minisogq103v-rl1-hfb1	306
17 sopp3-rl1-hfb1	306
19 dsfbfpm49i-rl1-hfb1	306
21 minisogq103v-rl1-hfb2	294
23 sopp3-rl1-hfb2	294
25 dsfbfpm49i-rl1-hfb2	294

Figure 115|Generation of inserts for LOV-rl1-hydrophobin. Gel electrophoresis of the PCR reactions (**a**) and expected lengths of the generated fragments (**b**) are depicted. Negative control (nc).

a

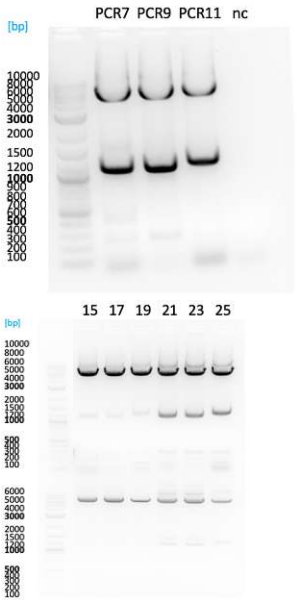

b

PCR	Expected length [bp]
7 (minisogq103v-rl1-mhgf1)	5581
9 (sopp3-rl1-mhgf1)	5581
11 (dsfbfpm49i-rl1-mhgf1)	5677
15 minisogq103v-rl1-hfb1	5584
17 sopp3-rl1-hfb1	5584
19 dsfbfpm49i-rl1-hfb1	5680
21 minisogq103v-rl1-hfb2	5585
23 sopp3-rl1-hfb2	5585
25 dsfbfpm49i-rl1-hfb2	5681

Figure 116|Generation of backbones for LOV-rl1-hydrophobin. Gel electrophoresis of the PCR reactions (**a**) and expected lengths of the generated fragments (**b**) are depicted. Negative control (nc).

a

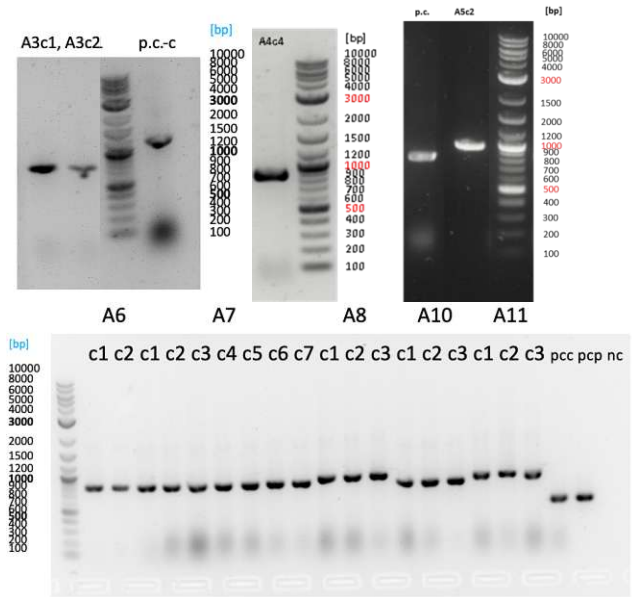

b

PCR	Expected length [bp]
A3 (minisogq103v-rl1-mhgf1)	865
A4 (sopp3-rl1-mhgf1)	865
A5 (dsfbfpm49i-rl1-mhgf1)	961
p.c.-c…positive control colony (supernova-rl1-mhgf1)	1258
A6 (minisogq103v-rl1- hfb1)	826
A7 (sopp3-rl1-hfb1)	826
A8 (dsfbfpm49i-rl1-hfb1)	922
A10 (sopp3-rl1-hfb2)	814
A11 (dsfbfpm49i-rl1- hfb2)	910
pcc (minisogq103v)	550
pcp (minisogq103v)	550

Figure 117|Colony PCR of LOV-rl1-hydrophobin. Gel electrophoresis of the PCR reactions (**a**) and expected lengths of the generated fragments (**b**) are depicted. Colony (c), positive control colony (pcc), positive control plasmid (pcp), negative control (nc). A9 (minisogq103v-rl1-hfb2) was not verified by colony PCR, but only by sequencing.

a **b**

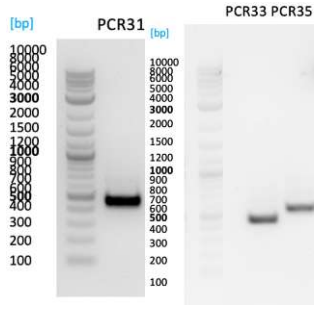

PCR	Expected length [bp]
31 (minisogq103v-rl1-mhgf1-rl2-minisogq103v)	417
33 (sopp3-rl1-mhgf1-rl2-sopp3)	417
35 (dsfbfpm49i-rl1-mhgf1-rl2-dsfbfpm49i)	513

Figure 118|Generation of inserts for LOV-rl1-hydrophobin-rl2-LOV. Gel electrophoresis of the PCR reactions (**a**) and expected lengths of the generated fragments (**b**) are depicted. Negative control (nc).

a

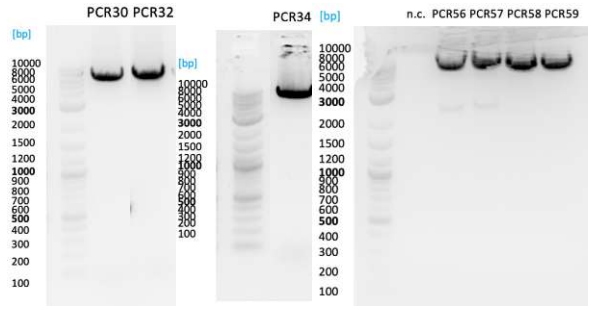

b

PCR	Expected length [bp]
30 (minisogq103v-rl1-mhgf1-rl2-minisogq103v)	5882
32 (sopp3-rl1-mhgf1-rl2-sopp3)	5882
34 (dsfbfpm49i-rl1-mhgf1-rl2-dsfbfpm49i)	5978
56 (sopp3-rl1-hfb1-rl2-sopp3)	5843
57 (dsfbfpm49i-rl1-hfb1-rl2-dsfbfpm49i)	5939
58 (sopp3-rl1-hfb2-rl2-sopp3)	5831
59 (dsfbfpm49i-rl1-hfb2-rl2-dsfbfpm49i)	5927

Figure 119|Generation of backbones for LOV-rl1-hydrophobin-rl2-LOV. Gel electrophoresis of the PCR reactions (**a**) and expected lengths of the generated fragments (**b**) are depicted. Negative control (nc).

a

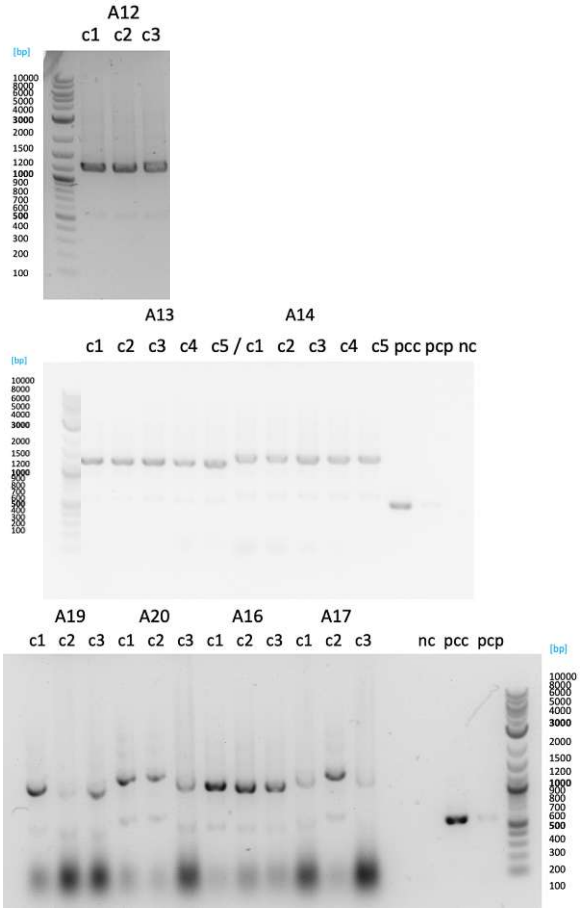

b

PCR	Expected length [bp]
A12 (minisogq103v-rl1-mhgf1-rl2-minisogq103v)	1231
A13 (sopp3-rl1-mhgf1-rl2-sopp3)	1231
A14 (dsfbfpm49i-rl1-mhgf1-rl2-dsfbfpm49i)	1423
A16 (sopp3-rl1-hfb1-rl2-sopp3)	1192
A17 (dsfbfpm49i-rl1-hfb1-rl2-dsfbfpm49i)	1384
A19 (sopp3-rl1-hfb2-rl2-sopp3)	1180
A20 (dsfbfpm49i-rl1-hfb2-rl2-dsfbfpm49i)	1372
pc (minisogq103v)	550

Figure 120|Colony PCR of LOV-rl1-hydrophobin-rl2-LOV. Gel electrophoresis of the PCR reactions (**a**) and expected lengths of the generated fragments (**b**) are depicted. Colony (c), positive control colony (pcc), positive control plasmid (pcp), negative control (nc).

a

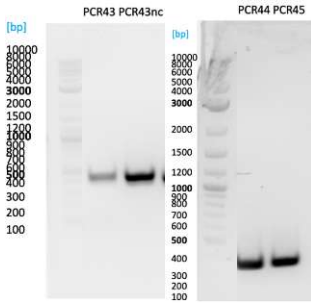

b

PCR	Expected length [bp]
43 (minisogq103v-rl1-mhgf1-flhis)	360
44 (sopp3-rl1-mhgf1-flhis)	360
45 (dsfbfpm49i-rl1-mhgf1-flhis)	360

Figure 121|Generation of inserts for LOV-rl1-mhgf1-flhis. Gel electrophoresis of the PCR reactions (**a**) and expected lengths of the generated fragments (**b**) are depicted. Negative control (nc).

a

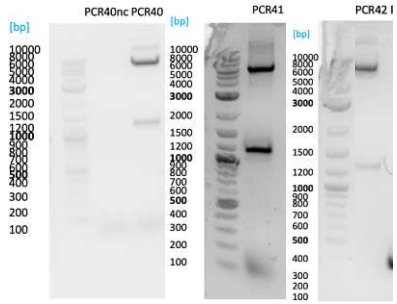

b

PCR	Expected length [bp]
40 (minisogq103v-rl1-mhgf1-flhis)	5596
41 (sopp3-rl1-mhgf1-flhis)	5596
42 (dsfbfpm49i-rl1-mhgf1-flhis)	5692

Figure 122|Generation of backbones for LOV-rl1-mhgf1-flhis. Gel electrophoresis of the PCR reactions (**a**) and expected lengths of the generated fragments (**b**) are depicted. Negative control (nc).

a

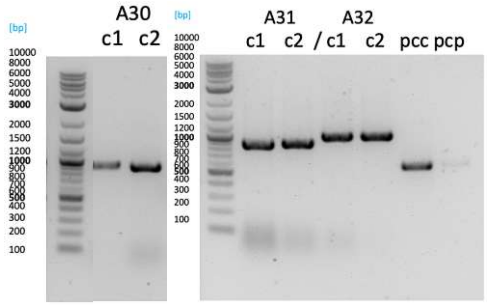

b

PCR	Expected length [bp]
A30 (minisogq103v-rl1-mhgf1-flhis)	895
A31 (sopp3-rl1-mhgf1-flhis)	895
A32 (dsfbfpm49i-rl1-mhgf1-flhis)	991
pc (miniSOGQ103V)	550

Figure 123|Colony PCR of LOV-rl1-mhgf1-flhis. Gel electrophoresis of the PCR reactions (**a**) and expected lengths of the generated fragments (**b**) are depicted. Colony (c), positive control colony (pcc), positive control plasmid (pcp), negative control (nc).

a

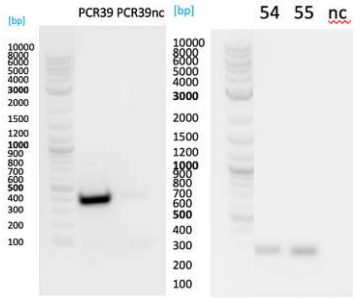

b

PCR	Expected length [bp]
39 (mhgf1-rl2-LOV)	323
54 (hfb1-rl2-LOV)	284
55 (hfb2-rl2-LOV)	272

Figure 124|Generation of inserts for hydrophobin-rl2-LOV. Gel electrophoresis of the PCR reactions (**a**) and expected lengths of the generated fragments (**b**) are depicted. Negative control (nc).

a

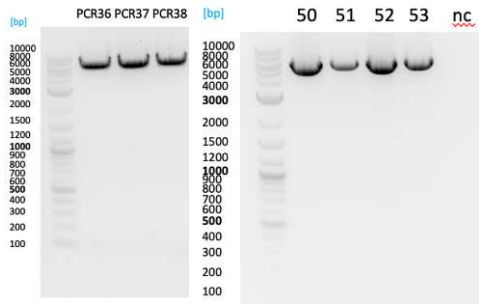

b

PCR	Expected length [bp]
36 (mhgf1-rl2-minisogq103v)	5607
37 (mhgf1-rl2-sopp3)	5607
38 (mhgf1-rl2-dsfbfpm49i)	5703
50 (hfb1-rl2-sopp3)	5607
51 (hfb1-rl2-dsfbfpm49i)	5703
52 (hfb2-rl2-sopp3)	5607
53 (hfb2-rl2-dsfbfpm49i)	5703

Figure 125|Generation of backbones for hydrophobin-rl2-LOV. Gel electrophoresis of the PCR reactions (**a**) and expected lengths of the generated fragments (**b**) are depicted. Negative control (nc).

a

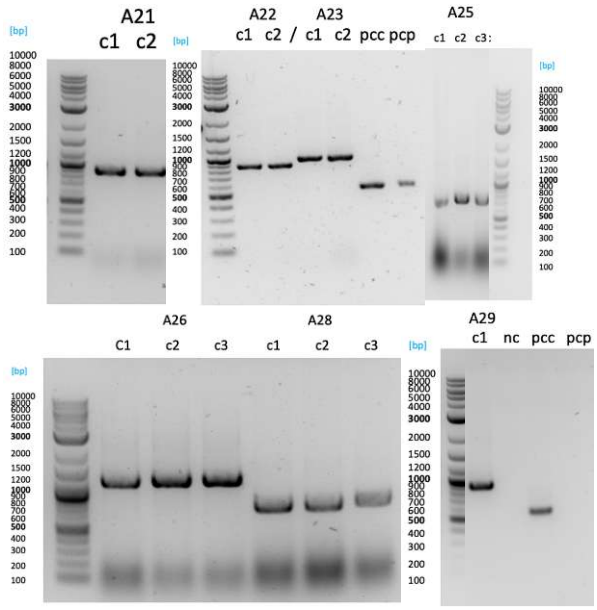

b

PCR	Expected length [bp]
A21 (mhgf1-rl2-minisogq103v)	865
A22 (mhgf1-rl2-sopp3)	865
A23 (mhgf1-rl2-dsfbfpm49i)	961
A25 (hfb1-rl2-sopp3)	826
A26 (hfb1-rl2-dsfbfpm49i)	922
A28 (hfb2-rl2-sopp3)	814
A29 (hfb2-rl2-dsfbfpm49i)	910
pc (miniSOGQ103V)	550

Figure 126|Colony PCR of hydrophobin-rl2-LOV. Gel electrophoresis of the PCR reactions (**a**) and expected lengths of the generated fragments (**b**) are depicted. Colony (c), positive control colony (pcc), positive control plasmid (pcp), negative control (nc).

a

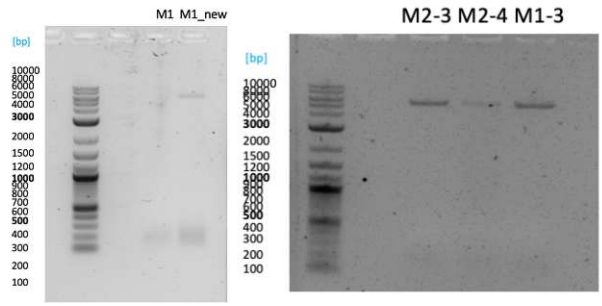

b

PCR	Expected length [bp]
M1 ((la)12-sopp3)	5636
M2 ((la)12-dsfbfpm49i)	5732

Figure 127|Q5® site-directed mutagenesis for generation of (la)12-LOV. Gel electrophoresis of the PCR reactions (**a**) and expected lengths of the generated fragments (**b**) are depicted. Negative control (nc).

a

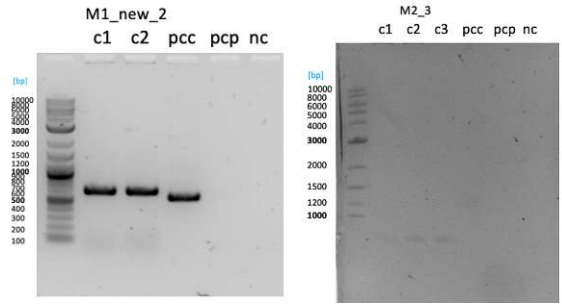

b

PCR	Expected length [bp]
M1 ((la)12-sopp3)	634
M2 ((la)12-dsfbfpm49i)	730
pc (minisogq103v)	550

Figure 128|Colony PCR of (la)12-LOV. Gel electrophoresis of the PCR reactions (**a**) and expected lengths of the generated fragments (**b**) are depicted. Colony (c), positive control colony (pcc), positive control plasmid (pcp), negative control (nc).

a

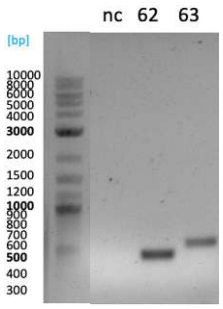

b

PCR	Expected length [bp]
62 (sopp3-(la)12-sopp3)	480
63 (dsfbfpm49i-(la)12-dsfbfpm49i)	576

Figure 129|Generation of inserts for LOV-(la)12-LOV. Gel electrophoresis of the PCR reactions (**a**) and expected lengths of the generated fragments (**b**) are depicted. Negative control (nc).

a

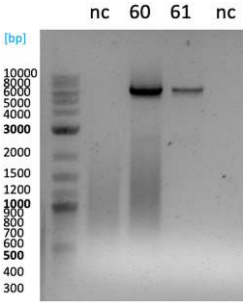

b

PCR	Expected length [bp]
60 (sopp3-(la)12-sopp3)	5549
61 (dsfbfpm49i-(la)12-dsfbfpm49i)	5645

Figure 130|Generation of backbones for LOV-(la)12-LOV. Gel electrophoresis of the PCR reactions (**a**) and expected lengths of the generated fragments (**b**) are depicted. Negative control (nc).

a

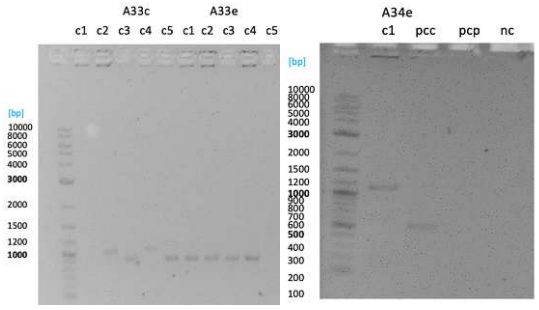

b

PCR	Expected length [bp]
A33 (sopp3-(la)12-sopp3)	961
A34 (dsfbfpm49i-(la)12-dsfbfpm49i)	1153
pc (minisogq103v)	550

Figure 131|Colony PCR of LOV-(la)12-LOV. Gel electrophoresis of the PCR reactions (**a**) and expected lengths of the generated fragments (**b**) are depicted. Colony (c), positive control colony (pcc), positive control plasmid (pcp), negative control (nc).

6.8.3 WCA

Gold is classified as a hydrophilic material; however, it is relatively hydrophobic as hydrophilic proteins do not adsorb on gold surfaces efficiently. In a research by Zhao et al., hydrophobin HFB1 self-assembled on a gold surface enabling immobilization of a choline oxidase.[137] Therefore, during this work, WCA measurements were done after incubation of SPR gold sensor slides with the LOV protein SOPP3 and the fusion protein SOPP3-mHGF1. The purified protein (3 µM, 800 µL) was added onto a SPR gold sensor slide. The surface was incubated at room temperature for 0.5 h, washed with 25 mL buffer (50 mM NaPi), and dried with an argon stream. WCA measurements were performed in triplicates (Table 44). In accordance with WCA measurements on PE, the fusion protein SOPP3-mHGF1 adsorbed more efficiently to the gold surface than the original LOV protein SOPP3.

Table 44: WCA of the gold surface after incubation with protein solutions[a]

	Control Buffer	SO	SO-mHGF1
SPR gold sensor slide	65.7 ± 0.8 °	62.4 ± 0.3 °	58.4 ± 0.9 °

[a] WCA measurements were performed on different areas of the sample surfaces, values are mean ± σ for n = 3. SPR gold sensor slides were used, 800 µl of 3 µM protein sample was added and incubated at room temperature for 0.5 h, then washed with 25 mL 50 mM NaPi buffer and dried with an argon stream.

6.8.4 ATR-FTIR spectra

a

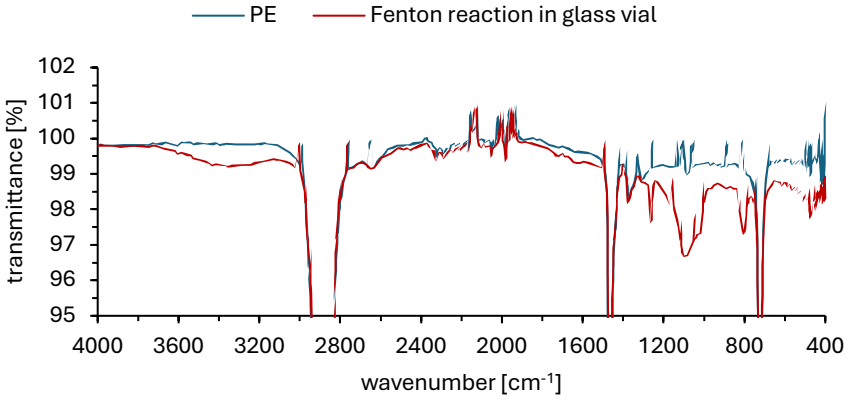

b

Functional group	Mode of vibration	Wavenumber [cm^{-1}]
Silanol	Si-O-H	<3000
Methylsilyl	Si-CH3	1260
Siloxane	Si-O-Si	1100

Figure 132|ATR-FTIR analysis of PE after Fenton in a glass vial. 10 mM Fe^{2+} and 15 % H_2O_2 were used at pH 3, exchanging solution each hour for 18 h in total. **a**, FTIR spectrum before and after incubation in Fenton reaction. **b**, Characteristic IR-bands for functional groups containing Si.

a

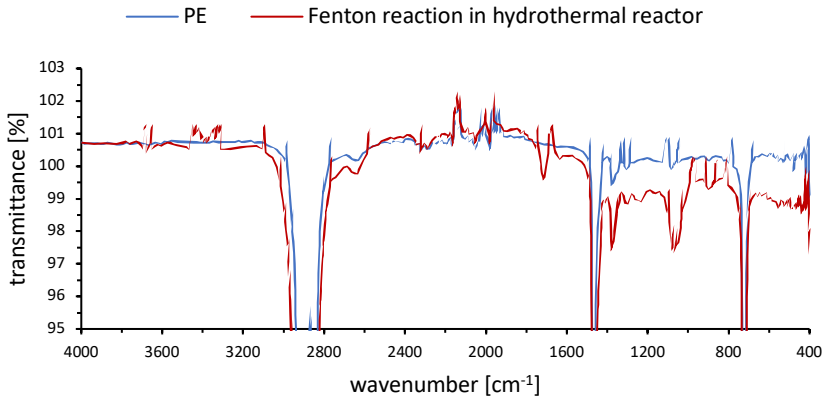

b

Functional group	Mode of vibration	Wavenumber [cm^{-1}]
Alcohol	O-H stretch	3600-3200
Carbonyl	C=O stretch	1870-1650
Alkene	C=C stretch	1670-1600
Alcohol, ether, ester, anhydride, acetal	C-O stretch	1300-1020

Figure 133|ATR-FTIR analysis of PE after Fenton reaction in a hydrothermal reactor. 4 mM Fe^{2+}, 200 mM H_2O_2, and 20 mM HCl were used, and it was incubated for 5 h at 140 °C. **a**, FTIR spectrum before and after incubation in Fenton reaction. **b**, Characteristic IR-bands for functional groups generated during oxidative PE degradation.

a

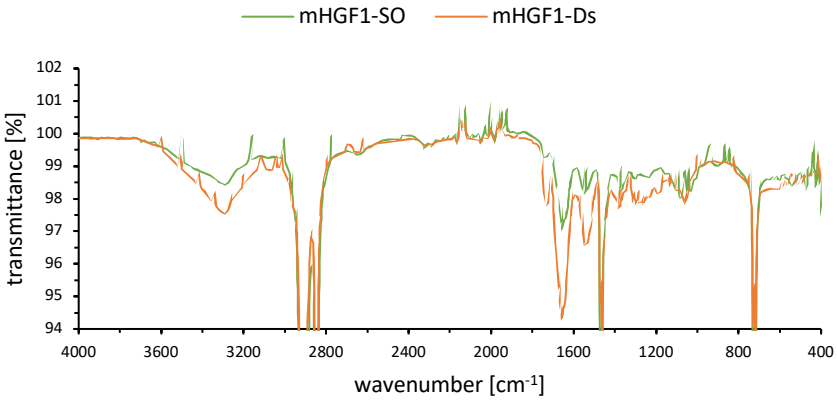

b

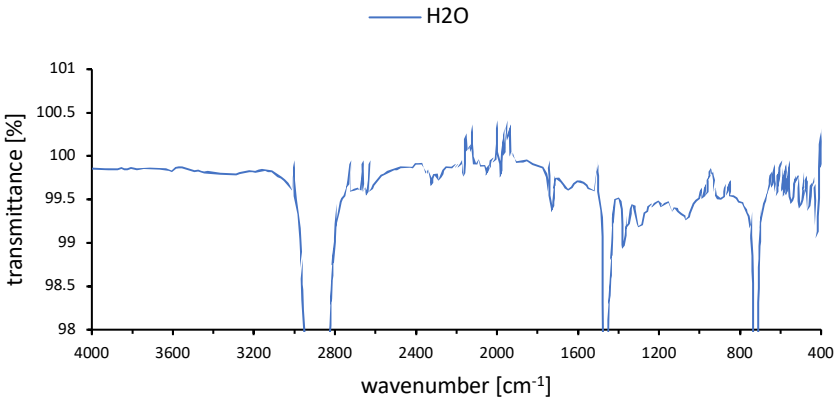

c

Peptide/protein signal	Mode of vibration	Wavenumber [cm^{-1}]
Amide A	N-H stretch	3400-3200
Amide I	C=O stretch	1680-1620
Amide II	N-H bend, C-N stretch	1550-1500

Functional group	Mode of vibration	Wavenumber [cm^{-1}]
Alcohol	O-H stretch	3600-3200
Carbonyl	C=O stretch	1870-1650
Alkene	C=C stretch	1670-1600
Alcohol, ether, ester, anhydride, acetal	C-O stretch	1300-1020

Figure 134|ATR-FTIR analysis PE degradation experiments in a flow setup. Incubation for 16 days with 1 µM fusion protein mHGF1-SOPP3, mHGF1-DsFbFpM49I (**a**, LYS_3 and LYS_4 respectively) or H_2O (**b**, LYS_5) under blue light (7.0 mW/cm^2) with a flow of 80 µL/min for 1 min within a cycle of 13.3 min (1 min flow, 12.3 min no flow) resulting in the addition of 80 µl every 13.3 min. SO = SOPP3, Ds = DsFbFpM49I. **c**, Characteristic IR-bands for amide bonds in a peptide/protein and for functional groups generated during oxidative PE degradation.

6.8.5 XPS spectra

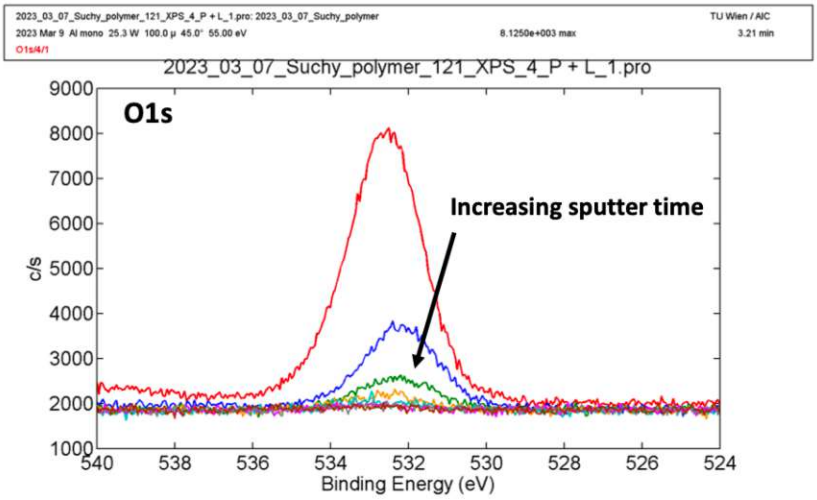

Figure 135|XPS analysis (detail spectra of the O1s region) of the PE degradation experiment using PE on Si and the fusion protein SOPP3-mHGF1-SOPP3. It was incubated with 3 µM fusion protein SOPP3-mHGF1-SOPP3 for 20 h, without exchanging the protein solution (P+L, 0323). The removal of loosely bound material by an Ar gas cluster ion gun is depicted.

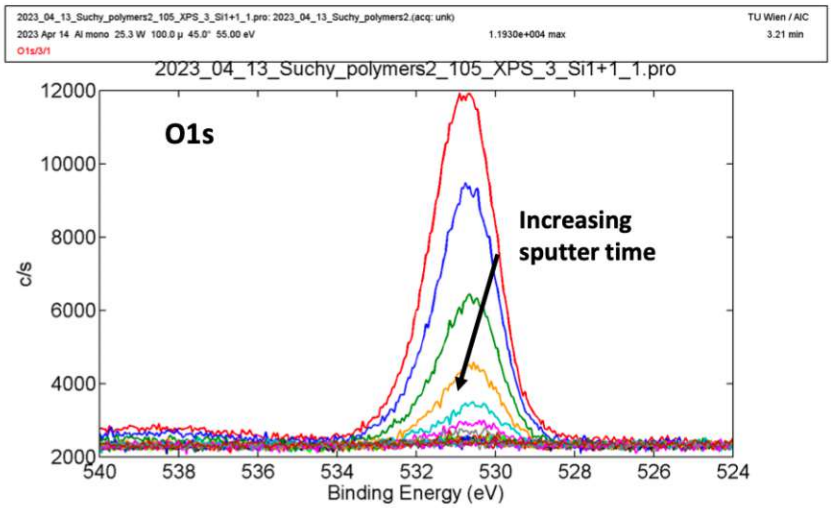

Figure 136|XPS analysis (detail spectra of the O1s region) of the second PE degradation experiment using PE on Si and the fusion protein SOPP3-mHGF1-SOPP3. It was incubated with 9 µM fusion protein SOPP3-mHGF1-SOPP3 for 9 h, while shaking (150 rpm), exchanging the protein solution every 3 hours (P+L Si, 0423). The removal of loosely bound material by an Ar gas cluster ion gun is depicted.

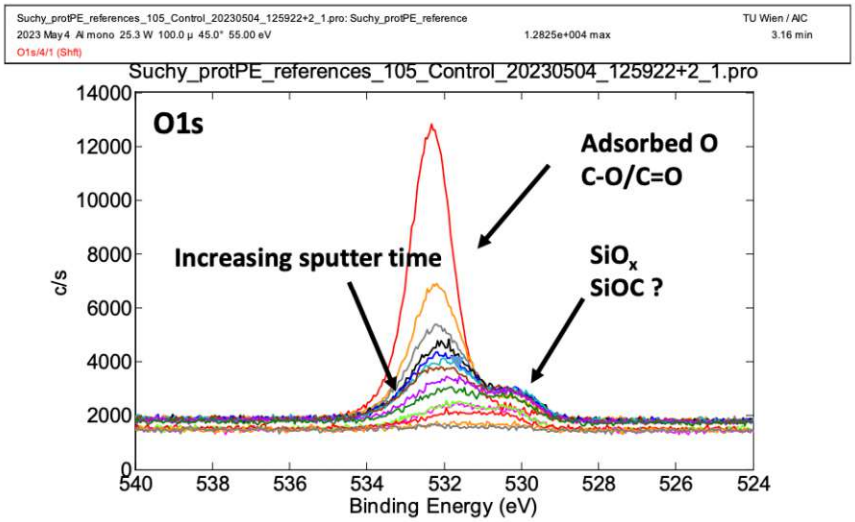

Figure 137|XPS analysis (detail spectra of the O1s region) of the PE degradation experiment by Fenton reaction in a glass vial. The PE sample was incubated with 10 mM Fe^{2+} and 15 % H_2O_2 for 1.5 h in a glass vial (Control, 0523). The removal of loosely bound material by an Ar gas cluster ion gun is depicted.

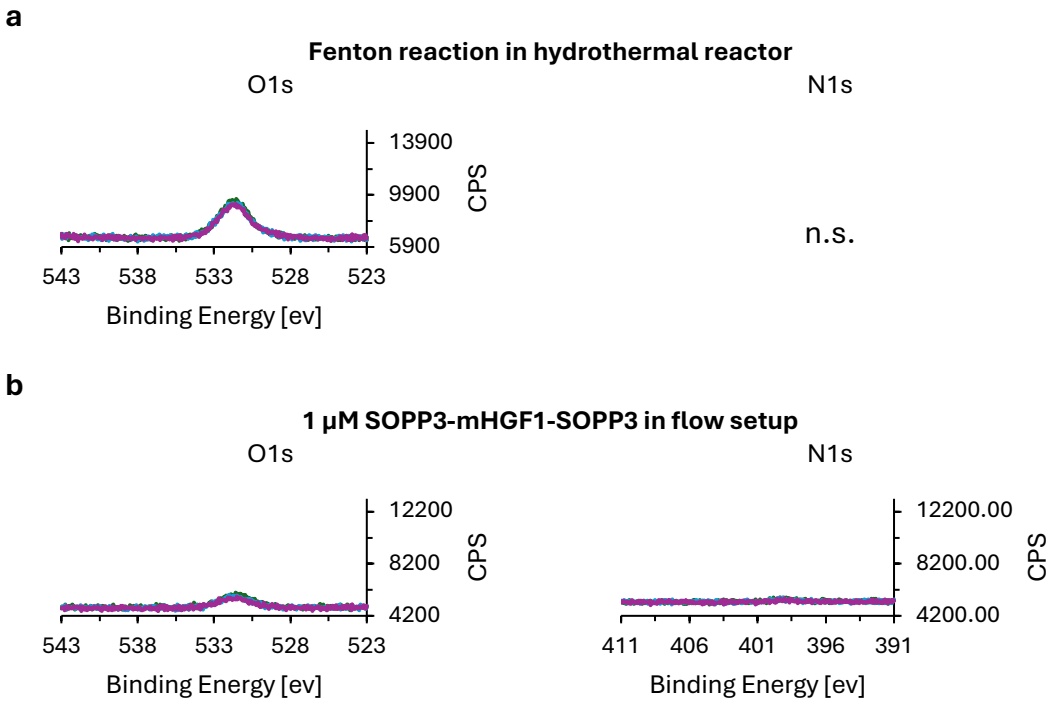

Figure 138|XPS analysis of different PE degradation experiments (detail spectra of the O1s and N1s regions). After the removal of loosely bound material by an Ar gas cluster ion gun, the last three sputter cycles before the fastest gas cluster ion beam setting are depicted. **a**, Incubation with Fenton's reagent for 5 h at 140 °C in a PTFE container (Lys2, 1023). **b**, Incubation with 1 µM fusion protein SOPP3-mHGF1-SOPP3 in a flow setup for 14 days, under illumination with blue light (7.0 mW/cm²) (Lys_3, 1023).

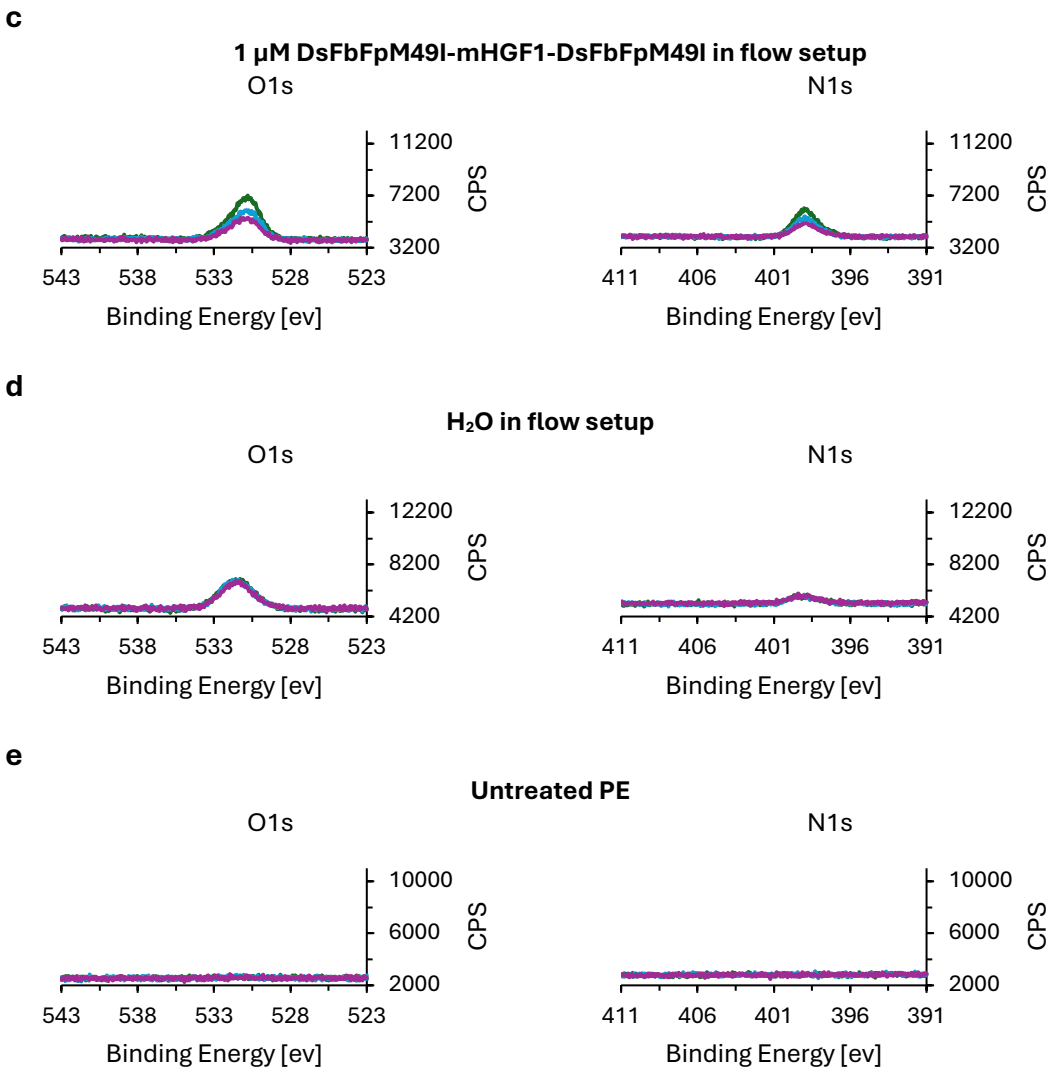

Figure 138| continued. c, Incubation with 1 µM fusion protein DsFbFpM49I-mHGF1-DsFbFpM49I in a flow setup for 14 days, under illumination with blue light (7.0 mW/cm^2) (Lys_4, 1023). **d**, Incubation with H_2O in a flow setup for 14 days, under illumination with blue light (7.0 mW/cm^2) (Lys_5, 1023). **e**, Untreated PE (Lys_10, 0724).

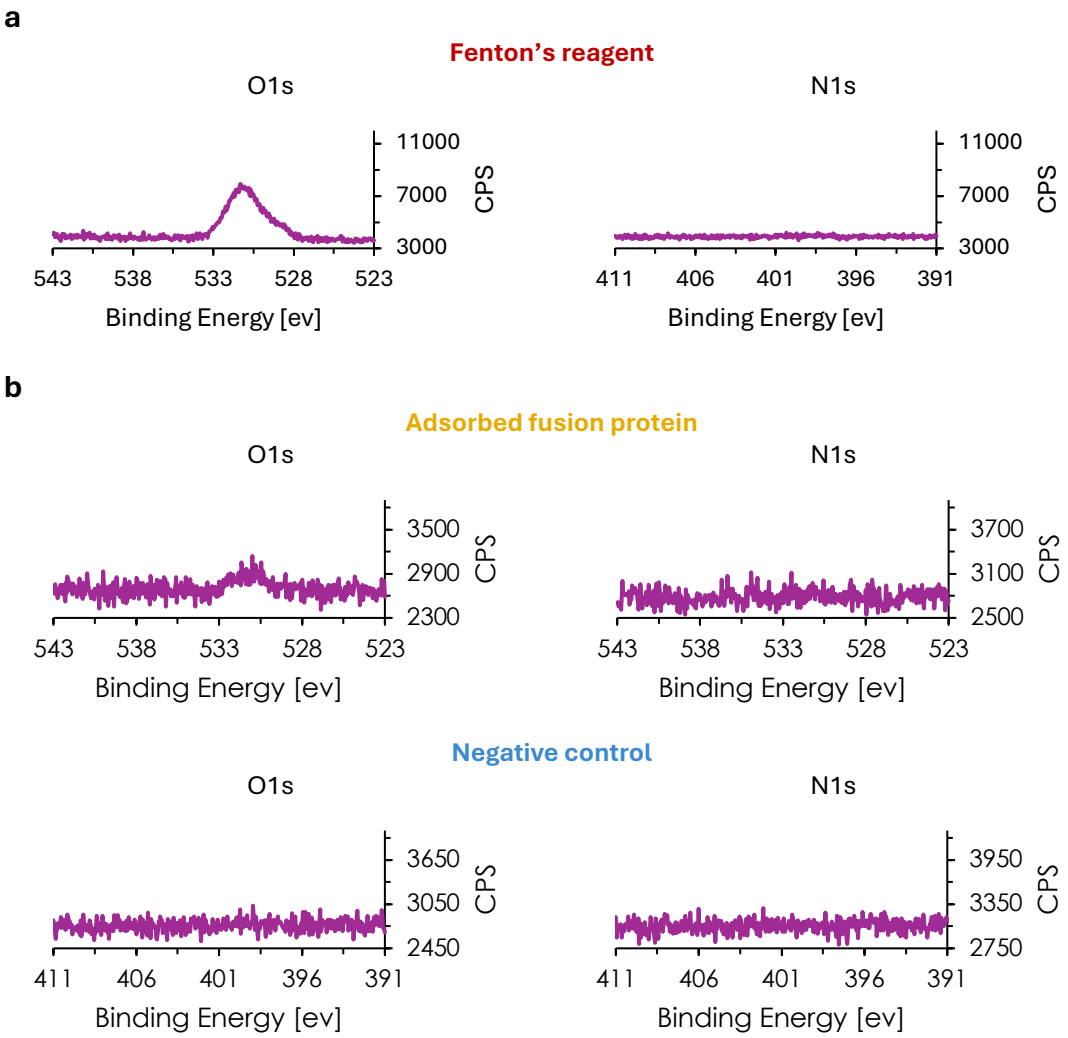

Figure 139|XPS analysis of PE degradation (detail spectra of the O1s and N1s regions). After the removal of loosely bound material by an Ar gas cluster ion gun, the first sputter cycle of the fastest gas cluster ion beam setting is depicted. **a**, Incubation with Fenton's reagent for 42 h in a PTFE container (Lys_1, 0224). **b**, Incubation with adsorbed fusion protein mHGF1-DsFbFpM49I for 42 h, irradiation with blue light (16.4 mW/cm^2) (Lys_8, 0724). Negative control (Lys_9, 0724).

7 Abbreviations

(LA)12	α-helix consisting of 12 units leucine and alanine
$(NH_4)_2SO_4$	ammonium sulfate
°C	degrees Celsius
$^1O_2$	singlet oxygen
3D	3-dimensional
aa	amino acid
ABTS	2,2'-azino-bis(3-ethylbenzothiazoline-6-sulfonate
AC	alternating current
AFM	atomic force microscopy
AIC	Analytical Instrumentation Center
ÄKTA	chromatography system for protein purification
Amp	ampicillin
APF	aminophenyl fluorescein
approx.	approximately
APS	ammonium persulfate
Ar	argon
at%	atomic percent
ATR-FTIR	attenuated total reflectance Fourier transform infrared spectroscopy
bacto	bacteriological
BCA	bicinchoninic acid assay
BE	binding energy
bp	base pairs
BSA	bovine serum albumin
C	carbon
$CaCl_2$	calcium chloride
CALI	chromophore assisted light inactivation
cam	chloramphenicol
$CDCl_3$	deuterated chloroform
CFE	cell free extract
CH_4	methane
CLEM	correlative light-electron microscopy
cm	centimeter
CO	carbon monoxide
CO_2	carbon dioxide
conc.	concentration
D_2O	deuterated water
DCM	dichloromethane
dH_2O	distilled water
DMF	dimethylformamide
DMPO	5,5-Dimethyl-1-pyrroline N-oxide
DMSO	dimethylsulfoxide
DNA	deoxyribonucleic acid
dNTP	Deoxynucleoside triphosphates
Ds	short form for the protein DsFbFpM49I
dsDNA	double strand DNA
E. coli	*Escherichia coli*
e.g.	for example (latin: exempli gratia)
EDTA	ethylenediaminetetraacetic acid
EG	ethylene glycol
Em	emission
ESR	electron spin resonance
EtOH	ethanol
eV	electronvolt
Ex	excitation
$FeSO_4$	iron(II) sulfate
FLHis	flexible linker followed by a 6 x His tag
FMN	flavin mononucleotide
g	gram
G	guanine
GC	guanine cytosine

GCIB	Gas cluster ion beams	mbar	millibar
GFP	green fluorescent protein	MeOH	methanol
GOI	gene of interest	Mg	magnesium
GPC	gel permeation chromatography	$MgCl_2$	magnesium chloride
h	hours	$MgSO_4$	magnesium sulfate
H_2	hydrogen	mL	milliliter
H_2O	water	mm	millimeter
H_2O_2	hydrogen peroxide	mM	millimolar
H_2SO_4	sulfuric acid	$MnCl_2$	manganese(II) chloride
HAc	acetic acid	MOPS	3-(N-morpholino)propanesulfonic acid
HCl	hydrochloric acid	MS	mass spectrometry
HDPE	high density polyethylene	mV	millivolt
His	histidine	mW	milliwatt
HNO_3	nitric acid	n.s.	not specified
$HO^{\bullet}$	hydroxyl radical	N/m	Newton/meter
HPLC	high pressure liquid chromatography	nA	nanoampere
HRP	horseradish peroxidase	Na_2HPO_4	disodium hydrogen phosphate
hv	the energy of a photon	NaCl	natrium chloride
IMAC	immobilized metal affinity chromatography	NaH_2PO_4	sodium dihydrogen phosphate
*i*PrOH	isopropyl alcohol	NaOH	sodium hydroxide
IR	infrared	NaPi	sodium phosphate buffer
kb	kilobyte	NbO_5	niobium pentoxide
KCl	potassium chloride	nc	negative control
kDa	kilodalton	NEB	New England Biolabs
KH_2PO_4	potassium dihydrogen phosphate	ng	nanogram
kHz	kilohertz	$NiSO_4$	nickel sulfate
KLD	kinase ligase and DpnI	nm	nanometer
KOAc	potassium acetate	NMR	nuclear magnetic resonance
kV	kilovolt	O_2	molecular oxygen
L	liter	$O_2^{\bullet-}$	superoxide
LB	lysogeny broth	OD_{590}	optical density at 590 nm
LDPE	low density polyethylene	pc	positive control
LIBS	laser induced breakdown spectroscopy	pcc	positive control colony
LLDPE	linear low density polyethylene	pcp	positive control plasmid
LOV proteins	light oxygen voltage sensing domain	PCR	polymerase chain reaction
M	molar (mol/L)	PDT	photodynamic therapy
max.	maximum	PE	polyethylene

PET	polyethylene terephthalate	SO	short form for the protein SOPP3
pg	picogram	SOC	super optimal broth with catabolite repression medium
pH	“potential of hydrogen”	SOD	superoxide dismutase
PLA	polylactic acid	SOSG	singlet oxygen sensor green
pmol	picomol	SPR	surface plasmon resonance
PMSF	phenylmethanesulfonyl fluoride	T_a	annealing temperature
PP	polypropylene	TEMED	tetramethylethylenediamine
ppm	parts per million	THF	tetrahydrofuran
Primer *fwd*	forward primer	TiO_2	titanium oxide
Primer *rev*	reverse primer	T_m	melting temperature
PS	polystyrene	Tris	tris(hydroxymethyl)aminomethane
PSP	photosensitizer protein	U	units
Pt	platinum	UHMWPE	Ultra High Molecular Weight Polyethylene
PTFE	Polytetrafluoroethylene	UV	ultraviolet
PVC	polyvinyl chloride	UVA	ultraviolet A (315-400 nm)
QCM	quartz crystal microbalance	V	volt
QWG	glutamine tryptophan glycine	W	watt
QYG	glutamine tyrosine glycine	WCA	water contact angle
R	organic residue	wt. %	weight percent
RbCl	rubidium chloride	x g	gravitational force
RBS	ribosome binding site	XPS	X-ray photoelectron spectroscopy
RL	rigid linker	XRD	X-ray diffraction
ROS	reactive oxygen species	ZnO	tin oxide
rpm	rounds per minute	Zr	zirconium
rt	room temperature	λ	wavelength
RU	relative units	µg	microgram
Ru	ruthenium	µL	microliter
SDS-PAGE	polyacrylamide gel electrophoresis	µm	micrometer
sec	seconds	µM	micromolar
SEM	scanning electron microscopy	v/v	volume percent
Si	silicium	ω/v	weight/volume

8 Curriculum Vitae

Lydia Suchy | Resume

lydiasuchy@gmail.com

Education

Vienna University of Technology — **Vienna**
Doctoral programme in Natural Sciences Technical Chemistry — *since december 2020*

Vienna University of Technology — **Vienna**
Master Thesis — *january 2020–february 2021*

University of Vienna — **Vienna**
Master of Science in Genetics and Developmental Biology — *since october 2018*

Cinvestav, Instituto Politécnico Nacional — **Mexico City, Mexico**
Master thesis — *march 2017–december 2017*

University of Bergen — **Bergen, Norway**
Exchange semester — *january 2016–june 2016*

University of Vienna — **Vienna**
Master of Science in Chemistry — *october 2015–june 2018*

University of Vienna — **Vienna**
Bachelor of Science in Chemistry — *october 2012–october 2015*

Filmschule Vienna — **Vienna**
Filmlehrgang-course in filmmaking — *october 2012–june 2013*

Experience

Department of Organic and Biological Chemistry — **Vienna University of Technology**
PhD thesis — *since march 2021*
under supervision of Assoc. Prof. Priv. Doz. Dr. Florian Rudroff
Detailed achievements:
- Supervision of students in lab courses and at examinations
- PhD thesis "Pioneering Light, Air, and Photosensitizing Proteins for the Degradation of Polyolefins"
- Paper draft "A bio-photocatalyst for the oxidative degradation of polyethylene"

Department of Organic and Biological Chemistry — **Vienna University of Technology**
Master thesis - Biology — *january 2020-february 2021*
under supervision of Assoc. Prof. Priv. Doz. Dr. Florian Rudroff
Detailed achievements:
- Master thesis "Enzymatic Cascades in *Escherichia Coli* based on the Equilibration of Reactive Aldehyde Intermediates"
- February 2021: Release of book chapter "Multi-Enzymatic Cascades In Vivo"
- January 2024: Release of paper "In situ Generation of Aldehydes for Subsequent Biocatalytic Cascade Reactions in Whole Cells"

Department of Microbiology, Immunobiology and Genetics **University of Vienna**
Research on molecular genetics and pathology *october-november 2019*
under supervision of Prof. Dr. Mikulits, Dr. Dolznig, and Prof. Dr. Müllner

Department of Organic and Biological Chemistry **Vienna University of Technology**
Cyanobacteria as host for a biocatalytic cascade reaction *september-october 2019*
under supervision of Prof. Dr. Rudroff

Institute of Organic Chemistry **Graz University of Technology**
New potential small-molecule inhibitors targeting ATGL *july-august 2019*
under supervision of Prof. Dr. Breinbauer

Department of Chromosome Biology **University of Vienna**
Eukaryotic model systems in chromosome biology *january 2019*
under supervision of Prof Dr. Loidl, Prof. Dr. Schlögelhofer, and Prof. Dr. Campbell

Department of Microbiology, Immunology and Genetics **University of Vienna**
Research on the potential function of the protein HNSΔ28 in E. coli *november 2018*
under supervision of Prof. Dr. Isabella Moll

Institute of Organic Chemistry **CINVESTAV, Instituto Politécnico Nacional**
Master thesis - Chemistry *march 2017–december 2017*
under supervision of Prof. Dr. Eusebio Juaristi
Detailed achievements:
- Master thesis "Dendron-Supported α, β-Dipeptides for the Organocatalytic Asymmetric Michael Reaction"
- May 2019: Release of paper "Dendrimeric α,β-dipeptidic conjugates as organocatalysts in the asymmetric Michael addition reaction of isobutyraldehyde to N-phenylmaleimides"

Institute of Chemical Catalysis **University of Vienna**
Research on phase transfer catalysts with dinaphthoazepinium backbone *january 2017*
under supervision of Prof. Dr. Michael Widhalm
Detailed achievements:
- March 2018: Release of paper "Economy of Catalyst Synthesis—Convenient Access to Libraries of Di-and Tetranaphtho Azepinium Compounds"

Department of Organic Synthesis **University of Vienna**
Research on chiral BINOL-based monophosphite ligands *december 2016*
under supervision of Prof. Dr. Nuno Maulide

Department of Botany and Biodiversity **University of Vienna**
Bachelor thesis *may 2015*
under supervision of Prof. Dr. Lothar Brecker and Dr. Johann Schinnerl
Detailed achievements:
- Bachelor thesis "Isolierung und Strukturaufklärung von Inhaltsstoffen aus Palicourea garciae Standl."

Scientific skills

Chemistry: Organic synthesis, purification and analysis (GC, HPLC, NMR)

Molecular biology: Molecular cloning, site-directed mutagenesis, protein production and purification

Biocatalysis: in vivo biocatalysis, in vitro biocatalysis

Polymer and Surface Chemistry: Spin coating of polymers, Ellipsometry, Surface plasmon resonance measurement, Water contact angle measurement, ATR-FTIR measurement, Atomic force microscopy, Analysis of XPS and LIBS data

Other scientific skills: Fluorescent assays for the analysis of reactive oxygen species, Measurement of oxygen

Computer skills

Microsoft Office: Word, Excel, PowerPoint

Chemistry and NMR Software: ChemDraw, ChemDoodle, TopSpin, Delta, MestreNova

Molecular Graphics Software: PyMol, RasMol, Chimera

Molecular Biology Software: Integrative Genomics Viewer, Gene Construction Kit, Primer3, SnapGene, GenomeCompiler, ApE-A Plasmid Editor, Gene Codes Sequencher, Jalview

Surface Analysis Software: MP-SPR Navi^{TM} (for Surface Plasmon Resonance measurement), Krüss Advance (for Water Contact Angle measurement), Cypher (for Atomic Force Microscopy)

Other Scientific Software: GeoGebra, LaTeX, ImageJ

Video Editing Software: Final Cut Pro, Motion, Soundtrack Pro

Languages

German: native — *mother tongue*

Czech: native — *mother tongue*

English: advanced — *Cambridge's Certificate (C1)*

Spanish: upper-intermediate

Norwegian: elementary

French: elementary

Publications

- Tharamak, S., Knittl-Frank, C., Manaprasertsak, A., Pengsook, A., Suchy, L., Schuller, P., Happl B., Roller A., Widhalm, M. Economy of Catalyst Synthesis–Convenient Access to Libraries of Di-and Tetranaphtho Azepinium Compounds, *Molecules*, **2018**, 23, 750.
- Landeros, J. M., Suchy, L., Ávila-Ortiz, C. G., Maulide, N., Juaristi, E. Dendrimeric α,β-dipeptidic conjugates as organocatalysts in the asymmetric Michael addition reaction of isobutyraldehyde to N-phenylmaleimides, *Monatshefte für Chemie-Chemical Monthly*, **2019**, 150, 777-788.
- Suchy, L., Rudroff, F. Multi-Enzymatic Cascades In Vivo, in *Enzyme Cascade Design and Modelling*, **2021**, 49-63.
- Suchy, L., Rudroff, F. In situ Generation of Aldehydes for Subsequent Biocatalytic Cascade Reactions in Whole Cells, *ChemCatChem*, **2024**, 16, e202301138.

9 References

1 https://plasticseurope.org/knowledge-hub/plastics-the-facts-2022/.

2 Bank, M. S. *Microplastic in the environment: pattern and process*. (Springer Nature, 2022). https://doi.org/10.1007/978-3-030-78627-4

3 Hamd, W., Daher, E. A., Tofa, T. S. & Dutta, J. Recent advances in photocatalytic removal of microplastics: mechanisms, kinetic degradation, and reactor design. *Front. mar. sci.*, **9**, 885614 (2022). https://doi.org/10.3389/fmars.2022.885614

4 Lee, Q. Y. & Li, H. Photocatalytic degradation of plastic waste: a mini review. *Micromachines* **12**, 907 (2021). https://doi.org/10.3390/mi12080907

5 Zhang, S. *et al.* Microplastics in the environment: A review of analytical methods, distribution, and biological effects. *TrAC, Trends Anal. Chem.* **111**, 62-72 (2019). https://doi.org/10.1016/j.trac.2018.12.002

6 Morrison, M. *et al.* A growing crisis for One Health: Impacts of plastic pollution across layers of biological function. *Front. Mar. Sci.* **9**, 980705 (2022). https://doi.org/10.3389/fmars.2022.980705

7 https://plasticseurope.org/de/knowledge-hub/plastics-the-fast-facts-2023/.

8 Sarkar, S., Diab, H. & Thompson, J. Microplastic pollution: Chemical characterization and impact on wildlife. *Int. J. Environ. Res. Public Health* **20**, 1745 (2023). https://doi.org/10.3390/ijerph20031745

9 Schmid, C., Cozzarini, L. & Zambello, E. Microplastic's story. *Mar. Pollut. Bull.* **162**, 111820 (2021). https://doi.org/10.1016/j.marpolbul.2020.111820

10 Seay, J. R. The global plastic waste challenge and how we can address it. *Clean Technol. Environ. Policy* **24**, 729-730 (2022). https://doi.org/10.1007/s10098-021-02271-0

11 Diana, Z. T., Virdin, J., Valiyaveettil, S., Li, H.-X. & Rittschof, D. Emerging challenges and solutions for plastic pollution. *Front. Mar. Sci.* 10, 1162680 (2023). https://doi.org/10.3389/fmars.2023.1162680

12 Hopewell, J., Dvorak, R. & Kosior, E. Plastics recycling: challenges and opportunities. *Philos. Trans. R. Soc., B.* **364**, 2115-2126 (2009). https://doi.org/10.1098/rstb.2008.0311

13 Peng, Y., Prabhu, A. & Rinke, C. Facing our plastic waste crisis: biorecycling as a promising solution. *Microbiol. Aust.* **44**, 52-56 (2023). https://doi.org/10.1071/MA23013

14 Patel, R. M. Types and basics of polyethylene. in *Handbook of Industrial Polyethylene and Technology: Definitive Guide to Manufacturing, Properties, Processing, Applications and Markets*, 105-138 (2017). https://doi.org/10.1002/9781119159797

15 Yuan, J. *et al.* Microbial degradation and other environmental aspects of microplastics/plastics. *Sci. Total Environ.* **715**, 136968 (2020). https://doi.org/10.1016/j.scitotenv.2020.136968

16 Inderthal, H., Tai, S. L. & Harrison, S. T. Non-hydrolyzable plastics–an interdisciplinary look at plastic bio-oxidation. *Trends Biotechnol.* **39**, 12-23 (2021). https://doi.org/10.1016/j.tibtech.2020.05.004

17 Tokiwa, Y., Calabia, B. P., Ugwu, C. U. & Aiba, S. Biodegradability of plastics. *Int. J. Mol. Sci.* **10**, 3722-3742 (2009). https://doi.org/10.3390/ijms10093722

18 Liu, S. *et al.* Reactive oxygen species-induced microplastics aging: Implications for environmental fate and ecological impact. *TrAC, Trends Anal. Chem.*, 117648 (2024). https://doi.org/10.1016/j.trac.2024.117648

19 Xing, R. *et al.* Free radicals accelerate in situ ageing of microplastics during sludge composting. *J. Hazard. Mater.* **429**, 128405 (2022). https://doi.org/10.1016/j.jhazmat.2022.128405

20 Bond, T., Ferrandiz-Mas, V., Felipe-Sotelo, M. & Van Sebille, E. The occurrence and degradation of aquatic plastic litter based on polymer physicochemical properties: a review. *Crit. Rev. Environ. Sci. Technol.* **48**, 685-722 (2018). https://doi.org/10.1080/10643389.2018.1483155

21 Gewert, B., Plassmann, M. M. & MacLeod, M. Pathways for degradation of plastic polymers floating in the marine environment. *Environ. Sci.:Processes Impacts* **17**, 1513-1521 (2015). https://doi.org/10.1039/C5EM00207A

22 Zhu, K. *et al.* Formation of environmentally persistent free radicals on microplastics under light irradiation. *Environ. Sci. Technol.* **53**, 8177-8186 (2019). https://doi.org/10.1021/acs.est.9b01474

23 Zhu, K. *et al.* Long-term phototransformation of microplastics under simulated sunlight irradiation in aquatic environments: Roles of reactive oxygen species. *Water Res.* **173**, 115564 (2020). https://doi.org/10.1016/j.watres.2020.115564

24 Wiles, D. M. & Scott, G. Polyolefins with controlled environmental degradability. *Polym. Degrad. Stab.* **91**, 1581-1592 (2006). https://doi.org/10.1016/j.polymdegradstab.2005.09.010

25 Duan, J. *et al.* ROS-mediated photoaging pathways of nano-and micro-plastic particles under UV irradiation. *Water Res.* **216**, 118320 (2022). https://doi.org/10.1016/j.watres.2022.118320

26 Suresh, B., Maruthamuthu, S., Kannan, M. & Chandramohan, A. Mechanical and surface properties of low-density polyethylene film modified by photo-oxidation. *Polym. J.* **43**, 398-406 (2011). https://doi.org/10.1038/pj.2010.147

27 Smith, L. M., Aitken, H. M. & Coote, M. L. The fate of the peroxyl radical in autoxidation: how does polymer degradation really occur? *Acc. Chem. Res.* **51**, 2006-2013 (2018). https://doi.org/10.1021/acs.accounts.8b00250.

28 Ghatge, S., Yang, Y., Ahn, J.-H. & Hur, H.-G. Biodegradation of polyethylene: a brief review. *Appl. Biol. Chem.* **63**, 1-14 (2020). https://doi.org/10.1186/s13765-020-00511-3

29 Agboola, O., Sadiku, R., Mokrani, T., Amer, I. & Imoru, O. Polyolefins and the environment. in *Polyolefin Fibres* **4**, 89-133 (2017). https://doi.org/10.1016/B978-0-08-101132-4.00004-7

30 Chamas, A. *et al.* Degradation rates of plastics in the environment. *ACS Sustainable Chem. Eng.* **8**, 3494-3511 (2020). https://doi.org/10.1021/acssuschemeng.9b06635

31 Campanale, C., Savino, I., Massarelli, C. & Uricchio, V. F. Fourier transform infrared spectroscopy to assess the degree of alteration of artificially aged and environmentally weathered microplastics. *Polymers* **15**, 911 (2023). https://doi.org/10.3390/polym15040911

32 Lange, J.-P. Managing plastic waste– sorting, recycling, disposal, and product redesign. *ACS Sustainable Chem. Eng.* **9**, 15722-15738 (2021). https://doi.org/10.1021/acssuschemeng.1c05013

33 Ellis, L. D. *et al.* Chemical and biological catalysis for plastics recycling and upcycling. *Nat. Catal.* **4**, 539-556 (2021). https://doi.org/10.1038/s41929-021-00648-4

34 Faust, K., Denifl, P. & Hapke, M. Recent advances in catalytic chemical recycling of polyolefins. *ChemCatChem* **15**, e202300310 (2023). https://doi.org/10.1002/cctc.202300310

35 Yeung, C. W., Teo, J. Y., Loh, X. J. & Lim, J. Y. Polyolefins and polystyrene as chemical resources for a sustainable future: challenges, advances, and prospects. *ACS Mater. Lett.* **3**, 1660-1676 (2021). https://doi.org/10.1021/acsmaterialslett.1c00490

36 Bäckström, E., Odelius, K. & Hakkarainen, M. Designed from recycled: turning polyethylene waste to covalently attached polylactide plasticizers. *ACS Sustainable Chem. Eng.* **7**, 11004-11013 (2019). https://doi.org/10.1021/acssuschemeng.9b02092

37 Su, H., Li, T., Zhu, L. & Wang, S. Catalytic reforming of the aqueous phase derived from diluted hydrogen peroxide oxidation of waste polyethylene for hydrogen production. *ChemSusChem* **14**, 4270-4279 (2021). https://doi.org/10.1002/cssc.202100913

38 Pichler, C. M., Bhattacharjee, S., Rahaman, M., Uekert, T. & Reisner, E. Conversion of polyethylene waste into gaseous hydrocarbons via integrated tandem chemical–photo/electrocatalytic processes. *ACS Catal.* **11**, 9159-9167 (2021). https://doi.org/10.1021/acscatal.1c02133

39 Lares, M., Ncibi, M. C., Sillanpää, M. & Sillanpää, M. Occurrence, identification and removal of microplastic particles and fibers in conventional activated sludge process and advanced MBR technology. *Water Res.* **133**, 236-246 (2018). https://doi.org/10.1016/j.watres.2018.01.049

40 Hu, K. *et al.* Microplastics remediation in aqueous systems: Strategies and technologies. *Water Res.* **198**, 117144 (2021). https://doi.org/10.1016/j.watres.2021.117144

41 Ortiz, D. *et al.* Insights into the degradation of microplastics by Fenton oxidation: From surface modification to mineralization. *Chemosphere* **309**, 136809 (2022). https://doi.org/10.1016/j.chemosphere.2022.136809

42 Hu, K. *et al.* Degradation of microplastics by a thermal Fenton reaction. *ACS ES&T Eng.* **2**, 110-120 (2021). https://doi.org/10.1021/acsestengg.1c00323

43 Nabi, I., Ahmad, F. & Zhang, L. Application of titanium dioxide for the photocatalytic degradation of macro-and micro-plastics: a review. *J. Environ. Chem. Eng.* **9**, 105964 (2021). https://doi.org/10.1016/j.jece.2021.105964

44 Jiao, X. *et al.* Photocatalytic conversion of waste plastics into C2 fuels under simulated natural environment conditions. *Angew. Chem., Int. Ed.* **59**, 15497-15501 (2020). https://doi.org/10.1002/anie.201915766

45 Gutierrez-Mata, A. *et al.* Recent overview of solar photocatalysis and solar photo-fenton processes for wastewater treatment. *Int. J. Photoenergy.* **2017**, 8528063 (2017). https://doi.org/10.1155/2017/8528063

46 Nosaka, Y. & Nosaka, A. Y. Generation and detection of reactive oxygen species in photocatalysis. *Chem. Rev.* **117**, 11302-11336 (2017). https://doi.org/10.1021/acs.chemrev.7b00161

47 Paiman, S. H., Noor, S. F. M., Ngadi, N., Nordin, A. H. & Abdullah, N. Insight into photocatalysis technology as a promising approach to tackle microplastics pollution through degradation and upcycling. *Chem. Eng. J.* **467**, 143534 (2023). 10.1016/j.cej.2023.143534

48 Ebrahimbabaie, P., Yousefi, K. & Pichtel, J. Photocatalytic and biological technologies for elimination of microplastics in water: Current status. *Sci. Total Environ.* **806**, 150603 (2022). https://doi.org/10.1016/j.scitotenv.2021.150603
49 Vital-Grappin, A. D. *et al.* The role of the reactive species involved in the photocatalytic degradation of HDPE microplastics using C, N-TiO2 powders. *Polymers* **13**, 999 (2021). https://doi.org/10.3390/polym13070999
50 Nabi, I. *et al.* Complete photocatalytic mineralization of microplastic on TiO2 nanoparticle film. *Iscience* **23** (2020). https://doi.org/10.1016/j.isci.2020.101326
51 Tofa, T. S., Kunjali, K. L., Paul, S. & Dutta, J. Visible light photocatalytic degradation of microplastic residues with zinc oxide nanorods. *Environ. Chem. Lett.* **17**, 1341-1346 (2019). https://doi.org/10.1007/s10311-019-00859-z
52 Mohanan, N., Montazer, Z., Sharma, P. K. & Levin, D. B. Microbial and enzymatic degradation of synthetic plastics. *Front. Microbiol.* **11**, 580709 (2020). https://doi.org/10.3389/fmicb.2020.580709
53 Zhu, B., Wang, D. & Wei, N. Enzyme discovery and engineering for sustainable plastic recycling. *Trends biotechnol.* **40**, 22-37 (2022). https://doi.org/10.1016/j.tibtech.2021.02.008
54 Demarche, P., Junghanns, C., Nair, R. R. & Agathos, S. N. Harnessing the power of enzymes for environmental stewardship. *Biotechnol. Adv.* **30**, 933-953 (2012). https://doi.org/10.1016/j.biotechadv.2011.05.013
55 Tournier, V. *et al.* Enzymes' power for plastics degradation. *Chem. Rev.* **123**, 5612-5701 (2023). https://doi.org/10.1021/acs.chemrev.2c00644
56 Bell, E. L. *et al.* Directed evolution of an efficient and thermostable PET depolymerase. *Nat. Catal.* **5**, 673-681 (2022). https://doi.org/10.26434/chemrxiv-2021-mcjh6
57 Weber, G., Bornscheuer, U. T. & Wei, R. *Enzymatic Plastic Degradation*. (Academic Press, 2021).
58 Li, A. *et al.* Discovery and mechanism-guided engineering of BHET hydrolases for improved PET recycling and upcycling. *Nat. Commun.* **14**, 4169 (2023). https://doi.org/10.1038/s41467-023-39929-w
59 Tournier, V. *et al.* An engineered PET depolymerase to break down and recycle plastic bottles. *Nature* **580**, 216-219 (2020). https://doi.org/10.1038/s41586-020-2149-4
60 https://www.carbios.com/fr/enzymatic-recycling/.
61 Zhang, Y., Pedersen, J. N., Eser, B. E. & Guo, Z. Biodegradation of polyethylene and polystyrene: From microbial deterioration to enzyme discovery. *Biotechnol. Adv.* **60**, 107991 (2022). https://doi.org/10.1016/j.biotechadv.2022.107991
62 Zhang, N., Ding, M. & Yuan, Y. Current advances in biodegradation of polyolefins. *Microorganisms* **10**, 1537 (2022). https://doi.org/10.3390/microorganisms10081537
63 Chen, Z. *et al.* Reactive oxygen species triggered oxidative degradation of polystyrene in the gut of superworms (Zophobas atratus larvae). *Environ. Sci. Technol.* **57**, 7867-7874 (2023). https://doi.org/10.1021/acs.est.3c00591
64 Murphy, M. P. *et al.* Guidelines for measuring reactive oxygen species and oxidative damage in cells and in vivo. *Nat. metab.* **4**, 651-662 (2022). https://doi.org/10.1038/s42255-022-00591-z
65 Paterson, M. J., Christiansen, O., Jensen, F. & Ogilby, P. R. Overview of theoretical and computational methods applied to the oxygen-organic molecule photosystem. *Photochem. Photobiol.* **82**, 1136-1160 (2006). https://doi.org/10.1562/2006-03-17-IR-851

66 Redmond, R. W. & Kochevar, I. E. Spatially resolved cellular responses to singlet oxygen. *Photochem. Photobiol.* **82**, 1178-1186 (2006). https://doi.org/10.1562/2006-04-14-IR-874
67 Wojtovich, A. P. & Foster, T. H. Optogenetic control of ROS production. *Redox biol.* **2**, 368-376 (2014). https://doi.org/10.1016/j.redox.2014.01.019
68 Bardaweel, S. K. *et al.* Reactive oxygen species: The dual role in physiological and pathological conditions of the human body. *Eurasian j. med.* **50**, 193 (2018). https://doi.org/10.5152/eurasianjmed.2018.17397
69 Zhang, Y., Dai, M. & Yuan, Z. Methods for the detection of reactive oxygen species. *Anal. Methods* **10**, 4625-4638 (2018). https://doi.org/10.1039/C8AY01339J
70 Babuponnusami, A. & Muthukumar, K. A review on Fenton and improvements to the Fenton process for wastewater treatment. *J. Environ. Chem. Eng.* **2**, 557-572 (2014). https://doi.org/10.1016/j.jece.2013.10.011
71 Tawfik, A. *et al.* Solar photo-oxidation of recalcitrant industrial wastewater: a review. *Environ. Chem. Lett.* **20**, 1839-1862 (2022). https://doi.org/10.1007/s10311-022-01390-4
72 Kusano, Y. Atmospheric pressure plasma processing for polymer adhesion: A review. *J. Adhes.* **90**, 755-777 (2014). https://doi.org/10.1080/00218464.2013.804407
73 Booth, J.-P., Mozetič, M., Nikiforov, A. & Oehr, C. Foundations of plasma surface functionalization of polymers for industrial and biological applications. *Plasma Sources Sci. Technol.* **31**, 103001 (2022). https://doi.org/10.1088/1361-6595/ac70f9
74 Michelin, C. & Hoffmann, N. Photosensitization and photocatalysis—Perspectives in organic synthesis. *ACS Catal.* **8**, 12046-12055 (2018). https://doi.org/10.1021/acscatal.8b03050
75 Baptista, M. S. *et al.* Type I and type II photosensitized oxidation reactions: guidelines and mechanistic pathways. *Photochem. Photobiol.* **93**, 912-919 (2017). https://doi.org/10.1111/php.12716
76 Trewin, A. J. *et al.* Light-induced oxidant production by fluorescent proteins. *Free Radical Biol. Med.* **128**, 157-164 (2018). 10.1016/j.freeradbiomed.2018.02.002
77 Endres, S. *et al.* An optogenetic toolbox of LOV-based photosensitizers for light-driven killing of bacteria. *Sci. Rep.* **8**, 1-14 (2018). https://doi.org/10.1038/s41598-018-33291-4
78 Sies, H. & Jones, D. P. Reactive oxygen species (ROS) as pleiotropic physiological signalling agents. *Nat. Rev. Mol.* **21**, 363-383 (2020). https://doi.org/10.1038/s41580-020-0230-3
79 Phaniendra, A., Jestadi, D. B. & Periyasamy, L. Free radicals: properties, sources, targets, and their implication in various diseases. *Indian J. Clin. Biochem.* **30**, 11-26 (2015). https://doi.org/10.1007/s12291-014-0446-0.
80 Wu, L. *et al.* Reaction-based fluorescent probes for the detection and imaging of reactive oxygen, nitrogen, and sulfur species. *Acc. Chem. Res.* **52**, 2582-2597 (2019). https://doi.org/10.1021/acs.accounts.9b00302.
81 Schweitzer, C. & Schmidt, R. Physical mechanisms of generation and deactivation of singlet oxygen. *Chem. Rev.* **103**, 1685-1758 (2003). https://doi.org/10.1021/cr010371d
82 Assenheim, H. M. *Introduction to electron spin resonance*. (Springer, 2014). https://doi.org/10.1007/978-1-4899-5502-9

83 https://www.picoquant.com/applications/category/materials-science/photocatalysis.
84 Bartosz, G. Use of spectroscopic probes for detection of reactive oxygen species. *Clin. Chim. Acta.* **368**, 53-76 (2006). https://doi.org/10.1016/j.cca.2005.12.039
85 Burns, J. M. *et al.* Methods for reactive oxygen species (ROS) detection in aqueous environments. *Aquat. Sci.* **74**, 683-734 (2012). https://doi.org/10.1007/s00027-012-0251-x
86 Sim Choi, H., Woo Kim, J., Cha, Y. N. & Kim, C. A quantitative nitroblue tetrazolium assay for determining intracellular superoxide anion production in phagocytic cells. *J. Immunoassay Immunochem.* **27**, 31-44 (2006). https://doi.org/10.1080/15321810500403722
87 Rhee, S. G., Chang, T.-S., Jeong, W. & Kang, D. Methods for detection and measurement of hydrogen peroxide inside and outside of cells. *Mol. Cells* **29**, 539-549 (2010). https://doi.org/10.1007/S1016-8478(23)12982-7
88 Harpaz, D., Eltzov, E., Ng, T. S., Marks, R. S. & Tok, A. I. Enhanced colorimetric signal for accurate signal detection in paper-based biosensors. *Diagnostics* **10**, 28 (2020). https://doi.org/10.3390/diagnostics10010028
89 Hou, J.-T. *et al.* Fluorescent detectors for hydroxyl radical and their applications in bioimaging: a review. *Coord. Chem. Rev.* **421**, 213457 (2020). https://doi.org/10.1016/j.ccr.2020.213457
90 Li, X., Yuan, L. & Zhao, L. A comparative study on oxidation of acidic red 18 by persulfate with ferrous and ferric ions. *Catalysts* **10**, 698 (2020). https://doi.org/10.3390/catal10060698
91 Xiong, Y., Tian, X. & Ai, H.-w. Molecular tools to generate reactive oxygen species in biological systems. *Bioconjugate Chem.* **30**, 1297-1303 (2019). https://doi.org/10.1021/acs.bioconjchem.9b00191
92 Bulina, M. E. *et al.* A genetically encoded photosensitizer. *Nat. Biotechnol.* **24**, 95-99 (2006). https://doi.org/10.1038/nbt1175
93 Hilgers, F. *et al.* Genetically encoded photosensitizers as light-triggered antimicrobial agents. *Int. J. Mol. Sci.* **20**, 4608 (2019). https://doi.org/10.3390/ijms20184608
94 Tsien, R. Y. Constructing and exploiting the fluorescent protein paintbox (Nobel Lecture). *Angew. Chem., Int. Ed.* **48**, 5612-5626 (2009). https://doi.org/10.1002/anie.200901916
95 Jiménez-Banzo, A., Nonell, S., Hofkens, J. & Flors, C. Singlet oxygen photosensitization by EGFP and its chromophore HBDI. *Biophys. J.* **94**, 168-172 (2008). https://doi.org/10.1529/biophysj.107.107128
96 Pletnev, S. *et al.* Structural basis for phototoxicity of the genetically encoded photosensitizer KillerRed. *J. Biol. Chem.* **284**, 32028-32039 (2009). https://doi.org/10.1074/jbc.M109.054973
97 Onukwufor, J. O. *et al.* Quantification of reactive oxygen species production by the red fluorescent proteins KillerRed, SuperNova and mCherry. *Free Radical Biol. Med.* **147**, 1-7 (2020). https://doi.org/10.1016/j.freeradbiomed.2019.12.008
98 Takemoto, K. *et al.* SuperNova, a monomeric photosensitizing fluorescent protein for chromophore-assisted light inactivation. *Sci. Rep.* **3**, 2629 (2013). https://doi.org/10.1038/srep02629

99 Das, S., Tiwari, M., Mondal, D., Sahoo, B. R. & Tiwari, D. K. Growing tool-kit of photosensitizers for clinical and non-clinical applications. *J. Mater. Chem. B* **8**, 10897-10940 (2020). https://doi.org/10.1039/D0TB02085K
100 Sarkisyan, K. S. *et al.* KillerOrange, a genetically encoded photosensitizer activated by blue and green light. *PLoS One* **10**, e0145287 (2015). https://doi.org/10.1371/journal.pone.0145287
101 Pletneva, N. V. *et al.* Crystal structure of phototoxic orange fluorescent proteins with a tryptophan-based chromophore. *PloS one* **10**, e0145740 (2015). https://doi.org/10.1371/journal.pone.0145740
102 Chia, H. E., Marsh, E. N. G. & Biteen, J. S. Extending fluorescence microscopy into anaerobic environments. *Curr. Opin. Chem. Biol.* **51**, 98-104 (2019). https://doi.org/10.1016/j.cbpa.2019.05.008
103 https://www.fpbase.org/protein/killerorange/.
104 https://www.fpbase.org/protein/killerred/.
105 Herrou, J. & Crosson, S. Function, structure and mechanism of bacterial photosensory LOV proteins. *Nat. Rev. Microbiol.* **9**, 713-723 (2011). https://doi.org/10.1038/nrmicro2622
106 Pudasaini, A., El-Arab, K. K. & Zoltowski, B. D. LOV-based optogenetic devices: light-driven modules to impart photoregulated control of cellular signaling. *Front. Mol. Biosci.* **2**, 18 (2015). https://doi.org/10.3389/fmolb.2015.00018
107 Losi, A., Gardner, K. H. & Möglich, A. Blue-light receptors for optogenetics. *Chem. Rev.* **118**, 10659-10709 (2018). https://doi.org/10.1021/acs.chemrev.8b00163
108 Seifert, S. & Brakmann, S. LOV domains in the design of photoresponsive enzymes. *ACS Chem. Biol.* **13**, 1914-1920 (2018). https://doi.org/10.1021/acschembio.8b00159
109 Wingen, M. *et al.* The photophysics of LOV-based fluorescent proteins–new tools for cell biology. *Photochem. Photobiol. Sci.* **13**, 875-883 (2014). https://doi.org/10.1039/C3PP50414J
110 Shu, X. *et al.* A genetically encoded tag for correlated light and electron microscopy of intact cells, tissues, and organisms. *PLoS Biol.* **9**, e1001041 (2011). https://doi.org/10.1371/journal.pbio.1001041
111 Pimenta, F. M., Jensen, R. L., Breitenbach, T., Etzerodt, M. & Ogilby, P. R. Oxygen-dependent photochemistry and photophysics of "MiniSOG," a protein-encased flavin. *Photochem. Photobiol.* **89**, 1116-1126 (2013). https://doi.org/10.1111/php.12111
112 Rodríguez-Pulido, A. *et al.* Assessing the potential of photosensitizing flavoproteins as tags for correlative microscopy. *Chem. Commun.* **52**, 8405-8408 (2016). https://doi.org/10.1039/C6CC03119F
113 Rodríguez-Pulido, A. *et al.* Fluorescent flavoprotein heterodimers: combining photostability with singlet oxygen generation. *ChemPhotoChem* **2**, 571-574 (2018). https://doi.org/10.1002/cptc.201800002
114 Barnett, M. E., Baran, T. M., Foster, T. H. & Wojtovich, A. P. Quantification of light-induced miniSOG superoxide production using the selective marker, 2-hydroxyethidium. *Free Radical Biol. Med.* **116**, 134-140 (2018). https://doi.org/10.1016/j.freeradbiomed.2018.01.014
115 Westberg, M., Bregnhøj, M., Etzerodt, M. & Ogilby, P. R. No photon wasted: an efficient and selective singlet oxygen photosensitizing protein. *J. Phys. Chem. B* **121**, 9366-9371 (2017). https://doi.org/10.1021/acs.jpcb.7b07831

116 Mogensen, D. J., Etzerodt, M. & Ogilby, P. R. Photoinduced bleaching in an efficient singlet oxygen photosensitizing protein: Identifying a culprit in the flavin-binding LOV-based protein SOPP3. *Journal of Photochem. Photobiol. A: Chemistry* **429**, 113894 (2022). https://doi.org/10.1016/j.jphotochem.2022.113894

117 Endres, S. *et al.* Structure and function of a short LOV protein from the marine phototrophic bacterium Dinoroseobacter shibae. *BMC Microbiol.* **15**, 1-16 (2015). https://doi.org/10.1186/s12866-015-0365-0

118 https://www.fpbase.org/protein/minisog/.

119 Bulina, M. E. *et al.* Chromophore-assisted light inactivation (CALI) using the phototoxic fluorescent protein KillerRed. *Nat. Protoc.* **1**, 947-953 (2006). https://doi.org/10.1038/nprot.2006.89

120 Jacobson, K., Rajfur, Z., Vitriol, E. & Hahn, K. Chromophore-assisted laser inactivation in cell biology. *Trends Cell Biol.* **18**, 443-450 (2008). https://doi.org/10.1016/j.tcb.2008.07.001

121 Zhou, Z., Song, J., Nie, L. & Chen, X. Reactive oxygen species generating systems meeting challenges of photodynamic cancer therapy. *Chem. Soc. Rev.* **45**, 6597-6626 (2016). https://doi.org/10.1039/C6CS00271D

122 Wang, B. *et al.* Mitochondria are targets for peroxisome-derived oxidative stress in cultured mammalian cells. *Free Radical Biol. Med.* **65**, 882-894 (2013). https://doi.org/10.1016/j.freeradbiomed.2013.08.173

123 Gerlach, T. *et al.* Photo-regulation of enzyme activity: the inactivation of a carboligase with genetically encoded photosensitizer fusion tags. *Front. Catal.* **2**, 835919 (2022). https://doi.org/10.3389/fctls.2022.835919

124 Püllmann, P., Homann, D., Karl, T. A., König, B. & Weissenborn, M. J. Light-Controlled Biocatalysis by Unspecific Peroxygenases with Genetically Encoded Photosensitizers. *Angew. Chem., Int. Ed.* **62**, e202307897 (2023). https://doi.org/10.1002/anie.202307897

125 Berger, B. W. & Sallada, N. D. Hydrophobins: multifunctional biosurfactants for interface engineering. *J. Biol. Eng.* **13**, 1-8 (2019). https://doi.org/10.1186/s13036-018-0136-1

126 Wösten, H. A. & Scholtmeijer, K. Applications of hydrophobins: current state and perspectives. *Appl. Microbiol. Biotechnol.* **99**, 1587-1597 (2015). https://doi.org/10.1007/s00253-014-6319-x

127 Schor, M., Reid, J. L., MacPhee, C. E. & Stanley-Wall, N. R. The diverse structures and functions of surfactant proteins. *Trends Biochem. Sci.* **41**, 610-620 (2016). https://doi.org/10.1016/j.tibs.2016.04.009

128 Linder, M. B., Szilvay, G. R., Nakari-Setälä, T. & Penttilä, M. E. Hydrophobins: the protein-amphiphiles of filamentous fungi. *FEMS Microbiol. Rev.* **29**, 877-896 (2005). https://doi.org/10.1016/j.femsre.2005.01.004

129 Lovett, B., Kasson, M. T. & Gandier, J.-A. Ecology drives the observed spectrum of hydrophobin protein diversity across Kingdom Fungi. *bioRxiv*, 2022.2008.2019.504535 (2022). https://doi.org/10.1101/2022.08.19.504535

130 Kirkland, B. H. & Keyhani, N. O. Expression and purification of a functionally active class I fungal hydrophobin from the entomopathogenic fungus Beauveria bassiana in E. coli. *J. ind. microbiol. biotech.* **38**, 327-335 (2011). https://doi.org/10.1007/s10295-010-0777-7

131 Puspitasari, N., Tsai, S.-L. & Lee, C.-K. Fungal hydrophobin RolA enhanced PETase hydrolysis of polyethylene terephthalate. *Appl. Biochem. Biotechnol.* **193**, 1284-1295 (2021). https://doi.org/10.1007/s12010-020-03358-y
132 Takahashi, T. *et al.* The fungal hydrophobin RolA recruits polyesterase and laterally moves on hydrophobic surfaces. *Mol. Microbiol.* **57**, 1780-1796 (2005). https://doi.org/10.1111/j.1365-2958.2005.04803.x
133 Espino-Rammer, L. *et al.* Two novel class II hydrophobins from Trichoderma spp. stimulate enzymatic hydrolysis of poly (ethylene terephthalate) when expressed as fusion proteins. *Appl. Environ. Microbiol.* **79**, 4230-4238 (2013). https://doi.org/10.1128/AEM.01132-13
134 Ribitsch, D. *et al.* Enhanced cutinase-catalyzed hydrolysis of polyethylene terephthalate by covalent fusion to hydrophobins. *Appl. Environ. Microbiol.* **81**, 3586-3592 (2015). https://doi.org/10.1128/AEM.04111-14
135 Paananen, A. *et al.* Structural hierarchy in molecular films of two class II hydrophobins. *Biochemistry* **42**, 5253-5258 (2003). https://doi.org/10.1021/bi034031t
136 Qin, M. *et al.* Bioactive surface modification of mica and poly (dimethylsiloxane) with hydrophobins for protein immobilization. *Langmuir* **23**, 4465-4471 (2007). https://doi.org/10.1021/la062744h
137 Zhao, Z.-X. *et al.* Self-assembled film of hydrophobins on gold surfaces and its application to electrochemical biosensing. *Colloids Surf. B: Biointerfaces* **71**, 102-106 (2009). https://doi.org/10.1016/j.colsurfb.2009.01.011
138 Gazzera, L. *et al.* Hydrophobin as a nanolayer primer that enables the fluorinated coating of poorly reactive polymer surfaces. *Adv. Mater. Interfaces* **2**, 1500170 (2015). https://doi.org/10.1002/admi.201500170
139 Yu, L. *et al.* Protein HGFI from the edible mushroom Grifola frondosa is a novel 8 kDa class I hydrophobin that forms rodlets in compressed monolayers. *Microbiology* **154**, 1677-1685 (2008). https://doi.org/10.1099/mic.0.2007/015263-0
140 Cheng, Y. *et al.* Soluble hydrophobin mutants produced in Escherichia coli can self-assemble at various interfaces. *J. Colloid Interface Sci.* **573**, 384-395 (2020). https://doi.org/10.1016/j.jcis.2020.04.012
141 Xu, L.-C. & Siedlecki, C. A. Effects of surface wettability and contact time on protein adhesion to biomaterial surfaces. *Biomaterials* **28**, 3273-3283 (2007). https://doi.org/10.1016/j.biomaterials.2007.03.032
142 Jeyachandran, Y. L., Mielczarski, E., Rai, B. & Mielczarski, J. A. Quantitative and qualitative evaluation of adsorption/desorption of bovine serum albumin on hydrophilic and hydrophobic surfaces. *Langmuir* **25**, 11614-11620 (2009). https://doi.org/10.1021/la901453a
143 Ausili, A., Sánchez, M. & Gómez-Fernández, J. C. Attenuated total reflectance infrared spectroscopy: A powerful method for the simultaneous study of structure and spatial orientation of lipids and membrane proteins. *Biomed. Spectrosc. Imaging* **4**, 159-170 (2015). https://doi.org/10.3233/BSI-150104
144 McArthur, S. L. Applications of XPS in bioengineering. *Surf. Interface Anal.* **38**, 1380-1385 (2006). https://doi.org/10.1002/sia.2498
145 https://en.wikipedia.org/wiki/X-ray_photoelectron_spectroscopy.
146 Walton, S., Fernsler, R. & Lock, E. *Preparation of ultra thin polystyrene, polypropylene and polyethylene films on Si substrate using spin coating technology*. (2008).

147 Guo, X. Surface plasmon resonance based biosensor technique: a review. *J. Biophotonics* **5**, 483-501 (2012). https://doi.org/10.1002/jbio.201200015
148 https://www.nottingham.ac.uk/isac/facilities/spr.aspx.
149 https://www.azooptics.com/Article.aspx?ArticleID=2083.
150 Pleshakova, T. O., Bukharina, N. S., Archakov, A. I. & Ivanov, Y. D. Atomic force microscopy for protein detection and their physicochemical characterization. *Int. J. Mol. Sci.* **19**, 1142 (2018). https://doi.org/10.3390/ijms19041142
151 Turner, K., Serantoni, M., Boyce, A. & Walsh, G. The use of proteases to remove protein-based residues from solid surfaces. *Process Biochem.* **40**, 3377-3382 (2005). https://doi.org/10.1016/j.procbio.2005.03.040
152 Li, X., Wei, X. & Husson, S. M. Thermodynamic studies on the adsorption of fibronectin adhesion-promoting peptide on nanothin films of poly (2-vinylpyridine) by SPR. *Biomacromolecules* **5**, 869-876 (2004). https://doi.org/10.1021/bm034266k
153 Green, R., Davies, J., Davies, M., Roberts, C. & Tendler, S. Surface plasmon resonance for real time in situ analysis of protein adsorption to polymer surfaces. *Biomaterials* **18**, 405-413 (1997). https://doi.org/10.1016/S0142-9612(96)00141-X
154 Serro, A., Degiampietro, K., Colaço, R. & Saramago, B. Adsorption of albumin and sodium hyaluronate on UHMWPE: a QCM-D and AFM study. *Colloids Surf. B: Biointerfaces* **78**, 1-7 (2010). https://doi.org/10.1016/j.colsurfb.2010.01.022
155 Malmsten, M. Ellipsometry studies of protein layers adsorbed at hydrophobic surfaces. *J. Colloid Interface Sci.* **166**, 333-342 (1994). https://doi.org/10.1006/jcis.1994.1303
156 van der Zee, M. *Handbook of biodegradable polymers.* (Rapra Technology, 2005). https://doi.org/10.1002/9783527635818
157 Bastioli, C. *Handbook of biodegradable polymers.* (Walter de Gruyter GmbH & Co KG, 2020). https://doi.org/10.1515/9781501511967
158 Yao, C., Xia, W., Dou, M., Du, Y. & Wu, J. Oxidative degradation of UV-irradiated polyethylene by laccase-mediator system. *J. Hazard. Mater.* **440**, 129709 (2022). https://doi.org/10.1016/j.jhazmat.2022.129709
159 Sudhakar, M., Doble, M., Murthy, P. S. & Venkatesan, R. Marine microbe-mediated biodegradation of low-and high-density polyethylenes. *Int. Biodeter. Biodegr.* **61**, 203-213 (2008). https://doi.org/10.1016/j.ibiod.2007.07.011
160 Hou, Y., Chen, J., Sun, P., Gan, Z. & Zhang, G. In situ investigations on enzymatic degradation of poly (ε-caprolactone). *Polymer* **48**, 6348-6353 (2007). https://doi.org/10.1016/j.polymer.2007.08.054
161 Phithakrotchanakoon, C. *et al.* Heterologous expression of polyhydroxyalkanoate depolymerase from Thermobifida sp. in Pichia pastoris and catalytic analysis by surface plasmon resonance. *Appl. Microbiol. Biotechnol.* **82**, 131-140 (2009). https://doi.org/10.1007/s00253-008-1754-1
162 Sinsereekul, N. *et al.* Recombinant expression of BTA hydrolase in Streptomyces rimosus and catalytic analysis on polyesters by surface plasmon resonance. *Appl. Microbiol. Biotechnol.* **86**, 1775-1784 (2010). https://doi.org/10.1007/s00253-010-2465-y
163 Sumner, C., Sabot, A., Turner, K. & Krause, S. A transducer based on enzyme-induced degradation of thin polymer films monitored by surface plasmon resonance. *Anal. Chem.* **72**, 5225-5232 (2000). https://doi.org/10.1021/ac000411y

164 Nakatani, H., Ohshima, Y., Uchiyama, T. & Motokucho, S. Degradation and fragmentation behavior of polypropylene and polystyrene in water. *Sci. Rep.* **12**, 18501 (2022). https://doi.org/10.1038/s41598-022-23435-y
165 Sommer, C., Nguyen, J., Menzel, T., Ruckdäschel, H. & Koch, M. Determining weathering-induced heterogeneous oxidation profiles of polyethylene, polypropylene and polystyrene using laser-induced breakdown spectroscopy. *Chemosphere* **343**, 140105 (2023). https://doi.org/10.1016/j.chemosphere.2023.140105
166 Sommer, C. *et al.* Weathering-induced oxidation: An investigation of artificially aged polystyrene samples using Laser-induced Breakdown Spectroscopy. *Polym. Test.* **112**, 107623 (2022). https://doi.org/10.1016/j.polymertesting.2022.107623
167 Willner, J. *et al.* Development of a simultaneous LA-ICP-MS & LIBS method for the investigation of polymer degradation. *J. Anal. At. Spectrom.* **38**, 2028-2037 (2023). https://doi.org/10.1039/D3JA00237C
168 Brunnbauer, L. *et al.* Combined LA-ICP-MS/LIBS: powerful analytical tools for the investigation of polymer alteration after treatment under corrosive conditions. *Sci. Rep.* **10**, 12513 (2020). https://doi.org/10.1038/s41598-020-69210-9
169 Harmon, R. S. & Senesi, G. S. Laser-induced breakdown spectroscopy–a geochemical tool for the 21st century. *Appl. Geochem.* **128**, 104929 (2021). https://doi.org/10.1016/j.apgeochem.2021.104929
170 Briggs, D., Brewis, D., Dahm, R. & Fletcher, I. Analysis of the surface chemistry of oxidized polyethylene: comparison of XPS and ToF-SIMS. *Surf. Interface Anal.* **35**, 156-167 (2003). https://doi.org/10.1002/sia.1515
171 Dorey, S., Gaston, F., Marque, S. R., Bortolotti, B. & Dupuy, N. XPS analysis of PE and EVA samples irradiated at different γ-doses. *Appl. Surf. Sci.* **427**, 966-972 (2018). https://doi.org/10.1016/j.apsusc.2017.09.001
172 Shard, A. G. *et al.* Argon cluster ion beams for organic depth profiling: results from a VAMAS interlaboratory study. *Anal. Chem.* **84**, 7865-7873 (2012). https://doi.org/10.1021/ac301567t
173 Cumpson, P. J., Portoles, J. F. & Sano, N. Observations on X-ray enhanced sputter rates in argon cluster ion sputter depth profiling of polymers. *Surf. Interface Anal.* **45**, 601-604 (2013). https://doi.org/10.1116/1.4793284
174 Cumpson, P. J., Portoles, J. F. & Sano, N. Material dependence of argon cluster ion sputter yield in polymers: Method and measurements of relative sputter yields for 19 polymers. *J. Vac. Sci. Technol. A* **31** (2013). https://doi.org/10.1116/1.4791669
175 https://www.novoprolabs.com/tools/codon-optimization.
176 https://www.genscript.com/tools/gensmart%2dcodon%2doptimization.
177 https://www.twistbioscience.com.
178 Studier, F. W. Stable expression clones and auto-induction for protein production in E. coli. in *Structural genomics: general applications*, 17-32 (2014). https://doi.org/10.1007/978-1-62703-691-7_2
179 Kadnikova, E. N. & Kostić, N. M. Oxidation of ABTS by hydrogen peroxide catalyzed by horseradish peroxidase encapsulated into sol–gel glass.: Effects of glass matrix on reactivity. *J. Mol. Catal. B Enzym.* **18**, 39-48 (2002). https://doi.org/10.1016/S1381-1177(02)00057-7
180 Christopher, L. P., Yao, B. & Ji, Y. Lignin biodegradation with laccase-mediator systems. *Front. Energy Res.* **2**, 12 (2014). https://doi.org/10.3389/fenrg.2014.00012

181 Zhao, B., Ranguelova, K., Jiang, J. & Mason, R. P. Studies on the photosensitized reduction of resorufin and implications for the detection of oxidative stress with Amplex Red. *Free Radical Biol. Med.* **51**, 153-159 (2011). https://doi.org/10.1016/j.freeradbiomed.2011.03.016
182 Ravanfar, R. & Abbaspourrad, A. The molecular mechanism of the photocatalytic oxidation reactions by horseradish peroxidase in the presence of histidine. *Green Chem.* **22**, 6105-6114 (2020). https://doi.org/10.1039/D0GC01972K
183 Dębski, D. *et al.* Mechanism of oxidative conversion of Amplex® Red to resorufin: pulse radiolysis and enzymatic studies. *Free Radical Biol. Med.* **95**, 323-332 (2016). https://doi.org/10.1016/j.freeradbiomed.2016.03.027
184 Younus, H. Therapeutic potentials of superoxide dismutase. *Int. J. Health Sci.* **12**, 88 (2018).
185 Zhao, B., Summers, F. A. & Mason, R. P. Photooxidation of Amplex Red to resorufin: implications of exposing the Amplex Red assay to light. *Free Radical Biol. Med.* **53**, 1080-1087 (2012). https://doi.org/10.1016/B978-0-12-405883-5.00001-6
186 Kim, S., Fujitsuka, M. & Majima, T. Photochemistry of singlet oxygen sensor green. *J. Phys. Chem. B* **117**, 13985-13992 (2013). https://doi.org/10.1021/jp406638g
187 Kiesslich, T., Gollmer, A., Maisch, T., Berneburg, M. & Plaetzer, K. A comprehensive tutorial on in vitro characterization of new photosensitizers for photodynamic antitumor therapy and photodynamic inactivation of microorganisms. *Biomed Res. Int.* **2013**, 840417 (2013). https://doi.org/10.1155/2013/840417
188 https://assets.thermofisher.com/TFS-Assets/LSG/manuals/mp36002.pdf.
189 https://de.lumiprobe.com/k/singlet-oxygen-sensor-green#:~:text=Singlet%20Oxygen%20Sensor%20Green%20(SOSG)%20is%20a%20fluorogenic%20probe%20for,2%20and%20various%20clinical%20applications.
190 Setsukinai, K.-i., Urano, Y., Kakinuma, K., Majima, H. J. & Nagano, T. Development of novel fluorescence probes that can reliably detect reactive oxygen species and distinguish specific species* 210. *J. Biol. Chem.* **278**, 3170-3175 (2003). https://doi.org/10.1074/jbc.M209264200
191 Control, C. f. D. *NIOSH pocket guide to chemical hazards*. (National Institute for Occupational Safety and Health, 1990).
192 Chen, X., Zaro, J. L. & Shen, W.-C. Fusion protein linkers: property, design and functionality. *Adv. Drug Deliv. Rev.* **65**, 1357-1369 (2013). https://doi.org/10.1016/j.addr.2012.09.039
193 Lewis, R. N. *et al.* A polyalanine-based peptide cannot form a stable transmembrane α-helix in fully hydrated phospholipid bilayers. *Biochemistry* **40**, 12103-12111 (2001). https://doi.org/10.1021/bi010555m
194 Lewis, R. *et al.* Studies of the minimum hydrophobicity of α-helical peptides required to maintain a stable transmembrane association with phospholipid bilayer membranes. *Biochemistry* **46**, 1042-1054 (2007). https://doi.org/10.1021/bi061891b
195 https://international.neb.com/protocols/2014/11/26/nebuilder-hifi-dna-assembly-reaction-protocol.
196 Thomas, S., Maynard, N. D. & Gill, J. DNA library construction using Gibson Assembly®. *Nat. Methods* **12**, i-ii (2015). https://doi.org/10.1038/nmeth.f.384
197 https://www.neb-online.de/en/cloning-synthetic-biology/dna-assembly/nebuilder-dna-assembly/.

198 https://www.neb.com/en/protocols/2013/12/13/pcr-using-q5-high-fidelity-dna-polymerase-m0491.
199 Mellbring, O., Kihlman Øiseth, S., Krozer, A., Lausmaa, J. & Hjertberg, T. Spin coating and characterization of thin high-density polyethylene films. *Macromolecules* **34**, 7496-7503 (2001). https://doi.org/10.1021/ma000094x
200 Amokrane, G., Falentin-Daudré, C., Ramtani, S. & Migonney, V. A simple method to functionalize PCL surface by grafting bioactive polymers using UV irradiation. *Irbm* **39**, 268-278 (2018). https://doi.org/10.1016/j.irbm.2018.07.002
201 Beyerer, J. & Pak, A. *Proceedings of the 2012 Joint Workshop of Fraunhofer IOSB and Institute for Anthropomatics, Vision and Fusion Laboratory*. (Karlsruhe: KIT Scientific, 2013). https://doi.org/10.5445/KSP/1000032956
202 https://nebuilder.neb.com/#!/.
203 https://tmcalculator.neb.com/#!/main.
204 https://nebasechangerv1.neb.com.
205 https://www.thermofisher.com/at/en/home/life-science/protein-biology/protein-biology-learning-center/protein-biology-resource-library/pierce-protein-methods/chemistry-protein-assays.html.
206 https://assets.thermofisher.com/TFS-Assets/LSG/manuals/mp22188.pdf.
207 https://tools.thermofisher.com/content/sfs/manuals/mp36002.pdf.
208 Aslan-Üzel, A. S. *et al.* An ultrasensitive fluorescence assay for the detection of halides and enzymatic dehalogenation. *ChemCatChem* **12**, 2032-2039 (2020). https://doi.org/10.1002/cctc.201901891
209 https://www.inrf.uci.edu/wordpress/wp-content/uploads/sop-wet-silicon-solvent-clean.pdf.
210 Vashist, S. K. A method for regenerating gold surface for prolonged reuse of gold-coated surface plasmon resonance chip. *Anal. Biochem.* **423**, 23-25 (2012). https://doi.org/10.1016/j.ab.2011.12.045
211 Macchia, E. *et al.* Label-free and selective single-molecule bioelectronic sensing with a millimeter-wide self-assembled monolayer of anti-immunoglobulins. *Chem. Mater.* **31**, 6476-6483 (2019). https://doi.org/10.1021/acs.chemmater.8b04414
212 Shirley, D. A. High-resolution X-ray photoemission spectrum of the valence bands of gold. *Phys. Rev. B* **5**, 4709 (1972). https://doi.org/10.1103/PhysRevB.5.4709
213 Tougaard, S. Universality classes of inelastic electron scattering cross-sections. *Surf. Interface Anal.* **25**, 137-154 (1997). https://doi.org/10.1002/(SICI)1096-9918(199703)25:3<137::AID-SIA230>3.0.CO;2-L
214 Scofield, J. H. Hartree-Slater subshell photoionization cross-sections at 1254 and 1487 eV. *J. Electron Spectrosc. Relat. Phenom.* **8**, 129-137 (1976). https://doi.org/10.1016/0368-2048(76)80015-1